INVESTIGATIONS ON PERFORMANCE ENHANCEMENT OF POWDER-MIXED NEAR-DRY ELECTRICAL DISCHARGE MACHINING

A THESIS SUBMITTED IN FULFILMENT OF

THE REQUIREMENT FOR THE AWARD OF THE DEGREE

OF

DOCTOR OF PHILOSOPHY

IN

MECHANICAL ENGINEERING

BY

SANJAY SUNDRIYAL

(ROLL NO-2K16/PH.D/ME/04)

GUIDED BY

Dr. R.S. WALIA **Dr.VIPIN**

Department of Mechanical Engineering,

Delhi Technological University

(Formerly Delhi College of Engineering)

Main Bawana Road, Shahabad Daulatpur, Delhi- 110042, India

CERTIFICATE

This is to certify that the work embodied in the thesis entitled **"Investigations On Performance Enhancement Characteristics Of Powder-Mixed Near-Dry Electrical Discharge Machining"** being submitted by **Sanjay Sundriyal (Roll No- 2K16/PhD/ME/04)** for the award of Doctor of Philosophy Degree (Ph. D) in Mechanical Engineering at Delhi Technological University, Delhi is an authentic work carried out by him under our guidance and supervision.

It is further certified that the work is based on original research and the matter embodied in this thesis has not been submitted to any other university/institute for award of any degree to the best of our knowledge and belief.

Dr. R.S Walia

Professor

Production and Industrial Engineering

Punjab Engineering College

Chandigarh- 160012

Dr. Vipin

Professor

Department of Mechanical Engineering

Delhi Technological University

Delhi-110042

ACKNOWLEDGEMENT

While bringing out this thesis to its final form, I came across a number of people whose contributions in various ways helped my field of research and they deserve special thanks. It is a pleasure to convey my gratitude to all of them.

First and foremost, I would like to express my deep sense of gratitude and indebtedness to my parents, supervisors (Prof. R.S Walia, Prof.Vipin) and friends (Himmat Singh, Dr. Parvesh Ali) for their invaluable encouragement, suggestions and support from an early stage of this research and providing me extraordinary experiences throughout the work. I also thanks for their support in my project research. Above all, their priceless and meticulous supervision at each and every phase of work inspired me in innumerable ways.

I specially acknowledge them for their advice, supervision, and the vital contribution as and when required during this research. Their involvement with originality has triggered and nourished my intellectual maturity that will help me for a long time to come. I am proud to record that I had the opportunity to work with an exceptionally experienced Professors like them.

Sanjay Sundriyal

PREFACE

In this thesis a newly developed hybrid form of Electric Discharge Machining have been described which is Powder-Mixed Near- Dry Electric Discharge machining and it would help the researchers to understand the technique how to get better surface characteristics by utilizing minimum amount of dielectric fluids. The contents of the thesis are as follows:

Chapter 1 This chapter includes the background of electric discharge machining and its evolution in modern world. Afterwards, its principle was discussed along with material removal mechanism. Details regarding EDM machine and its components were also discussed in elaborated manner. Further advantages, limitation and application of EDM were discussed. Lastly types of EDM and its hybrid forms were explained.

Chapter 2 This chapter deals with review of the literature study conducted by researchers in field of EDM and its hybrid forms. Several studies have been conducted related to surface finish, material removal rate, tool wear rate, micro-hardness and residual stress.

.**Chapter 3** This chapter includes preview of present investigation. The objectives of the present study and scope of the problem were evaluated by reviewing the literature review critically. Additionally, problem formulation was described for the lacking information pertaining to EDM process, thereafter the problems were described which needed to be solved through this present work.

Chapter 4 The Design of experiment was introduced in this chapter for experimentation planning. Further Taguchi methodology along with analysis of variance was studied for process optimization of the developed process of Powder Mixed Near Dry EDM. This chapter also gives information related to steps involved in Taguchi methodology and application of analysis of variation (ANOVA) in various research fields. Lastly scheme of experiments has been discussed along with instruments used for measurement of different response characteristics.

Chapter 5 This chapter includes information related to Electric Discharge Machine and design of powder mixed near dry electric discharge machining (PMND-EDM) setup and it's another form of gaseous assisted powder mixed near dry EDM (GAPMND-EDM) setup. The specification of the used parts was defined along with the operational condition of the indigenously developed setup. Afterwards, details of tool electrode fabrication and its design were also discussed.

Chapter 6 This chapter describes parameters selected for experimentation in powder mixed near dry EDM and gaseous assisted EDM. Afterwards selection of response characteristics was elaborated. Variable parameters such as tool type, metallic powder concentration, dielectric mist pressure, mist flow rate, types of gases, and types of metallic powders were discussed along with their range in order to optimize the process parameters for enhancing the machining performance in terms of increased material removal rate, improved surface finish, improved micro-hardness, reduction of residual stress and tool wear rate. Lastly, the instruments used for measuring response characteristics were discussed.

Chapter 7 This chapter includes thermal-physical based modeling for material removal in Powder Mixed Near-Dry Electric Discharge Machining. This research includes three-dimensional axisymmetric model for PMND-EDM. Thermal properties of material, heat source shape (Gaussian heat distribution), heat distribution percentage among workpiece, tool and dielectric fluid, pulse on, pulse off and material ejection efficiency were considered as significant elements for predicting the MRR in PMND-EDM.

Chapter 8 This chapter includes result and discussion related to present investigation. This section includes validation of model through experimental and analytical means. Further discussion was related to optimization of process parameters and their effect on output performance characteristics. The best combination of the parameters was found for improving the machining efficiency. Later confirmation experiments were conducted to verify the results. Lastly analysis of machining performance was done based on gaseous assisted EDM with powder additives.

Chapter 9 This chapter contains salient conclusions. Important conclusions of the investigation regarding MRR, Ra, TWR, MH and RS are stated in this end part of the thesis. This chapter also introduces scope for further research in this field. Significant findings have been drawn from performed experimentation.

CONTENTS

S.No	Title	Page No.
	Certificate	**i**
	Acknowledgement	**ii**
	Preface	**iii**
	List of Figures	**xi**
	List of Tables	**xv**
	Acronyms	**xviii**
	Abstract	**xx**
1	**CHAPTER 1- INTRODUCTION**	**1-20**
1.1	Background	1
1.2	Future of Electric Discharge Machining	1
1.3	Principle of Electric Discharge Machining	2
1.4	EDM MACHINE AND COMPONENTS	4
1.4.1	EDM Circuits	4
1.4.2	Dielectric Unit	5
1.4.3	Servo feed control	5
1.5	Benefits of EDM	5
1.6	Limitations of EDM	6
1.7	Applications	6
1.8	Advanced forms of Electric Discharge Machining Processes	7

1.8.1 Ram EDM 7

1.8.2 Small Hole (micro EDM) Drilling 8

1.8.3 Wire EDM 8

1.8.4 Electric discharge milling 9

1.8.5 Electric discharge grinding 10

1.9 Hybridizations in Electric Discharge Machining Process 10

1.9.1 Hybrid EDM Processes 10

1.9.2 Hybrid Process Of EDM In Gas Combined With Ultrasonic Vibration And AJM 11

1.9.3 Wire EDM in Gas 12

1.9.4 EDM by Using Water and Powder-Mixed Dielectric Fluid 13

1.9.5 Near-Dry Electric Discharge Machining 14

1.9.6 Laser assisted electrical discharge machining 15

1.9.7 Electro- chemical discharge machining 15

1.9.8 Abrasive wire electric discharge machining 16

1.9.9 Magneto rheological fluid assisted electrical discharge machining 16

1.9.10 Powder mixed near dry electric discharge machining 17

1.9.11 Dry EDM with dielectric medium of pressurized gas 18

1.10 Motivation for this research work 19

2 Chapter 2- LITERATURE REVIEW 21-35

2.1 The three basic major areas in EDM can be classified as given below 21

2.2 Literature Review 21

2.3 Research Gap 35

3 Chapter 3- PROBLEM FORMULATION 36-40

3.1 Preview of present investigation 36

3.2 Working of Powder Mixed Near Dry EDM 37

3.3 Problem Formulation 38

3.4 Objectives 39

3.5 Research Methodology 39

4 Chapter 4- EXPERIMENTAL DESIGN AND ANALYSIS 41-52

4.1 Steps Involved In Taguchi Method 42

4.2 Signal to Noise Ratios 43

4.3 Analysis of Variance 44

4.4 Scheme of experiments 44

4.4.1 Pilot Experiments 45

4.4.2 Single and Multi objective optimization 45

4.4.3 Gaseous Assisted Powder Mixed Near Dry EDM 46

4.4.4 Comparative study for Near Dry and PMND-EDM with compressed air 46

4.4.5 Thermo-Electric Modeling In Pmnd-Edm 47

4.5 Selection Of Workpiece And Tool 48

4.6 Measurement of Response Characteristics 49

4.6.1 Material Removal Rate 49

4.6.2 Surface Finish (Ra) 49

4.6.3 Micro-Hardness (MH) 50

4.6.4 Residual Stress (RS) 50

4.6.5 Scanning Electron Microscope 51

5 **CHAPTER 5 - DETAILS OF EXPERIMENTAL SETUP** **53-59**

5.1 EDM MACHINE 53

5.2 EDM control panel 54

5.3 Development Of Powder Mixed Near Dry Electric Discharge Machining Setup (PMND-EDM) 55

5.4 Gaseous assisted powder mixed near dry EDM (GAPMND-EDM) 57

5.5 Tool electrode design 58

6 CHAPTER 6 SELECTION OF PROCESS PARAMETERS AND EXPERIMENTATION **60-70**

6.1 Selection of process parameters 61

6.1.1 Concentration of Metallic Powder Additives 61

6.1.2 Tool Type 64

6.1.3 Dielectric Medium Flow Rate 65

6.1.4 Dielectric mist pressure 66

6.1.5 Type of Gases 67

6.1.6 Type of Powders 69

7 CHAPTER 7 THERMAL - PHYSICAL BASED MODELING FOR MATERIAL REMOVAL IN POWDER MIXED NEAR –DRY EDM **71-82**

7.1 Computational FEM Modeling and Simulation for material removal rate 73

7.1.1 MRR estimation through Finite Element Analysis 77

7.2 Mathematical modeling for material removal 78

7.3 Experimental material removal rate 81

8 CHAPTER 8 RESULT AND DİSCUSSİON 83-142

8.1 Model Validation for MRR in PMND-EDM 83

8.1.1 Effect of pulse-on time and powder's concentration on MRR 85

8.2 Optimization 88

8.2.1 Optimization of Material Removal Rate (MRR) in PMND-EDM 89

8.2.2 Performance characteristics estimation (MRR) 97

8.2.3 Confirmation Experiments for MRR 98

8.3 Optimization for surface finish (Ra) in PMND-EDM 99

8.3.1 Estimation of performance characteristics (Surface finish) 106

8.3.2 Confirmation of experiments for surface finish 106

8.4 Optimization for Residual Stress (RS) in PMND-EDM 108

8.4.1 Estimation of performance characteristics (Residual Stress) 120

8.4.2 Confirmation experiments for residual stress 121

8.5 Optimization for Tool Wear Rate (TWR) in PMND-EDM 121

8.5.1 Estimation of optimum performance characteristics (TWR) 126

8.5.2 Confirmation of tests 127

8.6 Optimization for Micro-hardness (MH) in PMND-EDM 128

8.6.1 Estimation of Performance Characteristics (Micro-Hardness) 136

8.6.2 Confirmation Experiments 137

8.7 Multi - Characteristic Optimization Using Utility Function 137

8.7.1 Multi-objective optimization of PMND-EDM through Taguchi method and Utility concept 138

8.7.2 Algorithm for multi-response optimization for MRR, Ra, RS, MH and TWR in PMND-EDM 140

8.7.3 Calculation of utility value 142

8.7.4 Estimation of performance characteristics (Utilities of MRR, Ra, MH, RS and TWR) 146

8.7.5 Confirmation of experiments for utilities (MRR, Ra, RS, MH and TWR) 148

8.8 Gaseous Assisted Powder Mixed Near-Dry Electric Discharge Machining 148

8.8.1 Effect of Gases with powder additives On MRR in GAPMND-EDM 150

8.8.2 Effect of Gases with powder additives on Surface finish in GAPMND-EDM 154

8.8.3 Effect of Gases with Powder Additives on Micro-Hardness in GAPMND-EDM 157

8.8.4 Effect of Gases with powder additives on Residual stress in GAPMND-EDM 160

8.9 Effect of Different Powder Additives on Machining Performance in PMND-EDM 162

8.9.1 Effect of Different Powder Additives on MRR 164

8.9.2 Effect of Different Powder Additives on Surface Finish (Ra) 165

9 Chapter 9 CONCLUSION AND FUTURE SCOPE OF WORK 170-173

9.1 Conclusion 170

9.2 Future Scope 173

10 References 174

11 Research publication 187

LIST OF FIGURES

Figure 1.1	Evolution of EDM	2
Figure 1.2	Complete mechanism of material erosion in EDM	4
Figure 1.3	Electric Discharge Machine	4
Figure 1.4 (a)	Automobile parts by Die Sinking EDM	6
Figure 1.4 (b)	Complex geometries generated by EDM	7
Figure 1.5	Sinker EDM used to produce blind cavities	7
Figure 1.6	Micro-hole drilling	8
Figure 1.7	Schematic representation of Wire cut EDM	9
Figure 1.8	Electric discharge milling	9
Figure 1.9	Electric discharge grinding	10
Figure 1.10	Hybrid Setup of EDM	12
Figure 1.11	Set up of Wire EDM in gas	13
Figure 1.12	Principle of powder mixed EDM	13
Figure 1.13	Schematic Diagram of NEAR DRY EDM setup	14
Figure 1.14	Electro- chemical discharge machining	15
Figure 1.15	Abrasive wire electric discharge machining	16
Figure 1.16	Magneto rheological fluid assisted electrical discharge machining setup	17
Figure 1.17	Powder mixed near dry electric discharge machining	18
Figure 1.18 (a)	Dry EDM with pressurized gas	19
Figure 1.18 (b)	Benefits of Dry EDM gas	19
Figure 1.19	Purpose of the research study	20
Figure 3.1	Powder Mixed Near-Dry Electric Discharge Machining	37
Figure 3.2	Schematic diagram of PMND-EDM	38
Figure 4.1	Complete summary for scheme of experiments	42
Figure 4.2	ZeGage optical profilometer	50
Figure 4.3	Micro-hardness measuring machine (Fischerscope instrument)	50
Figure 4.4	Portable XRD - residual stress analyzer in operation	51
Figure 4.5	Scanning electron microscope (TM-3000 table top microscope)	52
Figure 5.1	Sparkonix 35-A EDM machine	53
Figure 5.2	Developed experimental setup for PMND-EDM	56
Figure 5.3	Line diagram for indigenous developed setup for PMND-EDM	57

Figure 5.4	GAPMND-EDM setup for experimentations	57
Figure 5.5	Design of tool developed for PMND-EDM; all dimensions in mm	58
Figure 5.6	Design feature of developed tool	58
Figure 5.7 (a)	Hollow copper electrodes of different dimensions (all dimensions in mm)	59
Figure 5.7 (b)	Tool setup	59
Figure 6.1	Fish and Bone diagram for measurement of EDM response characteristics	60
Figure 6.2	Effect of metallic powder concentration on the MRR and Ra	61
Figure 6.3	Effect of metallic powder concentration on the RS and MH	62
Figure 6.4	Effect of metallic powder concentration on the TWR	63
Figure 6.5	Effect of tool type on the MRR and Ra	64
Figure 6.6	Effect of tool type on the RS	65
Figure 6.7	Effect of dielectric medium flow rate on the MRR and Ra	65
Figure 6.8	Effect of dielectric medium flow rate on the RS and MH	66
Figure 6.9	Effect of dielectric mist pressure on the MRR and Ra	66
Figure 6.10	Effect of dielectric mist pressure on the RS	67
Figure 6.11	Effect of type of dielectric gas on the RS	68
Figure 6.12	Effect of type of dielectric mixture on the Ra	68
Figure 6.13	Effect of type of dielectric gas on the MH and RS	69
Figure 7.1	Modeling and Analysis for MRR in PMND-EDM	71
Figure 7.2	Complete methodology for modeling	72
Figure 7.3	Diagram depicting the various boundary conditions used in mathematical modeling of PMND-EDM process	74
Figure 7.4	Diagram depicting the Gaussian heat distribution in PMND-EDM, at any instant of time ‘t’	75
Figure 7.5	A 3-D meshed model of workpiece	76
Figure 7.6	Heat flux conditions applied at workpiece for a particular powder concentration and total pulse duration value	76
Figure 7.7	Boundary conditions applied at workpiece for a particular powder concentration and total pulse duration value	77
Figure 7.8	Volume measurement method of a semi-toroidal crater	78
Figure 7.9	Gaussian distribution for thermal model	78

Figure 8.1	Temperature isotherms showing the extent of deformation zone obtained at discharge location (at the cross-section of the workpiece) corresponding to different pulse durations	83
Figure 8.2	Temperature distribution at various pulse durations corresponding to various N_{avg} (g/l) values	86
Figure 8.3	Graph between MRR and total pulse duration with metallic powder concentration of 5g/l	87
Figure 8.4	Graph between MRR and total pulse duration with metallic powder concentration of 10g/l	87
Figure 8.5	Graph between MRR and total pulse duration with metallic powder concentration of 15g/l	88
Figure 8.6	Machined workpiece samples	90
Figure 8.7 (a)	Effect of tool type on MRR (mg s^{-1})	92
Figure 8.7 (b)	Effect of flow rate on MRR (mg s^{-1})	93
Figure 8.7 (c)	Effect of powder concentration on MRR (mg s^{-1})	93
Figure 8.7 (d)	Effect of pressure on MRR (mg s^{-1})	94
Figure 8.8	SEM image of a machined surface with lower levels of parameters (image width: 68.8 µm, accelerating voltage 15.0 kV)	94
Figure 8.9	SEM image of a machined surface with higher levels of process parametric setting (image width: 68.8 µm, Accelerating voltage 15.0 kV)	95
Figure 8.10	Material deposit layers on machined surface at different magnification factor (a) 500x (b) 1.5kx (c) 2kx	95
Figure 8.11	XRD results of surface produced by PMND-EDM	96
Figure 8.12 (a)	EDAX spectrum for the region of machined sample	96
Figure 8.12 (b)	EDAX (Energy Dispersive Spectroscopy X-Ray) image of a machined sample by PMND-EDM	97
Figure 8.13 (a)	Effect of tool type on Ra	102
Figure 8.13 (b)	Effect of Flow rate on Ra	102
Figure 8.13 (c)	Effect of powder concentration on Ra	103
Figure 8.13 (d)	Effect of pressure on Ra	103
Figure 8.14	Study of surface topography of the machined surface by PMND-EDM	104
Figure 8.15	3-D image of surface roughness profile of machined surface by normal	104

	EDM	
Figure 8.16 (a)	SEM image of machined samples by PMND-EDM at different magnification factor (500x and 1.5kx)	105
Figure 8.16 (b)	SEM image of machined samples by normal EDM at different magnification factor (500x and 1.5kx)	106
Figure 8.17 (a)	Instrumental Residual stress (530 MPa)	109
Figure 8.17 (b)	Instrumental Residual stress (551 MPa)	110
Figure 8.17 (c)	Instrumental Residual stress (659 MPa)	110
Figure 8.17 (d)	Instrumental Residual stress (145 MPa)	111
Figure 8.17 (e)	Instrumental Residual stress (280 MPa)	111
Figures 8.17 (f)	Instrumental Residual stress (191 MPa)	112
Figure 8.18	Induced micro cracks in PMND-EDM	112
Figure 8.19	Magnitude of the strain of residual stress	115
Figure 8.20 (a)	Effect of tool type on RS (MPa)	115
Figure 8.20 (b)	Effect of Flow rate on RS (MPa)	116
Figure 8.20 (c)	Effect of powder concentration on RS (MPa)	116
Figure 8.20 (d)	Effect of pressure on RS (MPa)	117
Figure 8.21	Rapid solidification over the surface (SEM image)	118
Figure 8.22	SEM image of low metallurgical transformation (SEM image)	119
Figure 8.23	Localized in-homogenous plastic deformations (SEM image)	119
Figure 8.24 (a)	Effect of tool type on TWR	124
Figure 8.24 (b)	Effect of Flow rate on TWR	124
Figure 8.24 (c)	Effect of powder concentration on TWR	125
Figure 8.24 (d)	Effect of pressure on TWR	125
Figure 8.25	Wear of the sparking end of the tool	126
Figure 8.26 (a)	Effect of tool type on MH	130
Figure 8.26 (b)	Effect of Flow rate on MH	131
Figure 8.26 (c)	Effect of powder concentration on MH	131
Figure 8.26 (d)	Effect of pressure on MH	132
Figure 8.27 (a)	Instrument reading and plot of MH with respect to load applied	132
Figure 8.27 (b)	Instrument reading and plot of MH with respect to load applied	133
Figure 8.28	ZnC layer formation over the machined sample	133

Figure 8.29	SEM images of machined samples at different magnification factor (a) 500x (b) 1.0 kx (c) 1.5 kx (d) 2 kx	135
Figure 8.30	SEM micrograph of cross section with average values of micro-hardness	135
Figure 8.31	SEM micrograph of machined sample by EDM without metallic powder	136
Figure 8.32 (a)	Effect of tool type on utility	145
Figure 8.32 (b)	Effect of Flow rate on utility	145
Figure 8.32 (c)	Effect of powder concentration on utility	146
Figure 8.32 (d)	Effect of pressure on utility	146
Figure 8.33	Machined samples by GAPMND-EDM	150
Figure 8.34 (a)	SEM image of machined EN-31 sample by oxygen assisted with graphite powder	152
Figure 8.34 (b)	SEM image of machined EN-31 sample by argon assisted with copper powder	152
Figure 8.34 (c)	SEM image of machined EN-31 sample by oxygen assisted with zinc powder	153
Figure 8.34 (d)	SEM image of machined EN-31 sample by argon assisted with copper powder	153
Figure 8.34 (e)	SEM image of machined EN-31 sample by argon assisted with zinc powder additives	154
Figure 8.35 (a)	Surface profile with graphite additive (powder) in presence of argon gas	155
Figure 8.35 (b)	Surface profile with copper additive (powder) in presence of argon gas	155
Figure 8.35 (c)	Surface profile with zinc additive (powder) in presence of argon gas	156
Figure 8.35 (d)	Surface profile with copper additive (powder) in presence of oxygen gas	156
Figure 8.35 (e)	Surface profile with graphite additive (powder) in presence of oxygen	157
Figure 8.35 (f)	Surface profile with zinc additive (powder) in presence of oxygen gas	157
Figure 8.36 (a)	The reading of micro-hardness of the machined sample by GAPMND-EDM using zinc additive	158
Figure 8.36 (b)	The reading of micro-hardness of the machined sample by GAPMND-EDM using copper additive	159
Figure 8.36 (c)	The reading of micro-hardness of the machined sample by GAPMND-EDM using graphite additive	159
Figure 8.37 (a)	Debye Scherer rings with residual stress values of machined EN-31 samples by GAPMND-EDM with graphite and oxygen medium	160

Figure 8.37 (b)	Debye Scherer rings with residual stress values of machined EN-31 samples by GAPMND-EDM with copper and oxygen	160
Figure 8.37 (c)	Debye Scherer rings with residual stress values of machined EN-31 samples by GAPMND-EDM with zinc and oxygen	160
Figure 8.37 (d)	Debye Scherer rings with residual stress values of machined EN-31 samples by GAPMND-EDM with argon and graphite	161
Figure 8.37 (e)	Debye Scherer rings with residual stress values of machined EN-31 samples by GAPMND-EDM with argon and zinc	161
Figure 8.37 (f)	Debye Scherer rings with residual stress values of machined EN-31 samples by GAPMND-EDM with argon and copper	161
Figure 8.38(a-c)	Images of some machined EN-31 samples with micro cracks	163
Figure 8.39	Residual stress variations across the depth of the machined sample	163
Figure 8.40	MRR Vs different types of machining method	163
Figure 8.41	Ra Vs different types of metallic powder	166
Figure 8.42	Surface cracks over the machined surface by ND-EDM	166
Figure 8.43 (a)	Surface profile of machined workpiece sample by Silicon powder	167
Figure 8.43 (b)	Surface profile of machined workpiece by graphite powder	167
Figure 8.43 (c)	Surface profile of machined workpiece by aluminium powder	168
Figure 8.43 (d)	Surface profile of machined workpiece by Near Dry machining	168

LIST OF TABLES

Table 4.1	Experimental condition for pilot experiments	45
Table 4.2	Scheme for experiments	45
Table 4.3	Different scenarios of dielectric mediums for experimentations for MRR	46
Table 4.4	Process parameters for experimentation for ND-EDM and PMND-EDM	46
Table 4.5	Chemical composition and physical properties of workpiece (EN-31)	48
Table 4.6	Chemical and physical properties of copper tool	48
Table 5.1	Specifications of the EDM Machine	54
Table 5.2	Diameter of various tools developed for present study (sparking end)	59
Table 6.1	Properties of metallic powders	70
Table 7.1	Process parameters and their levels selected for experimentations	82
Table 8.1	Results obtained from experimentation, mathematical and finite element modeling and their error estimation	84
Table 8.2	Experimental Results for Material Removal Rate as per Taguchi L_9 OA	89
Table 8.3	Average values and Main effects: MRR (mg s^{-1})	92
Table 8.4	Pooled ANOVA raw data and S/N data for MRR	92
Table 8.5	Confirmation Experiments for MRR	99
Table 8.6	Experimental results of surface finish as per Taguchi L_9 OA	99
Table 8.7	Main effects table for surface finish (Ra)	101
Table 8.8	Pooled ANOVA raw data and S/N data for surface finish (Ra)	101
Table 8.9	Confirmation Experiments for surface finish	108
Table 8.10	Experimental Results of Residual stress as per Taguchi L_9 OA	108
Table 8.11	Average values and Main effects: Residual stress, RS (in MPa)	113
Table 8.12	Pooled ANOVA raw data and S/N data for Residual stress	113
Table 8.13	Confirmation experiments for Residual stress	121
Table 8.14	Experimental results for TWR as per L_9 orthogonal array	121
Table 8.15	Raw data and Signal to noise ratio for different parameters	122

Table 8.16	Pooled ANOVA raw data for TWR	122
Table 8.17	Predicted optimal values and results of confirmation experiments	128
Table 8.18	The experimental results for micro-hardness by PMND-EDM as per Taguchi L_9 OA	128
Table 8.19	Main effects table for micro-hardness	129
Table 8.20	Pooled ANOVA raw data and S/N data for micro-hardness	129
Table 8.21	Predicted optimal values and results of confirmation experiments	137
Table 8.22	Individual outcomes for MRR, Ra, RS, MH and TWR in PMND-EDM	141
Table 8.23	Optimal setting and values of process parameters for different output responses as per single objective optimization	141
Table 8.24	Utilities values of MRR, Ra, RS, MH and TWR	142
Table 8.25	Main effects and average values of output responses MRR, Ra, RS, MH and TWR in PMND-EDM	143
Table 8.26	ANOVA pooled S/N and raw data for multi responses MRR, Ra, RS, MH and TWR in PMND-EDM	143
Table 8.27	Confirmation experiments for quality characteristics	148
Table 8.28	Average value of Material Removal Rate by GAPMND-EDM using different experimental scenarios	149
Table 8.29	Summary of experimentations conducted by GAPMND-EDM under different experimental conditions	164

ACRONYMS

Fc	Heat distribution factor
V_b	Discharge or break down voltage (Volts)
I	Discharge current (Ampere)
Q-	Rate of heat supplied at workpiece (W)
q’	Heat supplied (J)
Q(t)	Rate of heat flux supplied (W/mm^2)
A	Area over which heat flux is acting (mm^2)
MRR_d	Material removal per discharge (mm^3)
MRR	Material removal rate (mg/s)
TWR	Tool Wear Rate (mg/s)
Ra	Surface finish (μm)
RS	Residual stress (MPa)
HV	Vickers hardness number
MH	Micro-hardness
γ_{cr}	Critical concentration ratio (N_{cr}/N_∞)
N_{cr}	Particle concentration at breakdown (g/l)
N_∞ or N_{avg}	Average particle concentration (g/l)
R_c	Critical radius (mm)
t_B	Break down time (μs)
$K_Ø$	Constant
η	Viscosity of dielectric medium (Pas)

x	Inter-electrode gap (mm)
s	Size of individual powder particles (mm)
E	Electric field at a location other than discharge region (V/mm)
Eo	Electric field at discharge region (V/mm)
P_{on}	Pulse-on time (μs)
P_{off}	Pulse-off time (μs)
V_{vt}	Total crater volume (mm^3)
j_i	Volume of individual cylindrical discs (mm^3)
W_i	Initial mass of the workpiece before machining (g)
W_f	Final mass of the workpiece after machining (g)
ρ	Density of the workpiece (g/mm^3)
T_m	Machining time for experiments (minutes/ sec).

ABSTRACT

EDM has played a vital role in machining industry but with advancement of technology, alternative advanced method of machining has been evolved such as powder mixed near-dry EDM (PMND-EDM). This technology have been proven more efficient than traditional EDM in terms of machining performance characteristics such as higher material removal rate (MRR), better surface finish (Ra) with low tool wear rate (TWR), residual stress (RS), and increased micro-hardness (MH) of the machined workpiece with high tolerance quality products. Powder mixed near-dry electric discharge machining (PMND-EDM) is an advanced method of machining very hard conductive materials with complex geometries which are very difficult to machine by any other conventional method. PMND-EDM is an eco-friendly process which uses minute amount of metal working fluids (MWF) along with conductive metallic powders for machining purposes. Improvement in heat distribution by the bridging effect at the machining gap due to presence of metallic powder particles results in obtaining better machined surfaces. In this research, an approach has been made to optimize the significant process parameters by using Taguchi L_9 orthogonal array (OA) along with ANOVA (analysis of variance) in order to obtain machined components with higher value material removal rate (MRR), micro-hardness (MH) with reduced residual stress (RS) and tool wear rate (TWR). The workpiece selected was EN-31 material due to its desirable mechanical properties and immense applications in manufacturing industry while the tool electrode selected was copper in material due to its higher thermal conductivity and other desirable properties for conducting experiments. The experiments were conducted on EDM machine (Sparkonix 35-A, Pune) in hybridization with setup made indigenously in Delhi technological university (D.T.U. India). In this present study a combination of conductive metallic powder (zinc) along with pressurized mist for powder mixed near dry electric discharge machining (PMND-EDM) has been utilized as a dielectric mixture in order to achieve higher material removal rate (MRR). The finished surface of the components was characterized for the microstructure study using SEM and XRD analysis. The analysis for X-ray diffraction of the finished workpiece was performed with X'Pert High Score tool. The oxide layers and molten material on workpiece surface was also observed from SEM images and these depositions were responsible for improving the surface properties.The maximum peak in the XRD graphs was found for iron oxide with a cubic crystal system. Additional peaks at different planes were found for a cubic crystal system. During the XRD interpretation some groups with lower peaks were discounted. It was also observed that some molten parts of the tool electrode got

embedded in the machined workpiece. The copper composition of molten copper material embedded in the machined workpiece was measured by energy dispersive spectroscopy X-Ray (EDAX). SEM images revealed that the surface characteristics of the machined workpiece were much better when machined by powder additives in near dry EDM as compared to simple EDM. The maximum material removal rate was found to be 0.11 mg s^{-1} at optimized parametric setting. It was found that PMND-EDM leads to generation of machined products with high surface quality characteristics (Ra ~1.113 µm). The PMND-EDM improved the efficiency of electrical discharging machining by the improved heat distribution at the machining gap. It was concluded from the results that the TWR can be significantly reduced by optimizing the parameters in PMND-EDM (TWR~1.15 mg/min). Confirmation experiments revealed that the highest value of micro-hardness was found to be 506.63 HV at optimized input process parameters. The minimum value of residual stress at optimized values of process parameters was found to be 106.32 MPa. Multi-Response optimization was performed for PMND-EDM by using Taguchi methodology and utility concept. At optimum settings, the experiments were performed and combined effect of input parameters was analysed on multi responses such as MRR, Ra, RS, MH and TWR. Confirmation experiments were performed and it was noticed that the values of the output results lies between the prescribed limit and range with 95 % confidence interval. The 95% confidence interval of the predicted mean for the material removal rate was 0.39 < MRR < 0.87; for Surface finish was 0.73< Ra < 0.85; for Residual stress was 285.33< RS< 286.67; for Micro-hardness was 248.58< MH< 249.42; for Tool wear rate was 0.95 < TWR < 1.19. Modeling was also performed for output process parameter –Material Removal Rate in PMND-EDM. The mathematical model was developed using the approach of Gaussian heat distribution. FEM (finite element method) modelling was done on ANSYS WORKBENCH 16.0 module. The experiments were performed and comparative study was done between the results obtained by modeling and experiments. The maximum experimental MRR was 7.68 mm^3/min and the error percentage between experimental, mathematical and FEM was under 15%. It was concluded that the modeling was done successfully and results obtained do comply with the methodology of the research. Study for different dielectric gases (argon and oxygen) along with metallic powder (Graphite and Zinc) was also conducted in GAPMND-EDM for output responses MRR, Ra, MH and RS. In this research, among the different metallic powder used, the largest cavities were formed by use of graphite powder because of its lower density and higher thermal/electrical conductivity as compared to other powders. It was also found that the maximum material removal rate (MRR 3.379 mg/min) was achieved with combination of (dielectric) oxygen gas with graphite

powder while highest surface finish (Ra 1.11 μm) was found to be with dielectric argon gas with graphite additives. SEM images revealed that graphite has excellent lubricity property which has a very good effect on wetting of the powder particles by the molten machined surface and the well-developed ordered microstructure of graphite material was also an added advantage. Highest micro-hardness and lowest residual stress was 820.30 (HV) and 229 MPa respectively found with dielectric combination of zinc additives with argon gas. Additional experiments were performed for different metallic powders (Aluminium, Graphite and Silicon) in terms of comparative study for material removal and surface finish of the machined EN-31 workpiece by using copper tool electrode. The highest MRR (4.5 mm^3/min) in PMND-EDM was found by using aluminium powder followed by graphite and silicon due to lowest resistivity of aluminium (5 μΩ-cm) amongst other metallic powders Gr (30 μΩ-cm) and Si (10000 μΩ-cm). The maximum surface finish (1.6 μm) was observed with Silicon powder followed by graphite and aluminium powder due to its low thermal and electrical conductivity. Silicon powder particles being smaller in size enter the machining gap in more quantity which resulted in even distribution of discharges over a large area. Therefore the surface finish achieved was higher in quality as compared to surface machined by other powder additives due to their large particle size. The developed technique is confirmed to be a better process for achieving products having high level of surface integrity.

This chapter includes the background of electric discharge machining and its evolution in modern world. Afterwards, its principle was discussed along with material removal mechanism. Details regarding EDM machine and its components were also discussed in elaborated manner. Further advantages, limitation and application of EDM were discussed. Lastly types of EDM and its hybrid forms were explained.

1.1 Background

Electrostatic phenomena were first noted in 1773 by English physicist Joseph Priestley. In 1766, it was also discovered by Priestly that electrical discharges causes erosion and leaves craters on the electrically conductive material. The history of invention of EDM and its principle dates back to 1943 by the two Russian scientists Boris and Natalya Lazarenko in Moscow. These two scientists were assigned with the task by the soviet government for investigation of the wear of the tungsten electrodes caused by the sparking at inter-space of the electrodes. The investigation was very critical, as it was needed for the automotive engines maintenance during Second World War. The sparks were found to be more stable by keeping the electrodes in oil. The Lazarenko's came with the idea of reverse phenomenon and used sparks in a controlled manner for erosion purposes. Although, the Lazarenkos could not prevent the wear problem but instead they were successful in inventing first EDM machine and "Lazarenko circuit" during the war, which was used to erode hard metals (i.e tungsten and tungsten carbide). Later in 1950's, the progress was made related to investigation of erosion phenomenon (Germer and Haworth, 1949, Zingerman, 1956). There was development of EDM machines by Swiss industries such as Agie Company and Ateliers des Charmilles during 1954-55. But the performance of machines was limited due to poor quality of the electronic parts. With the development of semiconductors in 1960's, the EDM machines were improved in performance characteristics. Later on, other form of EDM came into existence and better machined surface were produced with controlled quality.

1.2 Future of Electric Discharge Machining

Advanced materials were used for modern day industrial applications because of several advantages such as high stiff ness, high strength, better damping capacity, better fatigue and low thermal

expansion. These favourable properties of advanced materials makes them demanding in present manufacturing industries. There were several challenges faced by the present day manufacturing industries with respect to these advanced materials. Major challenges were difficulty in machining and reduced precision with high machining cost (Kozak and Rajurkar, 2001). The conventional machining processes failed to machine the advanced materials due to their improved mechanical, chemical and thermal properties. Conventional machining processes such as drilling, turning and milling were ineffective in machining these advanced materials because it resulted in improper material removal, poor surface finish and high wear of tool (Pandey and Singh, 2010). To solve this problem, advanced methodology was developed. Electric Discharge Machining (EDM) solved this trivial problem by using thermal energy and was successfully established in production industry for purposes such as forming of dies, tool and molds made of advanced materials. It was considered as one of the non-conventional machining method for accurate and precision machining of materials. Some research has been done related to improvement of EDM performance and making this process more reliable as shown in Figure 1.1 (Choudhary and Jadoun, 2014, Pandey and Singh, 2010).

.

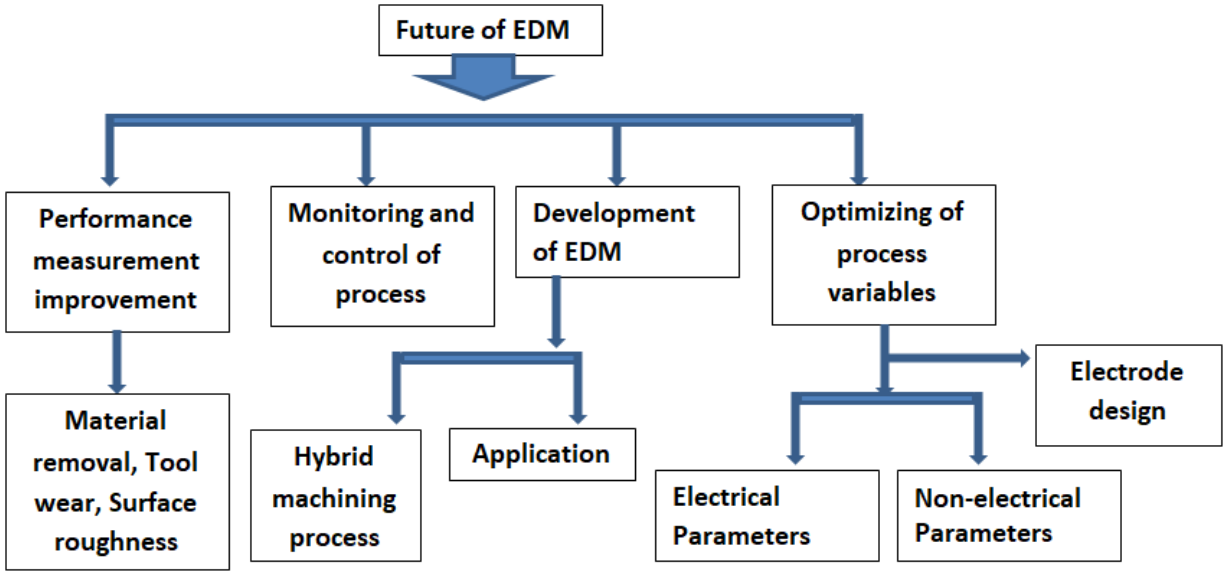

Figure 1.1 Evolution of EDM (Choudhary and Jadoun, 2014, Pandey and Singh, 2010)

1.3 Principle of Electric Discharge Machining

The material removal mechanism of EDM is still contentious and not defined absolutely, but the principle of conversion of electrical energy into thermal energy through electric discharges was most widely accepted for the erosion process in EDM (Tsai et al. 2003). There was a phenomenon of

movement of the accelerated electrons towards the anode from the cathode, when suitable voltage was applied across the submerged workpiece and tool in dielectric medium (Konig and Klocke, 1997). These liberated cold electrons collide with the dielectric medium, splitting them into electrons and ions. Due to this collision, a column of ionized molecules of the dielectric was established between the tool and workpiece leading to generation of sparks due to electrons avalanche. A compressed shock wave gets generated and high temperature range of 8000 to 12,000 °C gets developed between the electrodes resulting in melting and evaporation of the tool and workpiece (Shobert, 1983). Finally the molten tiny chips are evacuated by the mechanical blast resulting in formation of tiny craters over the electrodes (Panday and Shan, 2003).

Overall, the complete mechanism of material erosion can be stated in five different steps as shown in Figure 1.2 (a). A high potential was applied at a small gap between the electrodes as shown in Figure 1.2 (b), as there was no physical contact between the tool and workpiece. The electric field at the inter electrode gap was enhanced by the movement of the tool towards the workpiece, this continues till the breakdown voltage of dielectric was reached. The discharge takes place at the spot of nearest points of the electrodes (McGeough, 1988). However, the location of the spot may change due to the impurities (debris) present at the gap between the electrodes. Afterwards, there was drop in voltage and the discharge current flows from workpiece to the electrode by the ionization of the dielectric medium and leads to formation of plasma channel as shown in Figure 1.2 (c). There was intense heating of the workpiece by the interaction of the ions and the electrons. This intense heating leads to temperature rise creating molten metal pool and vaporization of particles takes place (Jameson, 2001). The plasma channel gets expanded during this period and molten metal pool gets enlarged (Figure 1.2 (d)).

In the final stage, the voltage is shut and pressure exerted by the dielectric causes the inward collapse of the plasma channel. This results in the evacuation of the molten metal by the dielectric and leaving a tiny cavity at the surface of the workpiece as shown in Figure 1.2 (e). The removed material was solidified and flushed away by the dielectric flow at the machining gap (Talla et al. 2017).

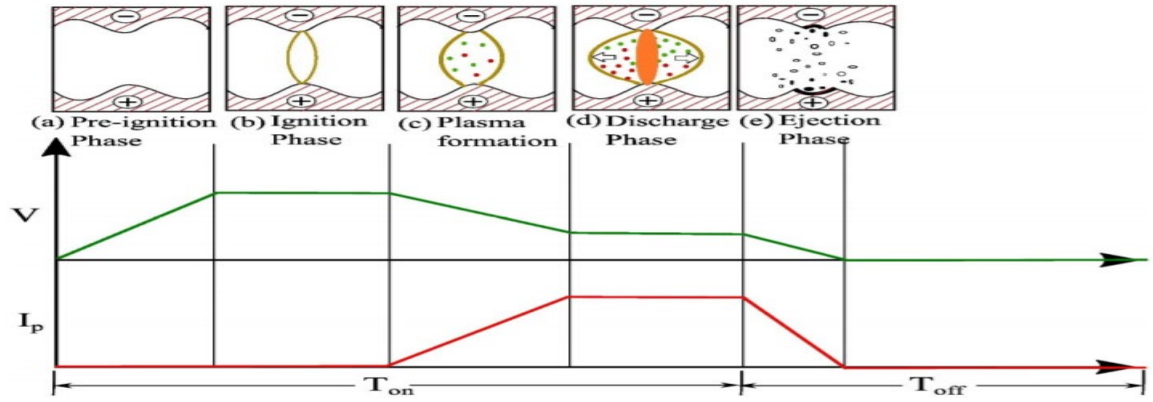

Figure 1.2 Complete mechanism of material erosion in EDM (Talla et al. 2017).

1.4 EDM MACHINE AND COMPONENTS

The EDM system generally consists of three main components: EDM circuit, Dielectric unit and Servo feed control as shown in Figure 1.3. The tool feed was controlled by the servo control mechanism. The DC pulse generates supplies the current in pulses for spark intitation at the machining gap between the conductive workpiece and tool electrodes. The pump provided was responsible for mantaining the circulation of the dielctric oil while pressure of the dielctric medium was maintained by the pressure gauge.

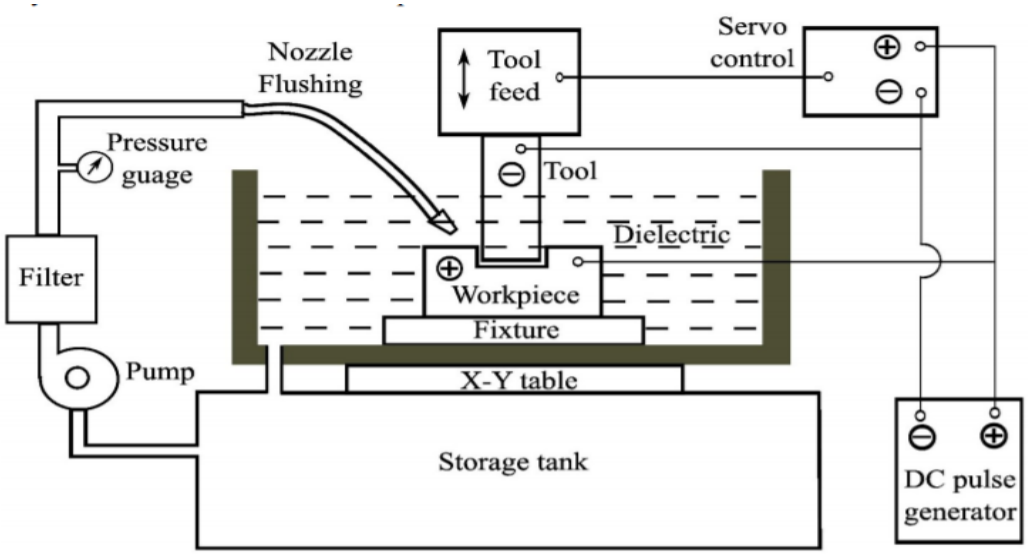

Figure1.3 Electric Discharge Machine (Talla et al. 2017).

1.4.1 EDM Circuits

The EDM circuit converts electrical energy to thermal energy and maintains the spark gap between the workpiece and tool electrodes. A capacitor was used as a storage device for electrical energy in

order to generate sparks in the electrical circuit (Bawa, 2004). Generally, Resistance –Capacitor (R-C) circuits, Pulse circuit and Generator circuits are used as powder supply source in EDM. The R-C circuit is recommended because of its simplicity and low cost. In R-C circuit, the capacitor of the condenser is charged by the resistance of the current. The charging continues till the potential of the condenser reaches the breakdown voltage of the inter electrode gap and finally spark initiation takes place (Shah et al. 2007).

1.4.2 Dielectric Unit

This unit comprises of dielectric tank, pump and filtration system for dielectric fluid. The dielectric fluid plays an important role in alternating the electrical field of the system and also controls the electrical discharges. Deionized water, mineral oil and kerosene oil were used as dielectric medium in EDM. Other purpose of dielectric fluid was to serves as a quenching medium for cooling effect and to solidify the vaporized eroded material due to discharges (Mishra, 1997).

1.4.3 Servo feed control

Since there was fluctuation in dielectric parameters, there is possibility for change of gap voltage between the electrodes. The machining gap voltage in maintained by incorporating a servo mechanism in the EDM system. Servo mechanism system was either operated by hydraulic means, solenoid driven or motor driven in order to maintain the machining gap (Pandey and Shan, 2003).

1.5 Benefits of EDM

a) Variety of shapes and sizes can be generated with EDM.
b) EDM can produce thin section as there is no contact between tool and workpiece electrodes.
c) Accuracy and finishes- Depending upon accuracy of electrode, high tolerance (0.0025 mm) can be achieved on the machined products.
d) EDM can machine very hard materials and therefore hardness is not a factor.
e) Threads can be machined into hardened parts such as carbide material.
f) It can perform micro machining.
g) Large pieces of objects can be machined.
h) Intricate details can be obtained on machined samples.
i) Fine finishes can be obtained.

1.6 Limitations of EDM

a) Material must be electrically conductive.
b) Electrical power consumption is high.
c) Slow material removal rate.
d) Additional cost and lead time used for developing sinker EDM electrodes.
e) Generation of sharp corners is difficult on the workpiece due to electrode wear.
f) Requirement of dielectric oil in bulk quantity which increases the risk of hazardous toxic fumes for occupational workers.
g) Problems related to discard of used EDM oil.

1.7 Applications

a) There are various applications of EDM in field of precision engineering; some of the complex parts generated by EDM are shown in Figure 1.4.
b) To generate blind cavity.
c) Produces machined parts with intricate details
d) Multi-cavity mold.
e) For medical casing and other applications such as surgical blades and instruments.
f) Automobile parts.
g) Aerospace industry.
h) Internal keyways.
i) Dental instruments.
j) Orthopedic, spinal, ear, nose, and throat implants.

Figure 1.4 (a) Automobile parts by Die Sinking EDM (https://www.avonbroach.com/)

Figure 1.4 (b) Complex geometries generated by EDM (http://www.mercatech.com)

1.8 Advanced forms of Electric Discharge Machining Processes

There are various other forms of EDM to enhance the machining characteristics such as higher material removal, better quality machined products etc. Some of the advance forms of EDM are as follows:

1.8.1 Ram EDM- The blind cavities in the samples were produced by conventional EDM or Ram EDM, Die sinker, Plunge EDM and Vertical EDM. It was used to generate blind cavities as shown in Figure 1.5. The spark jumps from tool electrode to workpiece electrode in Ram EDM due to which the material erosion takes place from the machined sample (Konig and Klocke, 1997). Additionally, there was no direct contact between tool electrode and workpiece electrode. Therefore there was elimination of mechanical chatter, stresses and induced vibration during machining.

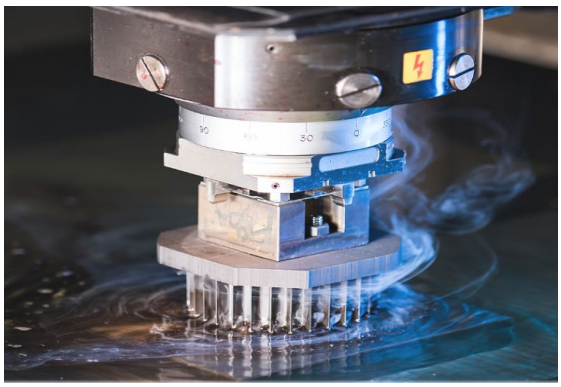

Figure 1.5 Sinker EDM used to produce blind cavities (https://www.basilius.com)

1.8.2 Small Hole (micro EDM) Drilling

Fast hole drilling or small hole drilling was used to drill micro holes (Masuzawa et al. 1989). Hollow electrodes were used as tool and erosion of material from the sample (workpiece) was achieved by means of mechanism of electrical discharge as shown in Figure 1.6. These days, small electrodes (0.1 mm) are used for drilling holes in curved surface at steep angles without drill (Kalpakjian and Schmid, 2014).

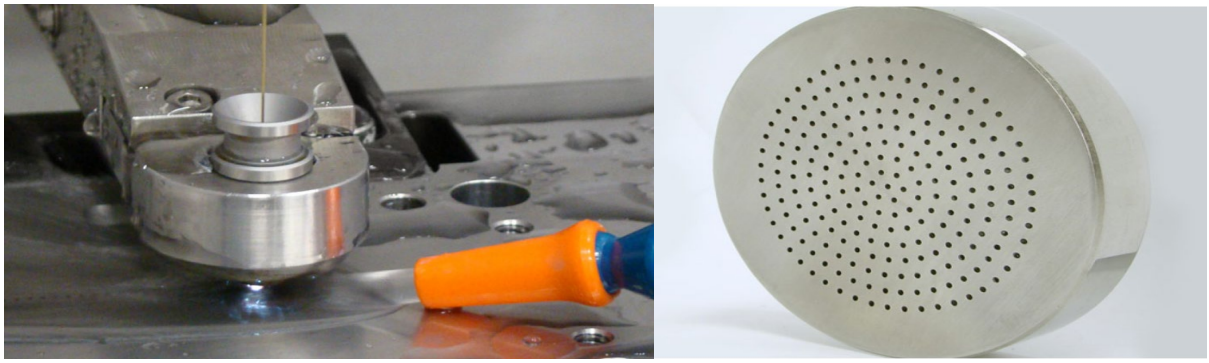

Figure 1.6 Micro-hole drilling (https://www.klhindustries.com)

Micro-EDM has got a lot of attention these days due to its capability to machine reduced sizes in recent trend. It can machine micro cavities, 3-D complex geometries, micro shafts and micro holes. Micro EDM has been classified into four types - micro-EDM milling, micro EDM drilling, die-sinking micro-EDM and micro-wire EDM. Micro –electrodes in micro EDM drilling can be used for micro holes drilling in workpieces.

1.8.3 Wire EDM

Wire cut EDM or wire EDM employs wire electrode as cutting tool, which are fed through guides (upper and lower) to cut workpieces and afterwards it is discarded (Kuriakose et al. 2003). The movement of the wire or the path of the cut was controlled by computer numeric control system. The variation in wire can from 0.0120 to 0.0008 inches in diameter and the schematic setup for wire electric discharge machining is shown in Figure 1.7.

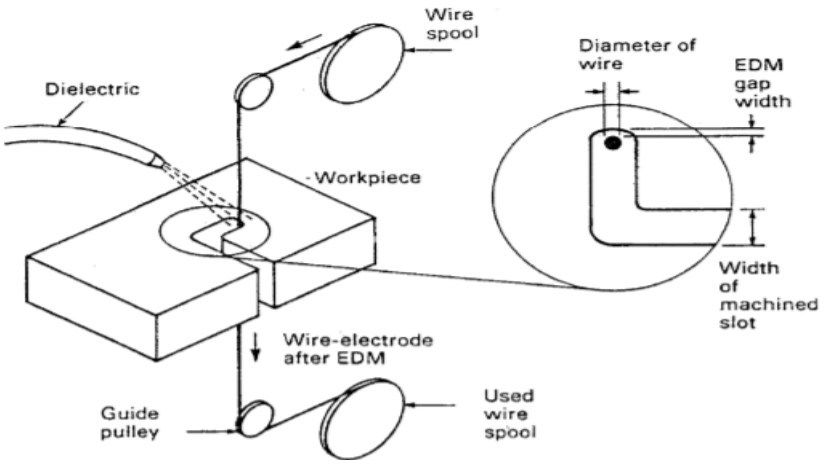

Figure 1.7 Schematic representation of Wire cut EDM (Kuriakose et al. 2003)

1.8.4 Electric discharge milling

It is advanced form of computer numeric control EDM. A programmed path by the CNC coding was followed by the rotating tool for obtaining desired shape or contour in the product to be machined. There was no need of customized electrodes in electric discharge milling as compared to sinking EDM. Layer by layer milling was performed by the tool electrode to obtain the 3-D geometry of the part by the repetitive sparks at the desired controlled programmed path (Ji et al. 2011). The feed rate was controlled by the discharge status of the sparks at the inter electrode gap as shown in Figure 1.8.

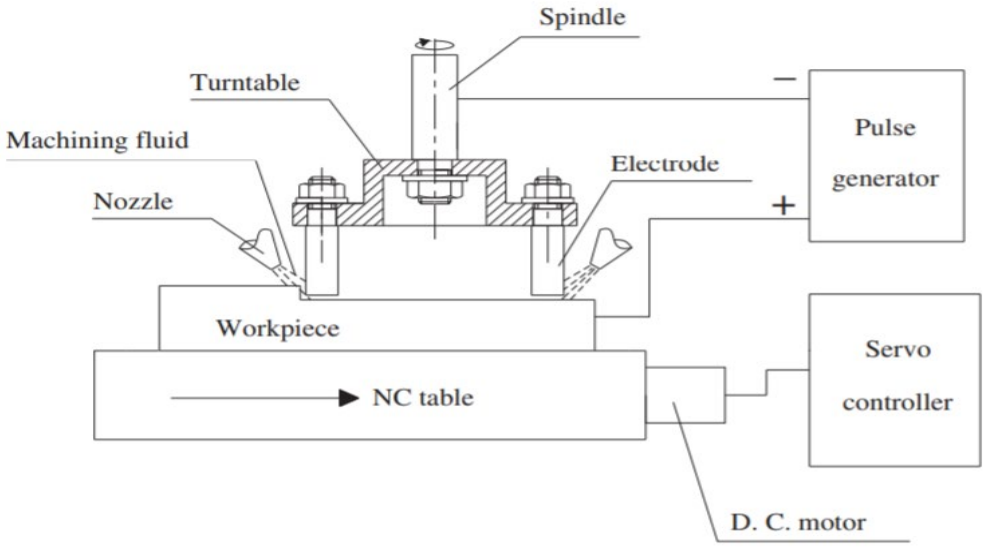

Figure 1.8 Electric discharge milling (Ji et al. 2011)

1.8.5 Electric discharge grinding

The principle of electric discharge grinding is same as that of EDM, but the tool is a rotating wheel made of conductive material (electrical) as shown in Figure 1.9 (Wang et al. 2020). The tool (cathode) and the workpiece were both immersed partially in the dielectric oil. The flow of the dielectric oil at the IEG (inter electrode gap) was regulated by the rotating motion of the tool wheel. Unlike conventional grinding, there was no physical contact between the tool wheel and the workpiece, therefore fragile parts can be machined as well. Electrical discharge grinding is also considered to be economical compared to the conventional diamond grinding.

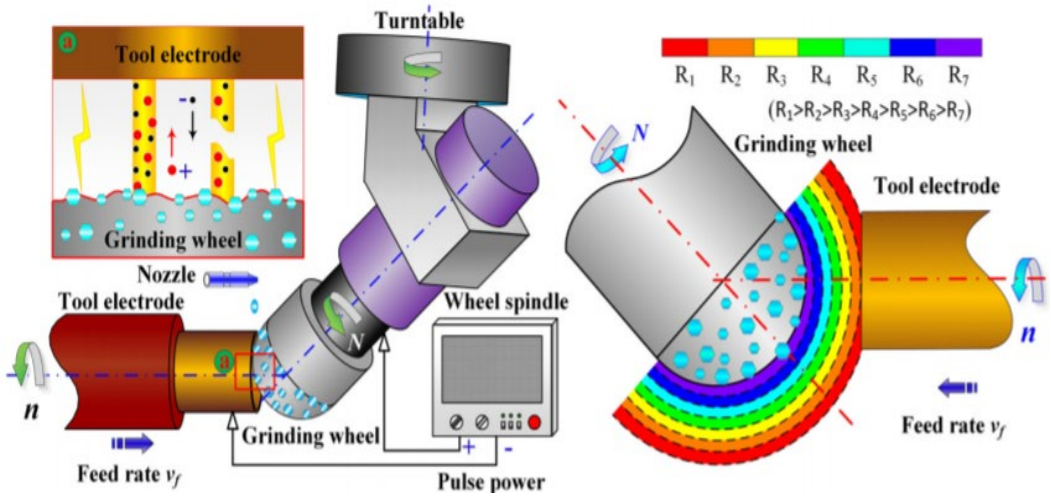

Figure 1.9 Electric discharge grinding (Wang et al. 2020)

1.9 Hybridizations in Electric Discharge Machining Process

There was also requirement of EDM hybridization so that, the cost of operator and adverse environmental effects produced by toxic EDM oil could be reduced. In this present work, an effort has been made to integrate the non-conventional EDM process with near dry dielectric medium and powder additives for better electrical discharging and improved EDM productivity and quality.

1.9.1 Hybrid EDM Processes

The Hybridization method of machining enhances the machining rates with economic benefits. The hybridization method was advantageous in performance enhancement by utilizing the benefits of other machining techniques in order to eliminate their shortcomings or adverse effects. Integration of EDM process by different non-traditional machining method has been performed by many researchers for improved material removal and better surface quality of machined samples.

Hybrid process of machining is categorized in two classifications:

a) Processes in which all constituents processes are directly interrelated with material removal and surface finish.
b) Processes in which there is single constituent who is responsible for enhanced material erosion and surface quality while other will be responsible for only material removal rate.

Various type of hybrid EDM can be classified as:

a) Hybrid Process Of EDM In Gas Combined With Ultrasonic Vibration And AJM.
b) Wire EDM in Gas.
c) EDM by Using Water and Powder-Mixed Dielectric Fluid.
d) Near-Dry Electric Discharge Machining .
e) Laser assisted electrical discharge machining.
f) Electro- chemical discharge machining.
g) Abrasive wire electric discharge machining.
h) Magneto rheological fluid assisted electrical discharge machining.
i) Powder mixed near dry electric discharge machining.
j) Dry EDM with dielectric medium of pressurized gas.

1.9.2 Hybrid Process Of EDM In Gas Combined With Ultrasonic Vibration And AJM

Lin et al. (2016) improved the machining performance and developed hybrid EDM by integrating various mechanisms. Abrasive jet machining and ultrasonic vibration were incorporated to develop hybrid EDM as shown in Figure 1.10. The input variables and effect of dielectric medium was examined on machining performance such as material removal, electrode wear and surface finish. The morphology of the machined surface was also studied and it was proved by the experimental results that hybrid EDM could improve the efficiency of the machine with higher quality of products. There was establishment of relationship between the input process parameters and machining characteristics for analysis of the potential of this process for industrial application. Effect of ultrasonic vibration assisted EDM was also investigated (Kremer et al. 1991). Ultrasonic vibrations were imparted to the tool and the positive effects were determined. The machining characteristics of Ti-6Al-4V alloy by ultrasonic assisted vibration in EDM was studied and results confirmed that overall efficiency of the machine could be increased in terms of increased material removal, reduction of recast layer and surface roughness.

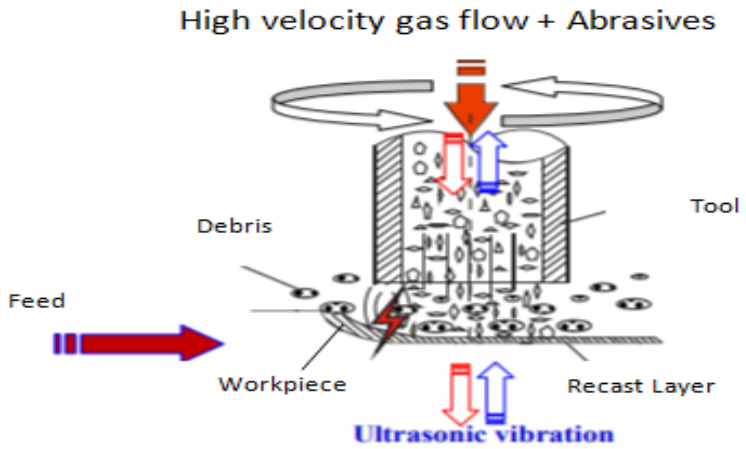

Figure 1.10 Hybrid Setup of EDM (Lin et al. 2016)

1.9.3 Wire EDM in Gas

Major cause of environmental concerns is the mineral based dielectric oil in EDM. Dry wire EDM (WEDM) utilizes gaseous medium as dielectric in place of liquid medium as shown in Figure 1.11 (Wang et al. 2003). The level of toxicity of wastes produced by normal wire EDM was undesired in industrial manufacturing. The breakdown of minerals at high temperature produced toxic fumes during machining. Secondly there were chances of fire hazards, therefore the dielectric oils are replaced by gases in emerging technology of dry wire EDM. This methodology was environmental friendly as it makes use of high pressurized gases with reduced generation of toxic gases. The high velocity gas was supplied with the help of nozzle at the machining gap between the tool and workpiece electrodes. The debris removal was facilitated by the high velocity gas and also prevents heating of wire.

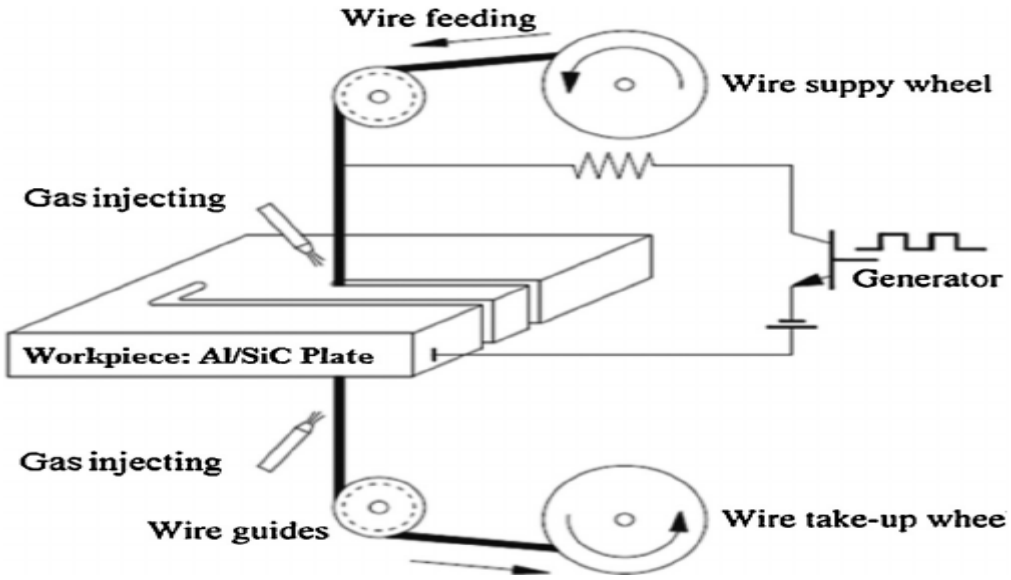

Figure 1.11 Set up of Wire EDM in gas (Wang et al. 2003)

1.9.4 EDM by Using Water and Powder-Mixed Dielectric Fluid

Metallic powders were suspended in dielectric oil to improve the machining rate of EDM (Kansal et al. 2005). The mechanism of powder mixed EDM (PMEDM) was completely different from normal EDM process. The powder particles at the machining gap increases the inter electrode gap from 25–50 to 50–150 mm when suitable voltage was supplied to the system. The powder particles get energized and behave in a zig-zag fashion as shown in Figure 1.12. These particles act as conductors when accelerated by the voltage. The particles organize themselves and behave as clusters. This cluster formation shows the phenomenon of bridging effect at the gap and causes early explosion due to which faster erosion takes place and the machining rate improves.

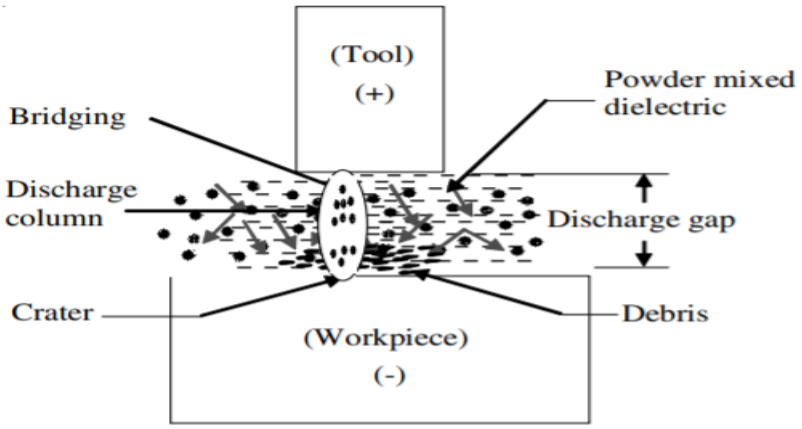

Figure 1.12 Principle of powder mixed EDM (Kansal et al. 2005)

Other factors influencing the machining were powder type, concentration and abrasive size. A small circulating system for dielectric medium was utilized in powder mixed electric discharge machining in order to avoid wastage of kerosene oil. Additionally, a stirring system was provided for avoiding the settling of powder particles. For better circulation of the powder laded dielectric medium, a micro pump was installed for proper functioning. The tank comprises of setup for pump and dielectric stirrer. Magnetic forces were used for separation of debris from the powder particles during machining and for constant re-use of powder dielectric.

1.9.5 Near-Dry Electric Discharge Machining

Very minute amount of dielectric oil was required for machining in near dry electric discharge method as shown in Figure 1.13 (Shen et al. 2016). Near dry EDM was developed as an alternative for flooded EDM, as there was reduced requirement of metal working fluids. The dielectric mixture of EDM oil and compressed air was supplied in the form of mist or aerosols to the machining gap. Atomisation results in generation of aerosols by the conversion of liquid form to spray form or by supplying liquid from the nozzle. Apparatus such as airbrush, carburettor, spray bottles and misters are some examples of atomisers. This application of droplets as metal working fluids for material removal in dry form is known as near dry electric discharge machining.

Both dry and near dry EDM are environmental friendly processes (Skrabalak et al. 2013). The dielectric medium (mist) was supplied through tubular hollow electrodes and does not possess health hazards to the operators. First research paper on dry EDM was published by NASA in 1985 and paved way for further prospective related to this type of machining. Dry EDM drilling was considered a possibility for drilling holes in samples using argon and helium gas.

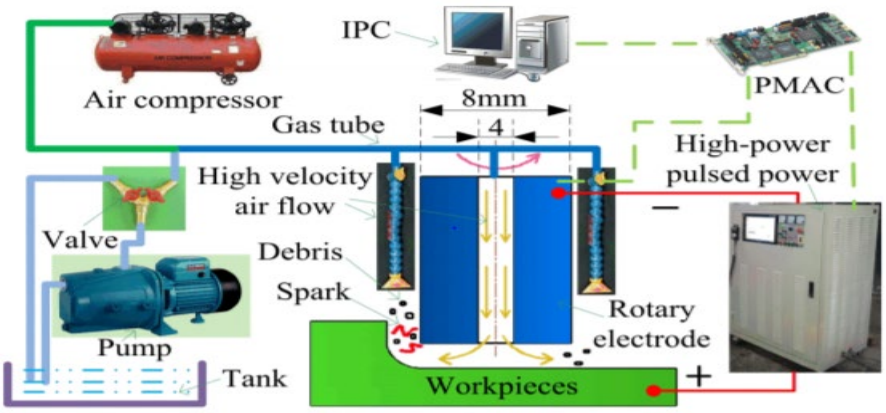

Figure 1.13 Schematic Diagram of NEAR DRY EDM setup (Shen et al. 2016)

1.9.6 Laser assisted electrical discharge machining

Laser assisted EDM is a layer by layer material removal mechanism from the surface of the product by the laser focussed high temperature beam (Vignesh and Ramanujan, 2020). The beam of heat vaporizes the material from the surface and gets flushed by the dielectric gases of liquids. Laser machining has been proven to be very efficient in machining at micro level with improved rate of accuracy, flexibility and its capability to machine any type of surface. The material removal rate by laser machining was high but the surface finish was not good. So, hybridization was performed for laser machining and micro drilling. By this technique the results obtained for material removal arte and surface finish were very satisfactory.

1.9.7 Electro- chemical discharge machining

The setup of Electro- chemical discharge machining consists of electrodes (tool and workpiece) immersed in electrolytic solution with an auxiliary anode (Singh and Dvivedi, 2016). Electro-chemical discharge machining is the combination of electro chemical machining and electric discharge machining. Its small size and simplicity in setup makes it suitable for micro-machining. Electro-chemical discharge machining process is shown in Figure 1.14. It has been found to be efficient in machining and micro drilling. It is considered as advantageous in fabrication of micro scale levels such as microwaves, micro-holes, micro channels and 3-D intricate shapes. Other advantages of this machining method are that it can machine electrically no conductive materials, thereby eliminating the drawback of traditional EDM process.

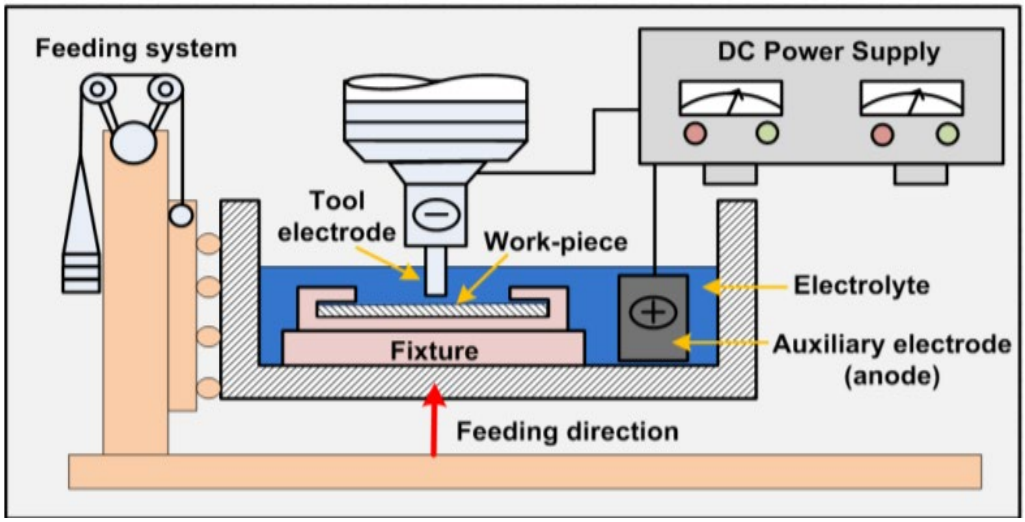

Figure 1.14 Electro- chemical discharge machining (Singh and Dvivedi 2016)

1.9.8 Abrasive wire electric discharge machining

Abrasive wire electric discharge machining (AWEDM) was performed with diamond abrasives (Menzies and Koshy, 2008). It was observed that material removal was increased with enhanced surface quality and the heat affected zone, recast layer decreased by AWEDM. There was a combine effect of electrical erosion and abrasion in abrasive wire electric discharge machining. The schematic illustration for abrasion in abrasive wire electric discharge machining is given in Figure 1.15. In this setup, abrasive laden wire was used in place of plain wire. The abrasives abrade the surface along with the repetitive discharges between the wire and the workpiece due to which the machining efficiency was enhanced. In simple wire EDM, there was a phenomenon of recast layer due to rapid heating and solidification which results in lower surface finish. These embedded abrasive eliminates this drawback of wire EDM by removing the recast layer from the machined surface which results in increased surface finish with higher material removal rate.

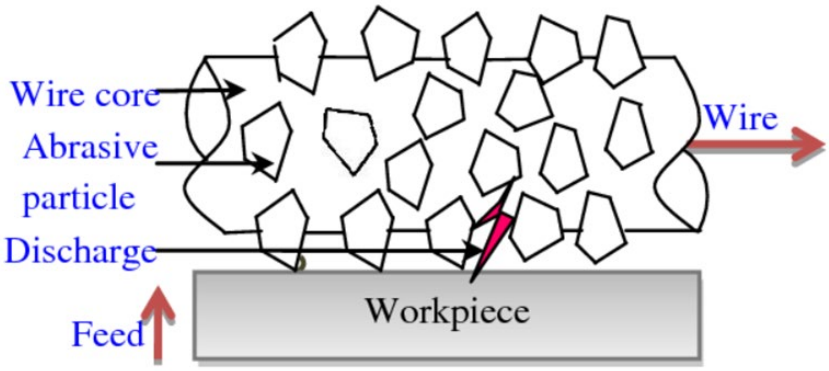

Figure 1.15 Abrasive wire electric discharge machining (Menzies and Koshy, 2008)

1.9.9 Magneto rheological fluid assisted electrical discharge machining

Magneto rheological fluid assisted electrical discharge machining makes use of rheological fluid instead of conventional EDM oils as shown in Figure 1.16 (Upadhyay et al. 2017). The polishing effect and the material removal rate were improved due to viscoelastic nature of rheological fluid. The magnetic field can modify the viscosity of the fluid which gives an additional advantage in providing the mirror like surface finish of the machined samples with improved machining rate.

Figure 1.16 Magneto rheological fluid assisted electrical discharge machining setup (Upadhyay et al. 2017)

1.9.10 Powder mixed near dry electric discharge machining

Powder mixed near dry EDM utilizes heterogenous mixture of dielectric medium in EDM process as shown in Figure 1.17 (Bai et al. 2012, a). Effect of powder additives in dielectric medium was also studied for performance enhancement (Kansal et al. 2005). In this hybridization, the dielectric oil was replaced by mixture of metallic powder along with EDM oil and compressed air. In Powder mixed near dry electric discharge machining, there was a reduction of the dielectric medium insulating strength between a tool and workpiece electrodes with the addition of liquid and conductive metallic powder to compressed air. This resulted in improved de-ionization effect and discharging conditions. Material removal was increased by the improved discharge frequency. The electric field strength of the dielectric medium was changed by the solid and liquid mixture and thus facilitates the discharge initiation (Bai et al. 2012, b). There was a phenomenon of sufficient heat dissipation due to enlarged gap at the machining gap, which results in more molten materials ejection by the explosive force by the gasification of solid and liquid phases. Cluster formation of metallic powder increases the conductivity at the machining gap which increases plasma intensity and results in more erosion.

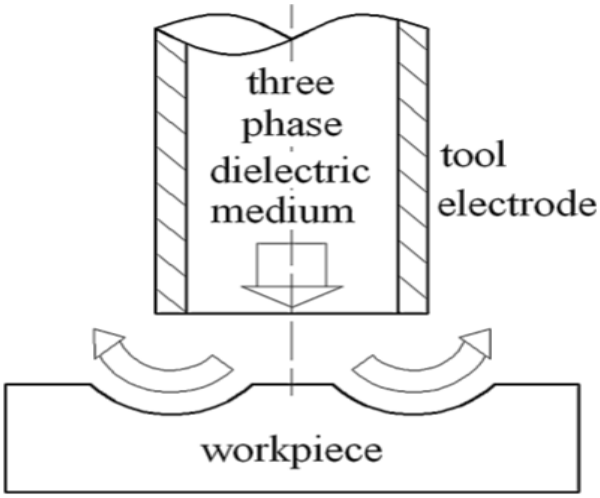

Figure 1.17 Powder mixed near dry electric discharge machining (Bai et al. 2012, a)

1.9.11 Dry EDM with dielectric medium of pressurized gas

Skrabalak et al. (2013) performed research in electro discharge machining with compressed air as dielectric medium as shown in Figure1.18 (a). This "green" technology uses pressurized gas as a dielectric medium instead of liquid oil or mineral based oil. This method of machining proved advantageous in terms of machining performance such as lower residual stress, reduced tool wear and high precision in machined samples. There could be numerous advantages to operator and end users in practical applications. The simplicity of the machine was an important factor because there was no requirement of dielectric circulation and cooling system. This led to the reduction cost of the overall manufacturing involved in the EDM dielectric supply setup.

The risk related to fire hazards were reduced by the absence of oils (flammable). Although Dry EDM was a promising method but still there was need of further research in this field before it could be used in large scale industry. Taking into consideration of benefits of Dry EDM as shown in Figure 1.18 (b), research centres and companies are working towards reduction of dielectric fluids by replacing them with water solutions of low concentration.

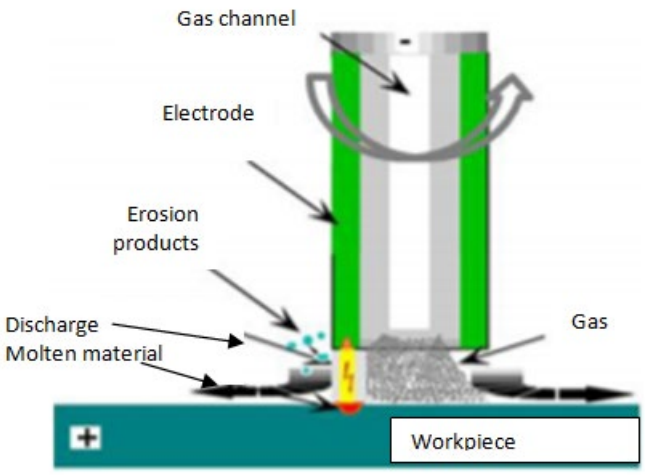

Figure 1.18 (a) Dry EDM with pressurized gas (Skrabalak et al. 2010).

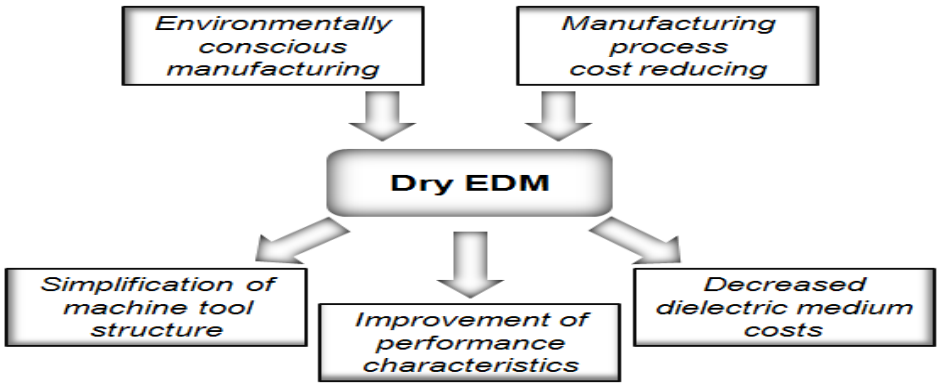

Figure 1.18 (b) Benefits of Dry EDM gas (Skrabalak et al. 2010).

1.10 Motivation for this research work

Due to economical, ecological and occupational pressure, the manufacturing industries are finding new methods to reduce the machining lubricants for cutting operations. MWF have the main side effects on respiratory and skin problems of the operators. Earlier this risk was limited to occupational operators, however these problems became airborne and there was formation aerosols from the MWF. There was health threat to 1.2 million operators who were exposed to these MWFs due to their toxic nature (National Institute of Occupational, Safety and Health, 1983). There were numerous risks associated with these aerosols and it's widespread. Therefore, it became important to find an alternative sustainable method so that the use of MWFs could be minimized in machining operations. Additionally, it was also important to determine optimum parametric cutting conditions in EDM and also maintaining accuracy of the machined samples with superior surface finish to achieve ecological benefits (Figure 1.19). Besides, there was high cost involved for EDM in

acquisition of MWFs along with its care and disposable. Although EDM have been globally accepted in the manufacturing industries but un-desirable characteristics such as low material removal rate, pores, cracks, surface pits and holes in the machined components makes this process quite inferior in terms of surface morphology, which needs to be improved through hybridization.

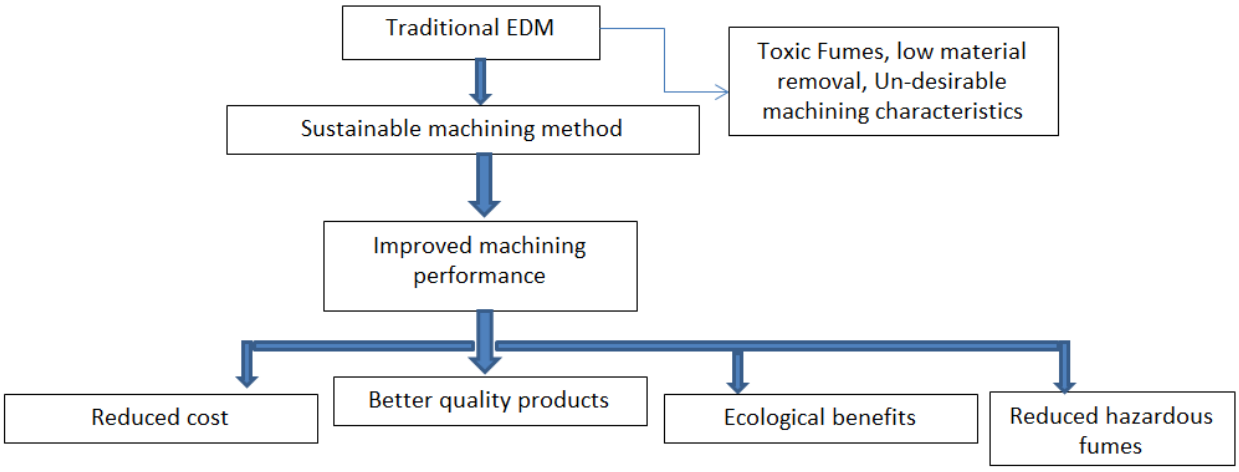

Figure 1.19 Purpose of the research study

Summary

a) Electric Discharge Machining (EDM) process is a non-conventional machining process with improved capabilities to finish those areas of a product which are inaccessible by any other traditional machining method.
b) This technology has got acceptance in many manufacturing sectors as electric discharge machining has been used widely for machining variety of products.
c) Low material removal in EDM and other defects in machined products is a limitation in existing EDM processes.
d) Near dry machining has been beneficial economically and ecologically, has immense scope for future studies related to EDM.
e) Concept of hybridization was implemented with EDM in order to improve the machining characteristics along with better economic capacities due to reduced amount of operator time and money.

This chapter deals with review of the literature study conducted by researchers in field of EDM and its hybrid forms. Several studies have been conducted related to surface finish, material removal rate, tool wear rate, micro-hardness and residual stress.

The complex geometries to be machined in hard materials was time taking process in the modern metal working industry which eventually increases the cost of machining and also results in operator health hazards. These hard to machine materials pose a challenge for operators and therefore EDM technology has been explored and enhanced day to day for better machining characteristics. In today's world EDM has replaced many conventional method of machining due to its capability of machining very hard materials with better surface characteristics. Researchers have worked extensively for improving this process by hybridization.

2.1 The three basic major areas in EDM can be classified as given below:

a) Experimental Research: There were various parameters which can affect the EDM performance such as dielectric oil pressure, flow rate, media concentration (powder particles), grain size, viscosity thermal conductivity and physical as well as chemical properties of tool and workpiece electrodes. In this present research, the effect of dielectric medium on material removal rate, micro-hardness, surface finish, residual stress and tool wear rate was analyzed and later optimization of process parameters was performed to get the desired results objective.

b) Evolution of Hybrid forms of EDM Process: In order to improve the effectiveness of the EDM process, an effort has been made to hybridize the machining method by utilizing other traditional methods of EDM.

c) Analytical Research: This section includes modeling of process parameters (Pulse On, Pulse Off, gap voltage etc.) for better process control.

2.2 Literature Review

Erden and Bilgin (1981) studied the effect of different additives or impurities in dielectric medium on MRR in EDM. It was revealed that artificial impurities enhance the MRR as these impurities improve the breakdown characteristics of the dielectric medium.

Jilani and Pandey (1982) prepared thermal model for EDM process to predict MRR by analysing the crater that each spark generates over the workpiece electrode. It was assumed in their study that the

geometry of the crater produced was of circular paraboloid nature and empirical relations were used to determine the diameter of the crater on the surface of the workpiece.

Tanimura et al. (1989) explored near dry machining (NDM) which can be performed in electric discharge machining which eventually led to new method of machining known as near dry EDM. Further investigations were performed on dielectric mixtures of mist with gases such as argon and nitrogen. This method of machining eliminated problems like improper flushing and debris attachment. At the same time this technology also led to reduction of harmful gases that are evolved while machining which made it an eco-friendly process. MRR gets increased with quality machined products with higher accuracy.

Merdan and Arnell (1991) stated that extreme temperature differences were developed on the surface of the machined samples due to high thermal sparking at the inter-electrode gap in EDM. Therefore rapid cooling leads to high residual stresses in the EDM'ed surfaces.

Ogata (1991) applied semi-empirical approach for the study of the nature of residual stress variation in the machined workpiece by EDM. It was revealed that residual stress increase from the top surface of the workpiece and reaches maximum limit up to some depth which was near to ultimate tensile strength of the workpiece. Afterwards, the stresses decrease to the minimum value and become compressive in nature.

Kunieda and Yoshida (1997) stated that although Dry-EDM eliminates requirement of bulk quantity of oil and toxic fumes but debris deposition becomes a main concern which consequently leads to lower MRR and also deteriorates the accuracy of the machined surfaces. They performed EDM in gas and it was ruled out that the tool wear rate (TWR) was negligible by this method of machining.

Wong et al. (1998) noted that some powders, such as graphite and silicon when mixed with dielectric in EDM, the distribution of spark at the discharge gap led to the creation of very fine glossy surfaces. The MRR increases and tool wear rate (TWR) decreases with the proper addition of metallic powders to the dielectric fluid.

Kruth and Bleys (2000) measured residual stress by using deflection method for removing influential stressed layer over the machined surface by wire EDM. An expression was deduced which gives a relationship between the curvature and the residual stress.

Chow et al. (2000) utilized SiC and Al powder in dielectric oil in EDM process. It was observed that addition of metallic powder resulted in increase of working gap between tool and workpiece. Due to

enlarged gap elucidate discrete sparks are generated and results in easy removal of material from the workpiece and also generates higher surface finish.

Tzeng and Lee (2001) stated that reason for achievement of uniform and smooth concave surface over the machined surface in powder mixed EDM. Molten material at the machining gap is not heavily pressed by the plasma and gas bubble, which reduces the entrapping of gas in the cavities. While presence of excessive powder particles results in over clustering of particles, which leads to short circuit due to which improper discharging takes place and surface roughness also increases.

Yadav et al. (2002) performed finite element analysis along with mathematical modeling for analysis of residual stress generated in the workpiece by EDM. It was stated that a part of the workpiece material near the spark expands more significantly due to higher temperature rise and results in a higher value of residual stresses because of the restraint effect produced by the material that expands less. The research was conducted on the mechanism of formation and distribution of residual stresses in EDM machined products by using molecular dynamics simulation technique. Maximum stress gradients were found near the melting region and the solid region connecting the melting area over the machined sample.

Zhao et al. (2002) illustrated that powder additives in powder mixed EDM (PM-EDM) reduces the insulating strength of the dielectric fluid as a result short circuit at the inter electrode gap (IEG) takes place due to which series discharge occurs and results in faster erosion. Metallic powder modifies the plasma channel between the electrodes and the sparking gets uniformly distributed. Consequently shallow craters are formed over the machined surface which produces machined parts with higher surface finish. The morphology of the machined components by powder additive EDM (PM-EDM) and capabilities of EDM was improved in terms of increased micro-hardness by powder additives.

Kunieda et al. (2003) studied the surface topography of machined surfaces using different gases as dielectric medium and it was revealed that large craters were formed on oxygen EDM'ed surfaces rather that argon gas EDM'ed surfaces due to exothermic reaction leading to oxidation and hence higher MRR.

Schulze et al. (2004) developed a model considering discharge voltage and discharge current as sole process parameters for prediction of the amount of heat transfer occurring from the tool and material removal per discharge in EDM. This same model had predicted the extent of thermally effected zone though finite element analysis.

Wu et al. (2005) introduced aluminium powder in the dielectric medium in EDM process and observed that by addition of metallic powder improves the heat distribution effect at the machining gap and surface finish was increased by 60% when the aluminium powder concentration was kept at 0.1gm/l.

Fong and Chen (2005) studied the effect of various metallic powder suspended dielectric oil on surface characteristics of machined SKD-11 material by EDM process. It was observed by them experimentally that metallic powder size plays a very crucial role in determining the surface finish of the machined part in powder mixed EDM (PMEDM) process. It was observed that smallest size of the powder particle (70nm- 80nm) generates higher surface finish while greater powder particles resulted in less improvement of surface finish. They also performed comparative study for surface roughness by using different metallic powders such as aluminium (Al), copper (Cu), chromium (Cr) and silicon carbide (SiC). Aluminium powder generated the best surface finish amongst the other metallic powders.

Kansal et al. (2005) studied phenomenon of metallic powder in EDM. It was stated dispersion of metallic powder in dielectric EDM oil results in reducing insulating strength and hence more energized and stable plasma is obtained at the machining gap which generates finer machined surfaces with higher MRR.

Murali and Yeo (2005) compared simulated residual stresses with experimental values of residual stress obtained by atomic force microscopy and nano-indentation technique in EDM. The stress value measure by nano-indentation was found to be 300 MPa at the spark eroded surfaces.

Marafona and Chousal (2006) utilized conversion of energy from one form to another (i.e. from electrical to thermal) to prepare model for predicting the temperature distribution within the plasma channel in EDM. Plasma channel as a semi-infinite cylindrical shape was utilized to make another electro-thermal model with disk shaped heat input with a consideration that equal amount of heat is distributed within the tool and workpiece.

Astakhov (2006) illustrated, near dry machining led to increase in tool life as compared to shorter tool life in dry machining or machining with dielectric in complete gaseous form without liquid aerosols. Near dry machining was proved advantageous in terms of good characteristics of product developed such as high quality of machined product which was quite economically produced. At the same time it led to reduction in harmful fumes evolved while machining.

Li et al. (2006) conducted experimental study for EDM in other gases as dielectric medium and it was concluded that oxygen gas as a dielectric medium yielded maximum MRR as compared to other gases due to its lower ionization energy.

Ekmekci et al. (2007) conducted study for peak value of residual stress in EDM and it was observed experimentally that the maximum value of these stresses are generated at depth of 40μm from the top surface of the workpiece and becomes negligible at depth of 200μm. The maximum value for the generated residual stress by EDM in workpiece was near the ultimate strength of the work material.

Kao et al. (2007) stated several advantages of ND-EDM, broad variety of liquids and gases could be used in order to change the liquid concentration in gas. Therefore dielectric properties could be tailored to meet different machining needs such as higher MRR enhanced surface finish and low tool wear rate. This also eliminates the bulk amount of EDM oil required unlike traditional EDM.

Yeo et al. (2008) reported that thermal erosion modeling process in EDM can be categorized into three parts- plasma channel, erosion of workpiece and erosion of tool. It was reported that the plasma channel expands in a cylindrical pattern as the duration of arc formation increases with time.

Kansal et al. (2008) stated that provision of metallic powder particles in dielectric medium reduces the dielectric strength in EDM. This further helps in uniform distribution of plasma heat in all directions. This resulted in the formation of stable arc and hence an increase in MRR.

Tao et al. (2008) stated that ND-EDM was eco-friendly as it utilizes very minute amount of oil therefore the fumes produced are lesser toxic in nature. Mirror like finish was achieved on machined surface by ND-EDM and the taper in the holes was considerably lower. The discharges in ND-EDM were easier to initiate and stable machining was achieved due to liquid phase presence in gaseous environment. This phase changes the electric field and also creates a large gap distance between the workpiece and tool electrodes. They also illustrated that MRR increases with increase in gas pressure because highly pressurised gas at high speed improves the cooling effect and better removal of debris takes place from the eroded surface of the machined workpiece.

Tan et al. (2008) suspended nano-powders of SiC and Al_2O_3 in μ-EDM processes in order to reduce the surface roughness by 14-24% in an average.

Gao et al. (2009) brought into feasibility of PMND-EDM and stated its benefits in terms of machining.

El-Hofy and Youssef (2009) stated that hydrocarbon oil is generally used as dielectric oil in EDM.

This EDM oil is a main source of aerosols, toxic fumes which can cause fire hazards.

Kung et al. (2009) conducted research in the field of EDM for performance enhancement characteristics such as improved material removal rate and better surface finish. Research on machining efficiency of PMND-EDM was done for the different material combination of tool and workpiece electrodes. It was illustrated that that brass tool electrode and W18Cr4V workpiece gain higher MRR.

Jahan et al. (2010), Bhattacharya et al. (2013) illustrated that metallic powder particles in dielectric fluid of EDM increases the electrical conductivity between the electrodes which increases the sparking frequency and also facilitates easy removal of debris from the machined surface.

Singh et al. (2011,b) performed FEM modeling for ultrasonic vibration assisted EDM and it was proven that ultrasonic vibration improve the debris flushing phenomenon and prevents the debris piling up in the machined area, thus preventing abnormal discharges

Singh (2012) used mathematical equations in EDM for modeling of shape of crater produced by erosion over the machined surface or depth of crater and heat distribution pattern.

Singh and Yeh (2012) explained that lighter and small powder particles produce superior surface quality and gives higher MRR in PM-EDM.

Kumar and Batra (2012) modified the die steel surface by tungsten powder additives in the dielectric medium of EDM. The surface morphology was improved by addition of metallic powder as there was carbon deposition at the top surface, which also increased the micro-hardness by 100%.

Mai et al. (2012) explained that in PM-EDM, the powder particles with comparatively lower density can balance themselves more uniformly against the surface forces due to which the particles are distributed evenly in the dielectric medium as compared to the same material particles of larger grain size.

Bai et al. (2012, a) proposed hybrid technique of powder mixed near-dry EDM (PMND-EDM) which combined the advantages of ND-EDM and PM-EDM in order enhances the machining performance characteristics. Research was performed on different combination of tool and workpiece electrodes in PMND-EDM to study effects of different process parameters on MRR. Gas –liquid- powder mixture of three phases was used in PMND-EDM for material removal process and it was revealed that MRR was much higher as compared to other EDM methods of

machining. They further improved PMND-EDM technology and enhanced the material removal rates and surface finish.

Bai et al. (2013 b, 2013 c) explained thermal phenomenon in powder mixed near-dry EDM and the tendency of variation in MRR was analyzed by varying each process parameter. It was proven that the plasma channel was much more stable in powder mixed EDM than the plasma formed in pure kerosene oil because the plasma generated in PMEDM was compressed by the electric bridge of conductive powder particles in EDM oil.

Yang et al. (2013) studied the nature of residual stresses in EDM of machined samples and it was illustrated that cracks are easy to be generated on the surface due to which the residual stresses were tensile in nature over the surface of the electrode while compressive in nature inside the electrode.

Kalajahi et al. (2013) investigated experimental and finite element analysis of EDM process for MRR by using response surface methodology. The model was prepared for single spark and mode of heat transfer was conduction while the workpiece was assumed to be stress free and homogenous in nature. Heat distribution at the cathode (workpiece) was predicted by applying Gaussian heat distribution method, and was analyzed to calculate the MRR. They utilized axisymmetric model and considered Fourier heat conduction equation for analysis.

Boopathi and Sivakumar (2013) utilized Taguchi L_{18} mixed orthogonal array (OA) to study the impact of process parameters in ND-EDM on output response such as MRR and Ra. Analysis of variance was performed to identify the most significant process parameters.

Liqing and Yingjie (2013) performed additional experiments based on previously mentioned advantages of dry EDM, with mixture of oxygen and other gases too in order to enhance the dry machining.

Jabbaripour et al. (2013) observed that shallow craters were formed over the machined surface due to decrease in discharge density by the removal of large amount of heat energy by the conductive powder in PM-EDM.

Prabhu et al. (2013), Prabhu and Vinayagam (2013) observed that mixing of carbon nanotubes tubes (CNTs) in the dielectric in PM-EDM, leads to higher thermal conductivity and also helps in the uniform distribution of discharge energy over the large surface area.

Prihandana et al. (2014) illustrated that beyond a certain limit over concentration leads to over clustering of powder particles in PM-EDM, resulting in arcing and therefore produces poor surface finish and low MRR.

Zain et al. (2014) improved the micro-hardness of stainless steel through powder mixed electric discharge machining and titanium carbide powder in dielectric oil was utilized to enhance the surface properties of stainless steel. It was illustrated that Vickers hardness value of 1200 was achieved over the machined surface by using titanium carbide powder (TaC) with the concentration of 25 g l^{-1} in kerosene oil.

Goyal and Singh (2014) conducted parametric study for PM-EDM in order to optimize the MRR and surface roughness. Experiments were conducted by utilizing Taguchi L_9 (OA) and keeping metallic powder concentration as one of the process parameters. It was observed that the grain size of powder and powder concentration has a great impact on MRR and surface finish.

Singh et al. (2014- 2016) used tungsten powder in EDM to machine AA6061/10%SiC composite and this additive resulted in increment of MRR by 48.43% and decrement of TWR by 51.12% due to stable and uniform discharges while surface defects such as crater size and deposits of recast were reduced due to decrease in insulating strength of the dielectric.

Singh and Singh (2014) utilized response surface methodology (RSM) for optimization in PM-EDM and effect of process parameters on MRR and tool wear rate (TWR) was studied. Powder concentration along with other parameters such as peak current, voltage, pulse-on time and duty cycle had a significant effect on MRR and TWR.

Dhakar et al. (2014) performed optimization of process parameters for comparative study between dry EDM (DEDM) and near dry EDM (ND-EDM) and it was revealed that NDEDM leads to higher MRR while DEDM leads to reduced TWR and tool electrode material played important role in determining MRR, TWR and surface finish (Ra).

Dhakar and Dvivedi (2015) observed better surface finish and lesser recast layer in machined products by ND-EDM as compared to conventional EDM.

Razak et al. (2015) used silicon powder as an additive along with dielectric oil in EDM to study MRR, Ra, and TWR by using RSM. PM-EDM leads to a reduction in machining time because the insulating strength of the dielectric gets reduced due to powder additives which result in rapid erosion. Analysis of MRR and electrode wear ratio (EWR) in PM-EDM was also studied by using

response surface methodology and it was revealed that MRR continues to increase with an increase in powder concentration up to a certain limit and after that, it tends to decrease.

Pattabhiraman et al. (2015) illustrated that higher material removal can be generated by spray EDM as compared to dry EDM and wet EDM for all possible combinations of discharge parameters. The spray-EDM technique reduces the percentage of debris particles which leads to better surface finish and also atomizes dielectric, reducing the tool wear rate as compared to dry and wet EDM. The experimental result obtained value of surface roughness of 2.66 μm.

Shen et al. (2015) made use of gases such as nitrogen or air as a dielectric medium instead of dielectric oil were used in Dry EDM which makes processing eco-friendly as this new methodology produces less harmful fumes and at the same time also eliminates the need of EDM oil. They conducted experiments in a high speed near-dry EDM of Ti6Al4V and achieved MRR of 648.22 mm^3/min. Increase of air flow rate, peak voltage of EDM, and electrode rotation speed, led to increase in surface finish (Ra).

Tlili et al. (2015) investigated MRR in EDM and simulation was performed by taking more realistic values and assumptions in order to predict the shape of the crater cavity. The study involved heat distribution factor of 0.18. Results were validated by making comparison with the experimental results but still concrete results were lacking as the effect of convection heat transfer was neglected due to which precise values for MRR were not obtained successfully.

Liu and Guo (2016, a) performed finite element modeling to simulate the EDM process by developing Gaussian heat flux model in order to predict heat distribution. A heat distribution factor of 0.42 was considered in the research but still this study had limitations, as the phase transformation effect was not taken into consideration and therefore the results obtained were not very precise.

Liu and Guo (2016, b) used finite element method for modeling of residual stresses in the workpiece machined by EDM. It was revealed by the study that the value of residual stresses at the subsurface of the workpiece was more than the top surface due to high surface roughness over the top surface and low discharge energy of the sparks was attributed to lower values of the residual stresses. The research on the prediction of residual stress in micro EDM by using finite element method was performed. A mathematical model was developed based on Gaussian distribution heat source. This approach for simulation was adopted because this was more near to real life situation.

Gill and Kumar (2016) utilized Cu-Mn tool made by powder metallurgy for machining die steel (H-11) by EDM process utilizing Taguchi technique. The micro-hardness was increased by 93.7 % for the machined samples under optimum experimental conditions. Evaluation for micro-hardness was carried out by using different powder metallurgy tools (Cu and Mn). There was improvement in micro-hardness by 93.7% by formation of cementite, ferrite and manganese carbide phases in the machined workpiece samples by utilizing composite tool. Under optimum process parameters conditions, the surface finish of 3.11 μm was obtained.

Kumar et al. (2016) investigated performance index in ultrasonic assisted EDM process by using graph theory and matrix approach. Theoretical and experimental investigations were performed in order to study the effect of additives such as metallic powder in dielectric fluid in EDM process. Role of influential factors such as flushing, cavitation's, abnormal discharge, dimensional accuracy, and surface morphology was studied on performance index of EDM. It was revealed that cavitation has a critical contribution in the EDM process and vibration assisted hybrid EDM shows high-performance index in terms of high dimensional accuracy and surface morphology as compared to customary EDM.

Rao et al. (2016) minimized the residual stress induced in the EDM'ed samples by optimization of process parameters by Taguchi methodology and it was stated that these stresses induced are very much dependent upon mechanical properties of the workpiece and the EDM process parameters.

Shabgard et al. (2016) applied finite element for analysis of residual stresses in vibration assisted EDM. Techniques like nano-indentation technique and Raman spectroscopy were adopted to measure the residual stress in AISI H13 tool steel machined by EDM process. X-ray cos α principle was utilized for residual stress analysis in vibration assisted EDM and it was revealed that micro-cracks were responsible for relieving some part of residual stress.

Lin et al. (2016) stated that the surface roughness (SR) obtained on machined parts by oxygen assisted D-EDM was very high due to the fact that oxygen assisted EDM resulted in high MRR which means that the craters produced over the surface of the machined workpiece will be deeper and wider which results in poor surface finish. While surface roughness was least in argon assisted DEDM because the MRR was also very low.

Wang et al. (2016) analysed the plasma channel characteristics in PM-EDM. It was proved that the plasma channel was much more stable in PM-EDM than the plasma formed in pure kerosene oil

because the plasma generated in PM-EDM was compressed by the electric bridge of conductive powder particles in EDM oil.

Singh and Sharma (2016) conducted research with different dielectrics on environmental and hazard and operability (HAZOP) analysis in PM-EDM, concluding that HAZOP analysis successfully reduced the wastage of dielectric, and minimized the machining cost and environmental hazards as compared to traditional EDM machining methods.

Dhakar et al. (2016) stated that ND-EDM was an environmentally friendly process with negligible tool wear rate (TWR) in comparison to other dielectric mediums.

Rana et al. (2016) performed parametric optimization of hybrid EDM process and the effect of a hybrid tool on erosion rate was studied. It was validated that tool with a material combination of copper and abrasive ceramic material enhanced the erosion rate thereby reducing the machining time required for removing the same volume of material by traditional EDM.

Zhao et al. (2016) utilized simple concept of joule heating for a heat transfer analysis of a single discharge in powder mixed EDM. They proposed that heat flux received by workpiece was solely depended upon the values of current, voltage and spark radius.

Li et al. (2016) illustrated that there was improvement in the EDM performance on machiningTi-6Al-4V by dispersing SiC particles (abrasives) in dielectric medium with magnetic stirring mechanism. The authors successfully achieved improved micro-hardness of the specimen surface due to formation of TiC and $TiSi_2$.

Marashi et al. (2016) produced high quality surfaces in PM-EDM of the machined components in comparison to other conventional EDM method.

Talla (2016, a) utilized graphite powder mixed dielectric to improve machining performance on Inconel 625. It was illustrated that, the tensile stress produced in machined parts by PM-EDM was comparatively lower as compared to that of conventional EDM, because addition of impurities (powder additives) decreases the discharge energy density due to large spark gap which in return also increase the fatigue strength of the machined components. It was also observed that some of the critical characteristics of metallic powders in PMND-EDM are size, density, thermal and electrical conductivity that affects the PM-EDM process significantly.

Tripathy and Tripathy (2017, a) studied the effect of different powder concentration of graphite powder on responses such as Ra, TWR and MRR on H-11 die steel, revealing that the addition of

graphite powder at a concentration of 6g/l enhances the MRR and surface finish while tool wear rate is decreased.

Tripathy and Tripathy (2017, b) utilized Taguchi L_{27} OA (orthogonal array) for optimization of process parameters in PM-EDM and used chromium powder additive for experimentation on H-11 die steel in order to increase micro-hardness of machined surface by powder mixed EDM. Analysis of variance (ANOVA) was utilized along with empirical model for optimization and prediction of micro- hardness. It was also observed that addition of metallic powder at 6gm/l concentration resulted in tremendous improvement of surface texture of machined component due to reduced recast layer and micro cracks.

Kumar et al. (2017) improved the micro hardness of cryogenically treated aluminium alloy by 94.85% in PM-EDM. Titanium carbide powder was used to improve the surface properties of the workpieces machined by powder mixed- EDM.

Khullar et al. (2017) utilized central composite design for experimentation on AISI 5160 material for predicting MRR and Ra in EDM by using response surface methodology (RSM). ANOVA (Analysis of variation) was utilized to study the influence of control factors on response. Non- dominating sorting genetic algorithm II (NSGA- II) was utilised to solve mathematical models. It was confirmed by the validation experiments that at optimal process parameter levels, the surface finish (Ra) and MRR were 1.280 μm and 1.167 g/min respectively. While NSGA-II predicted values gave better correlation with experimental values which were 1.327 μm and 1.149 g/min respectively.

Rahul et al. (2017) performed experiments as per Taguchi L_{25} orthogonal array by varying different process parameters at five levels in EDM. The study was performed on machining of Inconel 718 and the performance of the machine was based upon several outputs such as surface roughness, material removal rate etc. It was illustrated that discharging energy can be effectively dispersed by adding conductive aluminium powder in dielectric fluid to improve the machining efficiency. Scanning electron microscopy was used to study the morphology of the machined product and it was revealed that the powder additives improved the overall ophiology of the workpiece along with high surface finish.

Amorim et al. (2017) improved the micro-hardness of AISI H13 tool steel workpiece by using molybdenum-powder mixed dielectric medium in PM-EDM process. The migration of molybdenum and carbon particles leads to formation of white layer over the machined surface in form of Fe-Mo and MoxC which was responsible for improved micro-hardness.

Opoz et al. (2018) studied the impact of SiC powder concentration on surface topography, particle deposition, and subsurface structures in the PM-EDM of Ti-6Al-4V-ELI work material, and it was observed that a high suspended particle concentration in dielectric liquid enhance the material transfer mechanism in a particulate form. Sub-surface of Ti-6Al-4V-ELI workpiece in terms of micro-hardness was improved and it was revealed that unique mechanism of material transfer was responsible for formation of solid and harder sublayers over the machined surface.

Khundrakpam et al. (2018) performed comparative study between wet EDM, ND-EDM and PMND-EDM for machining performance characteristics in terms of Ra and TWR. Their study revealed that TWR and surface roughness of machined product was lowest in PMND-EDM as compared to wet EDM and ND-EDM.

Patel et al. (2018) stated that unlike EDM, powder mixed near dry-EDM has many advantages like low consumption of dielectric oil along with metallic powders, relatively more efficiency such as increase in productivity and high surface quality and low emission of toxic effluents.

Kumar et al. (2018, a) performed machining on Inconel 825 super alloys by powder mixed EDM. Nano graphene powder was used as an additive in dielectric medium and response surface methodology was utilized to perform experiments. Further field emission scanning electron microscope study was conducted over the machined surface and it was revealed that comparatively better surface finish was achieved over the machined surface by introducing nano-graphene powder in dielectric medium.

Kumar et al. (2018,b) performed optimization of the residual stress using X-ray cos α method in vibration- assisted hybrid EDM process over high carbon high chromium D2 tool steel workpiece. They made an investigation regarding the development of residual stresses during the ultrasonic vibration assisted Wire electrical discharge machining process (W-EDM). The influence of variation in process parameters on generation of residual stresses in the workpiece had been also studied. They supplied continuous and discontinuous vibrations for enhanced performance characteristics. It was revealed by the study that discontinuous vibration resulted in reduced residual stresses induced in the machined sample.

Gill and Kumar (2018) explored several methods regarding enhancement of the micro-hardness (MH) value and surface roughness of the machined components by powder-additive EDM methodology. Efforts were made to identify favorable conditions to enhance the surface MH of EN-31 tool steel using Cu–W tool manufactured by powder metallurgy in the electrical discharge alloying (EDA) process. The Taguchi method was followed to obtain a combination of process

variables for achieving the best MH. The presence of hard tungsten carbide (W_2C) and cementite (Fe_3C) on the machined surface was related to the observed substantial increase in MH (~150%).

Sahu et al. (2018) studied the influence and concentration of Sic powder additives in dielectric medium of EDM. Surface characteristics of Inconel 718 was studied and it was found that addition of powder additives such as Sic powder results in diminishing of surface irregularities and produces superior surface finish as compared to that of conventional EDM process. They made an observation which stated that powder mixed EDM'ed machined surface was enriched more with carbon element as compared to normal EDM (without powder). This carbon enrichment further increased the micro-hardness of the machined component.

Zou et al. (2018) used nitrogen plasma jet (NPJ) as dielectric medium to increase the discharge gap in μ-EDM in order to enhance the machining and surface quality characteristics. It was stated that in comparison to other gases as dielectric medium, NPJ was most effective in increasing machining efficiency.

Chundru et al. (2019) utilized Taguchi L_{18} orthogonal array for machining and surface modification of Ti6Al4V Alloy by dispersing nano and micron-sized TiC/Cu powder particles in dielectric of EDM process. ANOVA was performed to study the impact of process parameters on surface roughness (SR). Nano particles showed the positive influence on surface finish and the range of Ra in the investigation was between 1.88-4.44 μm. The microhardness was increased upto 912 HV (Vickers hardness).

Kumar et al. (2019) examined the machinability of titanium alloy (Ti–6Al–4V) during EDM. The performance was assessed in terms of MRR and TWR. The surface integrity of the machined specimen was evaluated in the purview of surface morphology and topographical features. It was evaluated that nanoparticle high reactive surface area made better surface alloying as compared to other tool materials and has displayed positive influence on micro-hardness on the machined surface. The generated carbides over the surface increased the micro-hardness to 912 HV. It was stated that pyrolysis of the dielectric media was responsible for significant carbon migration at the machined surface. Therefore, EDM'ed specimen shows existence of carbon rich surface (carbide layer). Formation of such carbide layer results in increased micro-hardness of the specimen while compared to that of 'as-received' parent material.

Sundriyal et al. (2020 a, 2020 b) performed research related to powder mixed near dry EDM (PMND-EDM) in terms of surface roughness, material removal rate, residual stress, tool wear rate

and micro hardness and it was proved that PMND-EDM was better in terms of performance enhancement characteristics as compared to traditional EDM.

2.3 Research Gap

a) Sufficient efforts are needed to be undertaken for the improvement of Near Dry EDM process efficiency/productivity in terms of more material removal rate, reduced tool wear rate and better surface quality.
b) More efforts needed for the optimization of process parameters from the component quality point of view.
c) Literature lacks in furnishing the consistent and sufficient theory and suitable models about the process mechanism. There are confliction opinions from the various researchers regarding the effect of some of the variables on the response parameters.
d) Still there is need to develop EDM which is environmental friendly and has higher material removal rate.
e) Limitation of the traditional process to correct the form geometry is not possible with the existing processes, requiring the development of new processes.

Summary

a) It was understood from the literature review, although many experiments have been performed till date in order to understand EDM process and associated parameters, but still there is lack of information for the detailed development process model due to variety of EDM applications.
b) There was lack of study related to different types of dielectric medium and its effect on output responses such as material removal and surface characteristics of machined sample.
c) Researchers have developed different hybrid forms of EDM in order to eliminate the drawbacks of traditional EDM.
d) Hybridization of EDM processes was achieved successfully by researchers for better performance characterstics.
e) There was need to explore more variety of Hybrid EDM processes as per the ingenuity of the inventors.

This chapter includes preview of present investigation. The objectives of the present study and scope of the problem were evaluated by reviewing the literature review critically. Additionally, problem formulation was described for the lacking information pertaining to EDM process, thereafter the problems were described which needed to be solved through this present work.

3.1 Preview of present investigation

In modern manufacturing techniques, researchers are always developing highly productive machining methods. In comparison to conventional EDM, a recent trend in technology and innovation has brought in hybrid Powder Mixed Near Dry EDM.

The use of optimum metal-working fluids leads to economic benefits and improved machining efficiency. Although research related to PMND-EDM has been done previously, but it was limited to a certain scope. This research was conducted to study the effect of three phase dielectric medium on various output performances.

Hybridization of EDM process with other machining process was performed as shown in Figure 3.1, in order to overcome the limitation of existing EDM methods such as debris accumulation, recast layer and high heat effected zone. These undesired effects pose a serious problem in traditional EDM because the end products achieved have deteriorated quality value and low reliability. Additionally, lower material removal rate and consumption of large volumes of dielectric oil results in formation of toxic fumes which cause hazard to operators and environment. This motivated the authors to develop a new setup so that these undesired factors are minimized and better machined products are achieved with low economic cost.

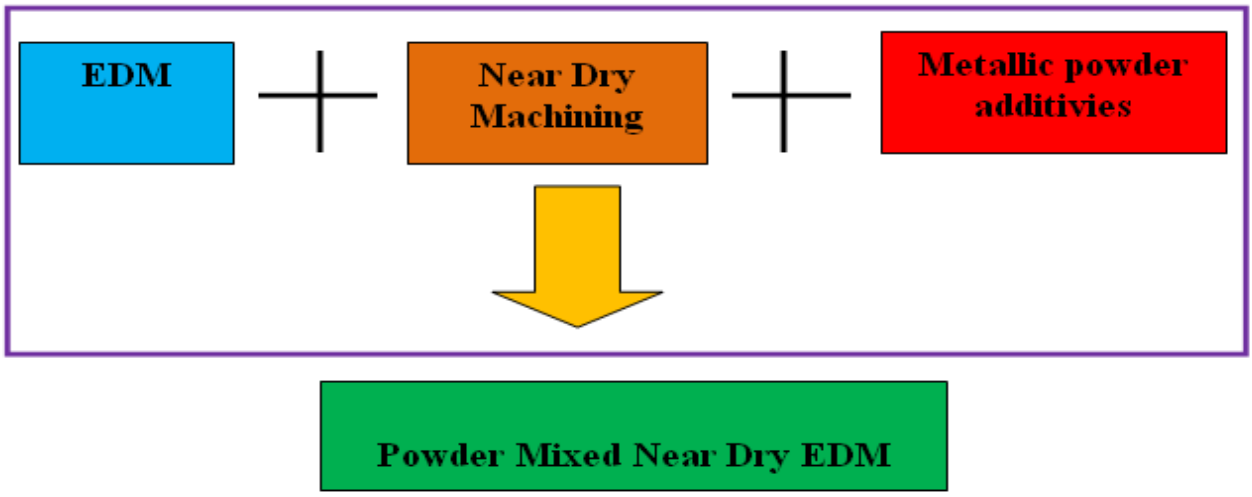

Figure 3.1 Powder Mixed Near-Dry Electric Discharge Machining

3.2 Working of Powder Mixed Near Dry EDM

Working principle of Powder Mixed Near Dry EDM is same as that of EDM but presence of metallic powder, compressed air and EDM oil in very minute amount along with glycerol as dielectric medium in PMND-EDM modifies the plasma channel or spark generation at the machining gap. The metallic powder works as an additive and helps in creating a chain-like structure of powder grain particles in the plasma channel (Kansal et al. 2005). This phenomenon reduces the insulating strength of dielectric medium and helps in rapid erosion as shown in Figure 3.2. The compressed air supplied from the compressor helps in the formation of dielectric mist and also assists in stabilizing arc at inter-electrode gap due to the increased pressure of supplied mist (Shen et al. 2015). The glycerol liquid of high viscosity was added to prevent the powder particles from settling down in the mixing chamber and thus provides a uniform concentration of powder particles in the dielectric oil. The mixture of dielectric medium (powder additives, glycerol and dielectric oil) was fed into the mixing chamber from the inlet of the tank and afterwards heterogeneous mist of dielectric mixture was supplied at IEG (Inter electrode gap or gap between the tool and the workpiece) at high pressure through hollow copper electrode tool with the help of tubes from the mixing chamber. The current was supplied to the electrodes from the powder supply of the EDM and the sparking phenomenon starts resulting in erosion process. The increased working gap due to the presence of metallic powder results in obtaining more uniformly energized plasma. The reason for an increase in working gap and energized plasma was attributed to the chain-like formation of powder particles due to interlocking of grains of powder particles at IEG which results in rapid sparking with high frequency (Bai et al 2012, a). This methodology of injecting heterogeneous mist at inter-electrode gap or working gap

was efficient in terms of machining and at the same time also led to the reduced requirement of EDM oil. The consumption rate of EDM oil in this methodology was very minute unlike in traditional EDM method where the requirement of EDM oil was in bulk quantity.

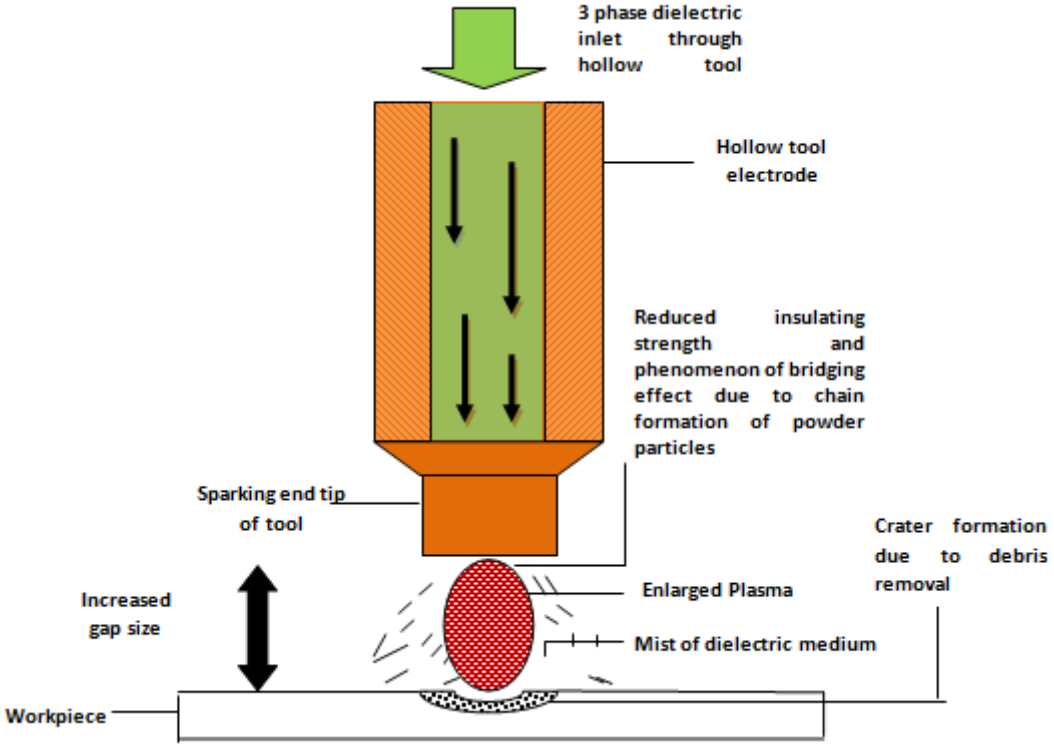

Figure 3.2 Schematic diagram of PMND-EDM

3.3 Problem Formulation

Problem formulation throws light on capabilities of the EDM and its hybrid forms and their application. By this developed technology, excellent process capabilities were achieved in terms of material removal and surface characteristics. During the literature review, following problems were observed in Electric Discharge Machining:

a) Evolution of different technique for production engineers for different challenges faced by them in manufacturing sector.

b) Improvement in existing machining process for reduced hazards to operators and environment along with reduced cost of machining.

c) The performance index in terms of material erosion and surface finish of traditional EDM was quite less as compared to Powder Mixed Near Dry EDM. The improved flushing technique can be used to obtained superior surface characteristics.

d) Consistent process control and analytical modeling for proposing the process mechanism.

e) Processing time can be reduced significantly by the process of PMND-EDM.

f) Argon and oxygen gases were used as dielectric medium with combination of different metallic powders.

3.4 OBJECTIVES

a) Design and development of the environmental friendly Powder Mixed Near Dry Electric Discharge Machining process termed as PMND-EDM which enhances material removal along with improved surface quality characteristics of work surface.

b) Experimental study of the effect of various process parameters on performance characteristics and to develop the empirical relationships between important process parameters and response characteristics.

c) Morphology and integrity study of the finished surfaces by PMND-EDM process.

d) Multi-response optimization of the process parameters of PMND-EDM process.

e) Developing suitable model for the PMND-EDM process based on soft computing techniques

3.5 Research Methodology

The methodology for the proposed research work involves the following phases.

a) The methodology begins with literature review that relates to this work for better understanding of subject and knowing state of the art
b) To identify appropriate process parameters in machining.
c) Design of experiment for synthesis of hybrid EDM with four control factors retaining three levels using Taguchi's L9 orthogonal array.
d) Synthesis of hybrid near dry EDM by powder additives technique in conjunction with different dielectric gases.
e) Microstructural, elemental, physical and mechanical characterization of developed hybrid process.
f) Depending upon characterization outcomes, parametric optimization of control factors for enhanced physical and mechanical properties

g) Investigations for surface roughness and machinability of developed machining methodology
h) Exhaustive investigation for behavior of different dielectric medium on machining characteristics.
i) Investigation related to behavior of different dielectric gases in PMND-EDM and their role in modifying the quality characteristics of the machined samples.
j) Thermo-electric modeling for performance enhancement in PMND-EDM.

Summary

a) PMND-EDM is hybridization of Electric Discharge Machining and Near Dry machining.

b) The toxic fumes evolved during machining in traditional EDM possess a serious health hazards to the operators. The operators were exposed directly to these fumes and were facing problems related to respiratory and skin diseases. Therefore sustainable machining EDM process was need of the hour, so that the toxic fumes could be reduced significantly.

c) There was a demand for development of process setup due to establishment of PMND-EDM process capability.

.

CHAPTER 4: EXPERIMENTAL DESIGN AND ANALYSIS

The Design of experiment was introduced in this chapter for experimentation planning. Further Taguchi methodology along with analysis of variance was studied for process optimization of the developed process of Powder Mixed Near Dry EDM. This chapter also gives information related to steps involved in Taguchi methodology and application of analysis of variation (ANOVA) in various research fields. Lastly scheme of experiments has been discussed along with instruments used for measurement of different response characteristics.

To obtain accurate conclusions from the experimental work, planned experiments was the basic requirement. Design of experiments (D.O.E) was very useful to accomplish this task or to obtain the desired results. D.O.E utilizes interference of different observations which were not exact but were subjected to variation in the study. Additionally, this technique helps in providing the experimental data by appropriate method with proper interpretations.

Taguchi L9 array along with ANOVA (Analysis of variation) was utilized for the design of experiments, which comprises of four parameters at three different levels. The selected process parameters were tool diameter, mist flow rate, metallic powder concentration, and dielectric mist pressure. The experiments were performed on EN-31 die steel material by using hollow copper tool. The selected parameters were selected based on previous literature review and their significance which affects the machining characteristics.

Further study was conducted in field of Gaseous Assisted Powder Mixed Near Dry EDM under different experimental for measurement of response characteristics such as material removal rate, surface finish, micro-hardness, residual stress and tool wear rate.

Additionally, thermo-electric modelling was performed for analysis of material removal rate by using ANSYS software by applying finite element methodology. In summary, the complete scheme of experiments is given in Figure 4.1.

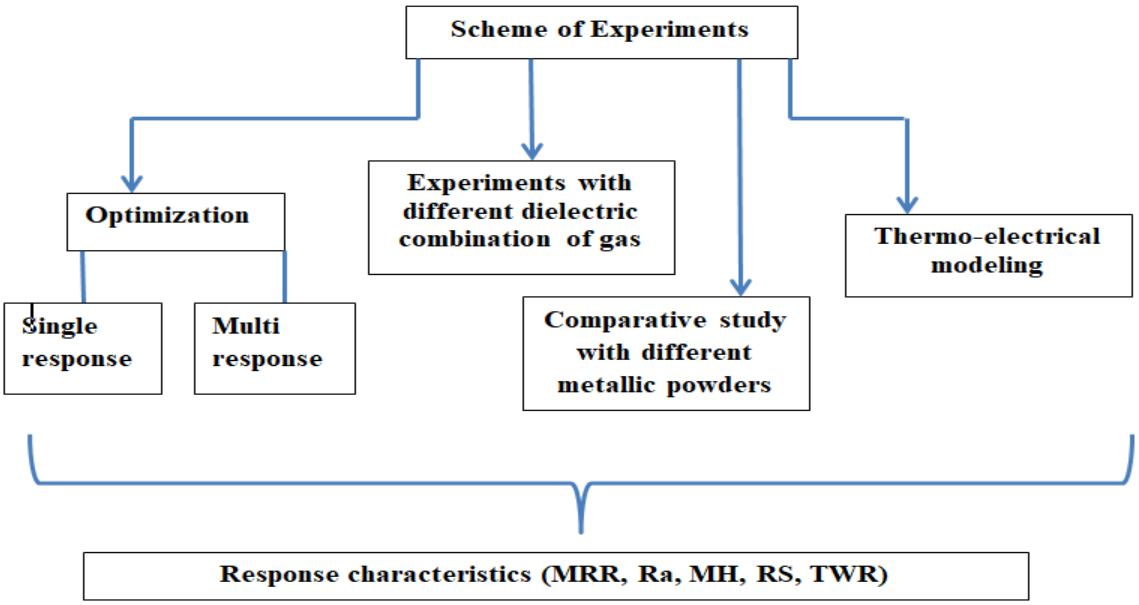

Figure 4.1 Complete summary for scheme of experiments

There were several advantages by the planning of experiments as per the design of experiments:

a) Identification of those variables which were effective in modifying the performance of the process.

b) This designing helps in reducing the number of trial experiments.

c) Optimum parametric setting can be determined in the process.

d) Experimental error can be found out.

e) The effect of interaction between the process parameters can be determined.

4.1 Steps Involved In Taguchi Method

The general steps involved in the Taguchi Method are as follows;

a) Defining the objective of the process or more accurately, the target value for measurement of performance such as pressure, flow rate, concentration etc. The performance measure of the target value can be maximum or minimum.

b) Determination of process parameters affecting the method. The process parameters are variable in nature which can be controlled easily. There should be specification of the number of levels for the particular parameter.

c) Creation of array (orthogonal) for design of parameters indicating the number of trails for each experiment. The levels of each parameters and its number determine the selection of orthogonal array.

d) Collection of data as per the experiments in the array.

e) Analysis of data to determine each parametric effect on performance measure.

There was tabulation of 18 orthogonal arrays by Taguchi which are called standard orthogonal array. The matrix for experiments can be planned as per any of the array from the table of orthogonal array. The number of experiments was represented by the number of rows of orthogonal array. For viable choice of an array, the rows should be equal to degree of freedom for a case study, while columns in an array determine the maximum number of factors. Furthermore, one should match the levels of factors with columns number in the array for use of standard orthogonal array. In order to reduce the expense of conducting experiments, smallest numbers of experiments are conducted that fulfils the case study requirement (Ross, 1996).

4.2 **Signal to Noise Ratios**

In Taguchi analysis signal to noise (*S/N*) ratios was calculated for desired and undesired values. These output characteristics were generally of three types such as higher the better (HB), lower the better (LB) and Nominal is better (NB). S/N is a technique of measurement in science and engineering to analyse the effect on output response relative to the target or nominal value under different noise condition (dB). In this study, the goal for experimentation was to measure MRR, Ra, RS, MH and TWR, therefore the noise conditions were involved during experimentations. The signal to noise quality was considered higher the better for output responses such as material removal rate (MRR), surface finish (Ra) and micro-hardness (MH) while signal to noise quality was considered lower the better for responses such as residual stress (RS) and tool wear rate (TWR). The expressions for the signal to noise ratios, higher the better, lower the better and nominal the better are given in Eqs. 4.1-4.3 respectively (Ross, 1988).

$$S/_N = -\log_{10}\left(\frac{1}{n}\sum_{i=1}^{n}\frac{1}{y_{ij}^2}\right) \quad (4.1)$$

$$S/_N = -log_{10}\left(\frac{1}{n}\sum_{i=1}^{n} y_{ij}^2\right) \quad (4.2)$$

$$S/_N = -log_{10}\sum_{i=1}^{n}(y_{ij} - y_o)^2 \quad (4.3)$$

Where:

n = Number of replications;

y_{ij}= observed response value

4.3 Analysis of Variance

The theory of analysis of variance was elaborated by Prof. R.A. Fisher and has been currently used in many fields of application. Further analysis and development of ANOVA was carried on by Prof. Snedecor and other researchers. Analysis of variance has been uses in various research fields such as education, industry, agriculture, engineering and other disciples. This technique was useful in multiple case studies. Z-test or t-test can be used to determine the significance of the difference between the means of the samples but real problem arises when there was need to determine the significance of differences between the means of more than two samples. Analysis of variance solves this problem and therefore it was widely used by the researchers in various fields of applications. By using this technique, we can determine whether the samples are from the population having the same mean or not. ANOVA is basically used for the homogeneity test for difference testing of different groups (Ross, 1988).

The variation of a set was divided into two types, attribution of amount to a cause and attribution of amount to a chance. There were variations within the sample and between the samples, which was solved by ANOVA for analytic purpose.

4.4 Scheme of experiments

The study for different response characteristics were performed in different experimental schemes. The different scheme of experiments carried out in this research work is as follows:

4.4.1 Pilot Experiments

Series of experiments were conducted in this developed hybrid setup, and responses, such as MRR, Ra, RS, and MH, were studied for powder mixed near dry EDM. The experimental condition for machining is shown in Table 4.1. The first set of experiments was performed with mist only (i.e., without any metallic powder); the second set of experiments was performed with 2% (2 g/l) powder concentration; the third set of experiments was done with 4% (4 g/l) powder concentration with four different tools. The main criteria for conducting the pilot experiments was to analyze the effect on machining performance by this new developed methodology of machining.

Table 4.1 Experimental condition for pilot experiments

Exp. no.	Powder Concentration [%]	Total experiments	Tool type
1	0%	4	1, 2, 3, 4
2	2%	4	1, 2, 3, 4
3	4%	4	1, 2, 3, 4
Pressure 0.6 MPa; time 10 min; T_{on} 500µs; T_{off}75 µs; discharge current 12A; gap voltage 25 V; tool electrode (copper); workpiece EN-31; mist flow rate 6 ml/min			

4.4.2 Single and Multi objective optimization

Series of experiments was planned for single response optimization and multi response optimization (utility concept) as per Taguchi L_9 (OA) as per Table 4.2. Each series of experiment was performed in three runs and a total of 27 experiments each were performed for analysis of material removal rate, surface finish, micro-hardness, residual stress and tool wear rate.

Table 4.2 Scheme for experiments

Symbol	**Process parameters**	**Unit**	**Level 1**	**Level 2**	**Level 3**
A	Tool diameter	mm	2	3	4
B	Mist flow rate	ml min^{-1}	5	10	15
C	Metallic powder concentration	g l^{-1}	2	5	8
D	Mist Pressure	MPa	0.4	0.5	0.6
*Values of other constant parameters: Machining time 10 mins; T_{on} 500µs; T_{off} 75 µs; Discharge current 12A; Voltage 30 V, Tool electrode Copper; Workpiece EN-31, Metallic zinc powder, powder grain size 15µm, glycerol 5%, EN-31 (30mmx15mmx15mm)					

4.4.3 Gaseous Assisted Powder Mixed Near Dry EDM

The experiments were conducted with different combination of dielectric gases as shown in Table 4.3. The effect of different dielectric gases was studied under different experimental scenarios on responses such as material removal, surface finish, micro-hardness and residual stress.

Table 4.3 Different scenarios of dielectric mediums for experimentations for MRR

Scenario	Dielectric combination
1	Copper + Argon
2	Copper + Oxygen
3	Zinc +Argon
4	Zinc + Oxygen
5	Graphite + Argon
6	Graphite + Oxygen
Dielectric oil: (LL-221), stabilizing agent: 5% glycerol, Powder concentration 6 (g/l) Flow meter of dielectric: 10 ml/min: Air and oil pressure: 0.1, 0.2, 0.3, 0.4 MPa, Cylindrical hollow copper rod ($ø_i$ =6mm, $ø_o$= 8mm)	

4.4.4 Comparative study for Near Dry and PMND-EDM with compressed air

Comparative study was also performed between near-dry EDM and PMND-EDM with different combination of metallic powders (aluminium, graphite and silicon) with compressed air. The process parameters selected for experiments and their values are shown in Table 4.4.

Table 4.4 Process parameters for experimentation for ND-EDM and PMND-EDM

Process parameter	Unit	ND-EDM	PMND-EDM
Dielectric medium	-	Pressurized air + Dielectric oil	Pressurized air + Dielectric oil + Powder
Machining time	Minutes	10	10
Discharge current	A	8	8
Pulse on	µs	60	60
Gap voltage	V	30	30
Working pressure	MPa	0.5	0.5
Metallic powder concentration	g/l	10	10
Type of powder	-	-	Aluminium, Graphite, Silicon
Dielectric oil flow rate	ml/min	10	10
Workpiece electrode – EN-31, Tool electrode – Copper			

4.4.5 THERMO-ELECTRIC MODELING IN PMND-EDM

Research on thermal-physical based modeling of material removal in Powder Mixed Near-Dry Electric Discharge Machining was also conducted. Three-dimensional axisymmetric model was prepared for PMND-EDM. Thermal properties of material, heat source shape (Gaussian heat distribution), heat distribution percentage among workpiece, tool and dielectric fluid, pulse on, pulse off and material ejection efficiency were considered as significant elements for predicting the MRR in PMND-EDM. Mathematical expressions for various physical parameters like material removal rate, time-lag, and heat flux were developed. In addition to this, values of these physical parameters were calculated by using their derived expressions. These values were further compared to the results of experimentation for validity of mathematical model.

The stepwise work carried out for the modeling was described as:

a) A geometric model of the workpiece was developed using design modeler platform of the given FEM software.
b) The assignment of material to the workpiece and the dielectric fluid was done.
c) After that, the boundary conditions and load assignment to the workpiece was done. Since this problem was transient thermal analysis, therefore a time varying heat load was applied at the specific location on the workpiece.
d) Meshing was carried out by using a3-D, 10 node tetrahedral elements for meshing. Apart from that, face meshing was also done on the certain faces so that even and uniform meshing can be obtained.
e) Transient analysis was carried out and the results in the form of contoured temperature plots, isotherms and temperature graphs at different locations on the workpiece were obtained. These results were further used for determining the deformed region on the workpiece which was further used for calculation of material removal rate. These material removal results were then compared with the experimental results which establish their validity.
f) The validity of FEM model and Mathematical model was established by doing comparison between FEM modelling and experimental results, Mathematical modelling and experimental results respectively.

4.5 SELECTION OF WORKPIECE AND TOOL

The workpiece selected was EN-31 (Workpiece dimensions: 30 mm x 25 mm x 25 mm), due to its high measure of hardness with compressive strength and abrasion resistance property. The excellent wear resisting property of this grade steel makes it desirable machine component. Additionally EN-31 has its immense applications in manufacturing industry, while the tool electrode selected was copper in material due to its higher thermal conductivity and other desirable properties for conducting experiments. The properties of workpiece and tool are given in Table 4.5 and Table 4.6 respectively.

Table 4.5 Chemical composition and physical properties of workpiece (EN-31**)**

Chemical properties		Physical properties	
ELEMENT	%	Thermal conductivity (W $m^{-1}K^{-1}$)	44.5
Carbon	0.90-1.20	Hardness(HRC)	63
Silicon	0.10-0.35	Yield stress (MPa)	450
Manganese	0.30-0.75	Tensile strength (MPa)	750
Sulphur	0.050	Density (kg m^{-3})	7850
Phosphorus	0.050	Melting point (ºC)	1540

Table 4.6 Chemical and physical properties of copper tool

Properties	Values
Atomic number	29
Atomic weight	63.546
Density(Kg m^{-3})	8960
Melting point (^{O}C)	1083
Boiling point (^{O}C)	2567
Thermal conductivity (Wm $^{-1}$ K^{-1})	385
Hardness (Mohs)	2.5-3
Tensile strength (MPa)	33.3
Bulk modulous (GPa)	140

4.6 Measurement of Response Characteristics

The response characteristics measured in present study are as follows:

a) Material Removal Rate (MRR)
b) Surface finish (Ra)
c) Micro-hardness (MH)

d) Residual stress (RS)

e) Tool wear rate (TWR)

4.6.1 Material Removal Rate

The response for material removal rate was measured using the relations given below:

$MRR = (W_i - W_f)/ T_m$,

Where W_i was the initial weight of the workpiece before machining, W_f was the final weight of the workpiece after machining, T_m was the time taken for machining.

Weight of the specimen was measured using an electronic balance of least count 0.001gram (Asia Techno weigh India).

4.6.2 Surface Finish (Ra)

Surface finish was checked by using a bench top ZeGage 3D optical profilometer (model TM3000, Figure 4.2). It enables precise and non-contact measurement of surface and characterization of micro surface features

Figure 4.2 ZeGage optical profilometer

4.6.3 Micro-Hardness (MH)

Micro-hardness analysis for product machined by PMND-EDM was performed with help of Fischerscope instrument (HM2000S model, USA) as shown in Figure 4.3. This instrument utilizes a carbide indenter which indents with respect to the increase in value of load applied.

Figure 4.3 Micro-hardness measuring machine (Fischerscope instrument)

4.6.4 Residual Stress (RS)

The residual stress measurements were taken by μX-360 Pulstec machine (Japanese built) as shown in Figure 4.4. The machine consists of mainly three parts which are computer, sensor unit and power unit. The setup consists of X- ray tube (30 KV) and 2-D X- ray sensor for visual analysis along with power supply unit to generate X-ray. X-ray takes 90 seconds to take one reading of residual stress. The machine has a special feature of air cooling for efficient performance. The X- ray tube current was 1mA and the sample distance from the X-ray focusing lens was 38mm. The incident angle for X- ray was set at 35 degree while the information regarding specimen to be analyzed were lattice constant, interplanar spacing and diffraction planes (h, k, l) , crystal structure, poisson's ratio, and Young's modulus. An AC supply of 240V and 50/60Hz specifications for the working of X-ray machine was utilized, however it could also run on a 24 V supply coming from a battery. Efficient working of this machine was ensured by a special provision of air cooling feature with the machine. The incidence angle set for X-ray striking the sample surface was set at 35^0 between the sample and focusing lens of the machine.

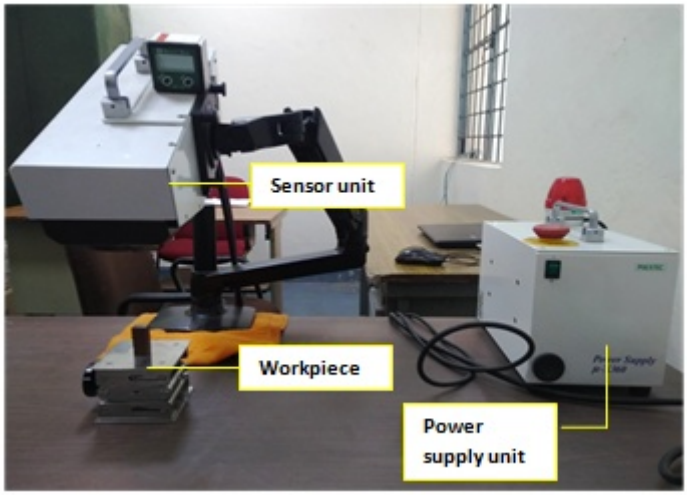

Figure 4.4 Portable XRD - residual stress analyzer in operation

4.6.5 Scanning Electron Microscope

A Hitachi Scanning electron microscope for the study of surface morphology of machines surface (Figure 4.5). The magnification range of the apparatus was 15X to 30000X. Scanning electron microscope makes use of electron optical system consisting of electron gun, objective lens and condenser lens to produce beam of electrons projecting over the specimen to be probed. The complete optical system is kept in vacuum chamber because the electrons would loose energy upon interaction in open environment.

Figure 4.5 Scanning electron microscope (TM-3000 table top microscope)

Summary

a) Present chapter discusses Taguchi design of experiment for experimental investigation. Classifications and relevant calculations for Signal to Noise have been discussed.

b) This chapter also includes discussions on suitability of various orthogonal arrays for robust design and analysis of variance for process parameter optimization. Here, four prevalent process variables along with three levels have been finalized in accordance with orthogonal array L9 for experimentation on developed setup.

c) The selection of parameters and their levels should be done before the starting of the experimental work, because the viability of design of matrix of experiments determines the correct results.

d) Comparison of process was also discussed in the present chapter in developed hybrid EDM by using different scheme of experiments.

e) Planning for thermo-electric model was done for analysis of material removal rate.

f) The instruments used for measurement of response characteristics were elaborated.

This chapter includes information related to Electric Discharge Machine and design of powder mixed near dry electric discharge machining (PMND-EDM) setup and it's another form of gaseous assisted powder mixed near dry EDM (GAPMND-EDM) setup. The specification of the used parts was defined along with the operational condition of the indigenously developed setup. Afterwards, details of tool electrode fabrication and its design were also discussed.

5.1 EDM MACHINE

To meet the demand of customers, EDMs were developed in various sizes with different types of flush and submerged machines. Variety of workpiece weighing thousands of pounds can be handled by large scale EDM and can machine samples up to twenty inches thick in size. Along with X-Y table, EDM has Z axis for tool electrode. The EDM system consists of power supply, computer numeric control, tool holder, programmable z-axis, filter system with anti –electrolysis circuitry. In this research the experiments were performed on Sparkonix 35-A EDM machine shown in Figure 5.1 and the specification of the machines is shown in Table 5.1.

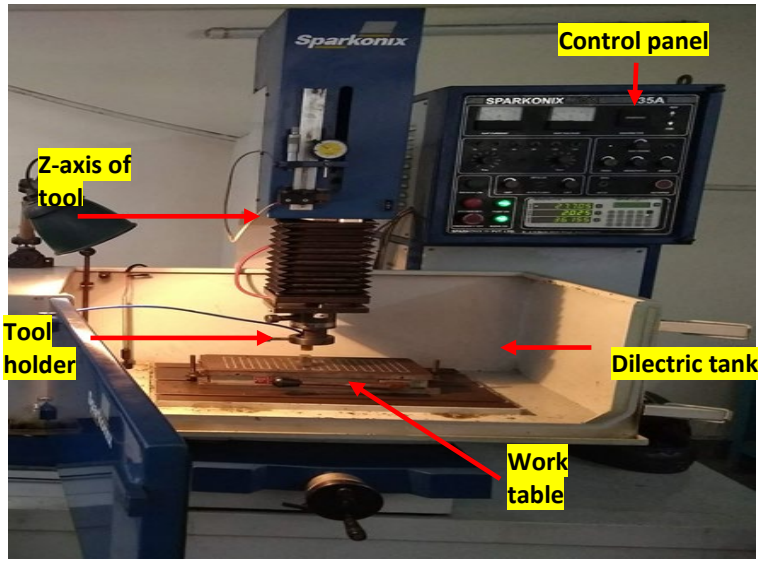

Figure 5.1 Sparkonix 35-A EDM machine

Table 5.1 Specifications of the EDM Machine

Machine model	SPARKONIX 35-A
Max table speed (L x W)	420x280
X Travel	300 mm
Y Travel	200 mm
Z Travel	200 mm
Maximum job weight	300 Kg
Maximum job height	250 mm
Pump Motor	0.5 Hp
Dielectric tank	150 Litre
Input power supply	3 phase, 50 Hz and 640 V
Dielectric fluid	LL-221 kerosene based oil

5.2 EDM control panel

The control panel of the EDM machine (Sparkonix Limited, Pune), consists of several parameters such as pulse on, pulse off, discharge voltage, peak current, sensitivity, feed and speed regulator. The various EDM parameters are as follows:

(a) **Pulse on Time**: The pulse on time determines the time duration in micro seconds for flow of current in each cycle when voltage was applied at the electrodes. These pulses determine the frequency and time period of sparks generated at the machining gap. The range of the Pulse off time was between 10- 2000 µs.

(b) **Pulse off time**: The pulse off time determines the time period in micro seconds between two successive sparks. The range of the Pulse off time was between 5- 500 µs

(c) **Peak current**: This current determines the maximum current and the spark energy of the pulse passing thought the electrodes. The maximum current capacity of the machine was 32 Ampere.

(d) **Discharge voltage**: This is also known as gap voltage, which was responsible for the spark gap. In the present machine, the range was between 0-99 volts.

(e) **Tool feed**: It determines the travel of tool path or feed of tool electrode for machining.

(f) **Sensitivity**: This regulator was used to control the movement of the tool.

(g) **Speed regulator**: This regulator controls the speed of z-axis lead screw.

5.3 DEVELOPMENT OF POWDER MIXED NEAR DRY ELECTRIC DISCHARGE MACHINING SETUP (PMND-EDM)

The setup for Powder Mixed Near Dry EDM was designed and developed in the Precision Manufacturing Laboratory (Delhi Technological University, Delhi). The experimental setup for PMND-EDM is shown in Figure 5.2 while its detailed line diagram is shown in Figure 5.3. It has a minimal input of resources, was relatively environmentally friendly and also gives the desired response characteristics. This indigenously developed setup of PMND-EDM used heterogeneous mixture of three phases (solid + liquid + gas) dielectric medium. There were several features in the panel of the setup. The panel of the setup includes dielectric mixing chamber, dielectric mist flow meter, manual regulators, and analogous gas pressure gauges which determine the working pressure of dielectric medium. The complete directional flow of dielectric medium in PMND-EDM is shown in Figure 5.3.

Main features of the Powder Mixed Near Dry EDM setup are as follows:

a) Mixing chamber

A mixing chamber was designed and manufactured in which oil along with metallic powder and glycerol was mixed in right proportion with compressed air supplied from the compressor at a high pressure, ranging from 0.4 MPa to 0.8 MPa. The designed chamber has a separate inlet for dielectric medium and, in case the pressure inside the chamber goes beyond operational limits, a safety valve was provided on top of it to release the pressure of compressed air.

b) Flow meter

A flow meter was integrated with the setup, which can vary the flow rate of dielectric mist within range of 0-20 ml/min. As the flow meter is a transparent body, the flow rate of mist can be easily read from the calibration marking/scale mounted on the flow meter. To avoid metallic powder particle settling, glycerol was added in the tank along with dielectric fluid from the inlet of the tank.

c) Mist pressure regulators

The setup also includes manually operated mist pressure regulators mounted on the control panel for regulating air and oil pressure. The setup comprises a display unit for oil and air pressure, which was analogous in nature.

d) Air compressor

Compressor (NU-air) of 2 horse power was used to supply compressed air. The maximum limit of pressure was 0.8 MPa. The working of air compressor was based on reciprocating mechanism**.**

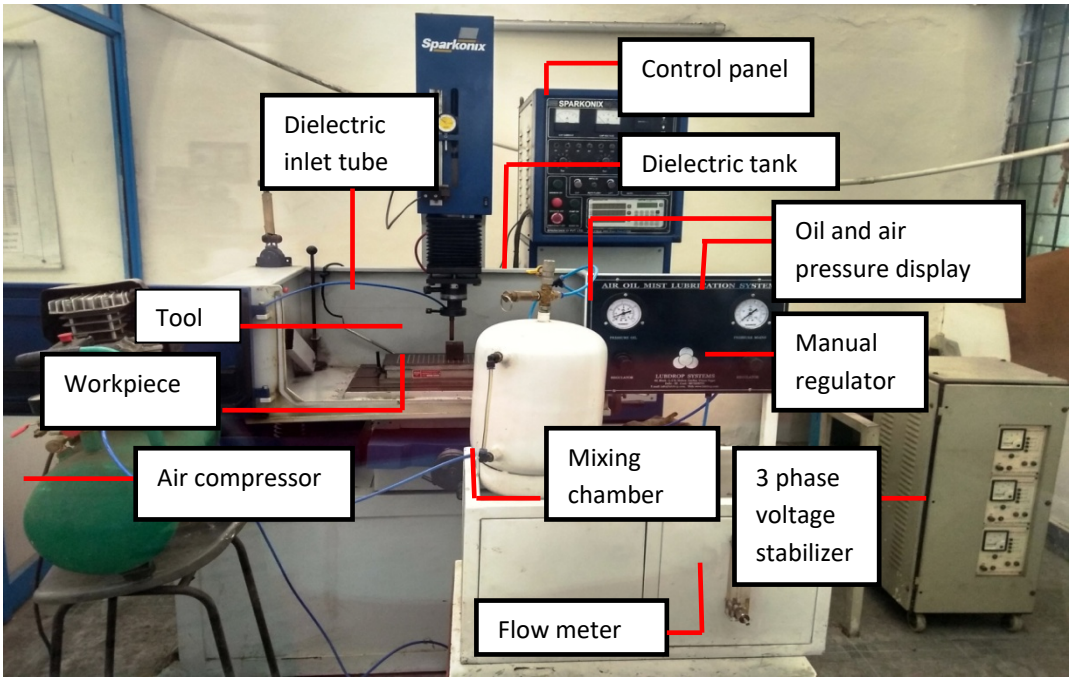

Figure 5.2 Developed experimental setup for PMND-EDM

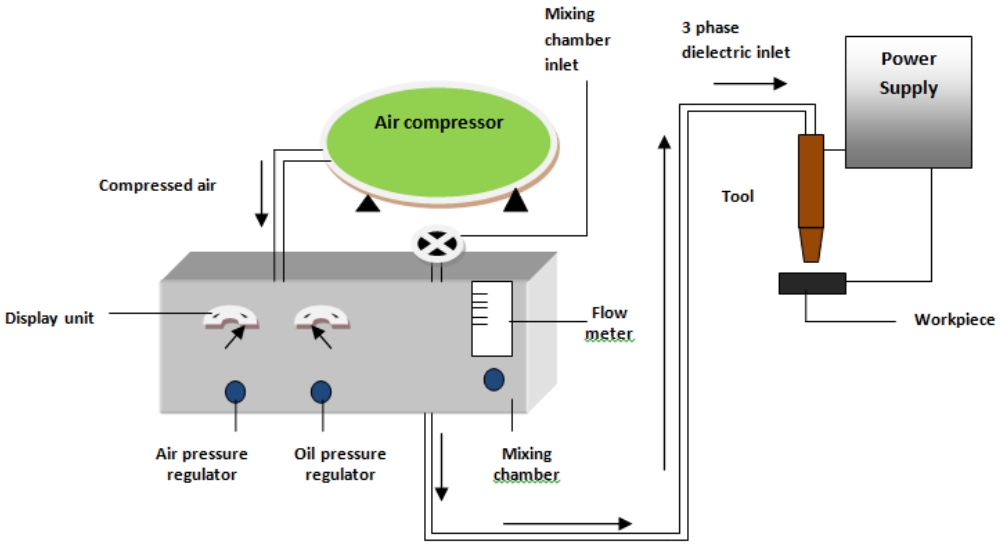

Figure 5.3 Line diagram for indigenous developed setup for PMND-EDM

5.4 Gaseous assisted powder mixed near dry EDM (GAPMND-EDM)

Another setup for gaseous assisted near dry EDM was also developed in order to study the influence of gases (argon and oxygen) in dielectric medium in place of compressed air as shown in Figure 5.4. Different metallic powders such as copper, zinc, silicon, graphite and aluminium powder were used as additives in the dielectric medium. Overall, the setup working was similar to PMND-EDM but in this case there were gases different from compressed air.

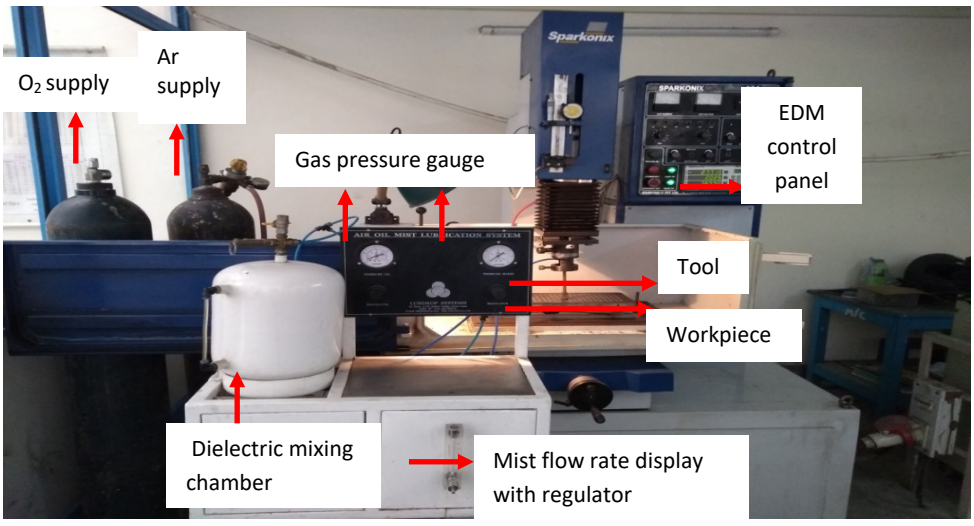

Figure 5.4 GAPMND-EDM setup for experimentations

5.5 Tool electrode design

The customized copper tools were developed in the precision manufacturing lab (Delhi Technological University, Delhi). The concept of design of tool electrodes was taken from previous study in field of near dry EDM (Shen et al. 2016). Figure 5.5 and Figure 5.6 shows the design feature of the tool electrodes. The other ends of hollow tubular copper were constant in dimension with 6.1 mm inner diameter and 8 mm outer diameter as shown in Figure 5.7 (a). The tool setup utilizes a flexible tube of 6 mm outer diameter inserted at the top end of the tool as shown in Figure 5.7 (b), while Table 5.2 shows the dimensions of various tools used in the present study.

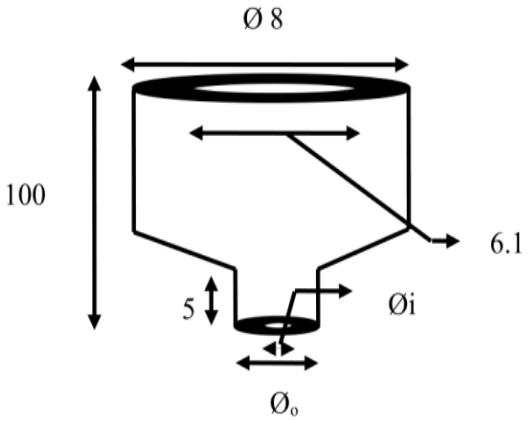

Figure 5.5 Design of tool developed for PMND-EDM; all dimensions in mm

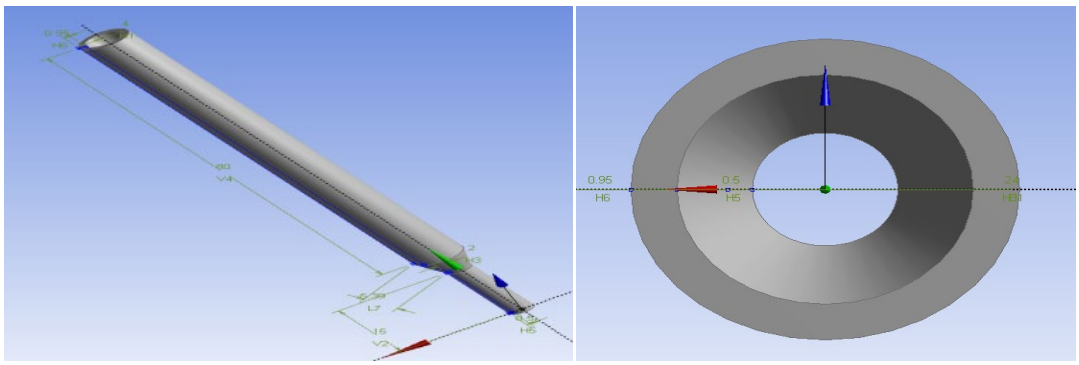

Figure 5.6 Design feature of developed tool

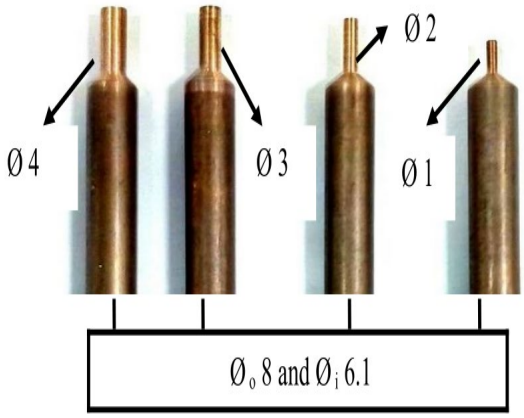

Figure 5.7 (a) Hollow copper electrodes of different dimensions (all dimensions in mm)

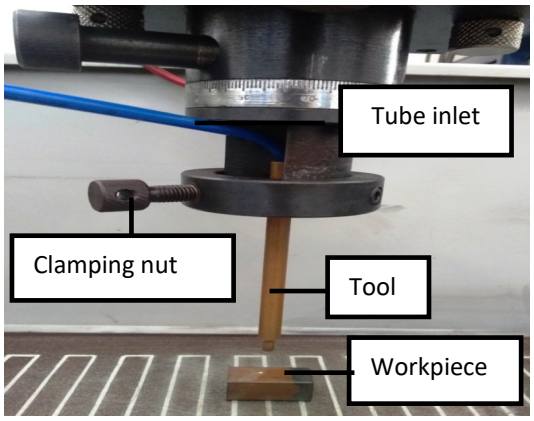

Figure 5.7 (b) Tool setup

Table 5.2 Diameter of various tools developed for present study (sparking end)

Tool type	Inner Diameter ($Ø_i$) [mm]	Outer Diameter ($Ø_o$) [mm]
Tool 1	1	2
Tool 2	2	3
Tool 3	3	4
Tool 4	4	5
Dimension of other end of hollow tubular copper tool: ($Ø_i$) 6.1 mm and ($Ø_o$) 8 mm.		

Summary

a) Specification of EDM machine with important parameters was discussed.
b) Setup for PMND-EDM was designed and fabricated with detailed features as per the requirement of the research.
c) Gaseous dielectric supply was incorporated with developed setup for new process of gaseous assisted powder mixed near dry EDM to study effects on material removal and surface characteristics of the machined samples.
d) Working of the developed setup was discussed.
e) Main features of the setup were discussed along with design of tool setup.

CHAPTER 6: SELECTION OF PROCESS PARAMETERS AND EXPERIMENTATION

This chapter describes parameters selected for experimentation in powder mixed near dry EDM and gaseous assisted EDM. Afterwards selection of response characteristics was elaborated. Variable parameters such as tool type, metallic powder concentration, dielectric mist pressure, mist flow rate, types of gases, and types of metallic powders were discussed along with their range in order to optimize the process parameters for enhancing the machining performance in terms of increased material removal rate, improved surface finish, improved micro-hardness, reduction of residual stress and tool wear rate. Lastly, the instruments used for measuring response characteristics were discussed.

In order to study the performance of any machining method, the important parameters and their range were selected for conducting the experiments. Experiments were conducted to study the effect of variables on response characteristics such as material removal rate, surface finish, micro-hardness, residual stress and tool wear rate as shown in Figure 6.1. All the EDM characteristics were measured for further analysis.

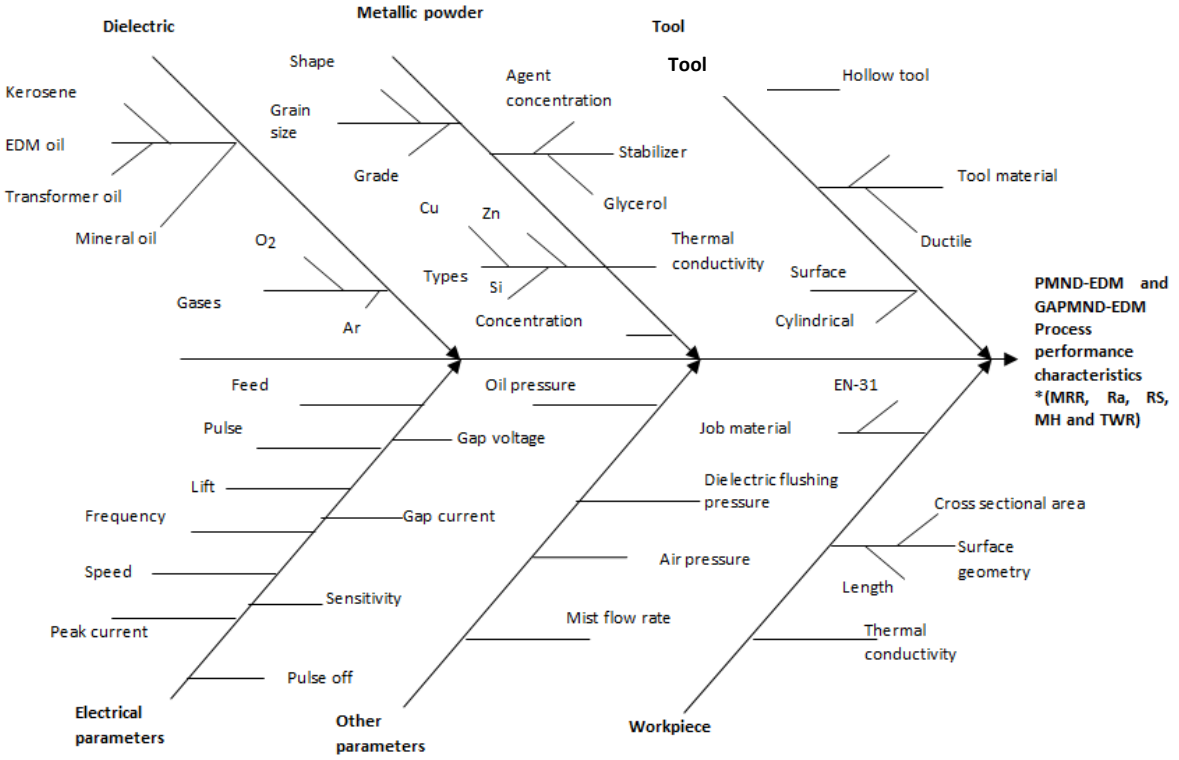

Figure 6.1 Fish and Bone diagram for measurement of EDM response characteristics

6.1 Selection of process parameters

Based on literature review, the process variables of PMND-EDM were arranged in the following categories:

a) **PMND-EDM setup based parameters**: Dielectric mist pressure and dielectric flow rate.
b) **Dielectric medium based parameters**: Metallic powder concentration, Metallic powder additives, type of powder, grain size, type of gas.
c) **Tool based parameter**: Tool material, tool type and tool geometry.

6.1.1 Concentration of Metallic Powder Additives

Comparative study was performed for Near Dry EDM (i.e machining without powder) and PMND-EDM. It was found from the literature review, with the addition of liquid and conductive metallic powder to compressed air, there was a reduction of the dielectric medium insulating strength between a tool and workpiece electrodes (Kansal et al. 2008). This resulted in improved de-ionization effect and discharging conditions. All these factors improve discharge frequency and material removal was thus increased. A solid and liquid mixture, such as mist assisted with metallic powder, changes the electric field strength of the dielectric medium and thus facilitates the discharge initiation (Bai et al. 2012, b).

Trial experiments were conducted to identify the effect of metallic powder concentration on the MRR and Ra, plotted in Figure 6.2.

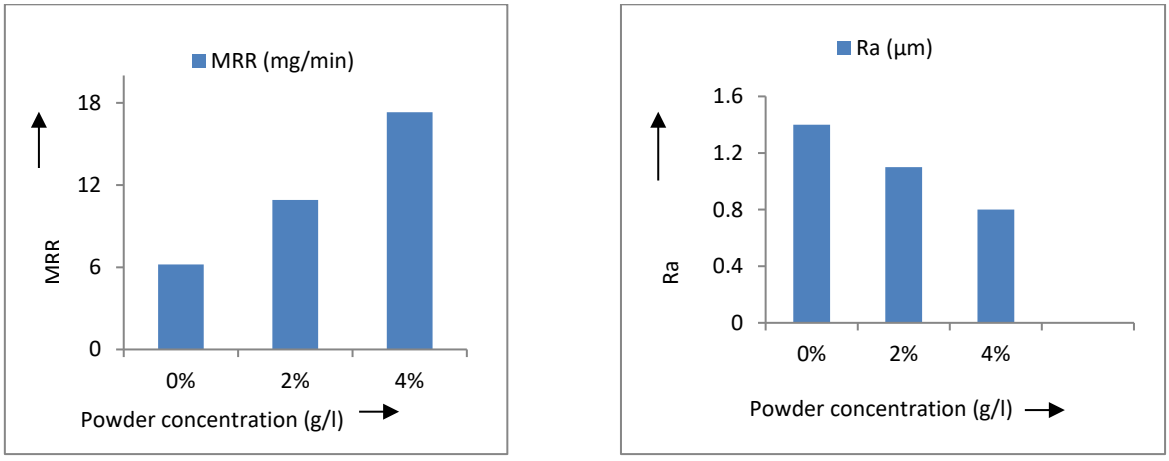

Figure 6.2 Effect of metallic powder concentration on the MRR and Ra

It was experimentally proved by trial experiments that the maximum percentage increase in MRR of PMND-EDM was 17.85% as compared to near- dry EDM (0%) (Figure 6.2). The plasma channel was small with a 2% concentration of powder due to which there were fewer craters over the

machined workpiece. A high energy enlarged plasma channel due to increased metallic powder concentration was the main reason for higher erosion (Wong et al. 1998). Metallic powder additives along with dielectric oil reduce the electric density and increase the spark gap, due to which the sparking over the machined surface was uniformly distributed (Zhao et al. 2002). It was observed that higher surface finish was achieved in machined products because the increased spark gap helped in effective debris removal from the machining area (Jeswani, 1981). Powder concentration was an important factor in influencing the spark gap. The maximum percentage increase in surface finish was 16.36% in PMND-EDM as compared to near-dry EDM. With a further increase of metallic powder concentration (4%), the plasma channel becomes more uniformly energized and distributed. which gives better surface finish than that of the 2% powder concentration (Figure 6.2).

The topography of the machined surface of the workpiece was improved by metallic powder in the dielectric medium because these additives were responsible for reducing the surface pits over the machined surface (Furutani et al. 2001). The micro-hardness of the die steel workpiece was increased by adding chromium powder to the dielectric medium (Tripathy and Tripathy, 2017, b). A micro-hardness of 1600 HV was achieved with the addition of titanium powder to the dielectric (Furutani et al. 2001).

Experiments were conducted to identify the effect of metallic powder concentration on the MH and RS, plotted in Figure 6.3.

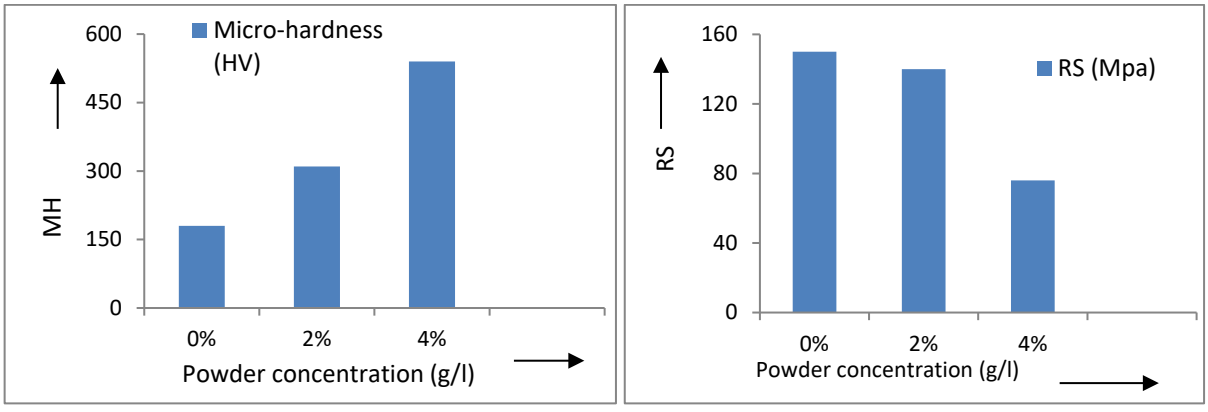

Figure 6.3 Effect of metallic powder concentration on the RS and MH

In trial experiments, the Vickers hardness number (HV) for machined part at 0% powder concentration was found to be 194 HV, but with powder additive machining this value increased to the maximum value of 520 HV at 4% powder concentration (Figure 6.3). The powder additives changed the surface topography of the machined surface which was responsible for surface modification and increased the micro-hardness by 69.63% (Sundriyal et al. 2016). The residual stress

analysis of machined surface at 0% powder concentration (ND-EDM) was performed. In ND-EDM, the residual stress measured by the machine was 164 MPa (tensile). The value of stress of the machined surfaces by PMND-EDM with 2% metallic powder concentration was 144 MPa (tensile), which was lower compared to the stresses in the workpiece machined by ND-EDM. On further increasing the metallic powder concentration to 4% in PMND-EDM, the residual stresses further reduced to a value of 72 MPa (tensile). The maximum decrease in residual stress was found to be 56.09% in PMND-EDM as compared to ND-EDM (Figure 6.3). The reason for the decrease in residual stresses in PMND-EDM can be attributed to the uniform distribution of heat or energy plasma over the machined surface and improved flushing condition, which ultimately relieves some part of the residual stresses over the machined surfaces (Ekmekci et al. 2016).

The addition of conductive metallic powder leads to reduced breakdown voltage and increase in the interspace between the electrodes for electric discharge (Jeswani, 1981). This phenomenon improves the stability of the machining process that caused a reduction in TWR. The dielectric fluid (LL-221) with added conductive powder has improved the efficiency of electrical discharging at the spark gap, preventing the tool electrode tip from further wear. Heat dissipation was improved because the phenomena of abnormal discharge and short circuit were minimized. The amount of heat conducted to the tool was also reduced due to proper heat dissipation. This makes the material temperature go below its melting point, which consequently reduces TWR (Bai et al. 2013, a).
There was a decrease in TWR was 18.80 % by PMND-EDM as compared to near dry EDM (i.e., without metallic powder) as shown in Figure 6.4.

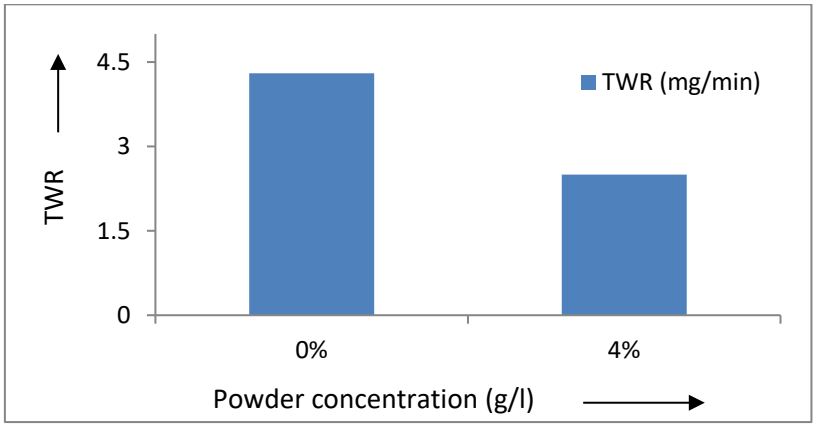

Figure 6.4 Effect of metallic powder concentration on the TWR

6.1.2 Tool Type

Tool geometry plays an important role in effecting response characteristics in PMND-EDM. The exit area for the dielectric medium from tool electrode tip changes the nature of discharge velocity (Shen et al. 2016). This nature of velocity of the dielectric medium enhanced the interaction of ions and molecules at machining gap which resulted in a high value of MRR.

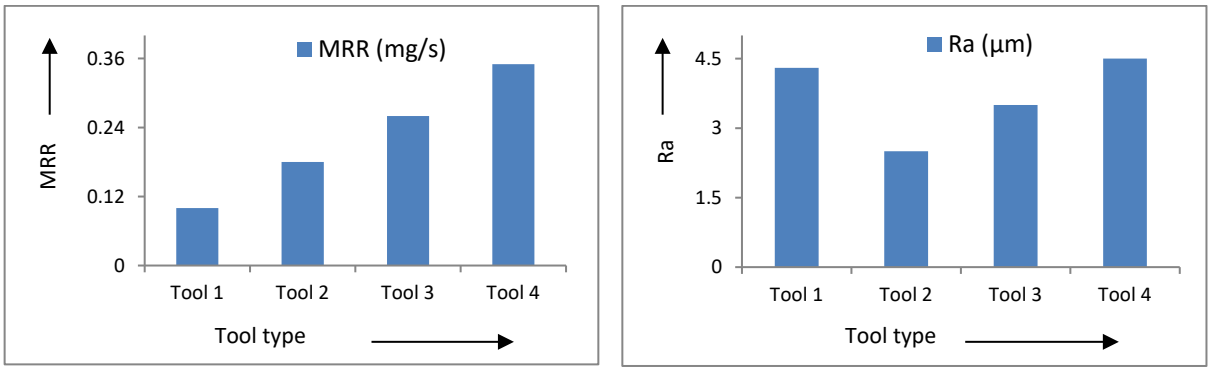

Figure 6.5 Effect of tool type on the MRR and Ra

The dielectric medium quantity at machining gap increased on further increase of tool tip diameter due to which MRR again displayed increasing trend (Figure 6.5). Appropriate dispersion results in stable discharging at the machining gap which results in reduction of surface roughness (Figure 6.5) over the machined surface (Fong and Chen, 2005). The discharge velocity of dielectric medium gets reduced on further increase of tool tip area, due to which the plasma reaction was not that significant and therefore the surface finish gets reduced to the lowest value (Figure 6.5).

The residual stress induced in the workpiece initially decreases with an increase in internal diameter of tool tip as shown in Figure 6.6. Better flushing takes place over the machined surface which provides a better cooling condition for dissipation of heat over the machined surface and therefore less heat was generated over the machined surface which results in reducing residual stress to the lowest value (Khundrakpam et al. 2018). Afterwards, rapid solidification was responsible for an increase in the value of RS (Kruth and Bleys, 2000).

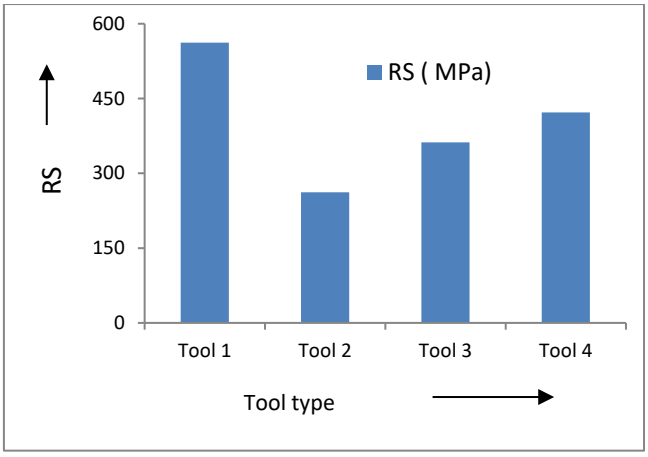

Figure 6.6 Effect of tool type on the RS

6.1.3 Dielectric Medium Flow Rate

It was noted from the literature review that MRR tends to increase with the increase in mist flow rate (Bai et al. 2012, a). High volume flow rate helps in faster flushing of debris and therefore results in faster erosion over the workpiece with improved surface finish (Tao et al. 2008). Additionally, the optimum dielectric flow which resulted in obtaining normal condition for discharges at the inter electrode gap resulted in improvement in surface finish. Similar trend was observed by experiments to identify the effect of dielectric medium flow rate on the MRR and Ra plotted in Figure 6.7.

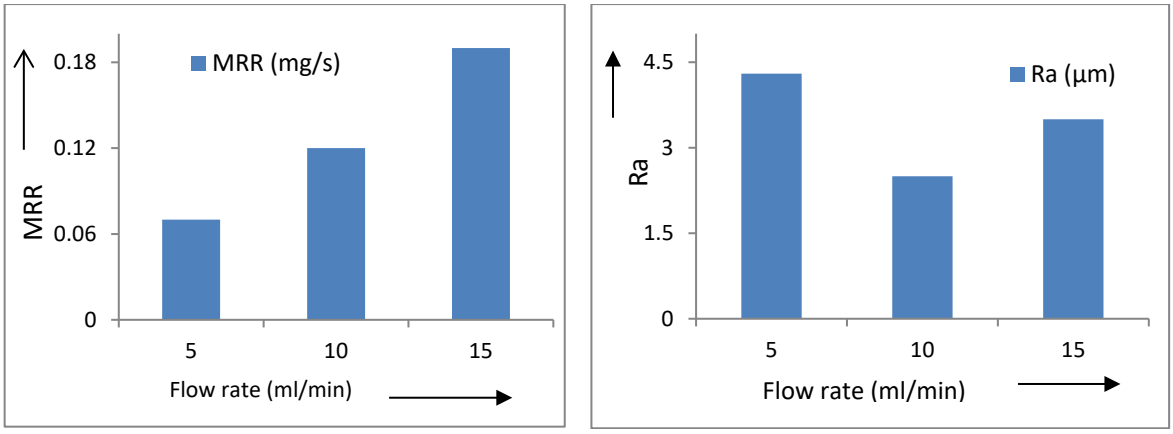

Figure 6.7 Effect of dielectric medium flow rate on the MRR and Ra

The RS value initially decreases with increase in flow rate values due to better heat dissipation at but with further increase of flow rate, there was a phenomenon of stress corrosion due to which the RS value increases to its peak value (Figure 6.8). Secondly flow rate was influential in increasing the micro-hardness value. Optimum suitable normal discharges at the machining zone along with powder

additives which results in higher value of micro-hardness on increasing the MH value (Gill and Kumar, 2016).

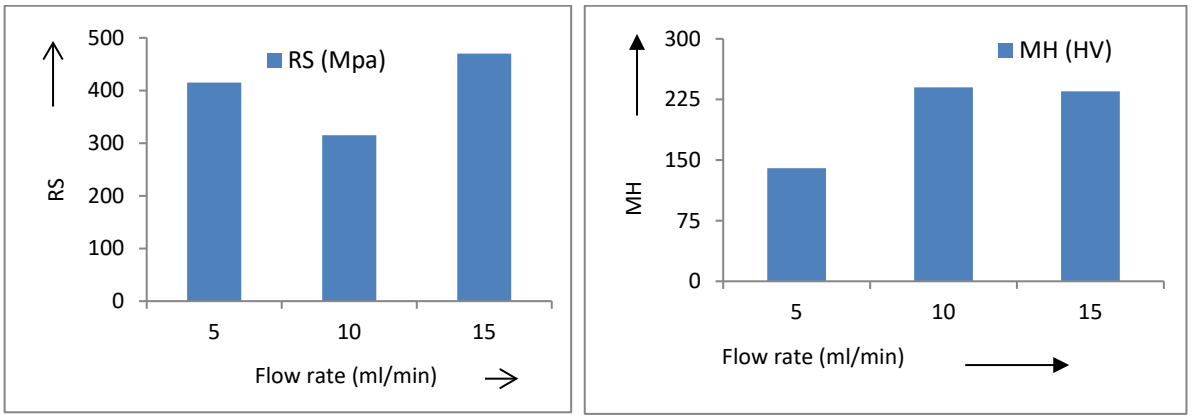

Figure 6.8 Effect of dielectric medium flow rate on the RS and MH

6.1.4 Dielectric mist pressure

The flushing effect over the machined area was improved significantly due to which there was a phenomenon of effective quenching and a good degree of fluidity, hence MRR increases with increase of dielectric mist pressure (Mane and Hargude, 2015). High pressurized mist assisted in removing the debris from the crater efficiently which provided favourable conditions for flushing and enhanced repetitive discrete discharge for an increase in MRR in machined products by PMND-EDM (Figure 6.9). The increased mist pressure provided excellent debris flushing and cooling conditions due to which enhanced surface finish was obtained (Figure 6.9).

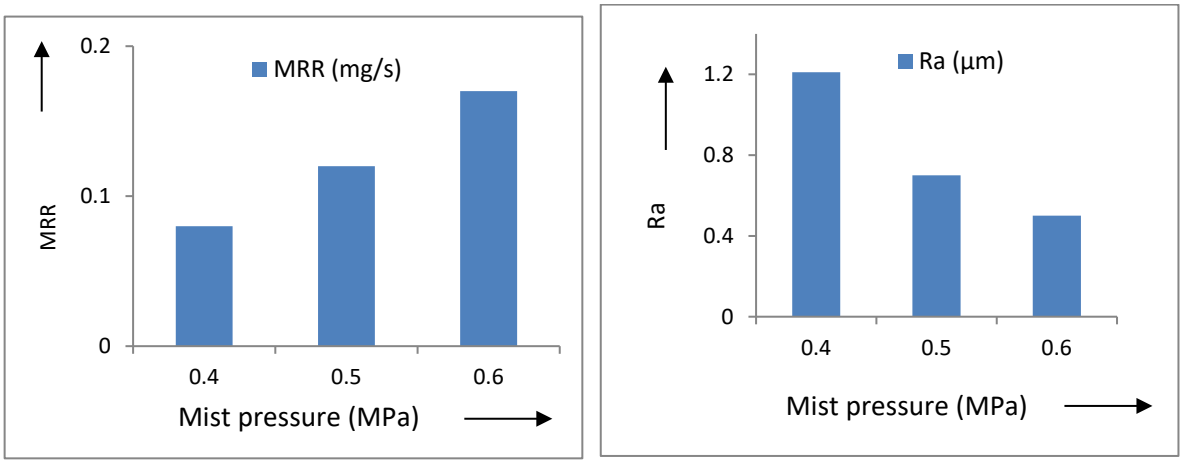

Figure 6.9 Effect of dielectric mist pressure on the MRR and Ra

The RS value decreases with the increase of mist pressure but afterwards, it increases with further increase of pressure (Figure 6.10). The molecules density initially gets increased with increase of mist pressure which improved deionization effect (Li et al. 2006). These conditions lead to better heat dissipation which reduces RS value. The relaxation time for residual stress gets decreased with an increase of mist pressure. These conditions were responsible for the increase in value of residual stress at higher mist pressure. Some trial experiments were conducted to identify the effect of dielectric mist pressure on the RS plotted in Figure 6.10.

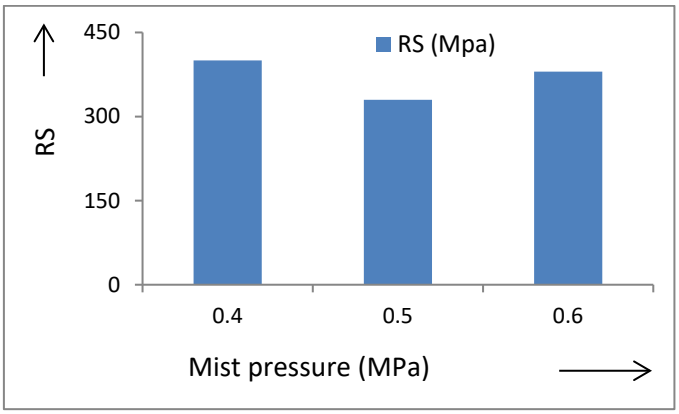

Figure 6.10 Effect of dielectric mist pressure on the RS

6.1.5 Type of Gases

Various experimental study related to gaseous assisted EDM has been done by researchers for increasing the productivity of existing EDM (Kuneida et al. 1997, Li et al. 2006, Lin et al. 2016, Liqing et al. 2013). In this present research, experiments were performed with metallic powders (copper, zinc, graphite) along with gases (argon and oxygen) at different operating pressure. Among the different metallic powders used, the graphite powder along with dielectric gas proved to be better in terms of higher erosion rate (Talla et al. 2017). The probable reason was that graphite powder has higher thermal conductivity as compared to zinc or copper additives along with dielectric gas. Secondly graphite additives have lower density as compared to zinc or copper additives which enables the grain particles of graphite to disperse more uniformly in the dielectric medium thus providing favourable machining conditions for erosion.

It was also visualize experimentally that among the different combination of metallic powders and gases, the dielectric mixture of graphite powder along with oxygen gas resulted in achievement of highest MRR (Kunieda et al. 2003).

Some trial experiments were conducted to identify the effect of type of dielectric gas with different powder additives on the MRR, plotted in Figure 6.11.

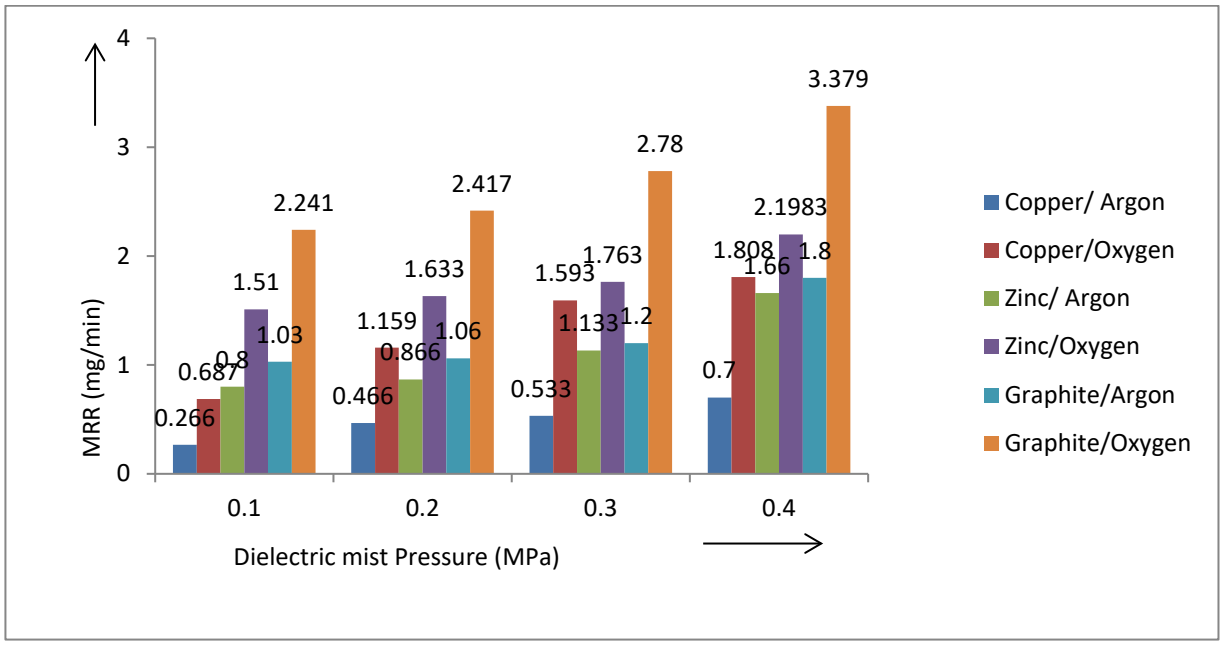

Figure 6.11 Effect of type of dielectric gas on the RS

Further preliminary experiments were carried out for surface finish and it was compared to conventional EDM, the surface finish obtained by GAPMND-EDM was quite high. The Ra value was found to be finest (1.11 µm) for machined sample with dielectric medium of graphite powder additive with argon gas as shown in Figure 6.12. Few properties of graphite powder were advantageous in terms of surface, electrical and thermal abilities which were responsible for generation of fine surfaces (Wong et al. 1998).

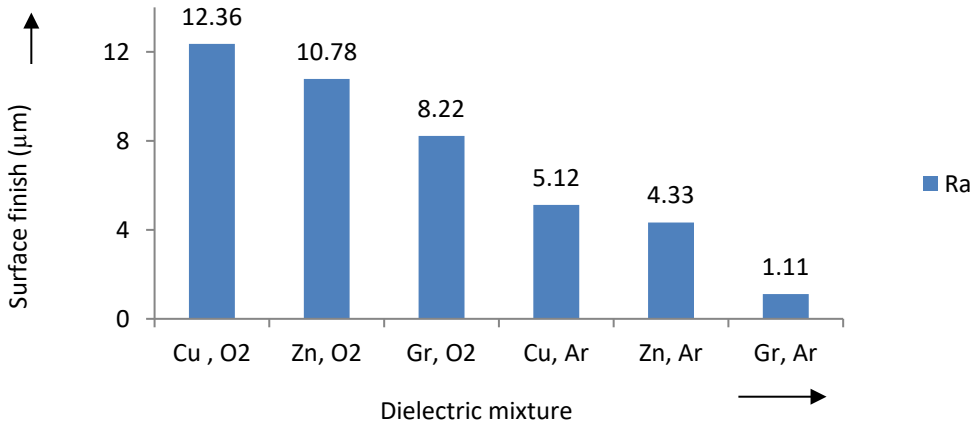

Figure 6.12 Effect of type of dielectric mixture on the Ra

It was observed that the micro-hardness at the machined area increased due to surface modification by using powder additives (Kumar and Batra, 2012). In the preliminary experiments in this research, the micro hardness was found to be maximum of 820.30 Vickers hardness number (HV) in case of zinc additive dielectric medium due to its high hardness and low electrical conductivity value followed by copper powder (671.1 HV) and graphite powder (194.13 HV) (Figure 6.13). Among all the three metallic powders, zinc additive laden dielectric medium obtained highest micro-hardness because the smallest spark gap at the machining area due to its low electrical conductivity. This small gap makes favourable conditions for piling of debris and in addition the amount of heat was removed from the machining area owing to low thermal conductivity of zinc powder. Therefore more amount of heat and quenching leads to harder surface (Talla et al. 2016, b).

The lowest value for residual stress (229 MPa) in machined EN-31 sample was with dielectric medium of copper additives with argon gas (Figure 6.13). Heat of fusion was considerably lower which resulted in lower value of thermal stresses and secondly lesser surface re-solidification phenomenon also contributed in reducing thermal residual stresses (Kruth and Bleys, 2000).

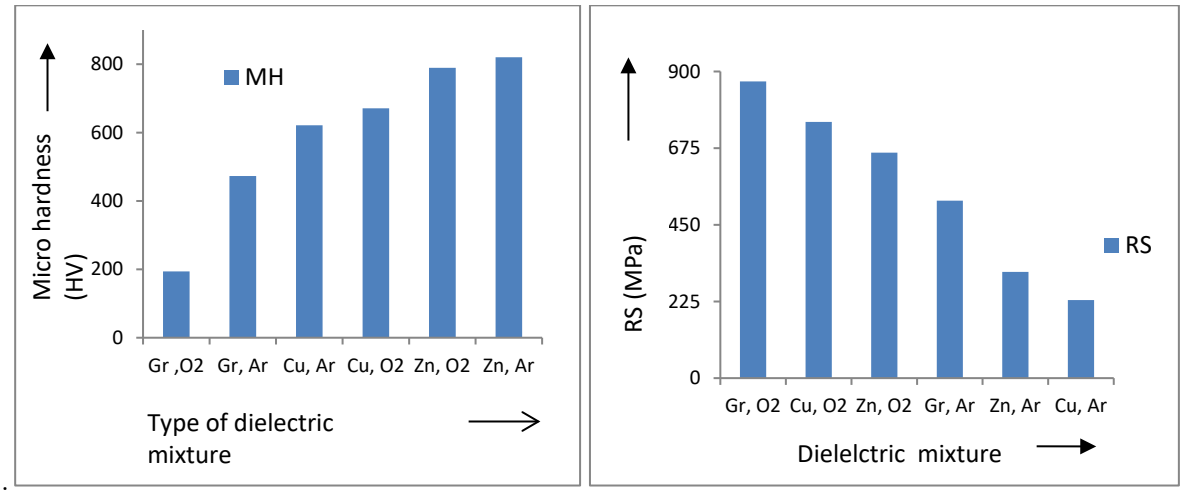

Figure 6.13 Effect of type of dielectric gas on the MH and RS

6.1.6 Type of Powders

The effect of different types of metallic powder on material removal rate and other response characteristecs was studied and there was significant improvement in PM-EDM efficiency by using correct type of metallic powders (Talla et al. 2017) . In this present study, further analysis was done for study of performance measure with different metallic powders in PMND-EDM. Comparitive study was performed between near-dry and powder mixed near-dry EDM for performance enhancement characterstics in terms of MRR, Ra and TWR by using aluminium, graphite and silicon powder. The properties of different powders used is shown in Table 6.1.

Table 6.1 Properties of metallic powders

Property (Units)	Graphite	Aluminium	Silicon
Electrical resistivity (μΩ-cm)	30	5	10000
Thermal conductivity (W/m-K)	25	238	163
Heat of fusion (kJ/mol)	117	10.79	50.21
Specific heat (J/kg-K)	710	910	710
Melting temperature (ºC)	3550	660	1414
Density (g/cm^3)	1.26	2.7	2.33
Mohs hardness (HV)	1.5	3	6.5

Summary

a) The range of process parameters was studied for further study and experimentation.

b) The different dielectric mixture were used to enhance the machining performance by using different gas and metallic powders

CHAPTER 7: THERMAL - PHYSICAL BASED MODELING FOR MATERIAL REMOVAL IN POWDER MIXED NEAR –DRY EDM

This chapter includes thermal-physical based modeling for material removal in Powder Mixed Near-Dry Electric Discharge Machining. This research includes three-dimensional axisymmetric model for PMND-EDM. Thermal properties of material, heat source shape (Gaussian heat distribution), heat distribution percentage among workpiece, tool and dielectric fluid, pulse on, pulse off and material ejection efficiency were considered as significant elements for predicting the MRR in PMND-EDM.

Many researchers had introduced different numerical methods for calculation of material removal per discharge and temperature distribution at electrodes in EDM. This area of research has been associated for developing a thermo-physical model for prediction of material removal under different experimental scenarios in Powder Mixed Near –Dry EDM as shown in Figure 7.1 while the complete methodology is shown in Figure 7.2. Finite Element method (FEM) modeling and simulation was carried out for prediction of material removal rate by using FEM software (ANSYS Workbench 16.0). This software programme clearly depicts the replica of the physical problem when identical constraints and boundary conditions were applied on it. Afterwards mathematical modelling was performed along with experimentation. Based on the results obtained, comparative study was performed for material removal rate.

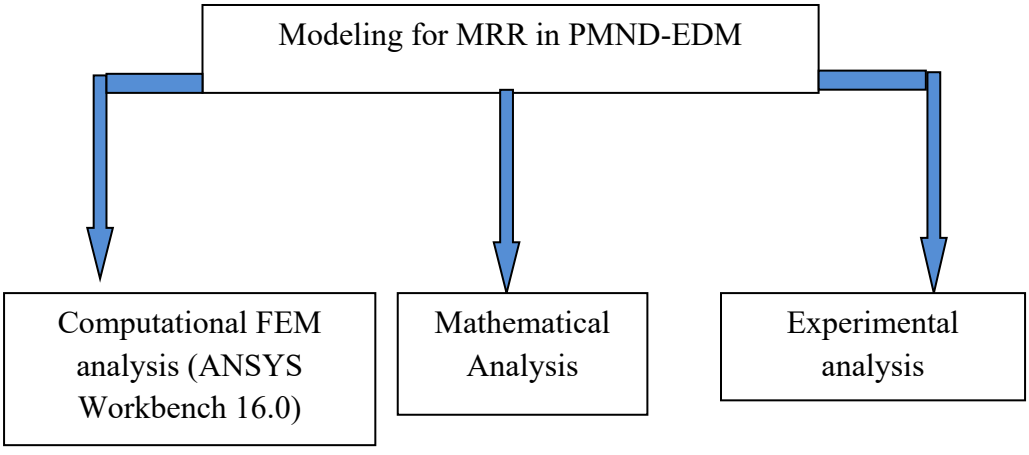

Figure 7.1 Modeling and Analysis for MRR in PMND-EDM

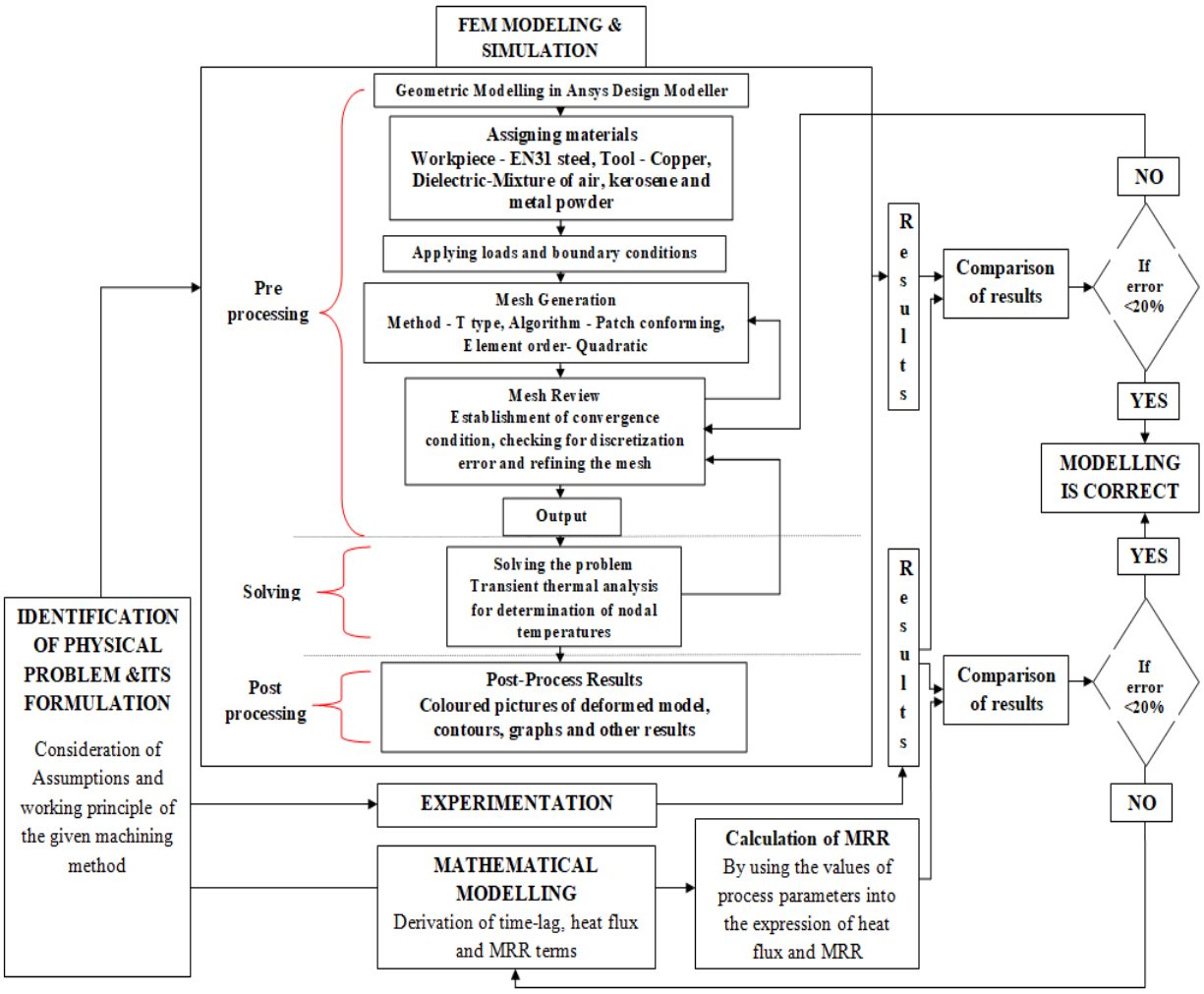

Figure 7.2 Complete methodology for modeling

The following assumptions were considered in order to obtain feasibility of the problem. Work piece and tool electrodes were assumed to be isotropic and homogenous in nature.

a) Single spark consideration was taken for modeling.
b) Properties of the workpiece and tool material were temperature dependent.
c) Variation in density and element shape for the workpiece were negligible, thermal expansion of the workpiece material did not change their values.
d) The radius of spark was function of time and discharge current.
e) Distribution of heat flux was following Gaussian distribution.
f) The spark zone was axisymmetric.
g) A certain fraction of total spark energy was received by the workpiece.
h) Absence of recast layers as the flushing efficiency was assumed to be 100 %.
i) Heat transfer mode for transfer of heat from plasma to workpiece and tool was conduction only.

j) The only possible mode of heat transfer between plasma and dielectric fluid was convection.
k) Transient un-steady thermal analysis was considered for studying the temperature variations during PMND-EDM process.
l) Workpiece material was not pre-stressed, neither thermally nor structurally prior machining.

7.1 Computational FEM Modeling and Simulation for material removal rate

For FEM modelling, a small portion was cut from the workpiece as shown in Figure 7.3 and several boundary conditions were applied over it to study the heat effect of the sparks by simulation over the machined sample. A single spark heat spark was applied on the surface of domain. Heat transfer by convection was applied over the remaining surface as cooling effect was provided by powder mixed dielectric fluid. It was assumed that there was no heat transfer on surface boundaries as they were far from spark radius zone.

Boundary conditions applied over the small portion of sample (PQRS) were K_1, K_2, K_3, K_4 and K_5:

For K_1: $0 \leq r \leq R$

$$K\frac{\partial T}{\partial z} = q_w(r) \tag{7.1}$$

Beyond spark radius, i.e. $R < r < \infty$:

$$K\frac{\partial T}{\partial z} = h(T - T_o) \tag{7.2}$$

For K_2, K_3, K_4 and K_5:

$$\frac{\partial T}{\partial z} = 0 \quad \text{(i.e. steady state)} \tag{7.3}$$

Where, h was heat transfer coefficient between powder mixed dielectric medium and the surface of the workpiece, heat flux $q_W(r)$ was created due to single spark, T_0 was the initial room temperature and T was the temperature attained after some time.

A Gaussian type heat source was considered and it was responsible for heating of the workpiece material. An incident plasma stream was responsible for heating phenomenon. This whole process is depicted clearly in Figure 7.4 (Kansal et al. 2008). The convection mode of heat transfer between two sparks was negligible and therefore was not considered in the present model. It was assumed in

previous models that all the heat was transferred to the workpiece from the plasma. It was later discovered that some percentage of heat was transferred to the dielectric medium and the tool electrodes as well, rendering this approach as unrealistic (Snoyes and VanDijck 1971, Jilani and Pandey 1982, Bhattacharya et al. 1996, Erden and Kaftanoglu 1981, Madhu et al. 1991, Marty 1977). They revealed by their work that anode and cathode absorbed 8% and 18% respectively and the rest goes to dielectric fluid. It was also proved by researchers that depending on type of dielectric medium and processing time, 40-45% was absorbed by the workpiece (Madhu et al. 1991, Dibitonto et al. 1989). Amount of total thermal energy that was transferred or conducted to the workpiece or F_c value assumed for this research was 18.3% (Schulze et al. 2004). Material flushing efficiency (MFE) was considered to be 100% in earlier models which meant that all the molten removed material from the workpiece was ejected out successfully. MFE was assumed to be 100% in present research study (Joshi and Pande 2010).

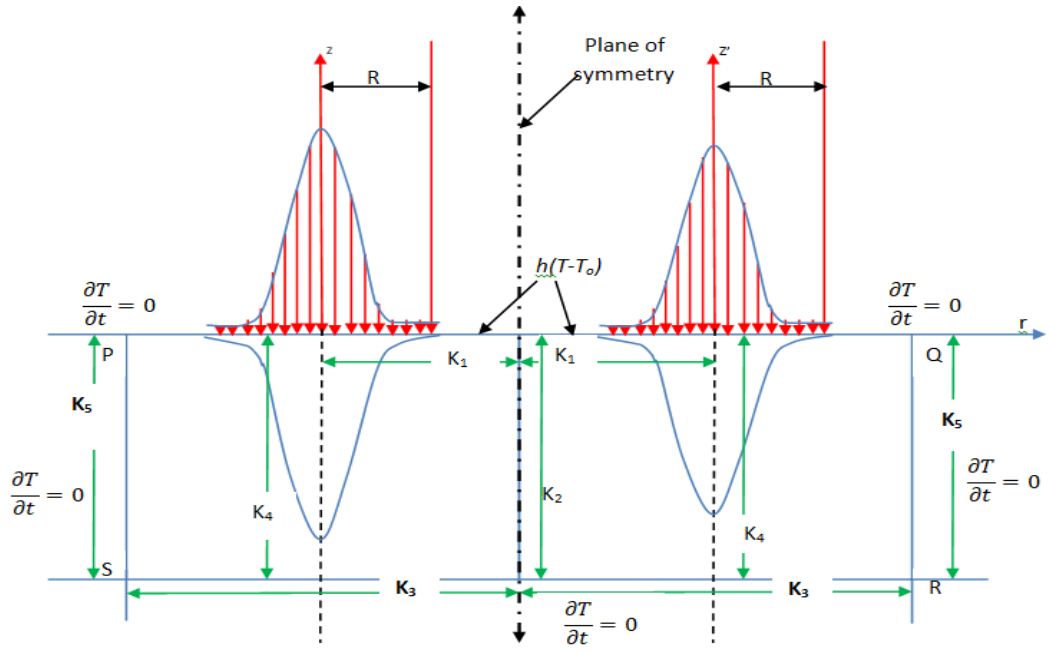

Figure 7.3 Diagram depicting the various boundary conditions used in mathematical modeling of PMND-EDM process

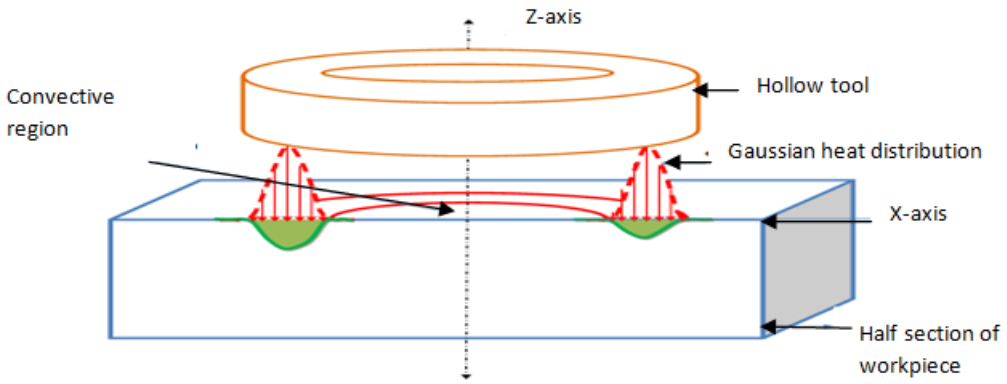

Figure 7.4 Diagram depicting the Gaussian heat distribution in PMND-EDM, at any instant of time 't'.

The governing equation (Eq. 7.4) was used for the calculation of heat flux applied on the workpiece in the presence of boundary conditions (like conduction, convection and regions of perfect insulation). In this way, a transient thermal problem was developed. In FEM model, boundary conditions were applied as a transient thermal load with time-steps in the order of microseconds on the workpiece.

$$\frac{1}{r}\frac{\partial}{\partial_r}\left(k_r r \frac{dt}{\partial_r}\right) + \frac{\partial}{\partial_r}\left(k_z \frac{dt}{\partial_{rz}}\right) = \rho\, C_p \frac{dt}{\partial_{rt}} \qquad (7.4)$$

Where T was temperature in kelvin, t is time (s), ρ was density (kg/m$^{3)}$, k_r and k_z were thermal conductivity (W/mK) coefficients in radial and axial direction respectively, C_p was specific heat capacity of workpiece material (J/Kg K), r and Z depict coordinate axis.

In modelling, a 3-D, 10 node tetrahedral axis-symmetric thermal solid element (SOLID87) was used for discretization of the continuum. Property like thermal conductivity which was temperature sensitive under the category of non-linear material properties was taken into the consideration. A very fine meshing was employed for building a precise and accurate FEM model and elemental size of 0.03 mm was considered for development. This optimized size was established by testing of vigorous convergence condition at 1, 0.5, 0.2, 0.15, 0.1, 0.015, 0.05, 0.04, 0.035 and 0.03 mm respectively. It was observed that the convergence condition was satisfied within 0.075- 0.03 mm and further miniaturization or diminishment of the element size was not giving the correct and justified results of temperature within the given time frame. A total of 7346748 nodes and 5019982 elements were present in the T-type meshed geometry. An additional refinement of conduction region at the level of 3 (highest level) was purposefully done to obtain smallest possible element.

This approach satisfies the convergence condition and ensures accurate interpolation of temperature values over that particular region. Due to this, fine temperature isotherms were obtained within that

region as this region was most prone for deformation due to high temperature. Aim of this analysis was solely to obtain the different sets of temperature isotherms over the workpiece during the machining.

Steps followed during FEM modeling of the given problem are as follows:

- Use of ANSYS mechanical enterprise product.
- Application of transient thermal analysis.
- Problem domain: Here, geometry of the workpiece was developed on Ansys Design modeler. The geometry of the workpiece was axis-symmetric about z-axis. Apart from that it was ensured that S.I units were right from geometric modeling to transient analysis. A meshed model of the given workpiece is shown in Figure 7.5.

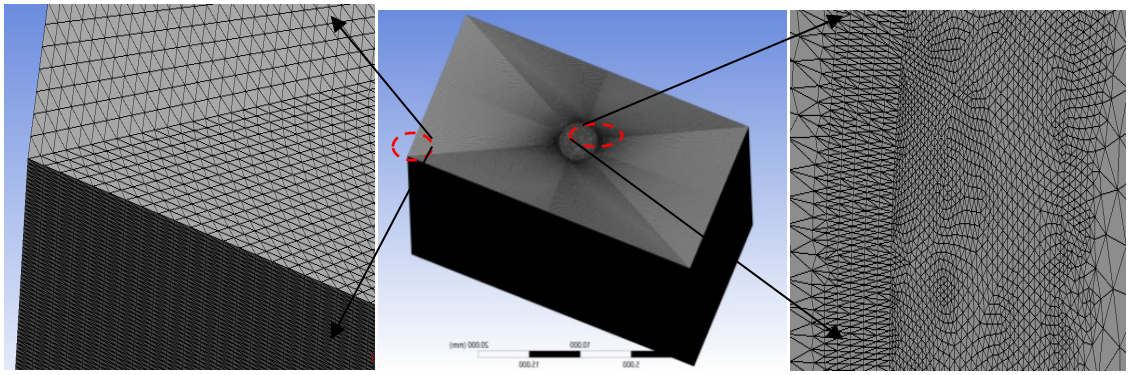

Figure 7.5 A 3-D meshed model of workpiece

This problem was solved by providing the calculated heat load value at the specified spark location and other boundary conditions as depicted in Figures 7.6 and 7.7 respectively. The time steps used for the problem were sum of P_{on} and P_{off}. Here, four different sets of P_{on} viz. 500, 200, 65 and 35µs were used with a constant P_{off} value of 125µs.

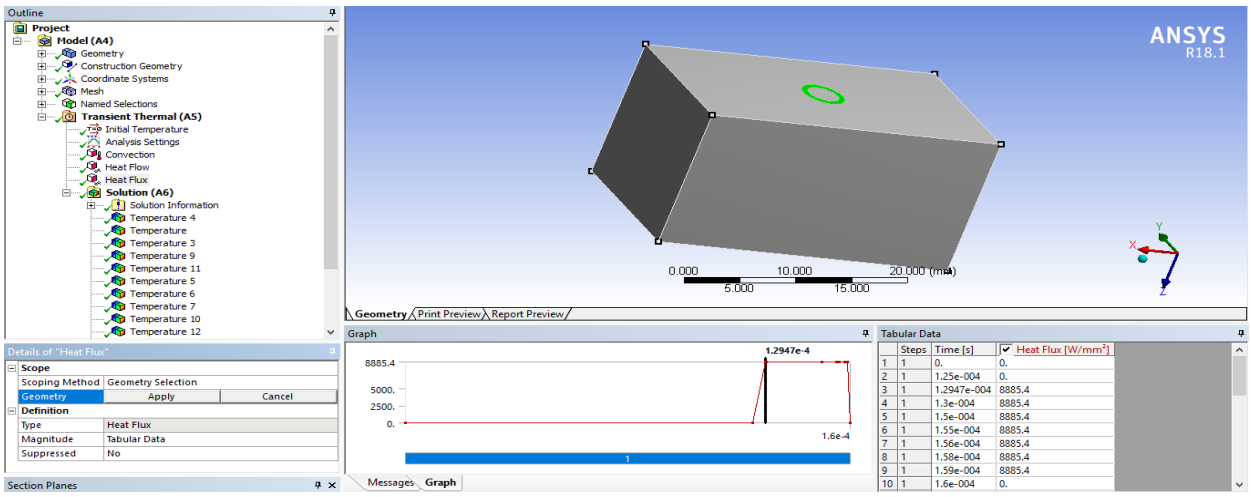

Figure 7.6 Heat flux conditions applied at workpiece for a particular powder concentration and total pulse duration value

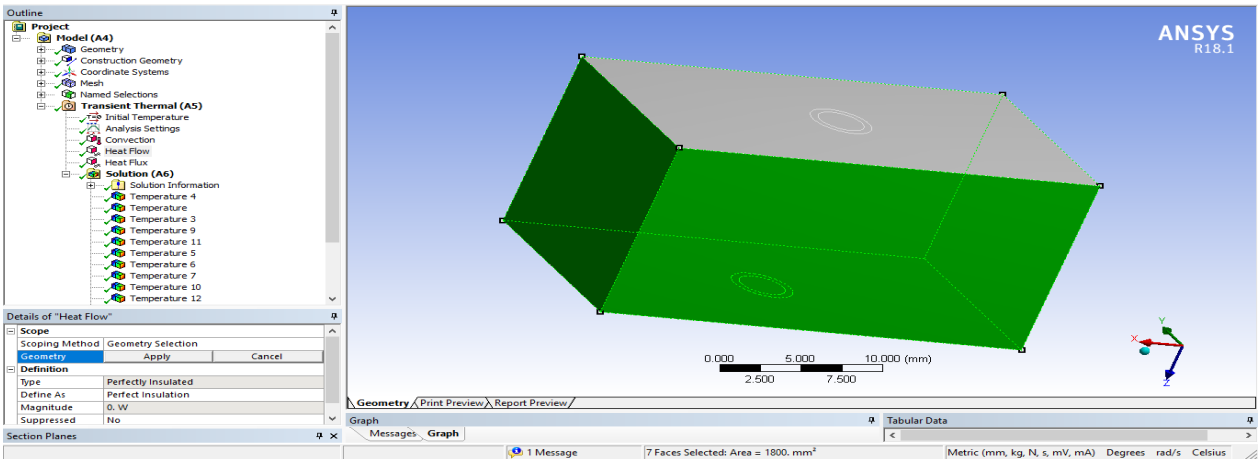

Figure 7.7 Boundary conditions applied at workpiece for a particular powder concentration and total pulse duration value

7.1.1 MRR estimation through Finite Element Analysis

a) Different temperature isotherms obtained after transient thermal analysis were used for investigation of amount of workpiece metal machined from the surface of the workpiece.

b) A region (area) was estimated as the deformed/eroded region within the sets of different temperature isotherms. The temperature of the isotherms was greater than the melting point of the workpiece material or perhaps more than 60-70^{0}C than melting point (conservatively). At these isotherms various nodes positions were determined which were further used to calculate the eroded material volume during machining.

c) Material removal calculation due to single spark discharge was done by calculating the volume of semi-toroidal shape obtained after machining of workpiece (region within which conduction has taken place). This semi-toroidal shape was further divided into numerous cylindrical discs as shown in Figure 7.8.The x,y and z coordinates of the node boundary generated by transient analysis were used for calculating the crater volume (Joshi and Pande 2010).

Total crater volume:

$$V_{vt} = \sum_{p=0}^{n} j_i \quad (7.5)$$

$$J_i = \pi\left(R_i^{\,2} - r_i^{\,2}\right) * \left|(z_o - z_i)\right| \quad (7.6)$$

Furthermore, MRR was given as;

$$MRR = \frac{60 * V_{vt}}{P_{on} - P_{off}} \left(mm^3/_{min}\right) \quad (7.7)$$

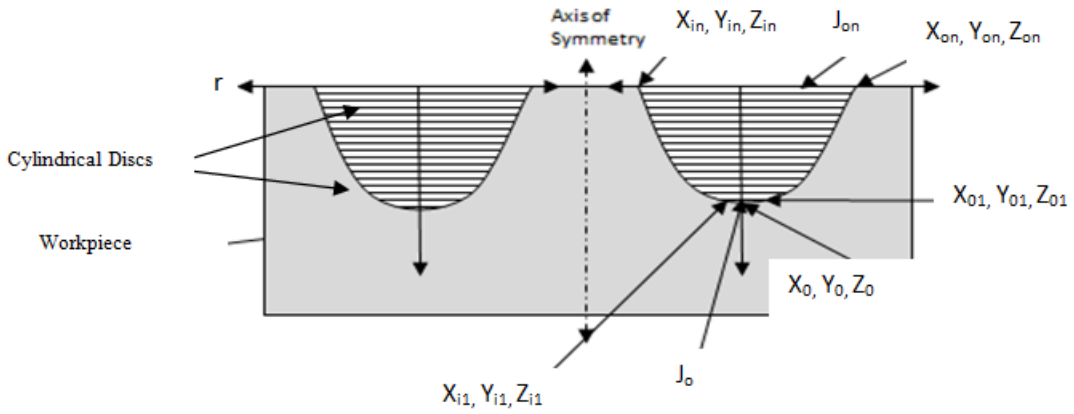

Figure 7.8 Volume measurement method ofa semi-toroidal crater

7.2 Mathematical modeling for material removal

The basic governing equation between workpiece and tool during spark was given by Fourier heat conduction given (Eq. 7.4). Gaussian distribution was used in order to obtain accurate isothermal curves in thermal model for PMND-EDM as shown in Figure 7.9 (Patel et al. 1989, Bhattacharya et al. 1996).

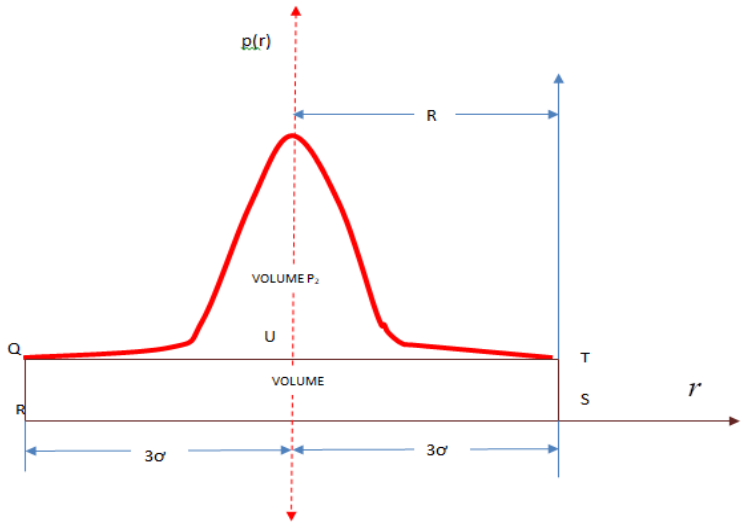

Figure 7.9 Gaussian distribution for thermal model

A representation of the heat distribution Gaussian curve with respect to random variable ‘ r’ is given by Eq.7.8.

$$p\,(r) = \frac{1}{\sqrt{2\pi\sigma}} e^{\frac{-r^2}{2\sigma^2}} \qquad (7.8)$$

Where $\frac{1}{\sqrt{2\pi}\sigma}$ indicated the maximum value that the distribution could attain and σ depicted standard deviation.

Mathematics proves that zero value of Gaussian curve could be possible only when random variable 'r' attained infinity. Due to this reason a definite region on the 'r' axis was considered for depicting the crater's bottom. Standard deviation (σ) varied between (−3σ to and +3σ) thus 99.75% of the values lies within the region (r = μ−3σ and r = μ+3σ). Three-dimensional representation of the crater was obtained by giving a complete rotation to the Gaussian curve about the vertical axis.

So, R = 3σ; putting the value of σ into above equation ie Eq. 7.8, a new Eq. 7.9 was obtained;

$$p(r) = \frac{3}{\sqrt{2\pi R}} e^{-4.5\left(\frac{r}{R}\right)^2} \quad (7.9)$$

p(r) refer to the amount of heat energy received by the work surface of the workpiece specimen, shown by q_W and was a function of ' r'

At r = 0, p(r) = q_0; (7.10)

Where, q_0 denote the maximum amount of heat energy received at the center of the work surface of the workpiece specimen. Heat flux of the system was given by Eq.7.5.

$$q_w(r) = q_o e^{-4.5\frac{r^2}{R^2}} \quad (7.11)$$

Thus the energy incident on the workpiece is given by Eq. 7.6:

$$\int q_w(r) dA = \int_o^R q_w(r) 2\pi r dr \quad (7.12)$$

On further calculation and simplification, Eqs. 7.13 and 7.14 were obtained;

$$= -\frac{\pi R^2}{4.5} q_o e^{-4.5\left(\frac{r}{R}\right)^2} \quad (7.13)$$

$$= 0.2191\, \pi\, q_o R^2 \quad (7.14)$$

The rate at which heat energy was incident on the workpiece was identical to the supplied electrical energy rate (Fc*V*I).

Where, F_c was the fraction of heat input to the workpiece, V_b was the breakdown voltage and I represent the current. Upon equating with Eq. 7.14; a new Eq. 7.16 was obtained.

$$F_c V_B I = 0.219\,\pi q_o R^2 \tag{7.15}$$

$$q_o = \frac{4.57\,F_c V_B I}{\pi R^2} \tag{7.16}$$

By putting the value of q_o from Eq.7.16 into Eq.7.11 and considering critical radius at which maximum heat flux was applied (R ˜ R_{pc}), the expression obtained is given in Eq.7.17.

$$q_w(r) = \frac{4.57\,F_c\,V_b I}{\pi\,Rc^2}\,e^{-4.5\left(\frac{r}{Rc}\right)^2} \tag{7.17}$$

Since critical radius was defined as (Joshi and Pande 2010),

$$R_c = (2.303e\text{-}3)\,I^{0.43}\,t_{on}{}^{0.44}\mu m \tag{7.18}$$

By using this value of Rc in Eq. 7.17, the heat flux equation derived and used in thermal model for EDM (Joshi and Pande 2010), all the corresponding 'r' value will now be time dependent 't' therefore $q_w(r)$ gets converted to $Q(t)$ and new expression for heat flux was obtained given in Eq.7.19;

$$\mathrm{Q(t)} = \frac{3.4878*10^5*F_c\,VI^{0.14}}{t_{on}{}^{0.88}}\left(e\left\{-4.5\,\left(\frac{t}{t_{on}}\right)^{0.88}\right\}\right) W/mm^2 \tag{7.19}$$

Above expression was rate of heat flux supplied from the tool to the work piece. Since, t_B or break down timing was defined as (Erden and Bilgin 1981);

$$t_B = \frac{6\pi\eta x^2\,ln\gamma_{cr}}{s^2(E-E_o)^2} \tag{7.20}$$

Q or rate of heat supplied at workpiece was obtained by multiplication of rate of heat flux with that area of workpiece over which the heat flux was acting.

$$Q = Q(t) * A \tag{7.21}$$

Therefore, *q'* or heat supplied at the workpiece within the break down interval was given by;

$$q' = Q * t_B \quad (7.22)$$

Material removed at each discharge was given as (Jain 2009);

$$MRR_d = K_{\emptyset} * q' \quad (7.23)$$

Where $K_{\emptyset}$ is a constant;

So, the MRR will be expressed by;

$$\text{MRR} = \frac{MRR_d * 60 * 10^9}{t_B}$$

$$\text{MRR} = \frac{K_{\emptyset} * q' * 60 * 10^9 * s^2 (E - E_o)^2}{6\pi\eta x^2 ln\gamma_{cr}} \quad (7.24)$$

While calculating heat flux through Eq.7.17 expression "*t*" was replaced by t_B as we are considering that whole heat energy in the form of plasma was released within that period of time after complete charging of the capacitor of RC circuit.

Further, t_B *(break down time)* was calculated by including critical concentration ratio. Eq. 7.20 gives a direct relationship between powder concentration and t_B. The Kø value was firstly determined form experimental results of MRR and then it was used in Eq. 7.23.

7.3 Experimental material removal rate

As per the literature review, effects of various machining parameters such as discharge current, pulse on time, current and voltage on output response i.e. MRR were studied. Multi-phase dielectric oil has been used as dielectric fluid throughout the tests. The experiments were conducted according to the given scheme of experiments as shown in Table 7.1. Effect of four process parameters was studied for analysis of MRR. The experimentation for MRR analysis was conducted as per the three different scenarios given below.

MRR was calculated by the formula given below:

$$MRR = (W_i - W_f)/(\rho \times T_m) \quad (7.25)$$

Table 7.1 Process parameters and their levels selected for experimentations

S. No	Symbol	Process Parameter	Level (Range)
1	A	Pulse on time (P_{on})	35-500
2	B	Voltage (V)	25
3	C	Current (I)	12
4	D	Powder concentration N_∞ (g/l)	5,10,15

- **Data used:**

I^st Scenario: V=25 V, I=12A, η=4.26 10^-3 Pas, γ_cr=7.8, N_∞=5g/l, s=12.5*10^-3 mm, t_B=2.334μs*

II^nd Scenario: V=25 V, I=12A, η=6.89 10^-3 Pas, γ_cr=1.6, N_∞=10g/l, s=12.5*10^-3 mm, t_B= 0.7213μs*

III^rd Scenario: V=25 V, I=12A, η=7.231 10^-3 Pas, γ_cr=6, N_∞=15g/l, s=12.5*10^-3 mm, t_B= 4.469μs*

The analysis for result of material removal in FEM modeling using ANSYS workbench and mathematical model are discussed in result and discussion part in chapter 8. The comaparative analysis has been done along with experimental approach for the validation of the results pertaining to material removal in PMND-EDM.

Summary

(a) Thermo-physical model was developed for prediction of material removal under different experimental scenarios in Powder Mixed Near –Dry EDM.
(b) FEM software, ANSYS Workbench 16.0 was used for modeling and simulation.
(c) Mathematical model was developed for the Powder Mixed Near –Dry EDM.
(d) A computational model was proposed for study of effect of metallic powder concentration, Pulse on, voltage and current on material removal.

This chapter includes result and discussion related to present investigation. This section includes validation of model through experimental and analytical means. Further discussion was related to optimization of process parameters and their effect on output performance characteristics. The best combination of the parameters was found for improving the machining efficiency. Later confirmation experiments were conducted to verify the results. Lastly analysis of machining performance was done based on gaseous assisted EDM with powder additives.

8.1 Model Validation for MRR in PMND-EDM

The proposed FEM model was validated through experimental and analytical modeling. MRR values calculated from analytical modeling (chapter 7) and experimental results were compared. MRR value was obtained by studying the temperature distribution of FEM model. Data regarding this comparison is shown in Table 8.1.

Experiments were conducted in three different scenarios (Refer Chapter 7). Results obtained from FEM modeling were in terms of set of temperature isotherms at different levels of time steps (i.e at different values of P_{on}). A different set of temperature isotherms were obtained at each average powder concentration level. From these isotherms variation in size of deformed region was clearly indicated in Figure 8.1. This could be checked by taking co-ordinates of extreme nodal points in each case. This meant that due to decrease in pulse on (*Pon),* the plasma size was increasing radially.

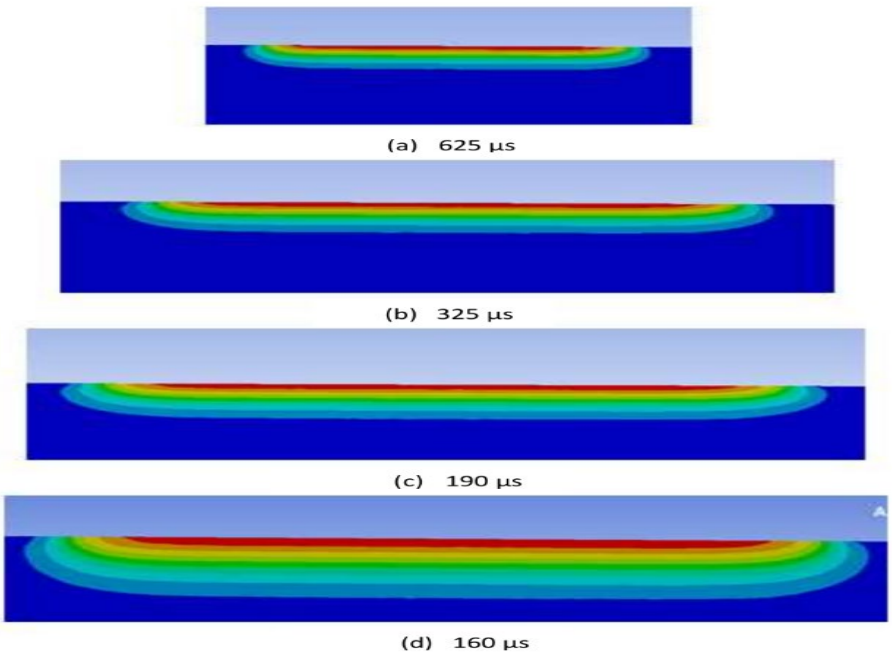

Figure 8.1 Temperature isotherms showing the extent of deformation zone obtained at discharge location (at the cross-section of the workpiece) corresponding to different pulse durations

Extent of deformation zone created during each pulse duration was clearly depicted in the Figure 8.1. One could observe that as the pulse duration kept on increasing, the spark area got increased which ultimately lead to material removal of larger volume.

Since metallic powder was used in PMND-EDM, a comparatively high degree of conduction takes place within the workpiece. Bridging effect or chain like phenomenon takes place at the machining gap due to introduction of metallic powder additives (Kansal et al. 2005). Interlocking of grains leads to chain like formation of powder particle due to which discharge gap between the tool and workpiece increases. This results in more energised spark plasma and due to this, heat gets distributed to a larger area of the workpiece as compare to traditional EDM process in the presence of same levels of process parameters used (current, voltage and pulse-on time) with reduced electrical density. These conditions resulted in increase of discharging frequency, further resulting in faster sparking at the workpiece surface due to which the erosion rate increases.

The experimental, theoretical and FEM results at all the three scenarios were obtained. Comparative study was conducted by means of graph plotted between total pulse duration and MRR at three different powder concentrations for all methods respectively. All the experiments in this study were repeated three times each to ensure the repeatability and final value are representation of average values in Table 8.1. Based upon these values graph for each case was plotted (Figures 8.3 – 8.5).

Table 8.1 Results obtained from experimentation, mathematical and finite element modeling and their error estimation

S.no	**P_{on} (µs)**	**q (W/mm²)**	Ist Scenario					q (W/mm²)	IInd Scenario					q (W/mm²)	IIIrd Scenario				
			MRR (mm³/min)						MRR (mm³/min)						MRR (mm³/min)				
			Error =(B-A)/B			Error =(C-A)/C			Error =(E-D)/E			Error =(F-D)/F			Error =(H-G)/H			Error =(I-G)/I	
			(A) Exp.	(B) Math.	Error %	(C) FEM	Error %		(D) Exp.	(E) Math.	Error %	(F) FEM	Error %		(G) Exp.	(H)Math.	Error %	(I) FEM	Error %

1	**500**	1743.90	0.92	0.99	7.0	1.10	16.36	1789.50	0.88	0.98	10.20	1.08	18.52	1691.40	0.25	0.28	10.71	0.31	19.35
2	**200**	3717.00	1.69	2.11	19.90	2.01	15.92	3937.70	1.76	2.05	14.14	2.17	18.89	3468.79	0.28	0.33	17.85	0.29	3.44
3	**65**	8950.40	3.87	4.77	18.86	4.55	14.94	10033.00	4.57	5.45	16.14	5.73	8.23	7134.60	0.56	0.68	17.64	0.69	18.84
4	**35**	12439.00	5.86	7.04	16.76	6.29	6.83	16257.30	7.68	8.82	12.92	8.77	12.43	8885.35	0.73	0.86	15.11	0.83	12.04

8.1.1 Effect of pulse-on time and powder's concentration on MRR

The volume of material removal was increased with decrease in pulse-on time. The reason attributed to this phenomenon was that due to decrease in pulse on time, the uniform supply of heat to the workpiece increased as more number of discharges takes place in this condition. Hence larger volume of the workpiece experienced temperatures higher than its melting point.

It was seen that as the value of N_{∞} or N_{avg} increased from 5 to 15 g/l, the heat supplied to the workpiece first increased, then decreased due to which volume of material removal also followed a similar pattern. As a result, the temperature variation over the workpiece surface also changed as shown in Figure 8.2.

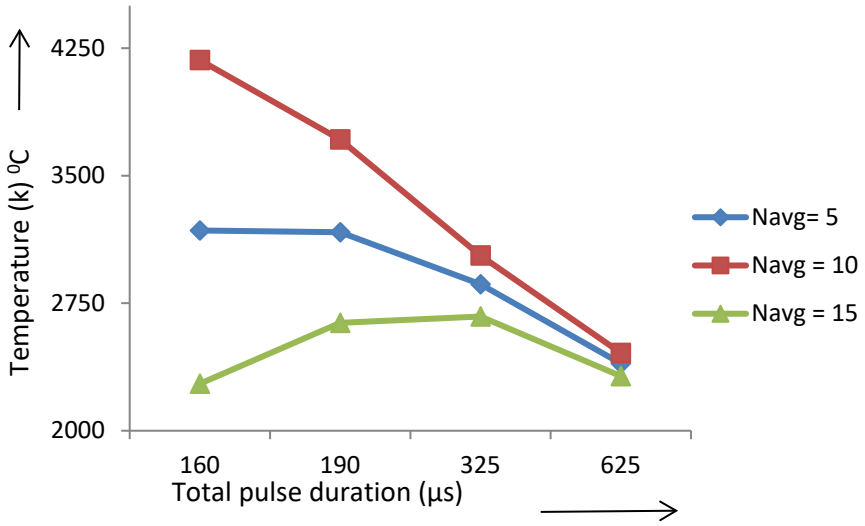

Figure 8.2 Temperature distribution at various pulse durations corresponding to various N_{avg} (g/l) values

This was also due to the fact that improper arcing occurred as the critical concentration value increased (due to increase in concentration of metallic powder in the dielectric medium). It was observed that significantly large changes in MRR were absent as the powder concentration was raised, because for copper and steel combination (for tool and workpiece respectively) the time-lag did not vary for a large extent. Also, the occurrence of short and open circuits was not very frequent in this case (Van Dijck and Dutre, 1974).

These small variations in time-lag value brought increase in net amount of heat delivered to the workpiece which resulted in increment of MRR value as N_{∞} increased from 5 to 10 g/l. But after N_{∞}=10 powder concentration increased so much that haphazard flow of heat took place within the IEG. As a result, a considerable amount of heat was lost to the surroundings and workpiece received a lesser amount of heat. A comparatively constricted (smaller in area) deformation zone was formed, which resulted in reduction of MRR. This increasing and decreasing nature of MRR at various powder concentration values corresponding to various pulse duration values is clearly depicted in Figure 8.3 – 8.5.

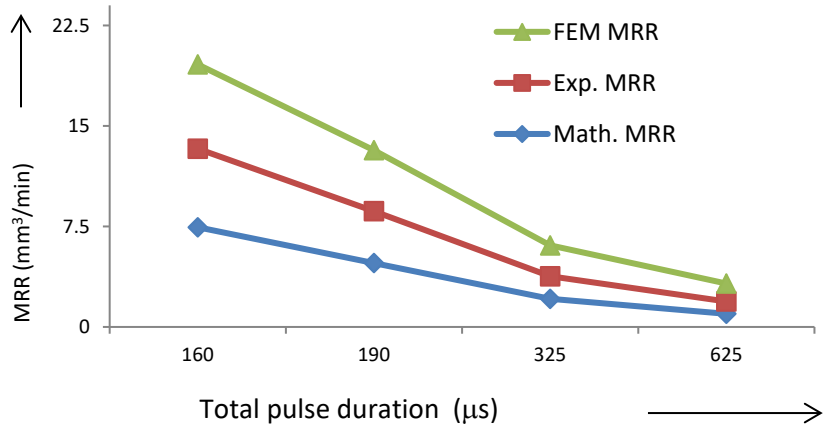

Figure 8.3 Graph between MRR and total pulse duration with metallic powder concentration of 5g/l

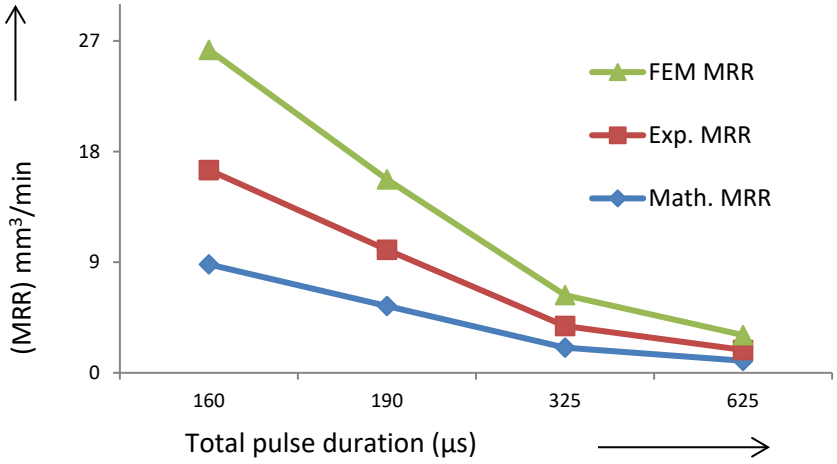

Figure 8.4 Graph between MRR and total pulse duration with metallic powder concentration of 10g/l

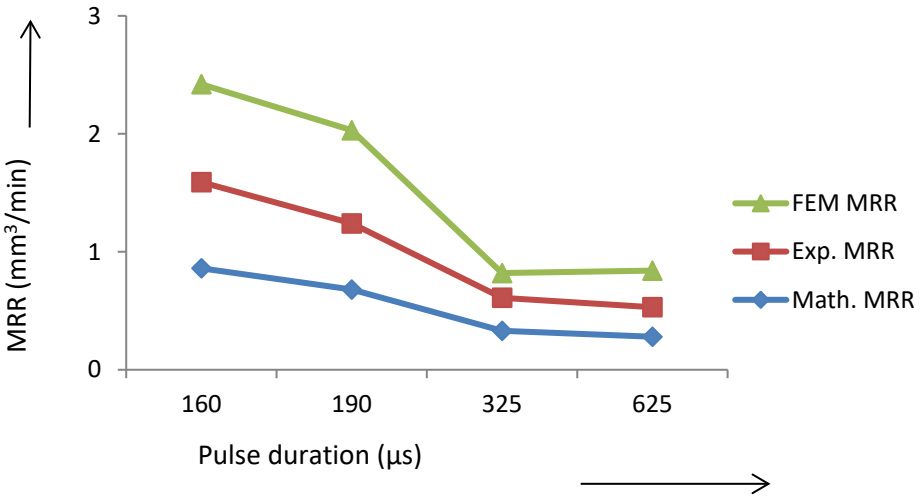

Figure 8.5 Graph between MRR and total pulse duration with metallic powder concentration of 15g/l

On increasing the powder concentration from 5 to 15 g/l, only a meagre change in time-lag would be observed which further would result in increase and then decrease vale of MRR. It was observed from the graphs that the MRR was very low for higher ranges of P_{on} but there was increasing trend in MRR as the P_{on} duration was decreased further. The MRR was maximum in scenario 2nd followed by 1st and 3rd respectively as shown in Figure 8.3 – 8.5.

The deformation region was decreasing as the powder concentration level had surpassed 5 g/l value to 10 g/l and 15 g/l. This fact suggested that an increase in metallic powder concentration level in dielectric was helping in widening of discharge channel due to increased level of conduction during machining. But too much increase in concentration level caused haphazard flow of heat over the workpiece, which ultimately lead to loss of most of the heat received by the workpiece.

8.2 Optimization

The experiments were conducted by Taguchi parametric approach. Optimization was performed and effect of parameters was studied on material removal rate, surface finish, micro-hardness, residual stress and tool wear rate. The plotting of graphs for raw value and S/N ratio was done in order to study the parametric effect. The analysis of variance (ANOVA) was carried out for raw data and S/N ratio to identify significant variables.

8.2.1 Optimization of Material Removal Rate (MRR) in PMND-EDM

Series of experiments were performed as per Taguchi L_9 (OA) as per Table 8.2 for material removal rate (MRR). Each series of experiment was performed in three runs and a total of 27 experiments each were performed for analysis of MRR respectively. The experiments were performed as per Taguchi L_9 (OA). The experiments were conducted for analysis of MRR. Each series of experiment was run for three trials and the results obtained are shown in Table 8.2.

Table 8.2 Experimental Results for Material Removal Rate as per Taguchi L_9 OA

Exp. No	Parameter trial condition				MRR (mg s^{-1})			S/N (dB)
	A	B	C	D	R1	R2	R3	
1	2	5	2	0.4	0.07	0.06	0.09	-24.11
2	2	10	5	0.5	0.22	0.10	0.21	-18.12
3	2	15	8	0.6	0.37	0.30	0.36	-11.04
4	3	5	5	0.6	0.01	0.01	0.01	-40.40
5	3	10	8	0.4	0.03	0.02	0.05	-30.29
6	3	15	2	0.5	0.08	0.05	0.01	-32.60
7	4	5	8	0.5	0.07	0.07	0.19	-23.21
8	4	10	2	0.6	0.10	0.07	0.10	-22.39
9	4	15	5	0.4	0.08	0.08	0.10	-22.74
Total					1.07	0.80	1.16	
Overall mean MRR ($\overline{MRR}$) = 0.11mg s^{-1}								

The average values and main effects values of MRR were calculated at different levels which were L1, L2 and L3 while the S/N ratio and raw data values at different levels of parameters are shown in Table 8.3. Pooled ANOVA (analysis of variance) for MRR at confidence level (95 %) is shown in Table 8.4. The tabulated value for F-ratio was 3.55 for raw data while the tabulated F-ratio value for S/N was 19. The average values of MRR was calculated and plotted as shown in Figure 8.6. It is clearly shown in Figure 8.6 that parameters A, B, C, and D at levels 1, 3, 3, 3 respectively were most effective in increasing MRR. Similarly, signal to noise ratios were also calculated and display the same trend in Figure 8.6. The parameter A at 1st level, parameter B at 3rd level, parameter C at 3rd level and parameter D at the 3rd level were most effective in increasing the MRR. Some of the machined workpiece samples are shown in Figure 8.6.

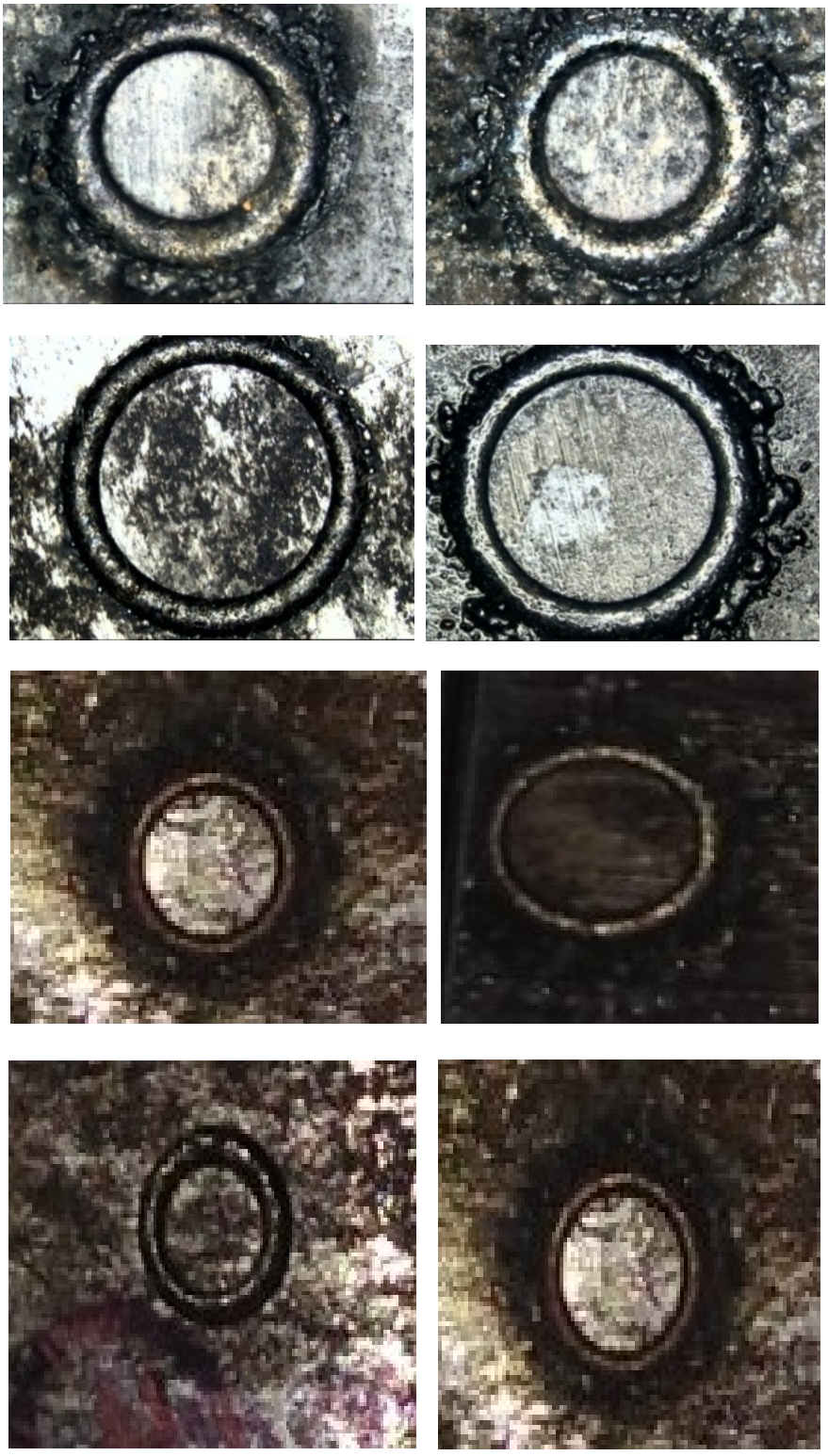

Figure 8.6 Machined workpiece samples

The exit area for the dielectric medium from tool electrode tip at level 1 was low due to which the velocity of the dielectric coming out from the tool tip was very high as per continuity law. The sparking was very vigorous at the inter-electrode gap due to this increased velocity of the medium along with the metallic powder. This nature of velocity of the dielectric medium enhanced the

interaction of ions and molecules at machining gap which resulted in a high value of MRR. The discharge velocity of dielectric medium gets reduced on further increase of tool tip area at level 2, due to which the plasma reaction was not that significant and therefore the MRR gets reduced to the lowest value. The dielectric medium quantity at machining gap increased on further increase of tool tip diameter at L_3 due to which MRR again displayed increasing trend as shown in Figure 8.7 (a). There was similar trend for MRR with respect to tool electrode pipe thickness as per the research conducted by Zhang et al. (2002).

The MRR tends to increase with the increase in mist flow rate (Figure 8.7 b). High volume flow rate helps in faster flushing of debris and therefore results in faster erosion over the workpiece. The effect of metallic powder as an additive in the dielectric mist led to increase in sparking frequency many times due to wide energized plasma which was obtained by the bridging effect of powder particles. The grains of powder particles interlock themselves which results in formation of bridge at the machining gap and they start behaving as the conductors. This phenomenon intensifies the electric field and early explosion of sparks gets initiated. This phenomenon also reduces the insulating strength of the dielectric medium. The machining gap gets increased due to which the plasma channel also increases, therefore, more heat was transferred between the tool and workpiece electrodes which results in higher erosion rates Figure 8.7 (c). Bai et al. (2013, b) also stated increase in material removal with the metallic powder additives. The material removal rate was more but upon further increase of metallic powder concentration, there was decrease of material removal rate due to over-clustering of powder particles. Therefore optimum range of experimentation was performed up to 8gm/l powder concentration.

Similarly, the pressure of dielectric mist also showed the same trend on MRR (Figure 8.7 d). The flushing effect over the machined area was improved significantly due to which there was a phenomenon of effective quenching and a good degree of fluidity. High pressurized mist assisted in removing the debris from the crater efficiently which provided favourable conditions for flushing and enhanced repetitive discrete discharge for an increase in MRR in machined products by PMND-EDM. The experimental work was comparable to research performed related to Near Dry machining with powder additives and similar trend was observed for effect of mist pressure on MRR (Bai et al. 2013 c). Similar trend for increase of MRR with respect to dielectric pressure was observed by Shen et al.2015.

Table 8.3 Average values and Main effects: MRR (mg s^{-1})

Process parameter	Level	Tool diameter (A)		Flow rate (B)		Powder concentration (C)		Pressure (D)	
Type of data		S/N Ratio	Raw data	S/N Ratio	Raw data	S/N Ratio	Raw data	S/N Ratio	Raw data
Average values (% MRR)	L1	-17.75	0.20	-29.24	0.06	-26.37	0.07	-25.71	0.07
	L2	-34.43	0.035	-23.60	0.10	-27.08	0.09	-24.64	0.11
	L3	-22.78	0.09	-22.12	0.16	-21.51	0.16	-24.61	0.15
Main effects (%MRR)	L2-L1	-16.67	-0.16	5.63	0.04	-0.71	0.01	1.06	0.04
	L3-L2	11.65	0.06	1.47	0.05	5.57	0.07	0.03	0.03
Differences (L3-L2)-(L2-L1)		28.32	0.22	-4.15	0.01	6.28	0.05	-1.03	-0.01

Table 8.4 Pooled ANOVA raw data and S/N data for MRR

Source	SS raw	SS S/N	SS' raw	SS' S/N	DOF raw	DOF S/N	V raw	V S/N	F-ratio raw	F-ratio S/N	P% raw	P% S/N
Tool Diameter	0.12	439.17	0.12	436.81	2	2	0.06	219.58	44.15	186.17	47.81	75.55
Flow rate	0.09	84.57	0.08	82.21	2	2	0.04	42.28	24.65	35.85	19.86	14.55
Powder concentration	0.04	55.14	0.03	52.78	2	2	0.02	27.57	14.18	23.37	15.35	9.48
Pressure	0.03	2.35	0.02	*	2	*	0.01	*	10.34	-	11.20	*
Error	0.02	2.35	0.03	9.43	18	2	0.001	1.17	-	-	9.74	0.40
Total	0.27	581.24	0.28	581.24	26	8	-	-	-	-	100	100

*Significant at 95% confidence level, F- critical=3.55 (Tabular value for raw data), SS- Sum of squares, DOF- Degree of freedom, V- variance , F- critical=19 (Tabular value for S/N data), SS'= Pure sum of squares.

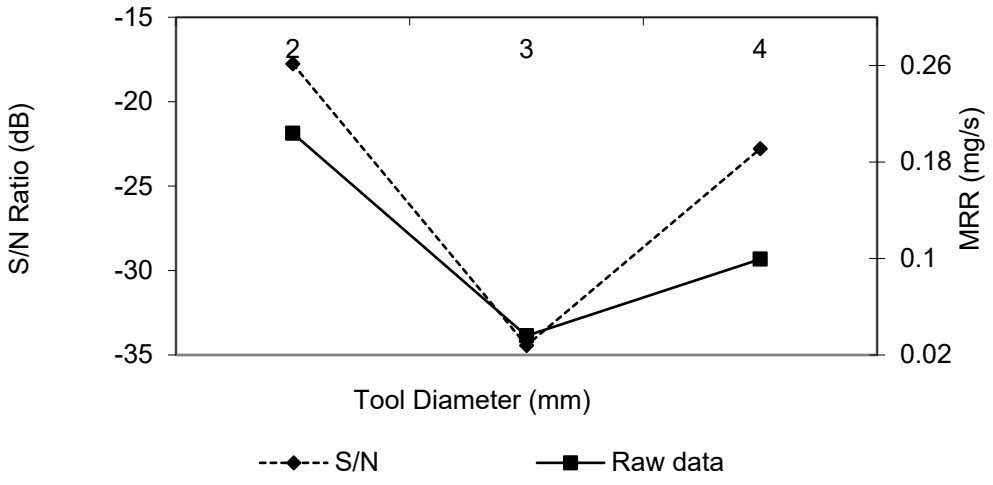

Figure 8.7 (a) Effect of tool type on MRR (mg s^{-1})

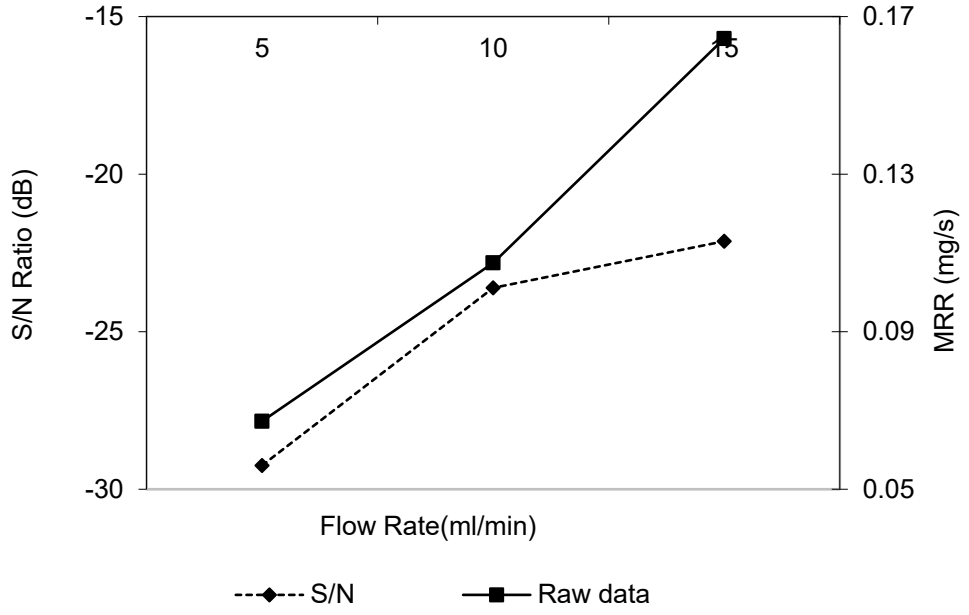

Figure 8.7 (b) Effect of flow rate on MRR (mg s^{-1})

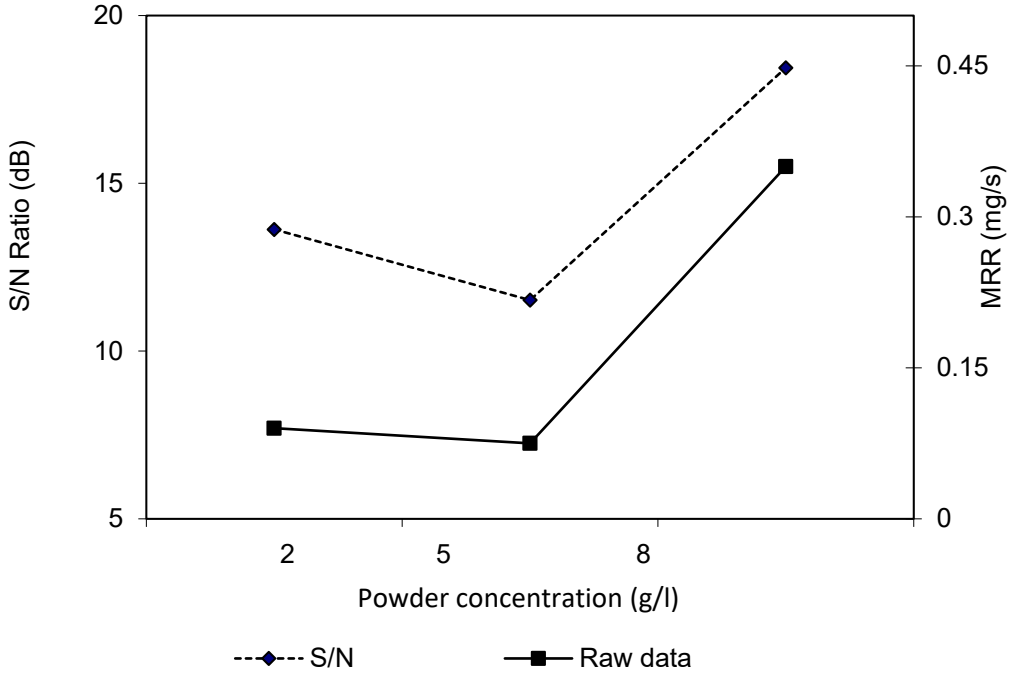

Figure 8.7 (c) Effect of powder concentration on MRR (mg s^{-1})

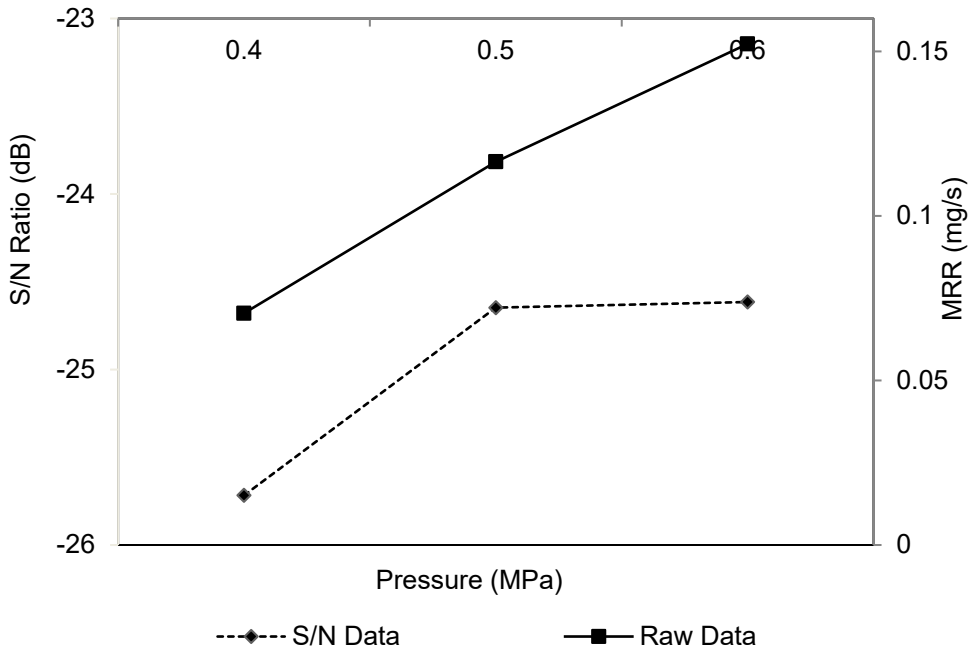

Figure 8.7 (d) Effect of pressure on MRR (mg s^{-1})

Overall, the plasma channel was small with lower levels of parametric setting due to which fewer craters can be seen after machining of the workpiece, as shown in Figure 8.8. Intensive craters over the machined surface were observed in Figure 8.9, which signifies that a higher erosion rate was achieved as the concentration of metallic powder was increased. A high energy enlarged plasma channel due to increased metallic powder concentration was the main reason for higher erosion. The electrical resistivity decreases, and the working gap expands due to the presence of metallic powder in EDM oil (Wong et al.1998). This phenomenon stabilizes the arc through better flushing and servo-hunting.

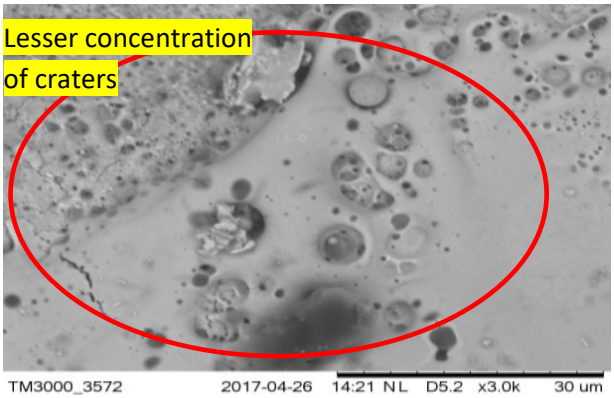

Figure 8.8 SEM image of a machined surface with lower levels of parameters (image width: 68.8 µm, accelerating voltage 15.0 kV)

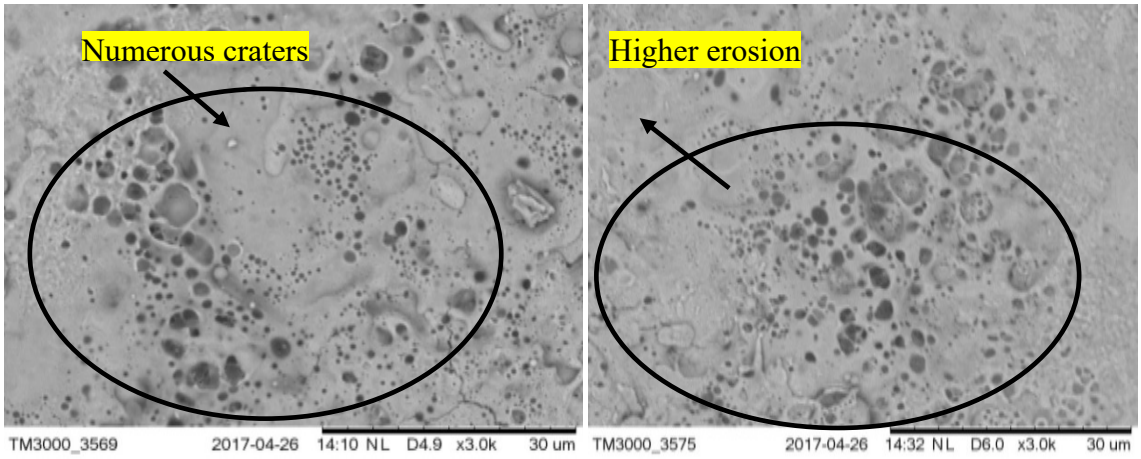

Figure 8.9 SEM image of a machined surface with higher levels of process parametric setting (image width: 68.8 µm, Accelerating voltage 15.0 kV)

Many material deposit layers were formed over the machined surface in PMND-EDM machining because, all the particles were not washed away and they remain as sticking because particles were partially in molten state as shown in Figure 8.10 with different magnification factors. It can be see from the SEM images that the structures formed were much more denser.The reason for this was product of melt penetrated deeper into the material causing larger microstructures.

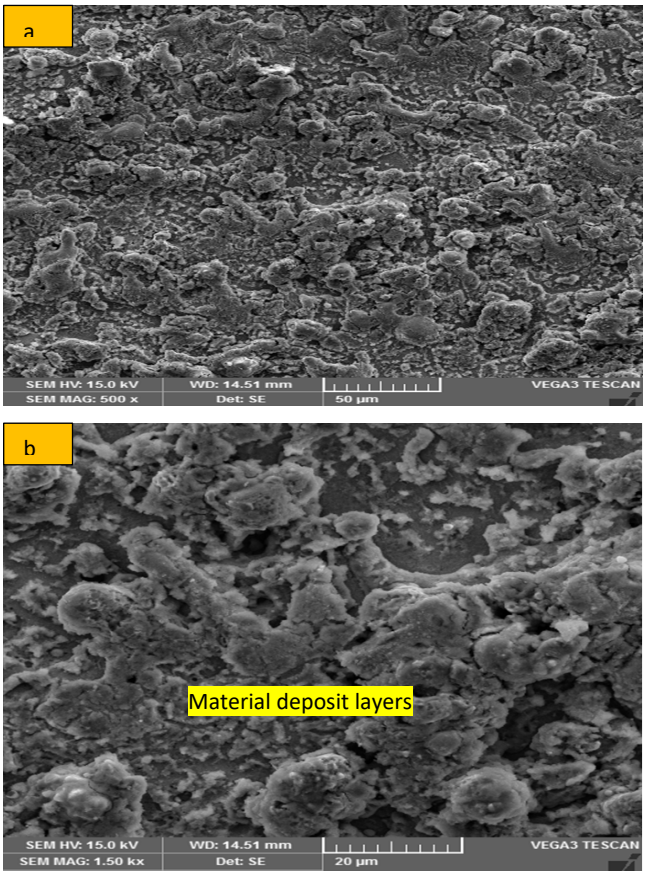

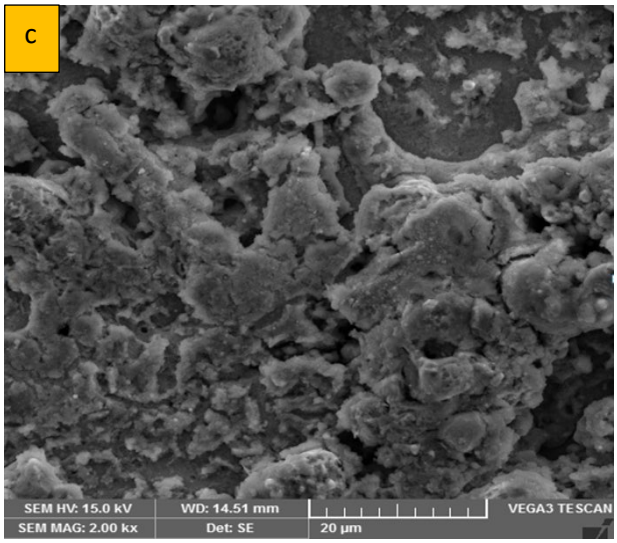

Figure 8.10 Material deposit layers on machined surface at different magnification factor (a) 500x (b) 1.5kx (c) 2kx

The analysis for X-ray diffraction of the finished workpiece was performed with X'Pert High Score tool. The XRD graph for the machined workpiece was shown in Figure 8.11. The maximum peak in the XRD graphs was found for iron oxide at 2θ degree for (201) plane with a cubic crystal system. Additional peaks were found for zinc oxide at 2θ degree of 35.61 degree and 50.48 degree at planes (111) and (211) planes respectively for a cubic crystal system. Some more peaks were found for copper oxide at 2θ of 37.28 degree and 51.23 degree at plane (211) and (103) respectively with hexagonal crystal system. During the XRD interpretation some groups with lower peaks were discounted.

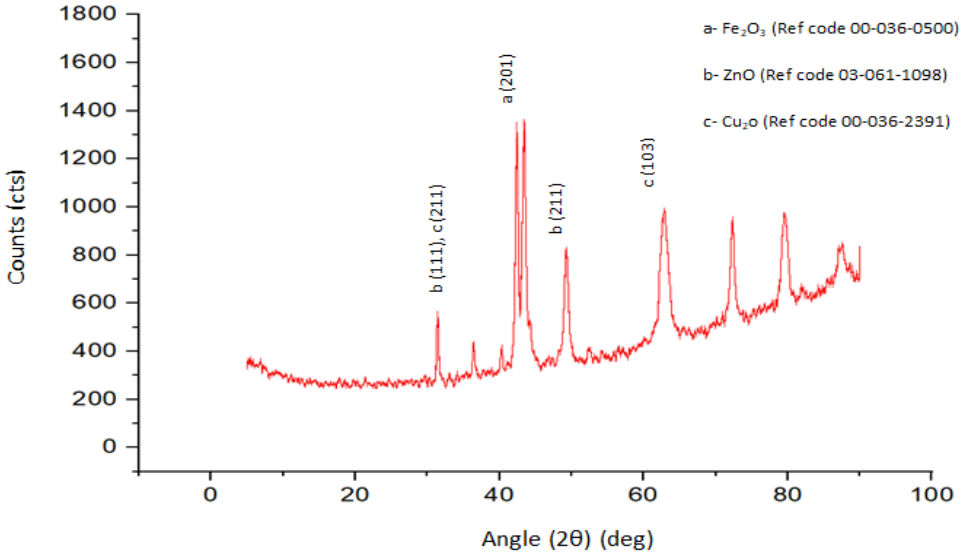

Figure 8.11 XRD results of surface produced by PMND-EDM

It was also observed that some molten parts of the tool electrode got embedded in the machined workpiece. The copper composition of molten copper material embedded in the machined workpiece was measured by energy dispersive spectroscopy X-Ray (EDAX) as shown in Figure 8.12.

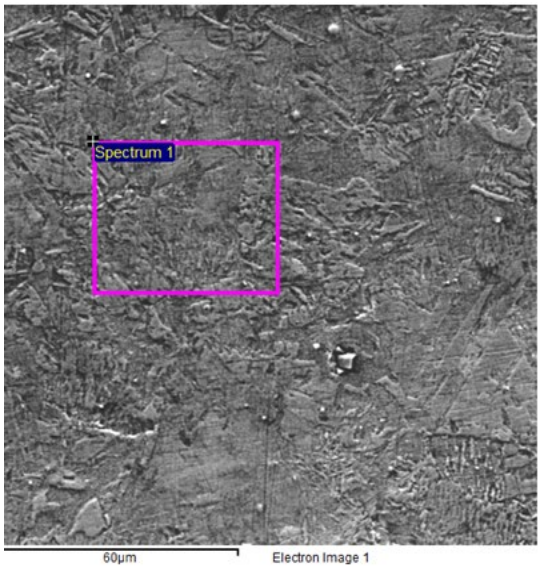

Spectrum processing:
Peak possibly omitted: 4.519 keV

Processing option: All elements analyzed (Normalised)
Number of iterations = 3

Standard:
C C 1-Jun-1999 12:00 AM
O_2 O_2 1-Jun-1999 12:00 AM
Cu Cu 1-Jun-1999 12:00 AM
Fe Fe 1-Jun-1999 12:00 AM

Element	Weight%	Atomic%
C	22.07	53.121
O_2	5.966	10.780
Fe	53.56	27.730
Cu	18.394	8.369
Totals	100.00	

Figure 8.12 (a) EDAX spectrum for the region of machined sample

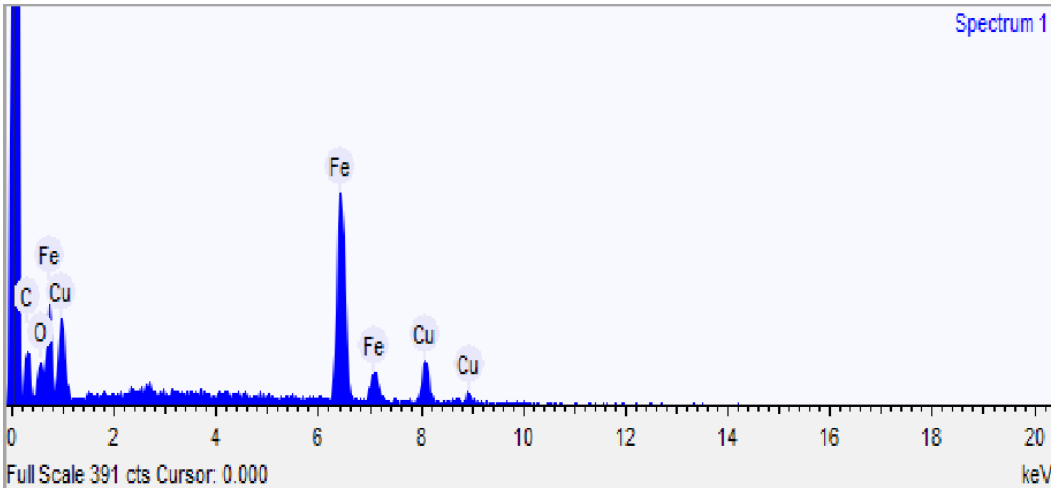

Figure 8.12 (b) EDAX (Energy Dispersive Spectroscopy X-Ray) image of a machined sample by PMND-EDM

8.2.2 Performance characteristics estimation (MRR)

In this section, the prediction for the response characteristic (material removal rate) has been performed along with their confidence intervals. Confirmation experiments were performed to validate the optimal results. The average value of the response must lie within 95% confidence interval.

Response characteristic MRR can be determined by using Eq. 4.1, (Walia et al. 2006) as:

$MRR = \overline{A_1} + \overline{B_3} + \overline{C_3} + \overline{D_3} - 3\overline{MRR}$ (8.1)

The confirmation experiments (CI_{CE}) and of population (CI_{POP}) at 95% confidence interval was calculated by using the following Eqs. 8.1 – 8.3:

$$CI_{CE} = \sqrt{F_a(1, f_e) V_e \left[\frac{1}{n_{eff}} + \frac{1}{R}\right]} \quad (8.2)$$

$$CI_{pop} = \sqrt{Fa\,(1, fe)\, Ve \,/\, n_{eff}} \quad (8.3)$$

Where, F_α (1, fe) was the F ratio at the confidence level of (1 –α) against DOF 1.

$F_{0.05}$ (1, 18) =3.5546 (Table 8.4)

$$n_{eff} = \frac{N}{1 + [\text{DOF associated in the estimate of mean response}]}$$

N (total number of experiments) = 27;

Treatment = 9, repetition = 3;

R (sample size for confirmation experiments) = 3.

V_e (error variance) = 0.001 (Table 8.4), f_e (error DOF) = 18 (Table 8.4).

F = 3.5546 (tabulated F value).

So, MRR= 0.357 (mg s^{-1}), CI_{CE}= ± 0.0397, CI_{POP}= ± 0.0198

The predicted optimal range of confidence interval of confirmation experiments (CI_{CE}) is:

Mean MRR − CI_{CE} < MRR (mg/s) < Mean MRR + CI_{CE}

i.e. 0.356 (mg s^{-1}) < MRR (mg s^{-1}) < 0.359 (mg s^{-1})

The 95% confirmation interval of the predicted mean is:

Mean MRR − CI_{POP} < MRR (mg s^{-1}) < Mean MRR + CI_{POP}

i.e. 0.337 (mg s^{-1}) < MRR (mg s^{-1}) < 0.377 (mg s^{-1})

8.2.3 Confirmation Experiments for MRR

Three repetitions of confirmation experiments for MRR were performed for process parameters at optimized levels. The confirmation test for MRR was performed at the experimental condition of A_1, B_3, C_3 and D_3 as shown in Table 8.5. The experimental material removal rate for three runs at optimized conditions was found to be 0.344 mg s^{-1}, 0.339 mg s^{-1} and 0.356 mg s^{-1} respectively. The mean experimental MRR calculated at the optimized process of parameters was 0.346 mg s^{-1} which was within the confidence interval of predicted MRR.

Table 8.5 Confirmation Experiments for MRR

Optimization type	Objective	Optimized process variables				Predicted Response (mg/s)	Confirmation Result (mg/s)
		Tool diameter (mm)	Flow rate (ml/min)	Powder concentration (g/l)	Mist pressure (MPa)		
Single response	Maximization of MRR	2	15	8	0.6	0.357	0.346

8.3 Optimization for surface finish (Ra) in PMND-EDM

Experiments were performed for optimization of surface finish (Ra) in PMND-EDM as per parametric condition at different levels as shown in Table 8.6. A total of 27 experiments were performed for getting the average value by repetitive trials of experiments.

Table 8.6 Experimental results of surface finish as per Taguchi L_9 OA

Exp. No	Parameter trial condition				Ra (μm)			S/N (dB)
	A	B	C	D	R1	R2	R3	
1	2	5	2	0.4	1.61	1.41	1.77	-4.10
2	2	10	5	0.5	1.66	1.38	1.35	-3.34
3	2	15	8	0.6	1.46	1.74	1.56	-4.03
4	3	5	5	0.6	1.33	1.19	1.07	-1.59
5	3	10	8	0.4	0.37	0.51	0.74	5.01
6	3	15	2	0.5	0.87	0.81	0.86	1.44
7	4	5	8	0.5	0.73	0.61	0.94	2.24
8	4	10	2	0.6	0.51	0.71	0.57	4.40
9	4	15	5	0.4	1.36	1.51	1.54	-3.35
Overall mean Ra ($\overline{Ra}$) = 1.113 μm								

The experiments were conducted as per L_9 (OA) and the experimental trials were run thrice for repeatability. The main effects and pooled ANOVA raw data for Ra are shown in Table 8.7 and Table 8.8 for different set of process parameters. The experimental process parameters at A_2, B_2, C_3, D_2 were most influential in reducing the surface roughness over the machined surface as shown in Figure 8.13. The average values of Ra were calculated and plotted as shown in Figure 8.13 (a-d). Tool type at level 2 was most significant in reducing the surface roughness because the dispersion of the dielectric medium was found to be most suitable at this level of tool tip diameter as shown in

Figure 8.13 (a). Appropriate dispersion results in stable discharging at the machining gap which results in reduction of surface roughness over the machined surface. Similarly, the S/N was also calculated and also shows the same trend. The discharges in PMND-EDM were easier to initiate and stable machining was achieved due to liquid phase with metallic powder additives presence in gaseous environment from the hollow tool electrodes.

Secondly the flow rate parameter was found to be most significant at level 2 in reducing the surface roughness as shown in Figure 8.13 (b). The flow rate of 10ml/min at level 2 provided optimum dielectric flow which resulted in obtaining normal condition for discharges at the inter electrode gap and the S/N ratio also followed the same trend. Similar comparative trend was seen for surface finish of the machined samples by using different dielectric medium in near dry EDM (Tao et al. 2008).

The surface roughness was found to be least at 3rd level of metallic powder concentration as shown in Figure 8.13 (c). It was observed that with increase in powder concentration the surface roughness reduced to a lowest value. The reason was that metallic powder at high concentration of 8gm/l resulted in reduction of short circuit and abnormal discharges. These favourable conditions resulted in obtaining well dispersed uniform plasma due to which the shallow craters were formed and consequently the surface achieved was very high in quality. Talla et al (2016, a) also stated the similar trend for study of surface integrity for advanced materials through PM-EDM.

Lastly the pressure of mist at 2nd level was most suitable value in reducing the surface roughness as shown in Figure 8.13 (d). The mist pressure at 0.5 MPa was found to be most suitable in reducing the surface roughness. This range of pressure provided excellent debris flushing and cooling conditions due to which enhanced surface finish was obtained. Further increase of mist pressure deteriorated the surface characteristics. Tomography test were conducted in order to validate the experimental results. The surface profile of machined samples is shown in Figure 8.14. The analysis was done with the help of Tomography instrument and 3D surface profilometer. It was clearly seen from Figure 8.14, that the irregularities produced were less over the machined surface by PMND-EDM. Shallow craters formed over the machined surface were a vital source for validation of smoother and fine machined surface by PMND-EDM. The similar trend for surface finish in near dry machining was depicted in research study related to near dry machining (Kao et al. 2007 and Kung et al. 2009).

Table 8.7 Main effects table for surface finish (Ra)

Process parameter	Level	Tool diameter (A)		Flow rate (B)		Powder concentration (C)		Pressure (D)	
Type of data		S/N Ratio	Raw data	S/N Ratio	Raw data	S/N Ratio	Raw data	S/N Ratio	Raw data
Avg. values (% Ra)	L1	-3.82	1.54	-1.14	1.18	0.58	1.01	-0.81	1.20
	L2	1.62	0.86	2.02	0.86	-2.76	1.37	0.11	1.02
	L3	1.09	0.94	-1.98	1.30	1.07	0.96	-0.40	1.12
Main effects (%Ra)	L2-L1	5.44	-0.86	3.16	-0.32	-3.64	0.36	0.92	-0.18
	L3-L2	-0.53	0.08	-4.00	0.44	3.83	-0.41	-0.51	0.10
Differences (L3-L2)-(L2-L1)		-5.97	0.94	-7.16	0.76	7.47	-0.77	-1.42	0.28

*L1, L2, L3 represent levels 1, 2 and 3 respectively of parameters. (L2-L1) is the average main effect when the corresponding parameter changes from Level 1 to Level 2. (L3-L2) is the main effect when the corresponding parameter changes from Level 2 to Level 3.

Table 8.8 Pooled ANOVA raw data and S/N data for surface finish (Ra)

Source	SS raw	SS S/N	DOF raw	DOF S/N	V raw	V S/N	F-ratio raw	F-ratio S/N	SS' raw	SS' S/N	P% raw	P% S/N
Tool Diameter	2.54	54.20	2	2	1.27	27.10	49.84	41.77	2.50	41.77	51.25	48.73
Flow rate	1.91	26.83	2	2	0.45	13.41	22.83	22.68	0.98	25.68	27.80	23.52
Powder concentration	0.87	21.21	2	2	0.25	13.10	18.01	20.20	0.87	20.20	17.99	22.95
Pressure	*	*	*	-		*	*	-	*	-	*	-
Error	0.51	1.29	20	2	0.02	0.64	-	-	0.63	-	12.94	4.78
Total	4.88	108.54	26	8	-	-	-	-	4.88	-	100	100

*Significant at 95% confidence level, F critical (raw) =3.55 (Tabular Value), F critical (S/N)=19 (Tabular Value), SS-Sum of Squares, DOF-Degree of Freedom, V-Variance, SS' Pure sum of Squares

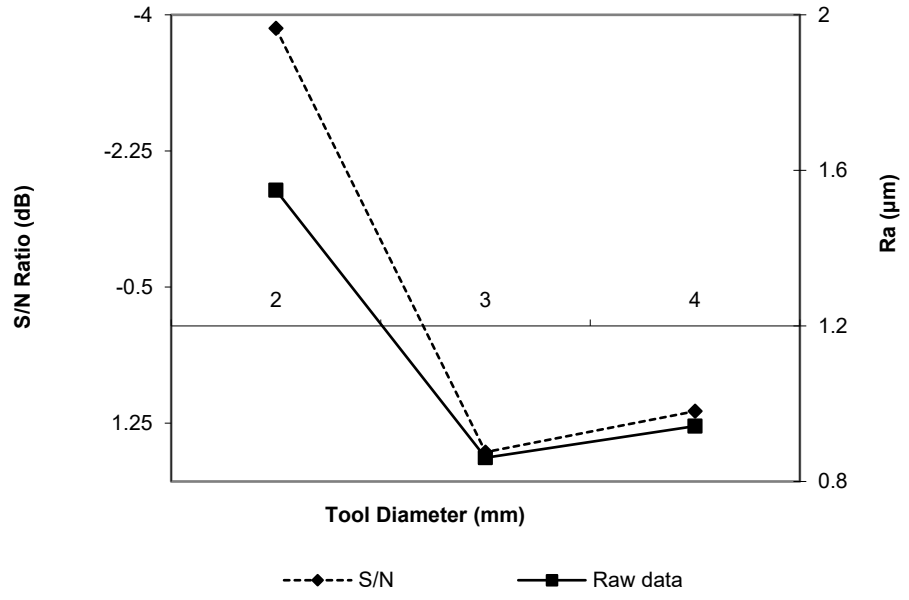

Figure 8.13 (a) Effect of tool type on Ra

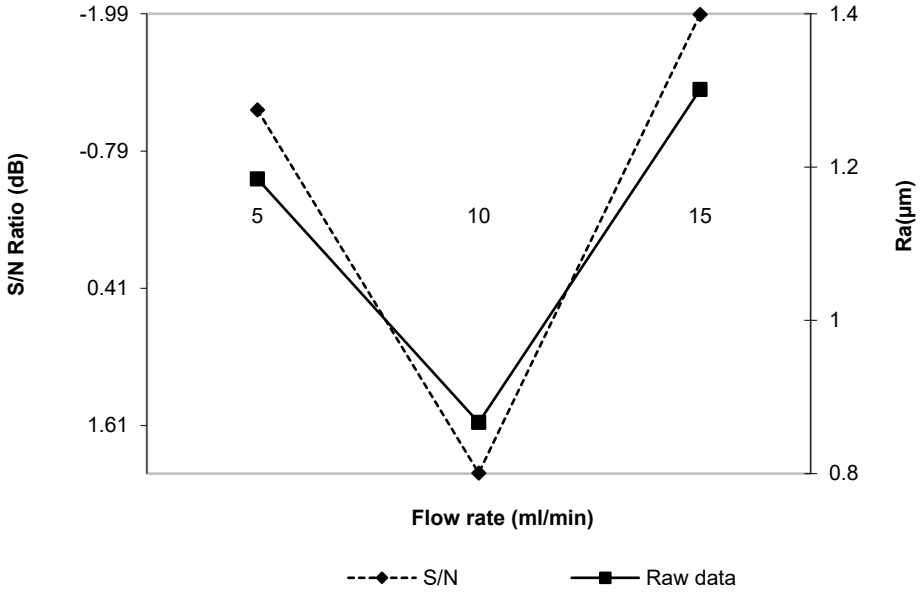

Figure 8.13 (b) Effect of Flow rate on Ra

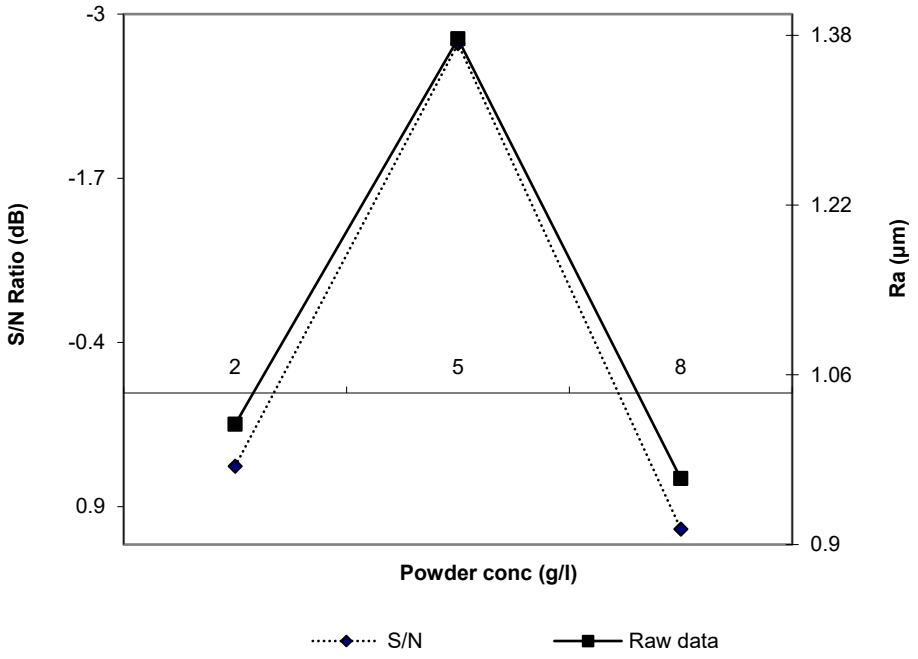

Figure 8.13 (c) Effect of powder concentration on Ra

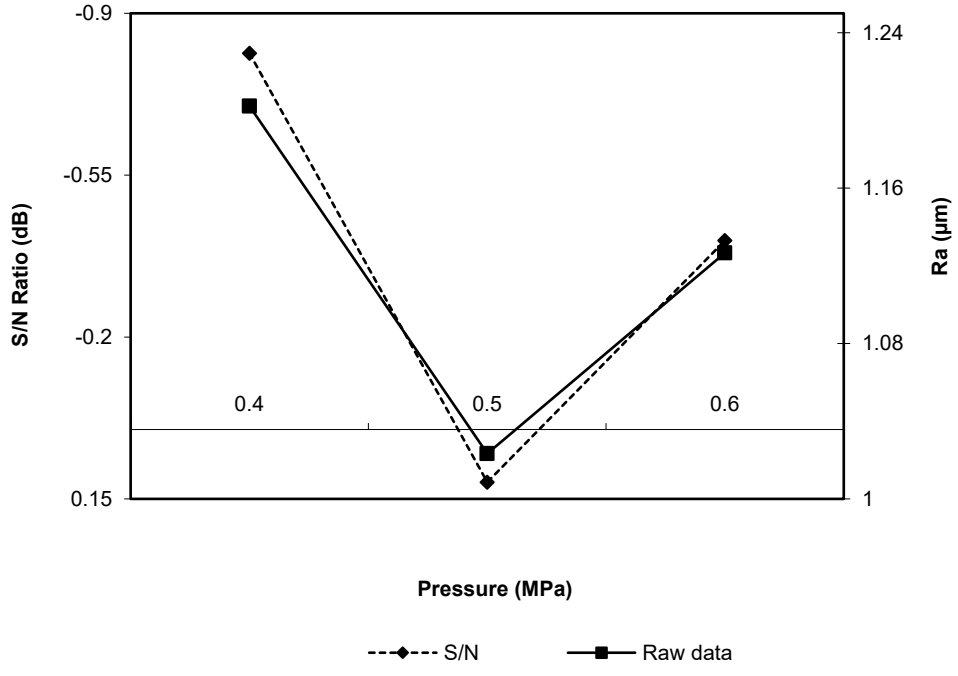

Figure 8.13 (d) Effect of pressure on Ra

The peaks in Figures 8.14 and 8.15 signify the height of the surface irregularities at different parts over the machined area. The variation of surface roughness in the images was signified by the pattern of yellow colour. The dark yellow colour of the image shows the area of lesser irregularities while

bright yellow colour signifies the area of high irregularities over the machined surface. The powder particles distribute the spark energy uniformly, which results in shallow craters on the workpiece surface. It was revealed that by the addition of metallic powder, the discharging energy dispersion improves because insulating strength of the dielectric fluid reduces with the addition of metallic powder. These favourable conditions give a refined machined surface with a high surface finish as compared machined sample by normal EDM as shown in Figure 8.15. This proves that a significant role was played by the metallic powder to modify the channel of the plasma, which gives even and uniform surfaces.

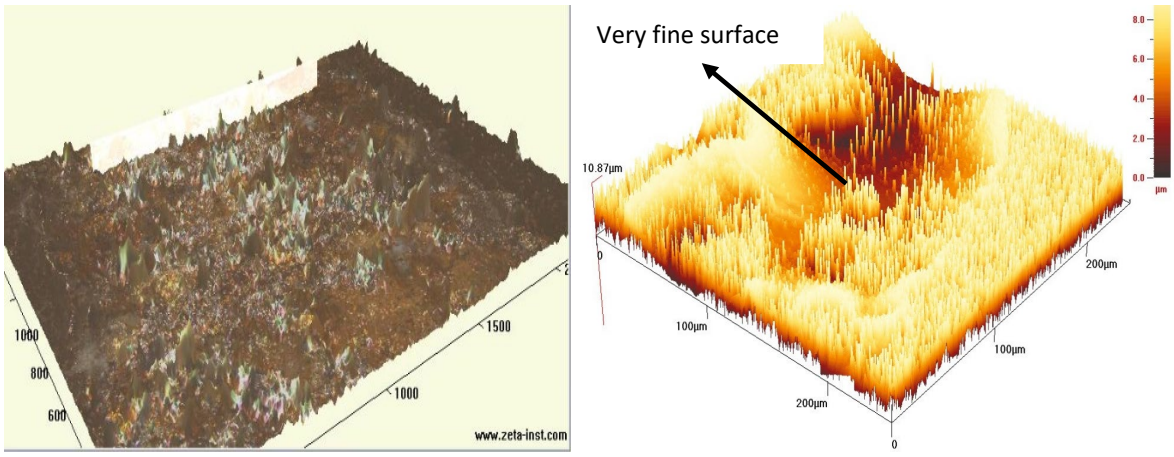

Figure 8.14 Study of surface topography of the machined surface by PMND-EDM

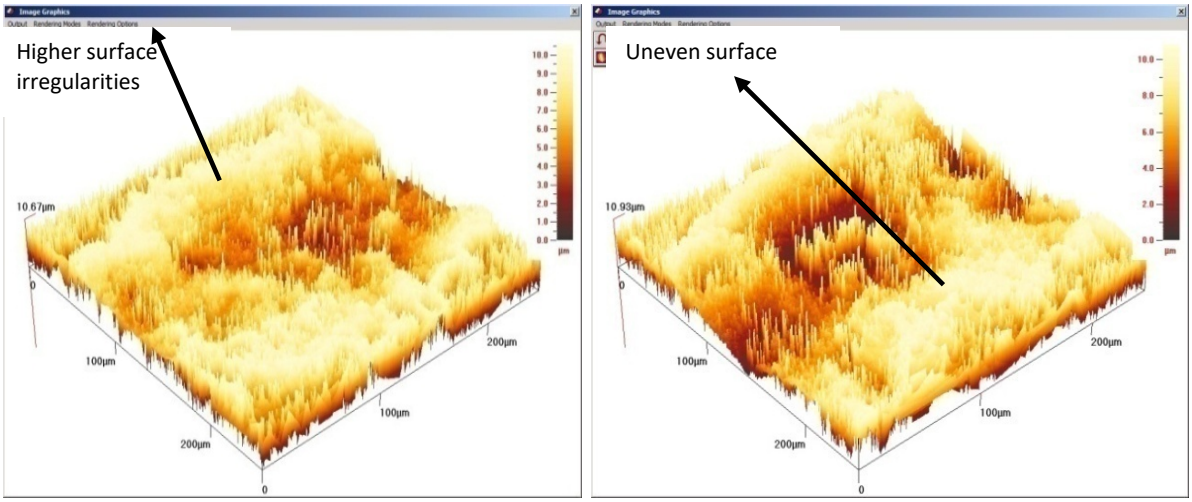

Figure 8.15 3-D image of surface roughness profile of machined surface by normal EDM

We can clearly make out from the SEM images that the surface finish was much better when work piece was machined by powder additives in near dry EDM as shown in Figure 8.16 (a) at different magnification factors**.**The crater formed were least in sample machined by PMND-EDM. In plain

EDM machining, molten material has come out in the chunks, which gets stuck to the surface**.** Bigger size of droplets sticking to the surface indicates that proper metal removal has not taken place which may lead to more uneven surface finish as shown in Figure 8.16 (b).

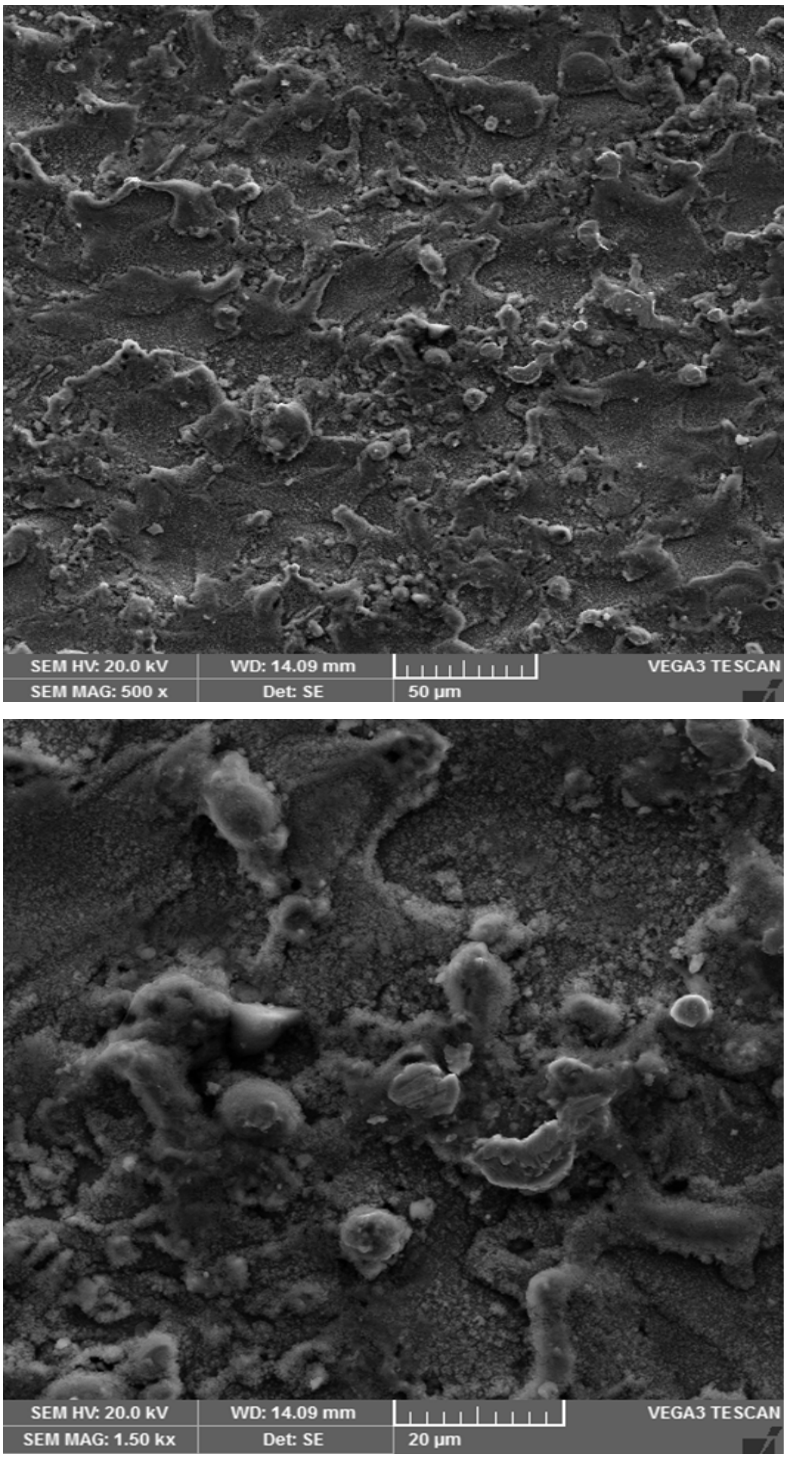

Figure 8.16 (a) SEM image of machined samples by PMND-EDM at different magnification factor (500x and 1.5kx)

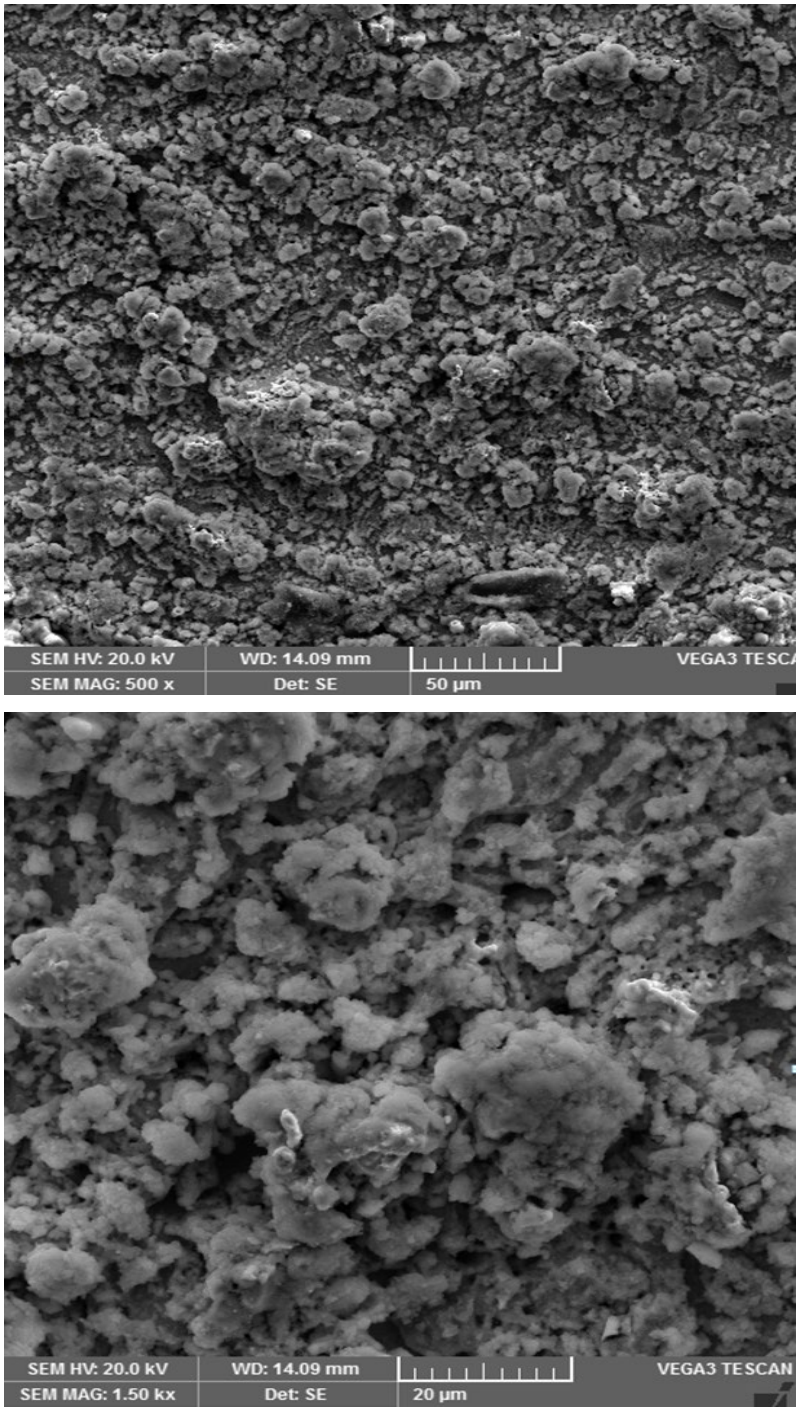

Figure 8.16 (b) SEM image of machined samples by normal EDM at different magnification factor (500x and 1.5kx)

8.3.1 Estimation of performance characteristics (Surface finish)

Response characteristic Ra can be determined by using Eq. 8.4, (Walia et al. 2006) as:

$$Ra = \overline{A_2} + \overline{B_2} + \overline{C_3} \ -3\overline{Ra} \qquad (8.4)$$

The parameter C (pressure of the mist) was insignificant therefore it was not considered into the Eq. (8.4).

The confidence interval of confirmation experiments can be determined by Eq. 8.5:

$$CI_{CE} = \sqrt{F_{\alpha}(1, f_e) V_e \left[\frac{1}{n_{eff}} + \frac{1}{R}\right]} = 0.177 \quad (8.5)$$

The Confidence interval of population can be determined by Eq. 8.6:

$$CI_{pop} = \sqrt{F\alpha\ (1, fe)\ Ve\ /\ n_{eff}} = 0.088 \quad (8.6)$$

Where, F_{α} (1, fe) was the F ratio at the confidence level of (1 –α) against DOF 1.

$F_{0.05}$ (1, 18) =3.5546 (Tabulated)

$$\boldsymbol{n_{eff}} = \frac{\boldsymbol{N}}{\textbf{1+[DOF associated in the estimate of mean response]}}$$

N (total number of experiments) = 27

Treatment = 9, repetition = 3

R (sample size for confirmation experiments) = 3

V_e (error variance) = 0.02 (Table 8.8), f_e (error DOF) = 26 (Table 8.8).

F = 3.5546 (tabulated F value).

So, Ra=0.3833 µm, CI_{CE}= ± 0.177, CI_{POP}= ± 0.088

The predicted optimal range of confidence interval of conformation experiments (CI_{CE}) is:

Mean Ra − CI_{CE}< Ra (µm) < mean Ra + CI_{CE}

i.e 0.206 µm< Ra (µm) <0.560µm

The 95% conformation interval of the predicted mean is:

Mean Ra− CI_{POP} < Ra (µm) < mean Ra+ CI_{POP}

i.e 0.295 µm < Ra (µm) < 0.471 µm

8.3.2 Confirmation of experiments for surface finish

The confirmation test was performed for Ra at A_2, B_2, C_3 and D_2 experimental conditions. The experimental Ra for optimized conditions was found to be 0.321µm, 0.303 µm and 0.351 µm respectively. The mean Ra calculated was 0.325 µm which lies within the confidence interval of predicted Ra as shown in Table 8.9.

Table 8.9 Confirmation Experiments for surface finish

Optimization type	Objective	Optimized process variables				Predicted Response (µm)	Confirmation Result (µm)
		Tool diameter (mm)	Flow rate (ml/min)	Powder concentration (g/l)	Mist pressure (MPa)		
Single response	Minimization of surface roughness	3	10	8	0.5	0.383	0.325

8.4 Optimization for Residual Stress (RS) in PMND-EDM

Series of experiments were performed as per Taguchi L_9 (OA) for residual stress (RS). Each series of experiment was run for three trials and the results obtained are shown in Table 8.10. Each series of experiment was performed in three runs and a total of 27 experiments each were performed for analysis of RS.

Table 8.10 Experimental Results of Residual stress as per Taguchi L_9 OA

Exp. No	Parameter trial condition				Residual stress (RS) (MPa)			S/N (dB)
	A	B	C	D	R1	R2	R3	
1	2	5	2	0.4	565	558	530	-54.82
2	2	10	5	0.5	621	551	550	-55.19
3	2	15	8	0.6	510	659	678	-55.85
4	3	5	5	0.6	370	361	340	-51.05
5	3	10	8	0.4	145	169	186	-44.48
6	3	15	2	0.5	239	279	280	-48.51
7	4	5	8	0.5	251	214	311	-48.35
8	4	10	2	0.6	230	209	191	-46.46
9	4	15	5	0.4	556	501	587	-54.79
Total					3478	3501	3653	
Overall mean RS ($\overline{RS}$)= 394.11 MPa								

The residual stress analysis performed by X-ray diffraction machine for series of experiments as per Taguchi L_9 (OA) is shown in Figures 8.17, depicting display diffraction ring, residual stress, peak

profile and FWHM along with their values for set of experiments as per Taguchi L_9 (OA). The full width at half maximum (FWHM) was an expression of the extent of a function (profile peak diffraction) whereas maximum and minimum values of peak diffraction were given as α-max and α-min respectively. The minimum value of residual stress was found to be 145 MPa among experimental values obtained from nine series of experiments as shown in Figure 8.17 (d). This obtained value of RS was much lower as compared to high RS achieved in previous work (Ekmekci et al. 2007). Residual stress decreased due to induced micro-cracks over the machined surface as shown in Figure 8.18, these cracks were responsible for relieving some of the residual stress, another reason can be attributed to the uniform distribution of heat over the machined surface and improved flushing condition which ultimately relieves some part of the residual stresses over the machined surfaces (Rao et al. 2016). The magnitude of the strain represented in Figure 8.19 was determined from the detected position of the Debye-Scherrer ring.

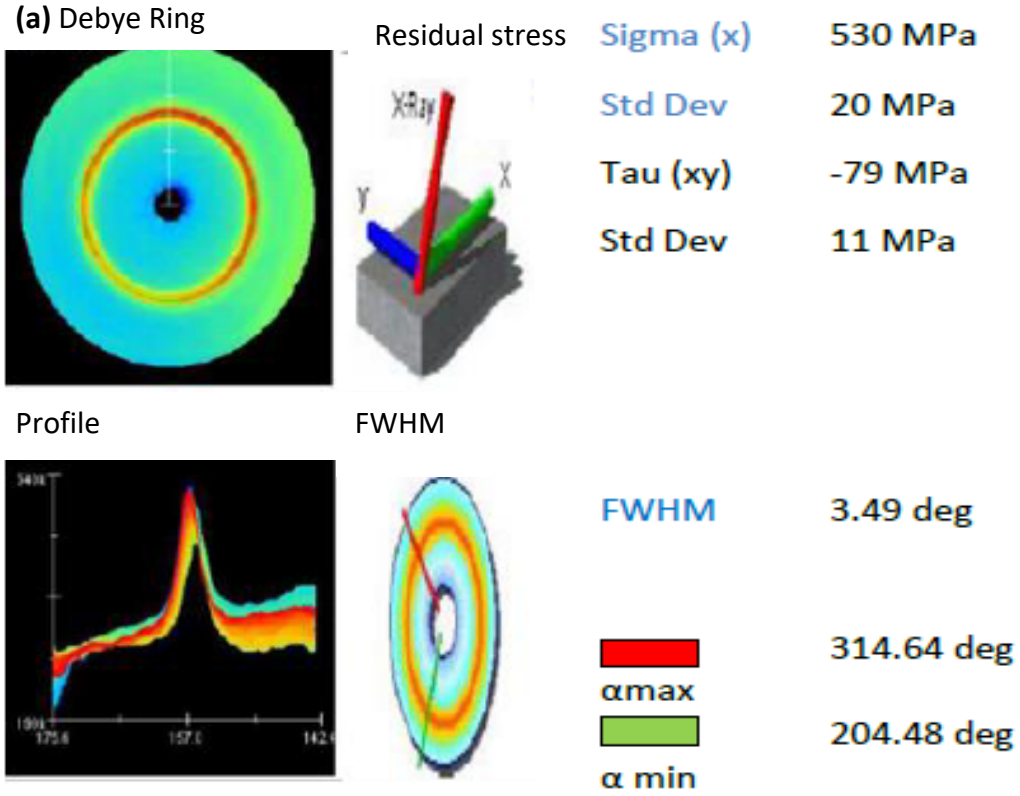

Figure 8.17 (a) Instrumental Residual stress (530 MPa)

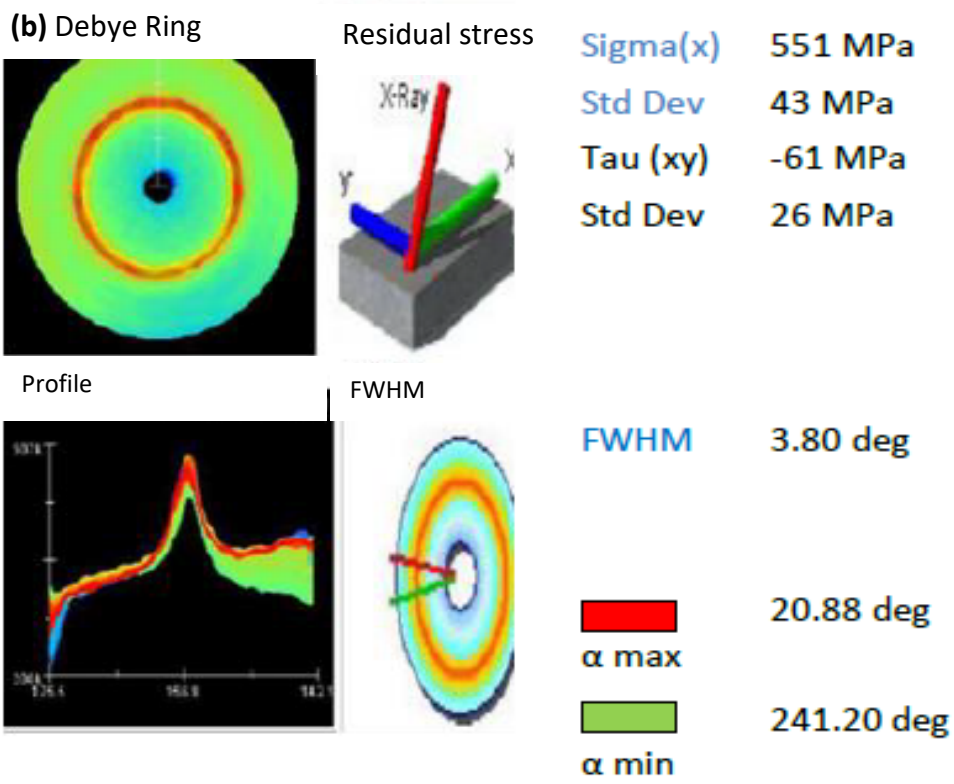

Figure 8.17 (b) Instrumental Residual stress (551 MPa)

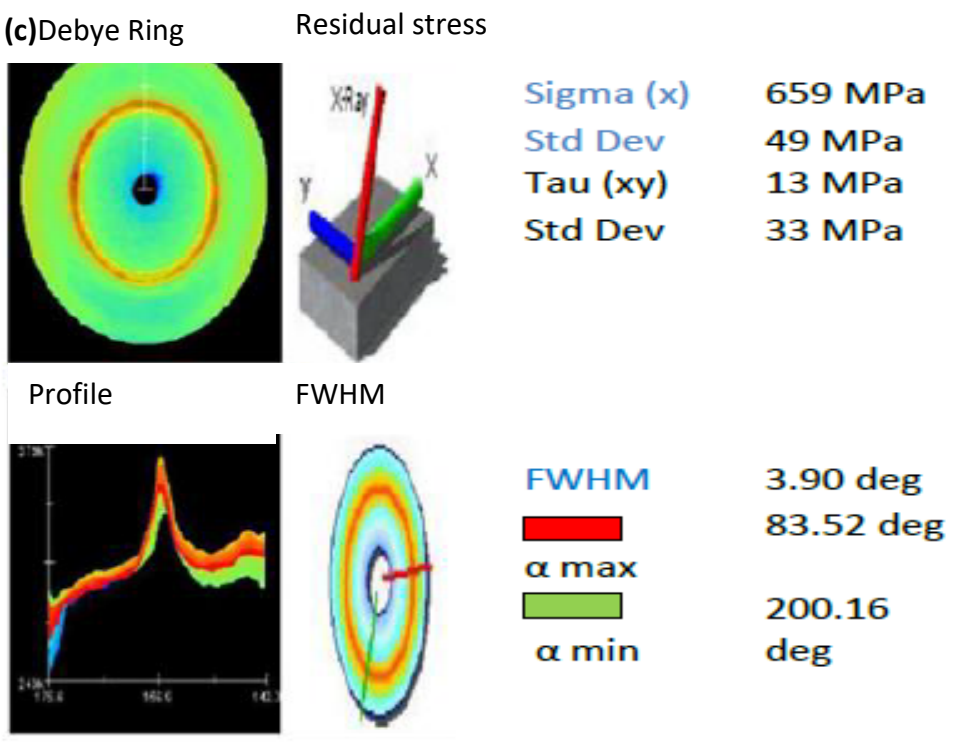

Figure 8.17 (c) Instrumental Residual stress (659 MPa)

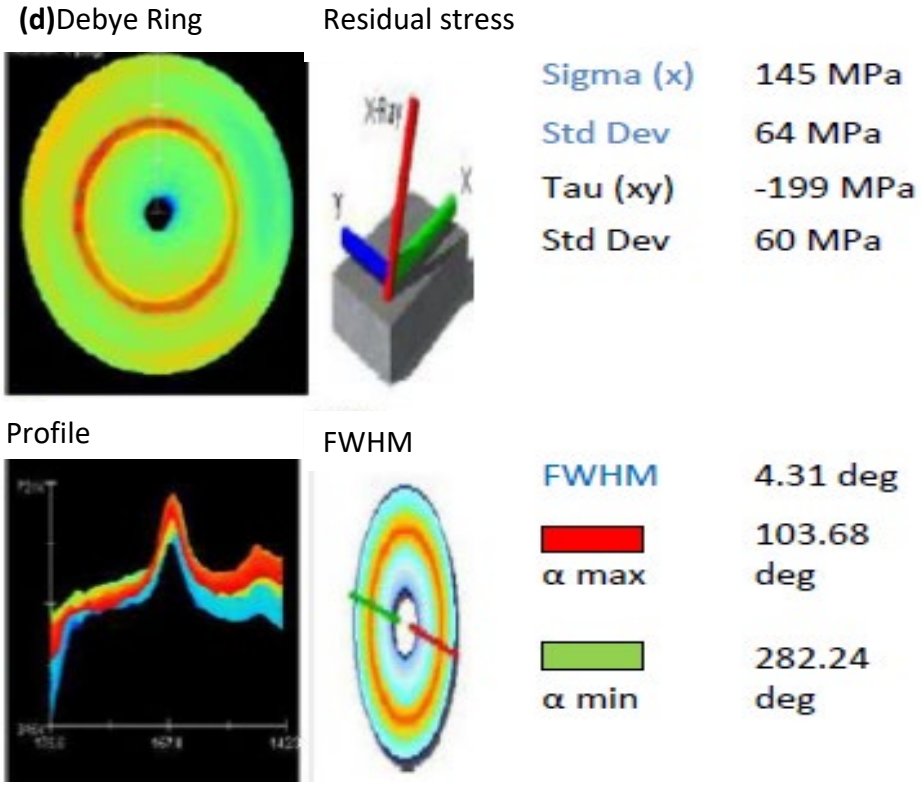

Figure 8.17 (d) Instrumental Residual stress (145 MPa)

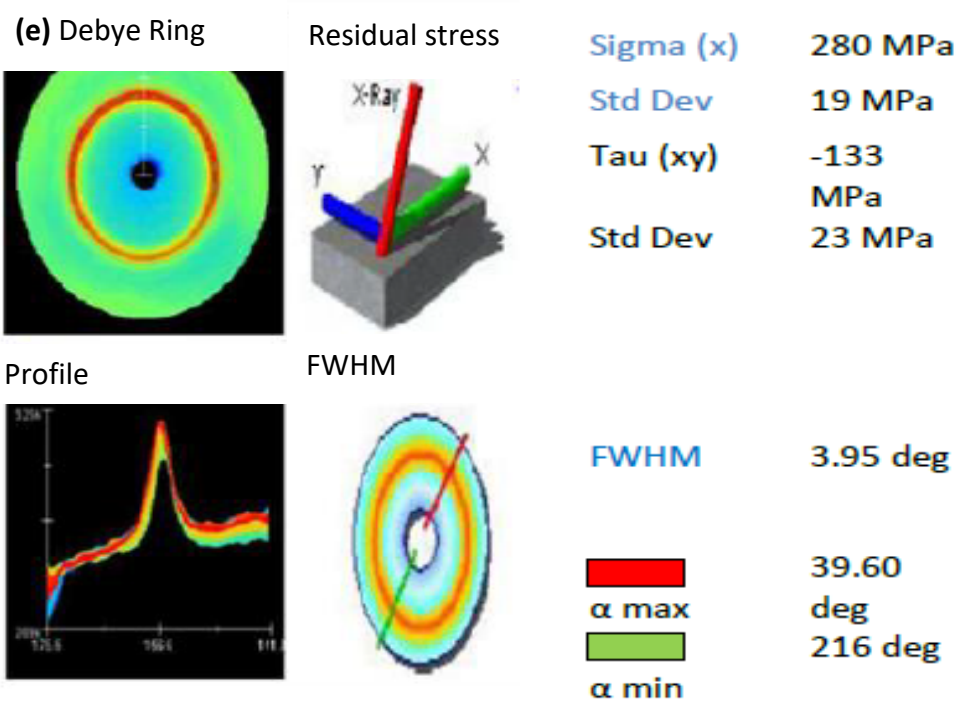

Figure 8.17 (e) Instrumental Residual stress (280 MPa)

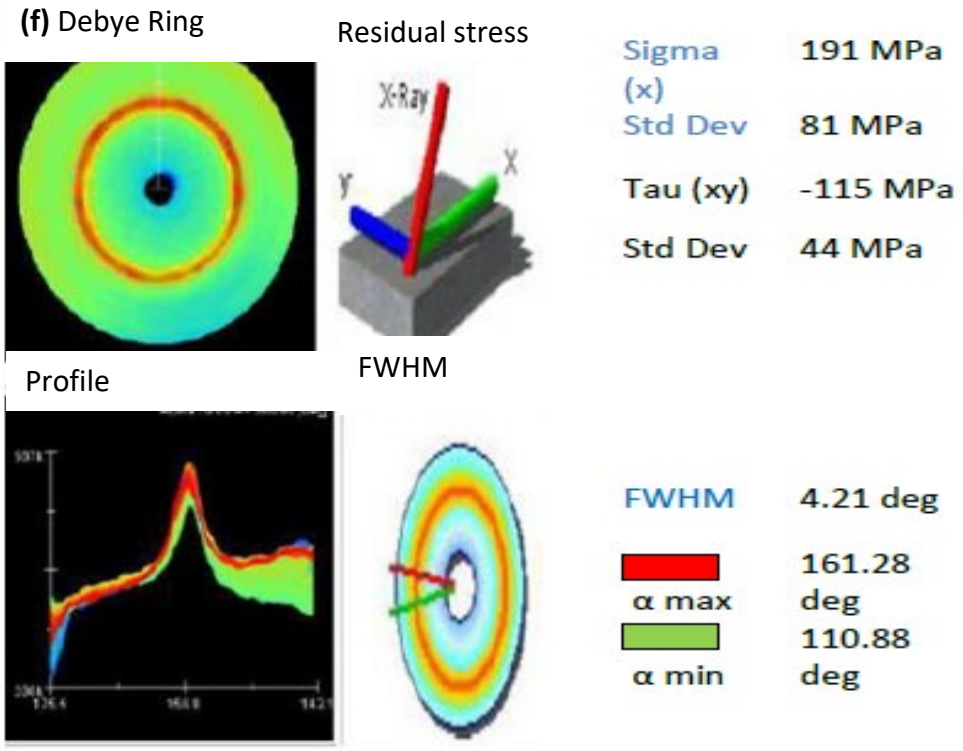

Figures 8.17 (f) Instrumental Residual stress (191 MPa)

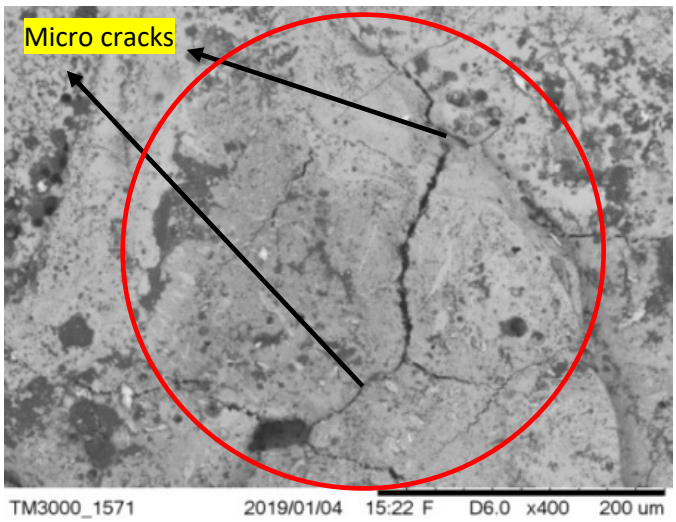

Figure 8.18 Induced micro cracks in PMND-EDM

The average values and main effects values of residual stress and their S/N ratios were calculated at different levels which were L1, L2 and L3 as tabulated in Table 8.11. Pooled ANOVA (analysis of variance) for raw data and S/N ratio for residual stress at 95 % confidence level is shown in Table 8.12. The tabulated value for F-ratio was 3.55 for raw data while the tabulated F-ratio value for S/N was 19.

Table 8.11 Average values and Main effects: Residual stress, RS (in MPa)

Process parameter	Level	Tool diameter (A)		Flow rate (B)		Powder concentration (C)		Pressure (D)	
Type of data		S/N	Raw data	S/N	Raw data	S/N	Raw data	S/N	Raw data
Average values (% RS)	L1	-55.29	580.22	-51.41	388.88	-49.93	342.33	-51.367	421.88
	L2	-48.01	263.22	-48.71	316.88	-53.68	493.00	-50.69	366.22
	L3	-49.87	338.88	-53.05	476.55	-49.56	347.00	-51.12	394.22
Main effects (% RS)	L2-L1	7.27	-317.00	2.69	-72.00	-3.74	150.66	0.67	-55.66
	L3-L2	-1.85	75.66	-4.34	159.66	4.11	-146.00	-0.43	28
Differences (L3-L2)-(L2-L1)		-9.12	392.66	-7.04	231.66	7.86	-296.66	-1.11	83.66
*L1, L2, L3 represent levels 1, 2 and 3 respectively of parameters. (L2-L1) is the average main effect when the corresponding parameter changes from Level 1 to Level 2. (L3-L2) is the main effect when the corresponding parameter changes from Level 2 to Level 3.									

Table 8.12 Pooled ANOVA raw data and S/N data for Residual stress

Source	SS Raw	SS S/N	SS' raw	SS' S/N	DOF raw	DOF S/N	V raw	V S/N	F-ratio raw	F-ratio S/N	P% raw	P% S/N
Tool Diameter	493368.6	85.63	489736	84.92	2	2	246684.30	42.81	135.81	121.16	62.67	58.54
Flow rate	132114.6	31.11	128482	30.40	2	2	66057.33	15.55	36.36	44.02	16.78	21.27
Powder concentration	115088.6	28.82	111456	28.11	2	2	57544.33	14.41	31.68	40.78	14.61	12.70
Pressure	13944.66	0.70	108954	23.87	2	--	6972.33	10.12	3.83	31.91	1.77	7.11
Error	32694	0.70	57536.67	2.82	18	2	1816.3	0.35	-	-	4.15	0.48
Total	787210.6	146.2	787210.7	146.2	26	8	*	-	-	-	100	100
*Significant at 95% confidence level, F- critical=3.55 (Tabular value for raw data), SS- Sum of squares, DOF- Degree of freedom, V- variance , F- critical=19 (Tabular value for S/N data), SS'= Pure sum of squares												

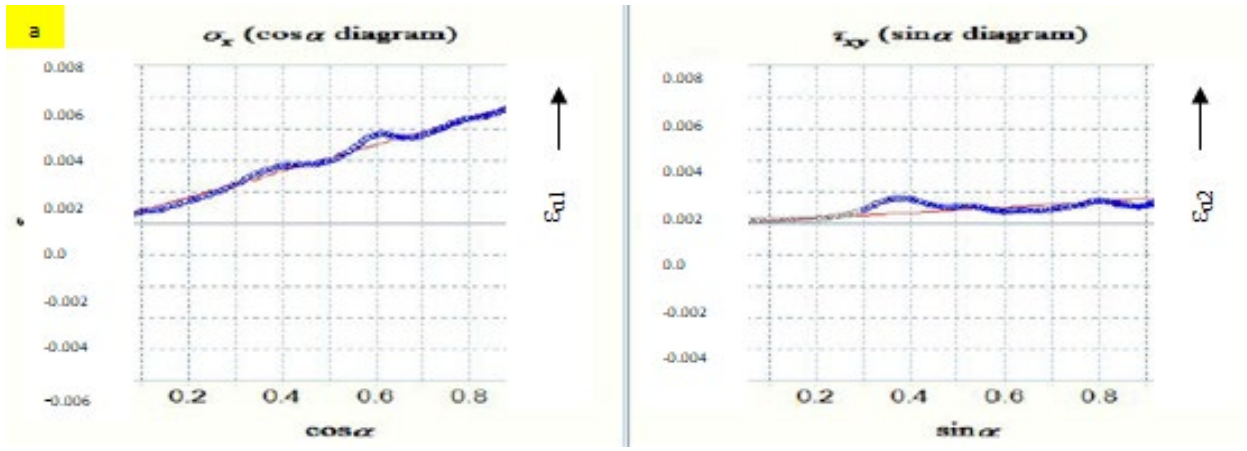

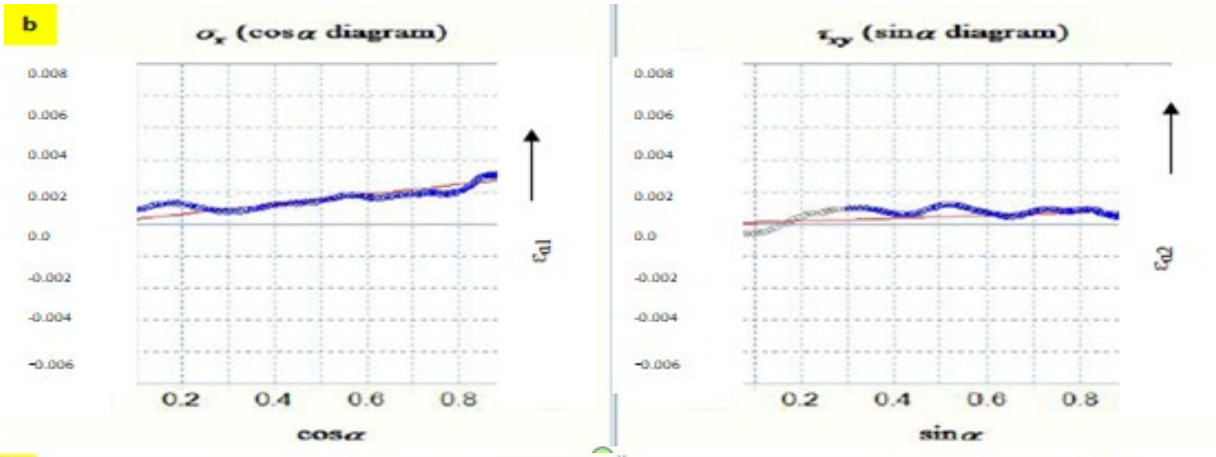
b
σ_x (cosα diagram)
τ_{xy} (sinα diagram)
0.008
0.006
0.004
0.002
0.0
-0.002
-0.004
-0.006
0.2
0.4
0.6
0.8
cosα
sinα
$\varepsilon_{\alpha 1}$
$\varepsilon_{\alpha 2}$

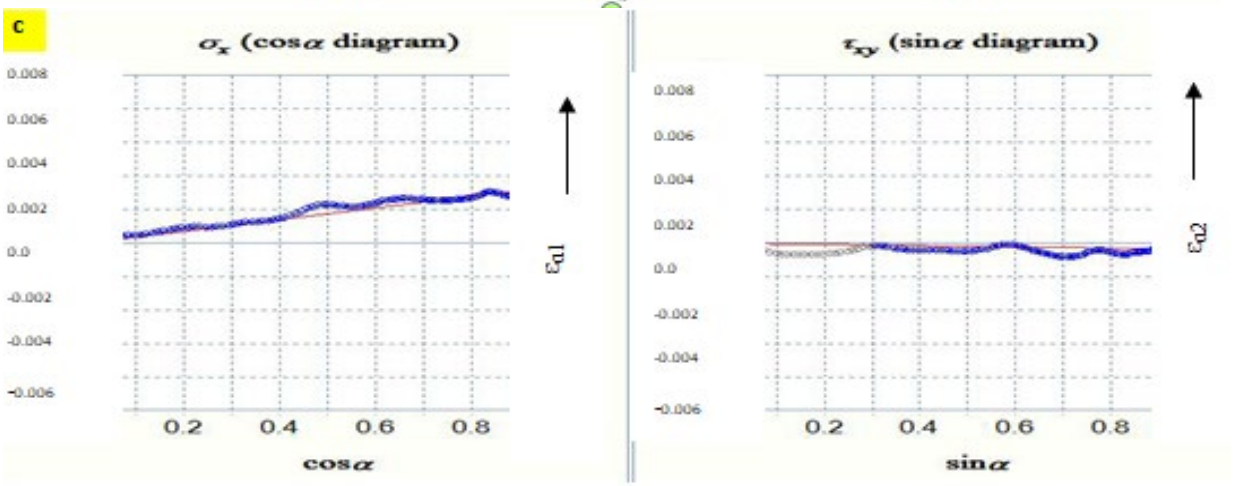
c
σ_x (cosα diagram)
τ_{xy} (sinα diagram)
0.008
0.006
0.004
0.002
0.0
-0.002
-0.004
-0.006
0.2
0.4
0.6
0.8
cosα
sinα
$\varepsilon_{\alpha 1}$
$\varepsilon_{\alpha 2}$

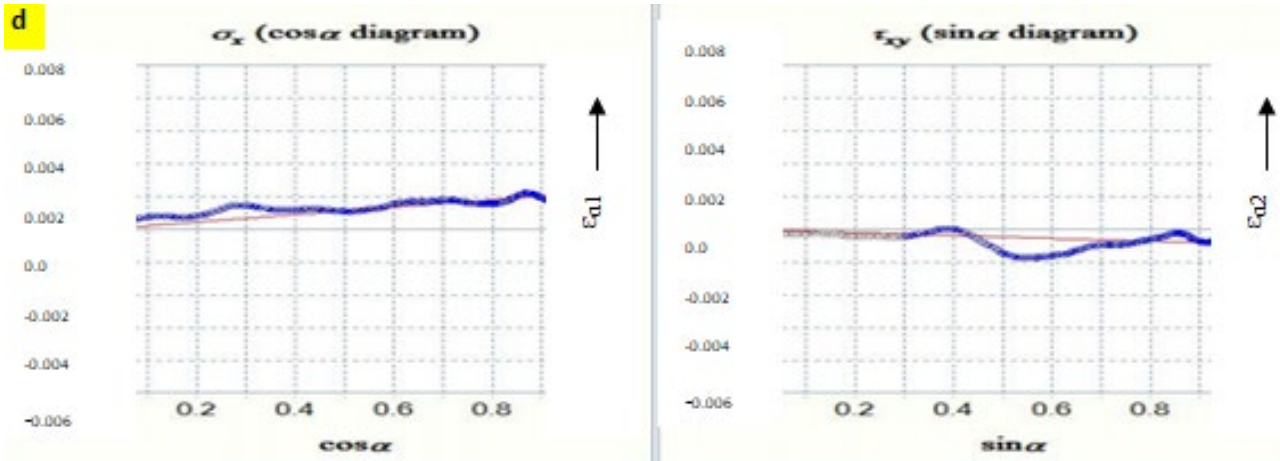
d
σ_x (cosα diagram)
τ_{xy} (sinα diagram)
0.008
0.006
0.004
0.002
0.0
-0.002
-0.004
-0.006
0.2
0.4
0.6
0.8
cosα
sinα
$\varepsilon_{\alpha 1}$
$\varepsilon_{\alpha 2}$

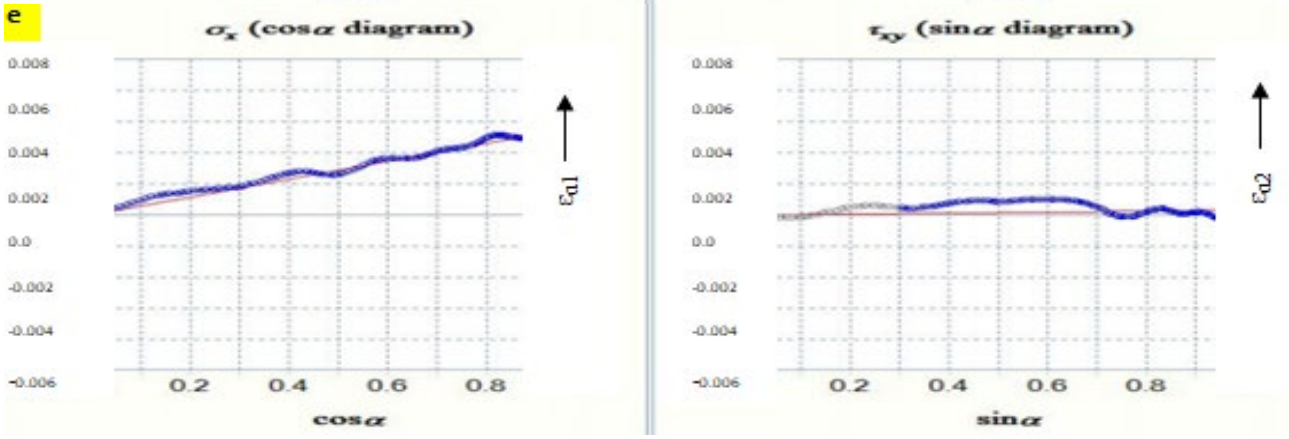
e
σ_x (cosα diagram)
τ_{xy} (sinα diagram)
0.008
0.006
0.004
0.002
0.0
-0.002
-0.004
-0.006
0.2
0.4
0.6
0.8
cosα
sinα
$\varepsilon_{\alpha 1}$
$\varepsilon_{\alpha 2}$

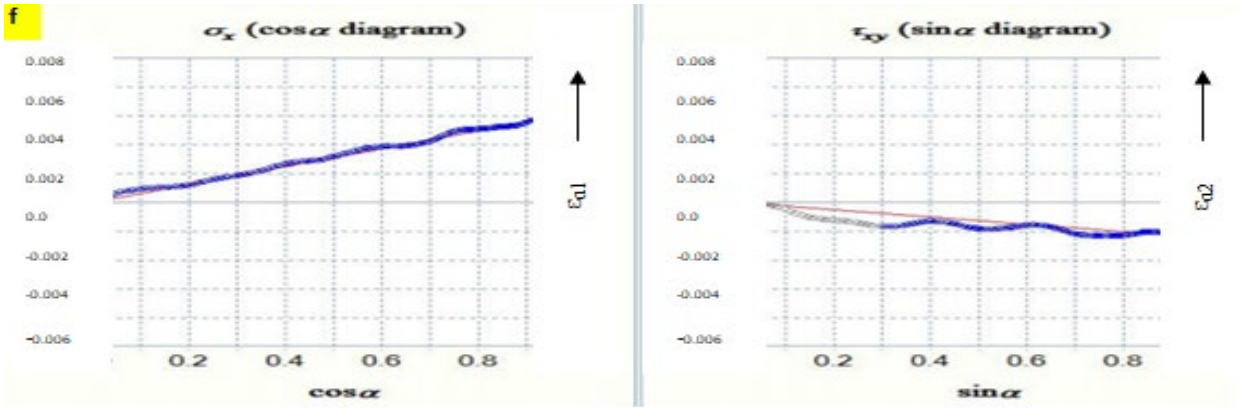

Figure 8.19 Magnitude of the strain of residual stress

The average values of residual stresses were calculated and plotted as shown in Figure 8.20. The parameters A, B, C, and D at levels 2, 2, 1, 2 respectively were most effective in reducing RS as shown in Figure 8.20. Similarly, the S/N ratios were also calculated and display the same trend in Figure 8.20. The parameter A at 2nd level, parameter B at 2nd level, parameter C at 1st level and parameter D at the 2nd level were most effective in reducing residual stress.

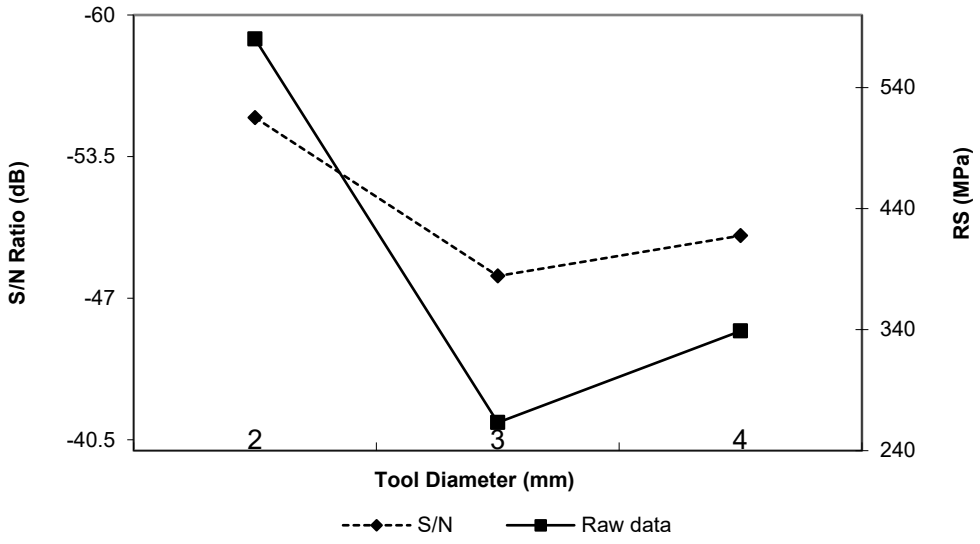

Figure 8.20 (a) Effect of tool type on RS (MPa)

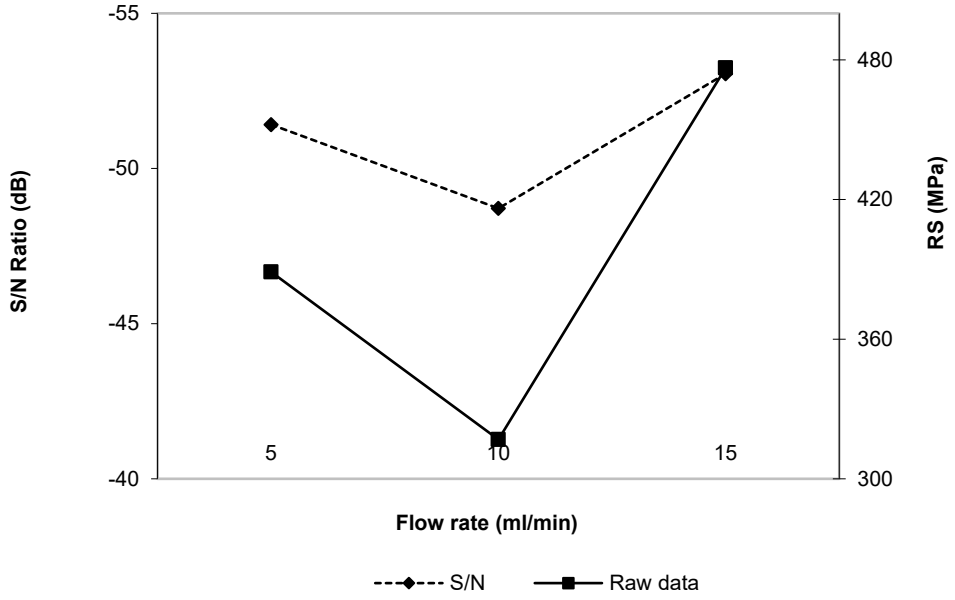

Figure 8.20 (b) Effect of Flow rate on RS (MPa)

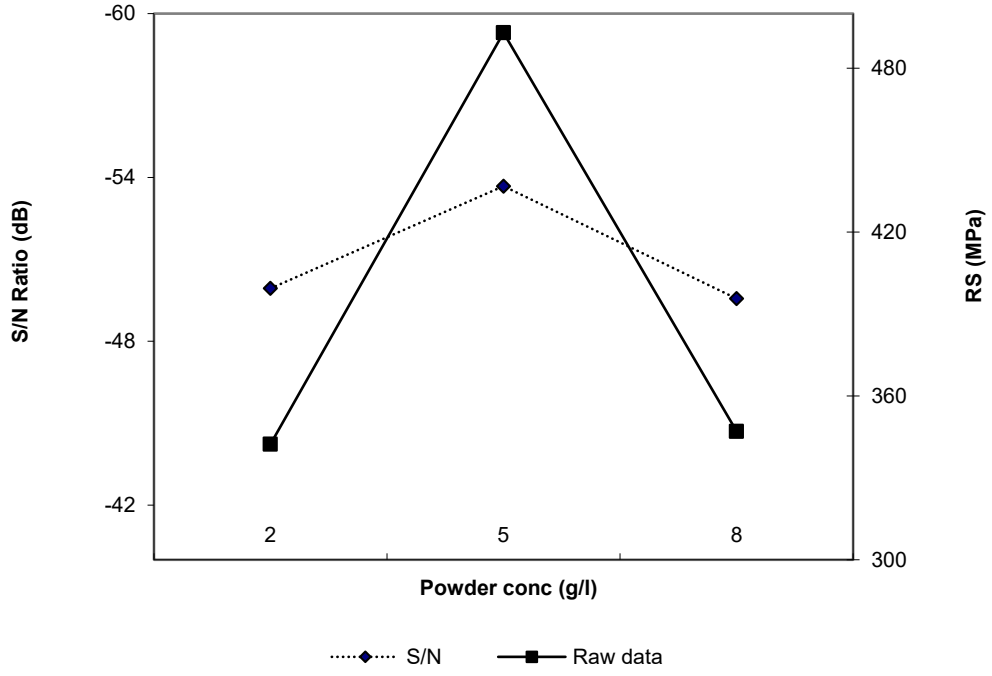

Figure 8.20 (c) Effect of powder concentration on RS (MPa)

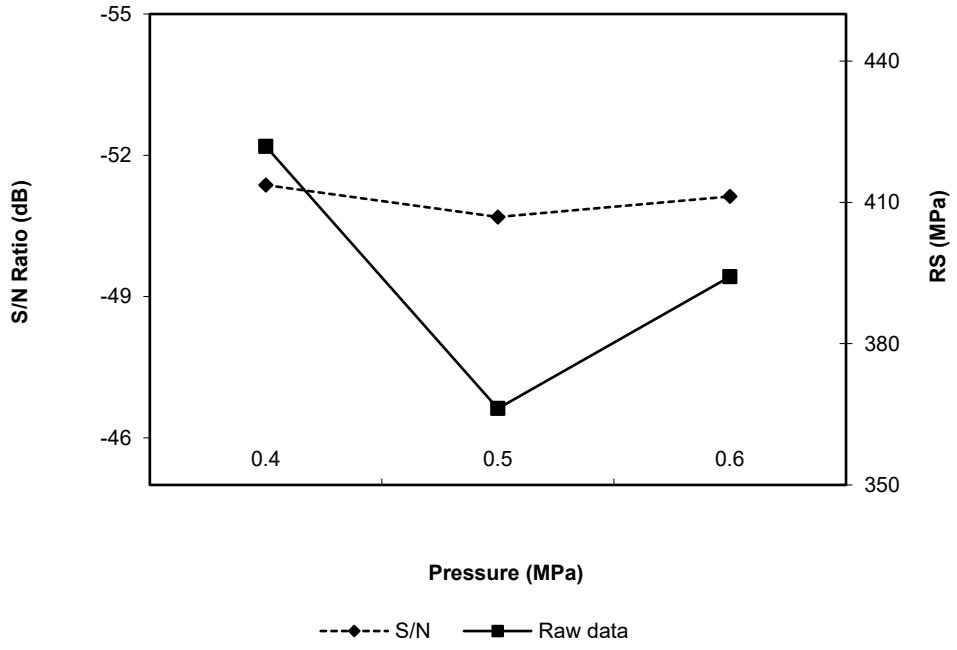

Figure 8.20 (d) Effect of pressure on RS (MPa)

The residual stress induced in the workpiece initially decreases with an increase in internal diameter of tool tip at 2nd level (L_2) as shown in Figure 8.20 (a). Better flushing takes place over the machined surface which provides a better cooling condition for dissipation of heat over the machined surface and therefore less heat was generated over the machined surface which results in reducing residual stress to the lowest value at L_2. At level 3 there was a phenomenon of rapid solidification. This rapid solidification was responsible for an increase in the value of RS (Kruth and Bleys, 2000). Rapid solidification led to solidification of sputtered melted liquid over the machined surface as shown in Figure 8.21. It can be clearly seen from Figure 8.21, there was non-homogenous solidified material over the machined surface which was responsible for the change in specific volume of the molten material and therefore the value of residual stresses was high.

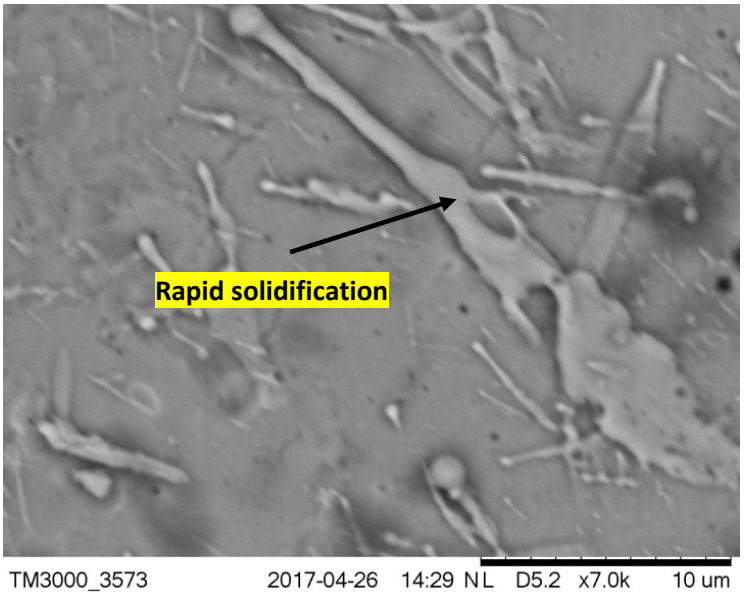

Figure 8.21 Rapid solidification over the surface (SEM image)

The RS value initially decreases with increase in flow rate values due to better heat dissipation at L_2 but with further increase of flow rate, there was a phenomenon of stress corrosion due to which the RS value increases to its peak value at L_3 as shown in Figure 8.20 (b). The residual stress initially increases with increases in powder concentration but afterwards decreases. Due to the presence of metallic powder particles the plasma channel becomes more energized and more heat was induced over the workpiece due to which high residual stress was found over the machined surface at L_2 as shown in Figure 8.20 (c). The heat density or heat flux at the machining gap was increased many times by the increase of metallic powder concentration. The bridging effect between the metallic powder grains gets increased and maintains favourable conditions for sparking and thus the temperature over the machined area gets very high which was responsible for higher values of residual stress. Further increase of powder concentration leads to improper spark discharges due to which low heat energy gets imparted to the workpiece. Over clustering of metallic powder particles at the inter-electrode gap resulted in the formation of small heat plasma and therefore the heat intensity at the machining gap gets reduced. The lower value of temperature at the inter-electrode gap was responsible for low metallurgical transformation over the machined surface as shown in Figure 8.22 and this result in reducing residual stress at L_3. Talla et al. 2017 stated the same trend in research related to residual stress in EDM with powder additives.

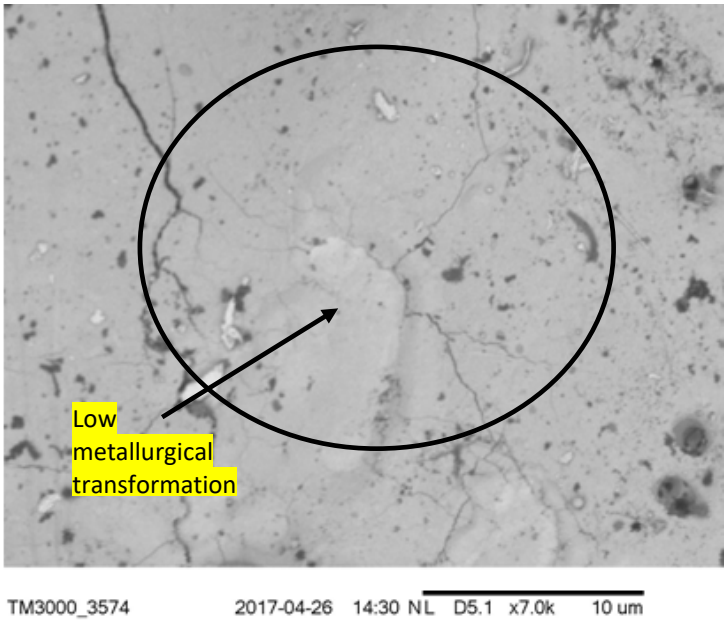

Figure 8.22 SEM image of low metallurgical transformation (SEM image)

RS value decreases with the increase of mist pressure but afterwards, it increases with further increase of pressure Figure 8.20 (d). The molecules density initially gets increased with increase of mist pressure which improved deionization effect. These conditions lead to better heat dissipation which reduces RS value at L_2. The relaxation time for residual stress gets decreased with an increase of mist pressure due to which there was a phenomenon of localized in-homogenous plastic deformation over the machined surface as shown in Figure 8.23. These conditions were responsible for the increase in value of residual stress at L_3. Sudden pressure change of mist at L_3 was very much significant in changing the grains structure of the surface layer of the machined part.

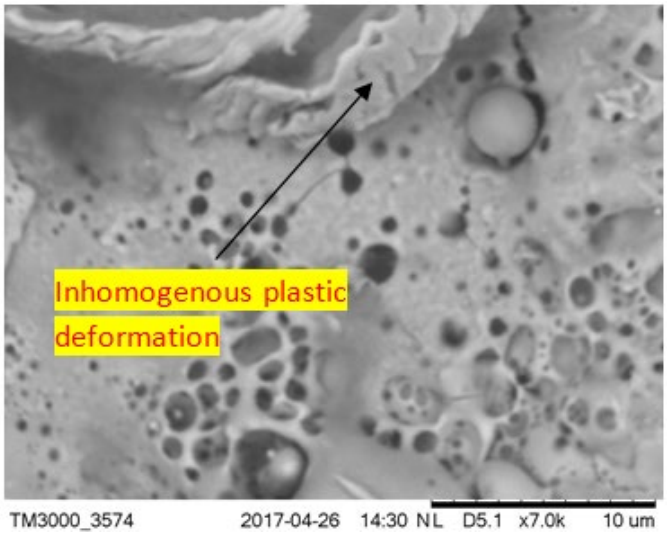

Figure 8.23 Localized in-homogenous plastic deformations (SEM image)

8.4.1 Estimation of performance characteristics (Residual Stress)

Response characteristic RS can be determined by using Eq. 8.7, (Walia et al. 2006) as:

$$RS= \overline{A_2} + \overline{B_2} + \overline{C_1} + \overline{D_2} - 3\overline{RS} \ , \quad (8.7)$$

The confidence interval of confirmation experiments can be determined by Eq. 8.8, (Walia et al. 2006):

$$CI_{CE} = \sqrt{F_\alpha\ (1, f_e\ )V_e[\frac{1}{n_{eff}} + \frac{1}{R}]}\ , \quad (8.8)$$

The Confidence interval of population can be determined by Eq. 8.9 (Walia et al. 2006):

$$CI_{POP} = \sqrt{\frac{F_\alpha\ (1, f_e\ )V_e}{n_{eff}}}, \quad (8.9)$$

Where, F_α (1, fe) = the F ratio at the confidence level of (1 –α) against DOF 1.

$F_{0.05}$ (1,18) =3.5546 (Tabulated)

$$n_{eff} = \frac{N}{1 + [\text{DOF associated in the estimate of mean response}]}$$

N (total number of experiments) = 27;

Treatment = 9, repetition = 3;

R (sample size for confirmation experiments) = 3.

V_e(error variance) = 1816.33 (Table 8.12), f_e (error DOF) = 18 (Table 8.12).

F = 3.5546 (tabulated F value).

So, RS=106.32 MPa, CI_{CE}= ± 53.56, CI_{POP}= ± 26.78

The predicted optimal range of confidence interval of conformation experiments (CI_{CE}) is:

Mean RS − CI_{CE}< RS (MPa) < mean RS + CI_{CE}

i.e 52.76 MPa < RS (MPa) < 159.88 MPa

The 95% conformation interval of the predicted mean is:

Mean RS − CI_{POP} < RS (MPa) < mean RS + CI_{POP}

i.e 79.54 MPa < RS (MPa) < 133.10 MPa

8.4.2 Confirmation experiments for residual stress

Three repetitions of confirmation experiments for RS were performed at optimized levels of process parameters. The confirmation test for residual stress was performed at the experimental condition of A_2, B_2, C_1 and D_2. The experimental residual stresses for three runs at optimized conditions were found to be 90.32 MPa, 110.39 MPa and 118.49 MPa respectively. The mean experimental residual stress calculated at the optimized process of parameters was 106.40 MPa which was within the confidence interval of predicted RS. Thus, it was proven by the range that the predicted value of RS lays in the optimum range as shown in Table 8.13.

Table 8.13 Confirmation experiments for Residual stress

Optimization type	Objective	Optimized process variables				Predicted Response (μm)	Confirmation Result (μm)
		Tool diameter (mm)	Flow rate (ml/min)	Powder concentration (g/l)	Mist pressure (MPa)		
Single response	Minimization of Residual stress	3	10	2	0.5	106.32	106.40

8.5 Optimization for Tool Wear Rate (TWR) in PMND-EDM

As per design of experiments, the experiments were conducted successfully for three runs. The results of TWR at different levels are shown in Table 8.14. The experiments were performed in three runs under same condition of parameter trial condition.

Table 8.14 Experimental results for TWR as per L_9 orthogonal array

Exp.No	Parameter trial condition				TWR			S/N (db)
	A	B	C	D	R1	R2	R3	
1	2	5	2	0.4	1.65	1.45	1.81	-4.31
2	2	10	5	0.5	1.70	1.42	1.39	-3.57
3	2	15	8	0.6	1.50	1.78	1.60	-4.24
4	3	5	5	0.6	1.37	1.23	1.11	-1.87
5	3	10	8	0.4	0.41	0.55	0.78	4.44
6	3	15	2	0.5	0.91	0.85	0.90	1.04
7	4	5	8	0.5	0.77	0.65	0.98	1.81
8	4	10	2	0.6	0.55	0.75	0.61	3.84
9	4	15	5	0.4	1.4	1.55	1.58	-3.59
Total					10.26	10.23	10.76	
Overall mean TWR ($\bar{T}$) = 1.15 mg/min								

There were two types of data available as per analysis such as raw data and S/N data at three levels L1, L2 and L3. The average % value was calculated for TWR for different parameters. After that

main effects % of TWR were calculated by expression (L2-L1) and (L3-L2). Finally the difference between L2, L1 and L3, L2 was calculated as shown in Table 8.15. Analysis of variance was done for TWR S/N ratio on the results obtained at 95% confidence level. Table 8.16 shows the pooled ANOVA raw data for TWR analysis at 95% confidence level and critical F-ratio of 3.55. The most optimum level of different input process parameter were A_2, B_2, C_3 and D_2.. Among the process parameters, nonlinear behaviour can be studied only if there are more than two levels of the parameters. Therefore, each parameter was analysed at three levels (Singh et al. 2011 a, Goyal et al. 2013, Walia et al. 2004).

Table 8.15 Raw data and Signal to noise ratio for different parameters

Process parameter	Level		Tool diameter (A)	Flow rate (B)		Powder Concentration (C)		Pressure (D)	
Type of data		S/N Ratio	Raw data	S/N Ratio	Raw data	S/N Ratio	Raw data	S/N Ratio	Raw data
Avg. values (% TWR)	L1	-4.04	1.58	-1.45	1.22	0.19	1.05	-1.15	1.24
	L2	1.20	0.90	1.56	0.90	-3.01	1.41	-0.24	1.06
	L3	0.68	0.98	-2.26	1.34	0.66	1.00	-0.75	1.16
Main effects (%TWR)	L2-L1	5.24	-0.68	3.01	-0.32	-4.23	0.36	0.91	-0.18
	L3-L2	-0.52	0.08	-3.82	0.44	3.67	-0.41	-0.51	0.10
Differences (L3-L2)-(L2-L1)		-5.76	0.76	-6.83	0.76	7.9	-0.77	-1.42	0.28
*L1, L2, L3 represent levels 1, 2 and 3 respectively of parameters. (L2-L1) is the average main effect when the corresponding parameter changes from Level 1 to Level 2. (L3-L2) is the main effect when the corresponding parameter changes from Level 2 to Level 3.									

Table 8.16 Pooled ANOVA raw data for TWR

Source	SS	SS (S/N)	DOF	DOF (S/N)	V	V (S/N)	F-ratio	F-ratio (S/N)	SS'	SS' (S/N)	P%	P% (S/N)
Tool Diameter	2.54	50.24	2	2	1.27	25.12	49.84	39.88	2.50	48.98	54.25	48.92
Flow rate	1.28	29.54	2	2	086	15.27	27.83	29.48	0.86	33.28	32.80	28.25
Powder concentration	0.91	24.08	2	2	0.45	14.04	17.99	19.12	0.51	22.82	10.99	20.79
Pressure	0.61	22.92	2	*	0.36	*	12.71	*	0.42	*	5.2	*
Error	0.51	1.25	20	2	0.02	0.62	-	-	0.63	5.03	12.94	5.03
Total	4.88	100.13	28	8	-	-	-	-	4.88	100.13	100	100
*Significant at 95% confidence level, F critical=3.55 (Tabular value), SS-Sum of squares, DOF- Degree of freedom, V-variance, SS' Pure sum of squares												

The TWR decreases with increase in dimensions of tool diameter because the flushing takes place more efficiently which provides better cooling condition at the tool tip which brings down the temperature at the sparking ends of the hollow tool electrodes. However with further increase in tool diameters there was no significant effect on TWR as seen in Figure 8.24 (a).

TWR first decreases at low flow rate due to poor heat dissipation and this resulted in some part of molten eroded material forming a solidified layer at the tool tip which reduces the wear at the tool end but further increases in flow rate facilitates material removal of the tool electrode because simultaneously more material is also gets eroded from the workpiece which consumes the tool tips rapidly due to better machining efficiency as shown in Figure 8.24 (b). The powder concentration affects the TWR in a certain manner. Similar analysis for TWR in powder mixed near dry EDM was performed and the results were comparable to trend of TWR with respect to dielectric mist flow rate (Bai et al. 2013, a).

Initially with increase of powder concentration, the TWR increases but afterwards with further increase in powder concentration the TWR starts decreasing as shown in Figure 8.24 (c).The reason was that powder concentration influences the heat received by the tool and adhesion of molten material on the face of the tool. Due to this phenomenon molten materials solidification takes place in discharge gap. As a result, materials that can adhere onto the surface of tool electrode are reduced, and therefore TWR was increased. On the other hand with further increase of metallic powder concentration, heat at discharge gap gets increased which forms adhesive layer over the tool end which reduces TWR. Powder concentration was significant factor affecting TWR.TWR increases with lower range of powder concentration but then decreases (Ojha et al. 2011).

TWR shows the decreasing trend when the air pressure changes from 0.4 MPa to 0.5 MPa as shown in Figure 8.24 (d).With increase of air pressure there were more molecules at the IEG which enhances discharging. The discharge gap got enlarged due to this phenomenon which led to improved deionization effect. Effects of abnormal short circuit and arc discharge were reduced which eventually led to better heat dissipation and reduced heat transfer at the tool. All these factors contributed to reduction in TWR till 0.5 MPa. But with further increase of pressure the gap voltage increases due to which the plasma generated is not uniformly distributed and improper erosion takes place which led to increase in TWR. The similar experimental outcome of the results was comparable to research performed (Mane and Hargude, 2015).

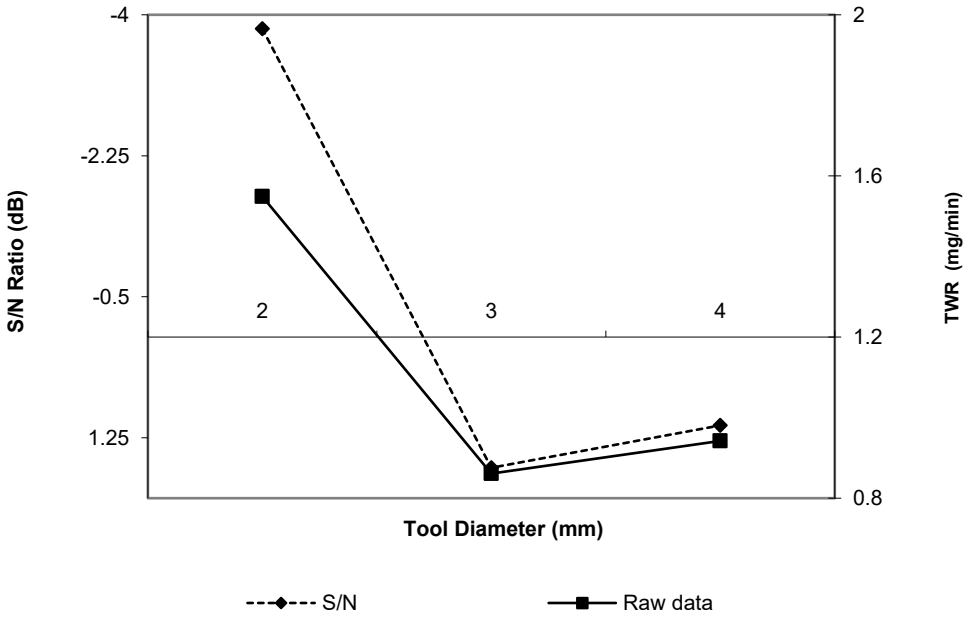

Figure 8.24 (a) Effect of tool type on TWR

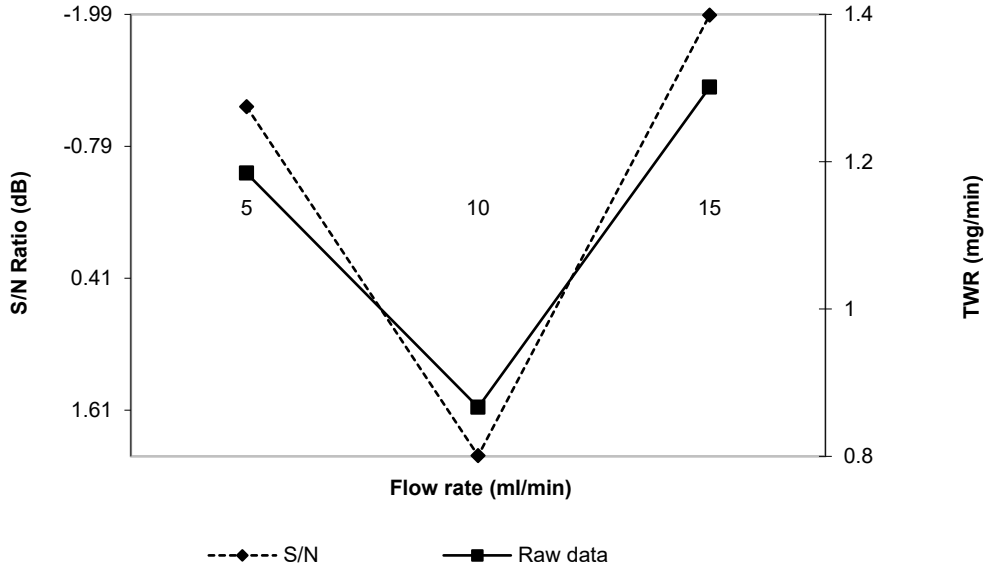

Figure 8.24 (b) Effect of Flow rate on TWR

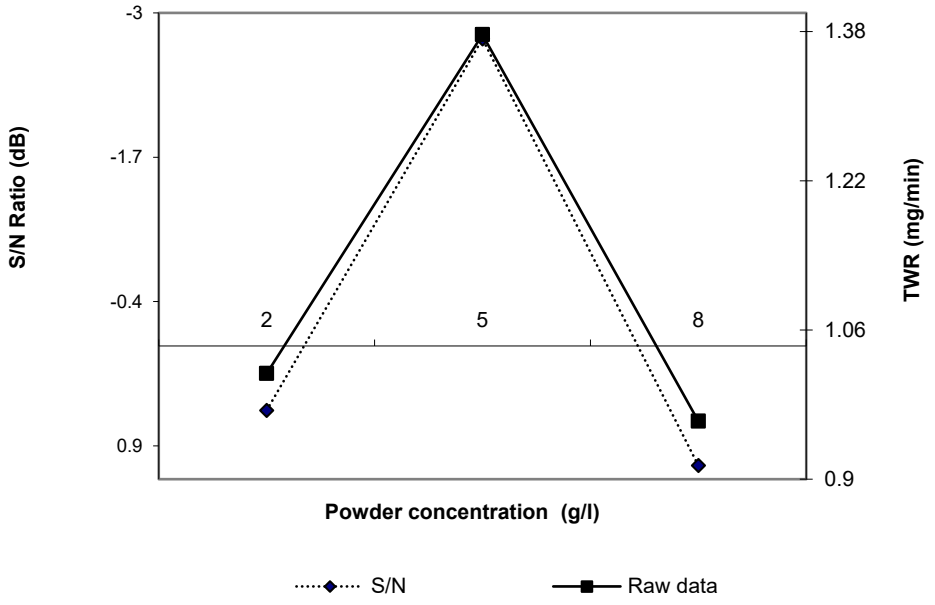

Figure 8.24 (c) Effect of powder concentration on TWR

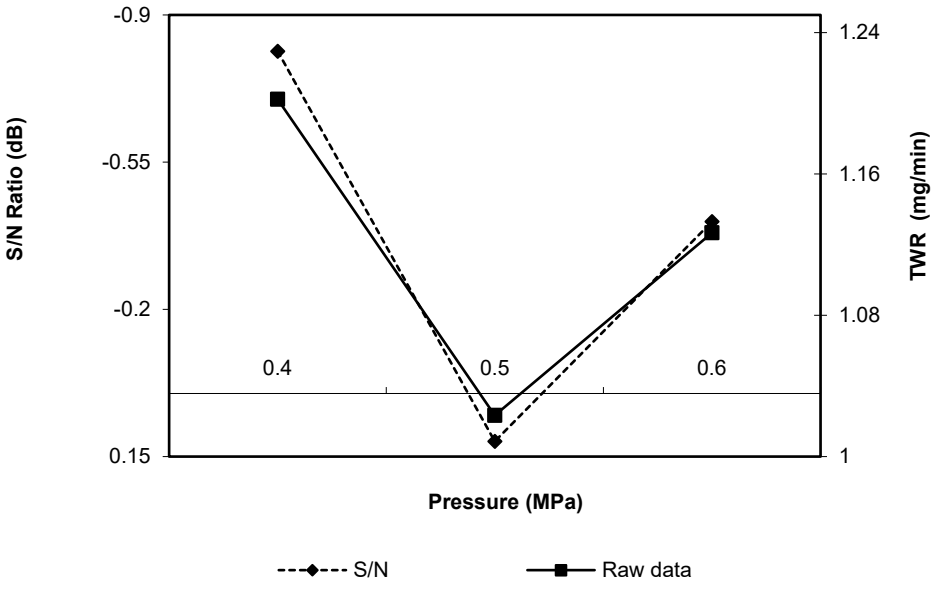

Figure 8.24 (d) Effect of pressure on TWR

Parametric optimization of TWR was studied with different combination of tool electrode composition such as half of the chemical composition of tool was made up of conductive material such as copper and another half of the tool composition was made up of conductive abrasive (Jeswani, 1981). It was revealed with the study that with abrasives, the TWR tends to decrease as

compared to simple conductive tool without any conductive abrasive particles embedded in the tool. By addition of graphite powder the discharge gap was increased and stable machining was initiated with reduced gap voltage which reduced the TWR (Jeswani, 1981). The wear of the sparking ends of the tool electrode tip after experimentation is shown in Figure 8.25.

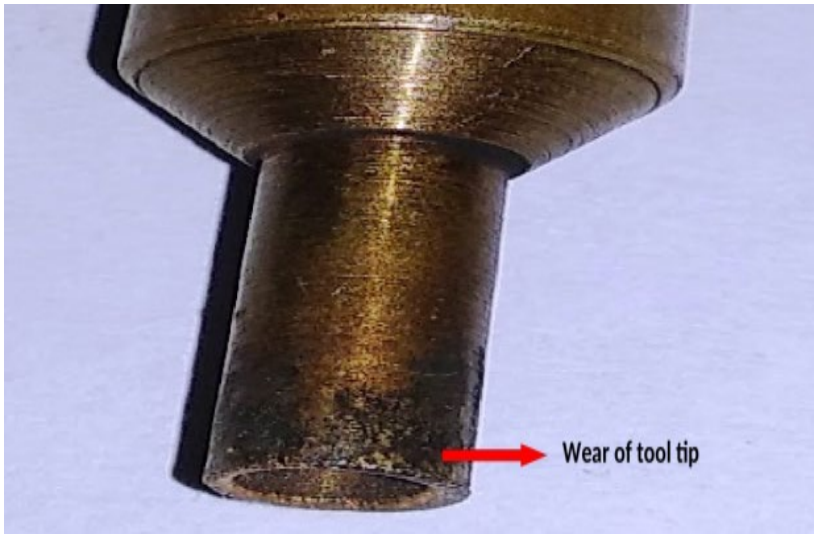

Figure 8.25 Wear of the sparking end of the tool

8.5.1 Estimation of optimum performance characteristics (TWR)

The optimum value of TWR was predicted at the selected levels of significant parameters $A_2B_2C_3D_2$. The estimated mean of the response characteristic (TWR) can be determined by Eq. 8.10 (Walia et al. 2006) as:

$$TWR = \overline{A_2} + \overline{B_2} + \overline{C_3} + \overline{D_2} - 3\bar{T} \quad (8.10)$$

Where $\bar{T}$ (overall mean of TWR) = 1.15 mg/min (Table 8.14), A_2 (Average TWR at the second level of tool diameter) = 0.90 mg/min, B_2 (Average TWR at the second level of flow rate) = 0.90 mg/min, C_3 (Average TWR at the third level of powder concentration) = 1.00 mg/min, D_2 (Average TWR at the second level of pressure) = 1.06 mg/min.

Upon substituting the above values in Eq. 8.10,

TWR = 0.90 + 0.90 + 1.00 +1.06 - 3 × 1.15 = 0.41 mg/min.

The 95% confidence interval of conformation experiments (CI_{CE}) and confidence interval of population (CI_{POP}) was calculated by using the following Eqs. (8.11 - 8.12):

$$CI_{CE} = \sqrt{F_{\alpha}(1, f_e)V_e\left[\frac{1}{n_{eff}} + \frac{1}{R}\right]} = \pm 0.21, \quad (8.11)$$

$$CI_{POP} = \sqrt{\frac{F_\alpha(1,f_e)V_e}{n_{eff}}} = \pm 0.15 \quad (8.12)$$

Where, F_α (1, f_e) = the F ratio at the confidence level of (1 –α) against DOF 1.

$$n_{eff} = \frac{N}{1+[\text{DOF associated in the estimate of mean response}]} = 3$$

N (Total number of experiments) = 27;

Treatment = 9, repetition = 3;

R = sample size for confirmation experiments = 3.

V_e(error variance) = 0.02 (Table 8.16), f_e (error DOF) = 20 (Table 8.16).

F = 3.5546 (tabulated F value).

So, CI_{CE}= ± 0.21, CI_{POP}= ± 0.15

The predicted optimal range of confidence interval of conformation experiments (CI_{CE}) is :

Mean TWR − CI_{CE}< TWR (mg/s) < mean TWR + CI_{CE}

i.e 0.20 mg/min < TWR (mg/min) < 0.62

The predicted optimal range of confidence interval of population (CI_{POP}) is :

Mean TWR − CI_{POP}< TWR (mg/min) < mean TWR+ CI_{POP}

i.e 0.26 mg/min < TWR (mg/min) < 0.56 mg/min

Thus, it is proven by the range that the predicted value of TWR lies in the optimum range.

8.5.2 Confirmation of tests

Confirmation tests were performed in three runs in order to bring out the validation between predicted and experimental results. The experiments were performed at most optimum levels of different input process parameters. It was revealed by experiments that the predicted values were within +/- 5% error range as shown in Table 8.17. The experiments conducted at optimum levels of four parameters gave TWR of 0.43 mg/min. The three set of experiments were conducted under optimized conditions as shown in Table 8.17.

Table8.17 Predicted optimal values and results of confirmation experiments

Optimization type	Objective	Optimized process variables				Predicted Response (mg/min)	Confirmation Result (mg/min)
		Tool diameter (mm)	Flow rate (ml/min)	Powder concentration (g/l)	Mist pressure (MPa)		
Single response	Minimization of Tool wear rate	3	10	8	0.5	0.41	0.43

8.6 Optimization for Micro-hardness (MH) in PMND-EDM

The experiments were performed as per experimental conditions of process parameters at different levels given in Table 8.18. Taguchi L_9 OA was utilized for design of experiments and the tests for micro-hardness were performed thrice for repeatability. A total of twenty seven experiments were performed (three repeatability for each set of process parameter condition).

Table 8.18 The experimental results for micro-hardness by PMND-EDM as per Taguchi L_9 OA

Exp. No.	Parameter trial condition				Micro-hardness			*S/N* [dB]
	A	B	C	D	R1	R2	R3	
1	2	2	15	0.4	175	100.25	338.93	41.52
2	2	5	20	0.5	450	350.78	345.08	49.69
3	2	8	25	0.6	505.63	501.78	540.89	52.47
4	3	5	15	0.6	59.37	45.96	50.26	32.39
5	3	8	20	0.4	112.23	259	189	42.13
6	3	2	25	0.5	132.23	55.63	62.38	34.96
7	4	8	15	0.5	148.96	192.85	200.56	43.15
8	4	2	20	0.6	237	215	350.22	46.23
9	4	5	25	0.4	201	222.37	245	45.11
Overall mean Vickers micro-hardness ($\overline{HV}$)= 232.86 load of micro-hardness measurements300N/20s								

The main effects and *S/N* ratio for average micro- hardness and pooled ANOVA are given in Tables 8.19 and 8.20 respectively for different process parameters. The effect of input parameters at different levels on micro-hardness value (average) was plotted as shown in Figure 8.26 while instrumental reading is depicted in Figure 8.27. It was observed that process parameters at A_1, B_2, C_3 and D_3 were most significant in enhancing the micro-hardness of EN-31 workpiece machined by PMND-EDM. The force applied for micro-hardness testing was 300 N/20s by the Fischer micro-hardness machine.

The average % value was calculated for micro-hardness for different parameters. After that main effects % of micro-hardness were calculated by expression (L2-L1) and (L3-L2). Finally the difference between L2, L1 and L3, L2 was calculated. Analysis of variance was done for TWR S/N ratio on the results obtained at 95% confidence level.

Table 8.19 Main effects table for micro-hardness

Process parameter	Level	Tool diameter(A)		Flow rate (B)		Powder concentration (C)		Pressure(D)	
Type of data		S/N Ratio	Raw data	S/N Ratio	Raw data	S/N Ratio	Raw data	S/N Ratio	Raw data
Avg values (%micro-hardness)	L1	47.8	367.5	39	145.7	40.9	185.1	42.9	204.7
	L2	36.4	107.3	46	278.7	42.3	218.8	42.6	215.3
	L3	44.8	223.6	44.1	274.1	45.9	294.5	43.7	278.4
Main effects (**%**micro-hardness)	L2-L1	-11.3	-260.2	6.9	132.9	1.4	33.6	-0.3	10.6
	L3-L2	8.3	116.3	-1.8	-4.6	3.5	75.6	1.0	63.0
Differences (L3-L2)-(L2-L1)		19.7	376.5	-8.8	-137.5	2.0	41.9	1.4	52.4
*L1, L2, L3 represent levels 1, 2 and 3 respectively of parameters. (L2-L1) is the average main effect when the corresponding parameter changes from Level 1 to Level 2. (L3-L2) is the main effect when the corresponding parameter changes from Level 2 to Level 3.									

Table 8.20 Pooled ANOVA raw data and S/N data for micro-hardness

Source	SS raw	SS S/N	DOF raw	DOF S/N	V raw	V S/N	F-ratio Raw	F-ratio S/N	SS' raw	SS' S/N	P% raw	P% S/N
Tool diameter	305936.46	208.81	2	2	152968.2	104.40	42.21	109.04	298690.1	206.90	53.46	62.78
Flow rate	102445.57	79.03	2	2	51222.78	39.51	14.13	41.27	95199.25	77.12	17.04	23.40
Powder concentration	56465.03	39.77	2	2	28232.52	19.88	7.79	20.76	49218.71	37.85	8.81	11.48
Pressure	28569.57	*	2	*	14284.79	*	3.94	*	21323.25	*	3.81	*
Error	65216.86	1.91	18	2	3623.15	0.95	-	-	94202.14	7.65	16.86	2.32
Total	558633.51	329.54	26	8	-	-	-	-	558633.5	329.54	100	100
*Significant at 95% confidence level, F critical (raw) =3.55 (tabular value), F critical (S/N)=19 (tabular value),SS-Sum of Squares, DOF-Degree of Freedom, V-Variance, SS' - Pure sum of Squares P - Probability of obtaining the observed results of a test												

Parameter A (Tool type) at level 1 was most significant in increasing the micro-hardness value of the machined EN-31 sample as shown in Figure 8.26 (a). At this level the dielectric medium dispersion from the tool tip was found to be very suitable. Due to this proper dispersion, stable discharging was observed at the inter electrode gap (IEG) which results in higher value of micro-hardness. The signal to noise ratio (*S/N*) in the graph plotted also shows the same trend.

Secondly flow rate was found to be most influential at 2nd level in increasing the micro-hardness value as shown in Figure 8.26 (b). At this level, the flow rate of the dielectric medium at 10ml/min

was most optimum in providing suitable normal discharges at the machining zone along with powder additives which results in higher value of micro-hardness.

The micro-hardness value was found to be highest at 3rd level of powder additives (metallic) concentration as shown by the trend of plot in Figure 8.26 (c.) The micro-hardness value increased with respect to increase in metallic powder concentration which can be observed in the Figure 8.26 (c). Zinc carbide (ZnC) hard layer was formed over the top surface of the workpiece due to rich amount of zinc deposition at the melting and re-solidification zone over the surface of the sample (Figure 8.28) while machined surface is given in Figure 8.29. As stated that pyrolysis of dielectric results in diffusion of oxygen and carbon which also results in formation of hard carbides and oxides over the top layer of the machined workpiece. All these factors resulted in achieving the best micro-hardness value at 3rd level of process parameter. This increased the micro hardness of the surface which was similar with the results obtained by Gill and Kumar (2016).

Dielectric mist pressure at 3rd level (0.6MPa) was most significant in enhancing the micro-hardness value as shown in Figure 8.26 (d) and the *S/N* also shows the same trend in the plot. The trend displayed that the micro-hardness value increased with increase in the mist flow pressure. Excellent debris removal and cooling effect over the machined sample at this mist pressure resulted in achieving the maximum micro-hardness value at the sample surface.

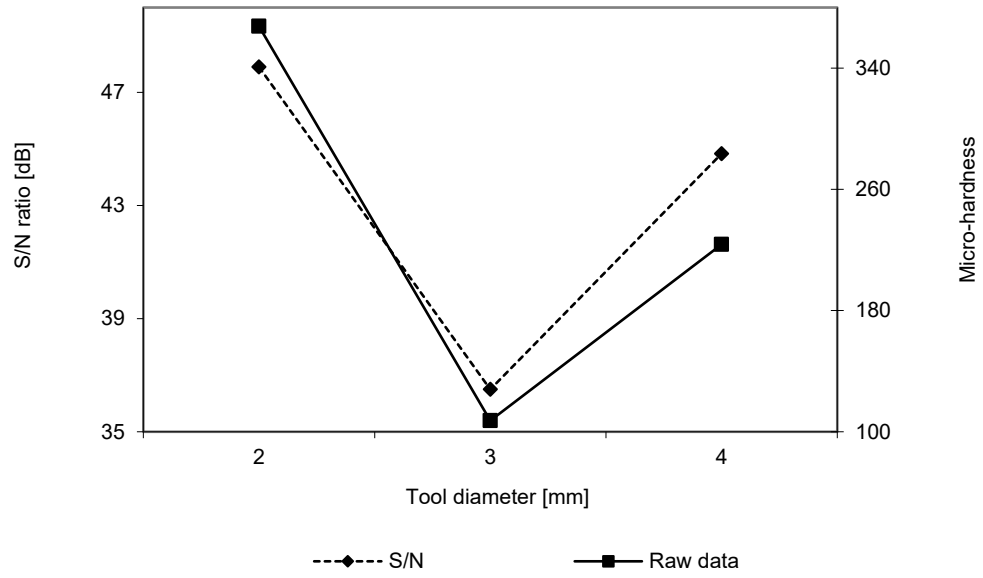

Figure 8.26 (a) Effect of tool type on MH

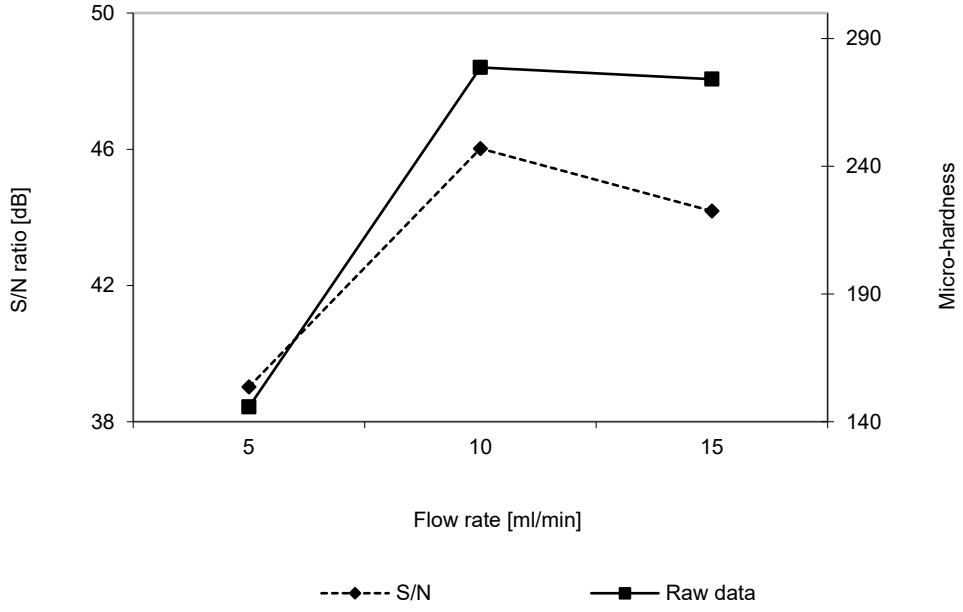

Figure 8.26 (b) Effect of Flow rate on MH

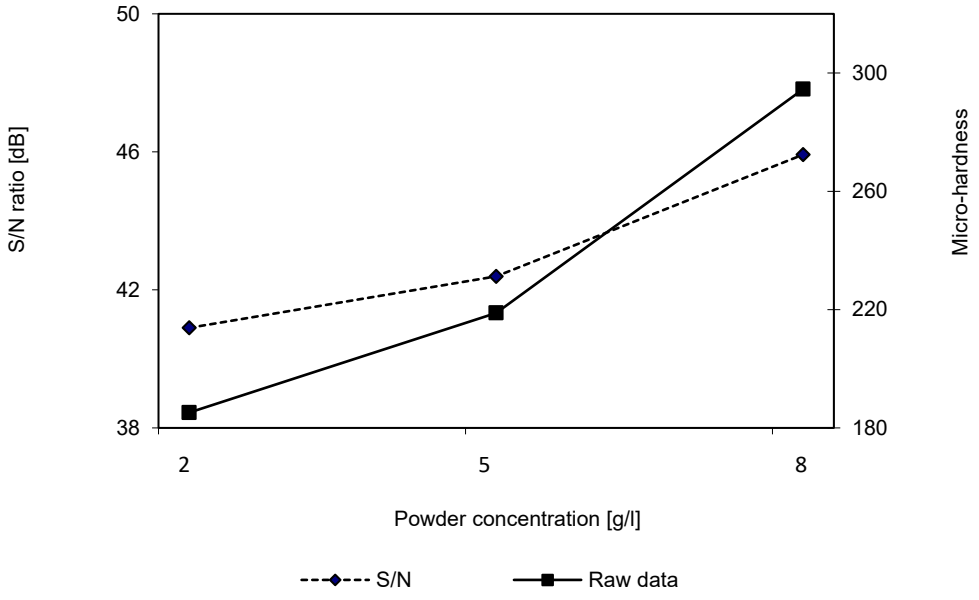

Figure 8.26 (c) Effect of powder concentration on MH

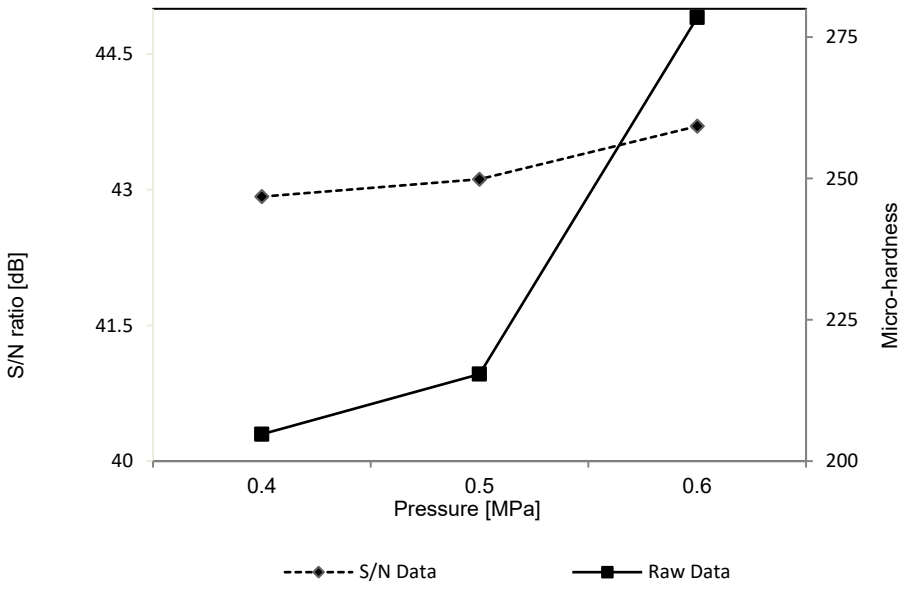

Figure 8.26 (d) Effect of pressure on MH

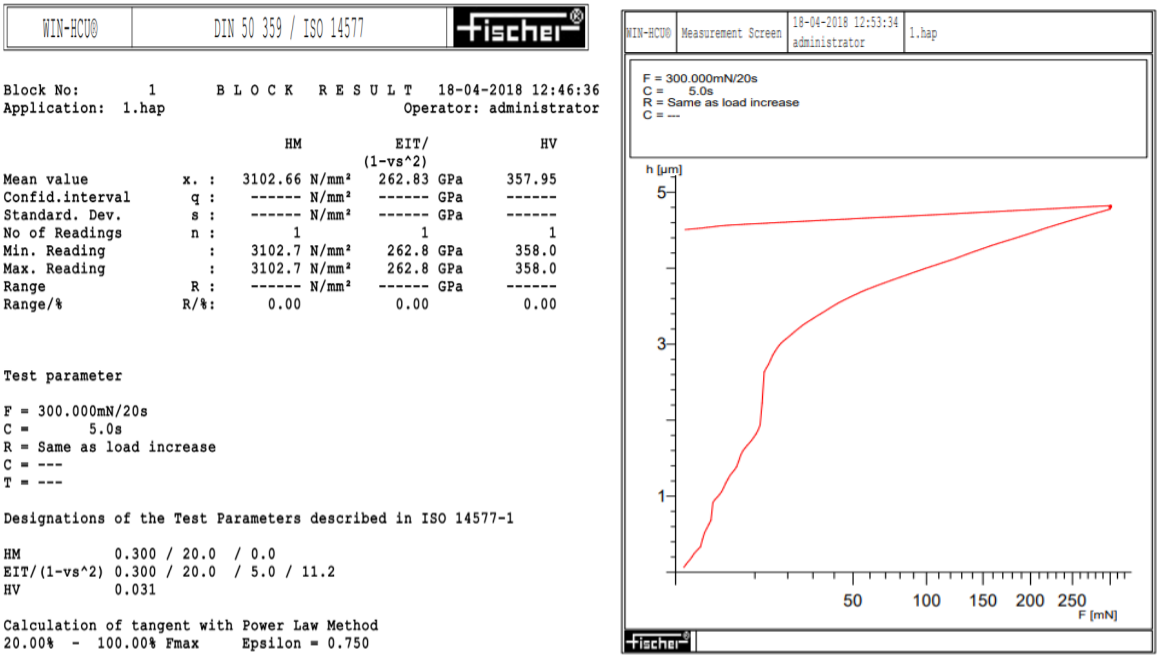

WIN-HCU® | DIN 50 359 / ISO 14577 | Fischer®

Block No: 1 B L O C K R E S U L T 18-04-2018 12:46:36
Application: 1.hap Operator: administrator

		HM	EIT/(1-vs^2)	HV
Mean value	x. :	3102.66 N/mm²	262.83 GPa	357.95
Confid.interval	q :	------ N/mm²	------ GPa	------
Standard. Dev.	s :	------ N/mm²	------ GPa	------
No of Readings	n :	1	1	1
Min. Reading	:	3102.7 N/mm²	262.8 GPa	358.0
Max. Reading	:	3102.7 N/mm²	262.8 GPa	358.0
Range	R :	------ N/mm²	------ GPa	------
Range/%	R/%:	0.00	0.00	0.00

Test parameter

F = 300.000mN/20s
C = 5.0s
R = Same as load increase
C = ---
T = ---

Designations of the Test Parameters described in ISO 14577-1

HM	0.300 / 20.0 / 0.0
EIT/(1-vs^2)	0.300 / 20.0 / 5.0 / 11.2
HV	0.031

Calculation of tangent with Power Law Method
20.00% - 100.00% Fmax Epsilon = 0.750

Figure 8.27 (a) Instrument reading and plot of MH with respect to load applied

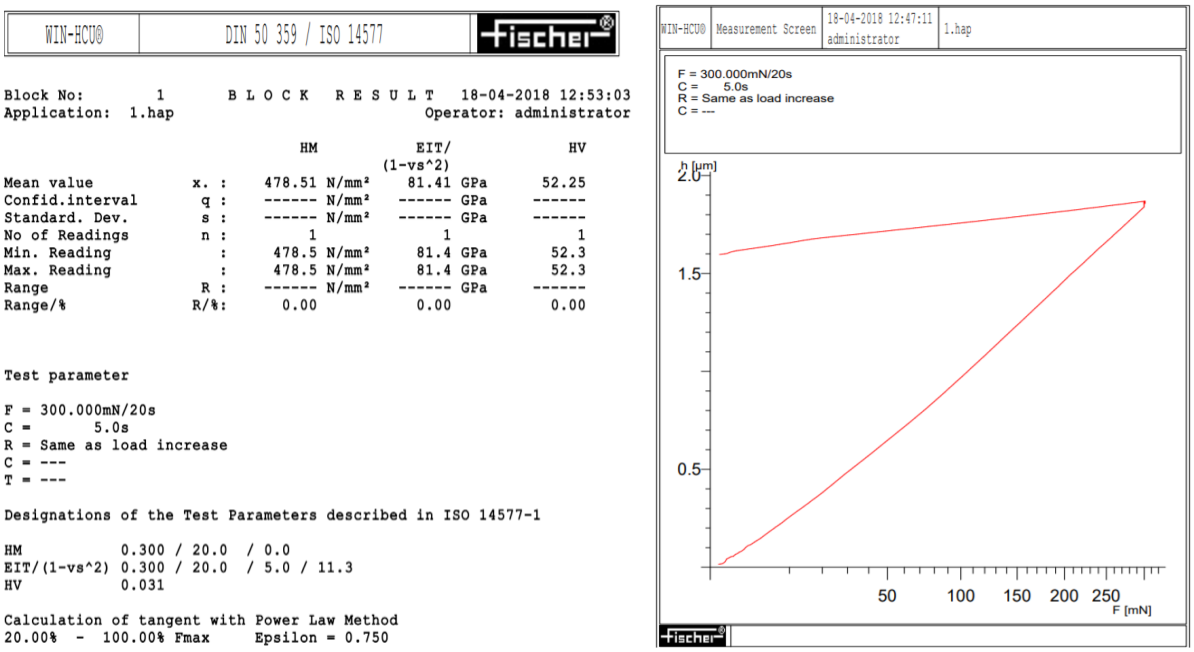

WIN-HCU® | DIN 50 359 / ISO 14577 | Fischer

Block No: 1 B L O C K R E S U L T 18-04-2018 12:53:03
Application: 1.hap Operator: administrator

		HM	EIT/(1-vs^2)	HV
Mean value	x. :	478.51 N/mm²	81.41 GPa	52.25
Confid.interval	q :	------ N/mm²	------ GPa	------
Standard. Dev.	s :	------ N/mm²	------ GPa	------
No of Readings	n :	1	1	1
Min. Reading	:	478.5 N/mm²	81.4 GPa	52.3
Max. Reading	:	478.5 N/mm²	81.4 GPa	52.3
Range	R :	------ N/mm²	------ GPa	------
Range/%	R/%:	0.00	0.00	0.00

Test parameter

F = 300.000mN/20s
C = 5.0s
R = Same as load increase
C = ---
T = ---

Designations of the Test Parameters described in ISO 14577-1

HM	0.300	/ 20.0	/ 0.0
EIT/(1-vs^2)	0.300	/ 20.0	/ 5.0 / 11.3
HV	0.031		

Calculation of tangent with Power Law Method
20.00% - 100.00% Fmax Epsilon = 0.750

Figure 8.27 (b) Instrument reading and plot of MH with respect to load applied

The microstructure of the machined workpiece changes by re-crystallization phenomenon due to rapid heating and cooling during machining process (Singh et al. 2017). The shape of the material grains and subsequently the surface properties of the machined workpiece are determined by the heating and cooling rate.

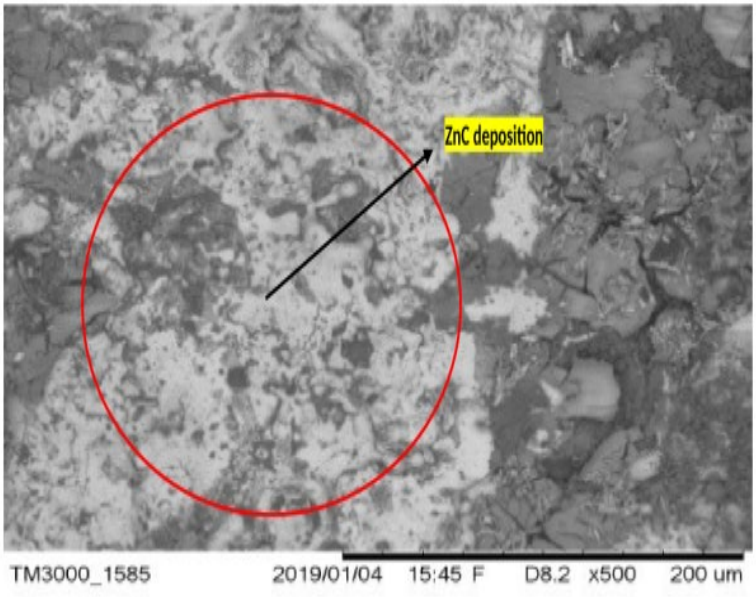

Figure 8.28 ZnC layer formation over the machined sample

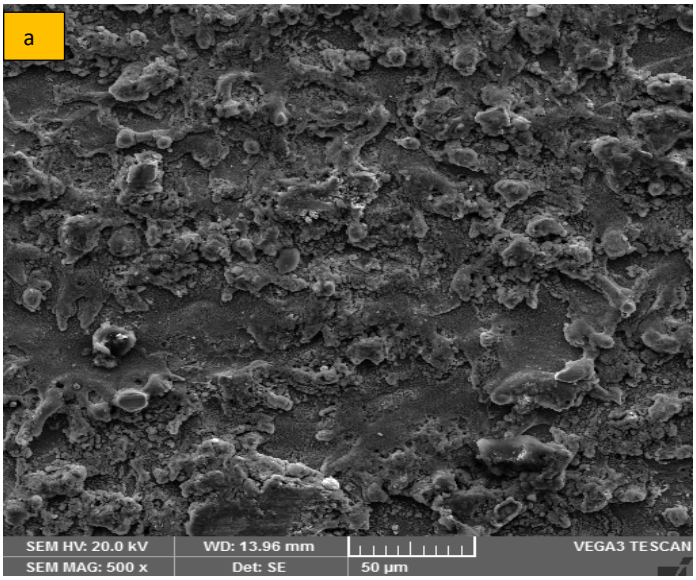
a
SEM HV: 20.0 kV
WD: 13.96 mm
VEGA3 TESCAN
SEM MAG: 500 x
Det: SE
50 µm

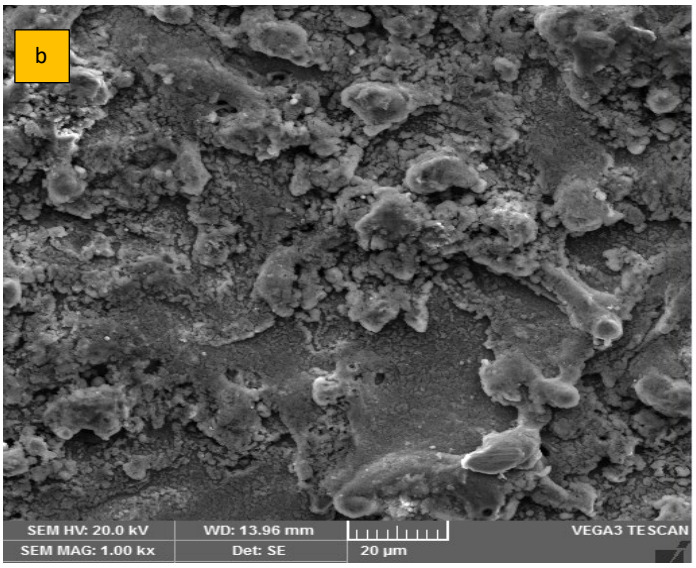
b
SEM HV: 20.0 kV
WD: 13.96 mm
VEGA3 TESCAN
SEM MAG: 1.00 kx
Det: SE
20 µm

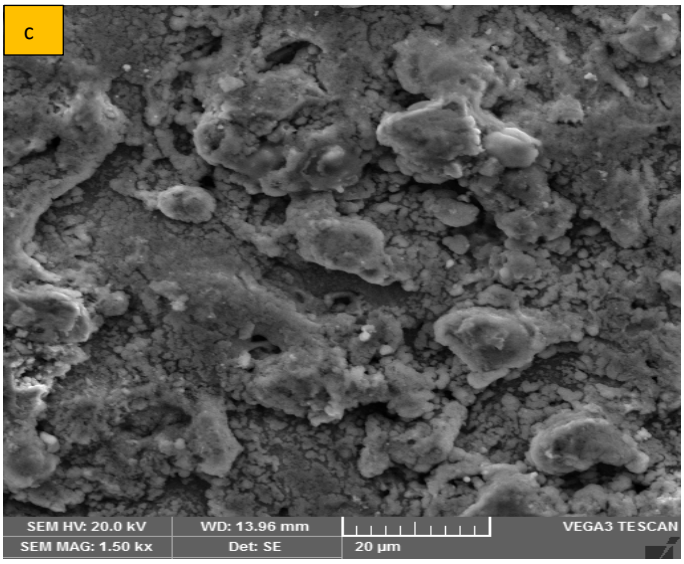
c
SEM HV: 20.0 kV
WD: 13.96 mm
VEGA3 TESCAN
SEM MAG: 1.50 kx
Det: SE
20 µm

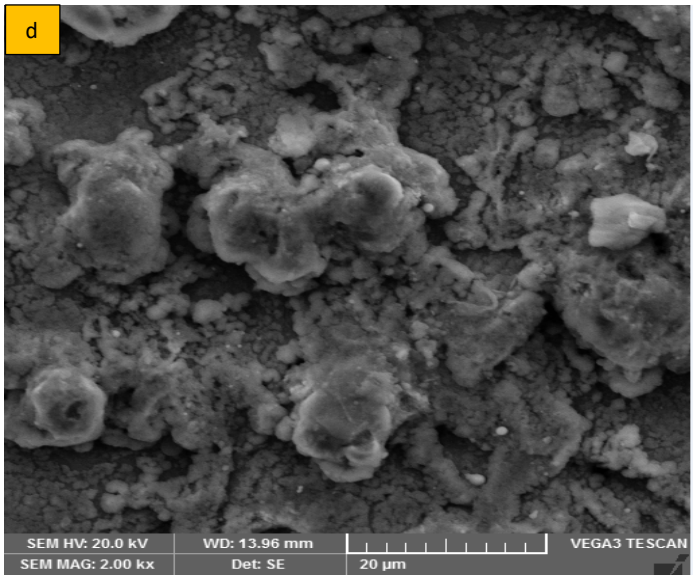

Figure 8.29 SEM images of machined samples at different magnification factor (a) 500x (b) 1.0 kx (c) 1.5 kx (d) 2 kx

Figure 8.30 shows recast layer at the top altered surface due to meting and re-solidification of the molten material. Due to change in chemical composition and rapid cooling by flushing here was a metallurgical structural change. Heat affected zone was found below the recast layer due to heat generated by the plasma at the inter electrode gap (IEG). The white layer indicated the metallographic phase due to adequate carbon present which results in formation of ZnC deposits (10 µm) along with the solidified molten material while comparison was also made with machined sample without metallic powder and there was negligible metallurgical transformation as shown in Figure 8.31.

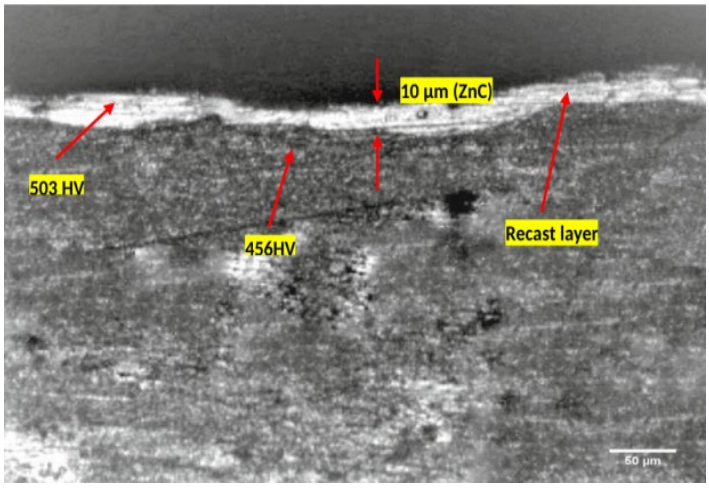

Figure 8.30 SEM micrograph of cross section with average values of micro-hardness

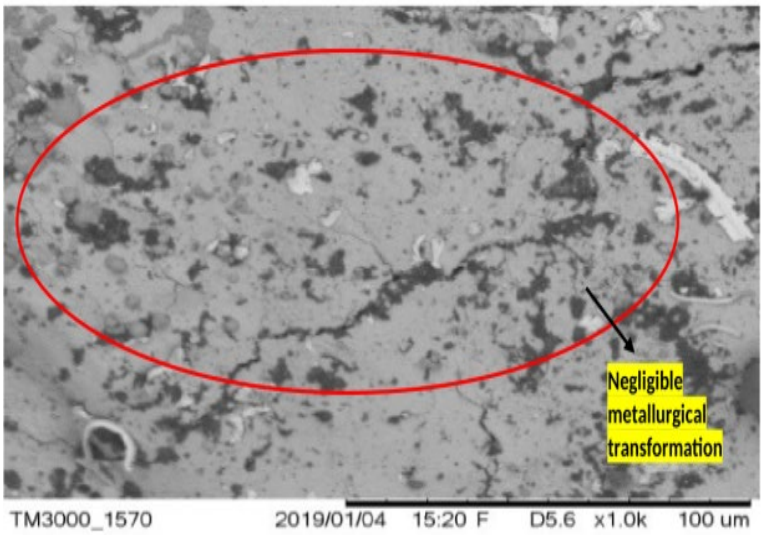

Figure 8.31 SEM micrograph of machined sample by EDM without metallic powder

8.6.1 Estimation of Performance Characteristics (Micro-Hardness)

Response characteristic micro-hardness can be determined by using Eq. 8.13, (Walia et al. 2006) and (Brar et al. 2015):

$$Micro\text{-}hardness = \overline{A_1} + \overline{B_2} + \overline{C_3} + \overline{D_3} - 3\overline{HV} = 520.7\ HV. \quad (8.13)$$

The confidence interval of confirmation experiments can be determined by Eq. 8.14:

$$CI_{CE} = \sqrt{F_a(1, f_e) V_e \left[\frac{1}{n_{eff}} + \frac{1}{R}\right]} = 75.65 \quad (8.14)$$

The confidence interval of population can be determined by Eq. 8.15:

$$CI_{pop} = \sqrt{Fa\ (1, fe)\ Ve\ /\ n_{eff}} = 37.82, \quad (8.15)$$

where, $F_\alpha(1, fe)$ is the F ratio at the confidence level of $(1 - \alpha)$ against DOF 1.

$F_{0.05}(1,18) = 3.5546$ (Tabulated)

$$n_{eff} = \frac{N}{1 + [\text{DOF associated in the estimate of mean response}]} = 9,$$

Where: Total number of experiments $N = 27$; Treatment is 9, repetition 3; and sample size for confirmation experiments, R, is= 3.

V_e, error variance = 3623.15 (Table 8.20), f_e, error DOF = 26 (Table 8.20), $F = 3.5546$ (tabulated F value),

So, micro-hardness is 520.7, $CI_{CE} = \pm 75.65$, $CI_{POP} = \pm 37.82$

The predicted optimal range of confidence interval of conformation experiments (CI_{CE}) is:

Mean micro-hardness− CI_{CE}<micro-hardness< mean micro-hardness+ CI_{CE}

i.e. 445.05<micro-hardness< 596.35

The 95% conformation interval of the predicted mean is:

Mean micro-hardness− CI_{POP}<micro-hardness< mean micro-hardness+ CI_{POP}

i.e 482.88<micro-hardness< 558.52

The confirmation tests for micro-hardness were performed by setting machining conditions at the optimal process parameters values given below:

Tool diameter at level 1 (2mm);

Flow rate at level 2 (10ml/min);

Powder concentration at level 3 (8 g/l);

Dielectric mist pressure at level 3 (0.6 MPa);

8.6.2 Confirmation Experiments

The confirmation test was performed for micro-hardness at A_1, B_2, C_3 and D_3 experimental conditions as shown in Table 8.21. The confirmation tests were run thrice in order to get the average value in order to reduce the percentage error in experimentations. The micro-hardness values achieved were 449.30 HV, 510.39 HV and 560.21 HV respectively for three trials and the average value was 506.63 HV. The mean micro-hardness calculated was within the confidence interval of predicted micro-hardness.

Table8.21 Predicted optimal values and results of confirmation experiments

Optimization type	Objective	Optimized process variables				Predicted Response (HV)	Confirmation Result (HV)
		Tool diameter (mm)	Flow rate (ml/min)	Powder concentration (g/l)	Mist pressure (MPa)		
Single response	Maximization of micro-hardness	2	10	8	0.6	520.7	506.21

8.7 Multi - Characteristic Optimization Using Utility Function

This section includes multi response characteristic optimization using utility function. A unified index term was used as criteria for overall effectiveness or usefulness by taking into consideration

the individual utility of each different quality characteristics of the process. Afterwards, plotting was performed by using ANOVA technique for multi responses. At the end, confirmation experiments were performed for each response characteristics.

A number of different techniques have been established till date for multi response characteristic optimization. In this present research study, a simplified methodology by using utility concept with Taguchi's approach has been used to determine the optimal setting of process parameters for multi – objective responses. In fact this multi methodology was brain child of research work carried for different case study (Byrne and Taguchi, 1987).

8. 7.1 Multi-objective optimization of PMND-EDM through Taguchi method and Utility concept

Taguchi method along with utility concept was utilized for multi-response optimization (MRR, Ra, RS, MH and TWR) for determining the process parameters optimal settings in PMND-EDM. Utility concept was defined as the usefulness of the process with respect to the users' expectation. A unified index term was used as criteria for overall effectiveness or usefulness by taking into consideration the individual utility of each different quality characteristics of the process.

Suppose let us consider, Xi was the usefulness measure of a quality characteristics 'i' and if there are 'n' attributes evaluating the outcome, so combined utility function was expressed as (Derek,1982):

$$U(X_1, X_2, \ldots, X_n) = f(U_1(X_1), U_2(X_2), \ldots, U_n(X_n)) \quad (8.16)$$

Where,

Where Ui (Xi) was the utility of the ith attribute. The expression for sum of individual utilities was given by overall utility function for independent attributes by (Derek, 1982):

$$U(X_1, X_2, \ldots, X_n) = \sum_{i=1}^{n} U_i(X_i) \quad (8.17)$$

While, overall utility function after assigning weights to the attributes can be expressed as:

$$U(X_1, X_2, \ldots, X_n) = \sum_{i=1}^{n} W_i U_i(X_i) \quad (8.18)$$

Where W_i was the weight assigned to the attribute *'i'*.

A scale (preference) was constructed for each quality characteristics for utility value determination. Preference numbers (P; (0-9)) were assigned for just acceptable and best value. The P_i number was given as (kumar et al. 2000):

$$P_i = A \log\left(\frac{Xi}{Xi'}\right) \quad (8.19)$$

where *Xi*= value of any quality characteristic or attribute i, Xi' = just acceptable value of quality characteristic or attribute i, A=constant, $P_i = 9$ (Assumed at optimum value)*;*

Where A was calculated by:

$$A = \frac{9}{\log\frac{X^*}{X_i'}} \quad (8.20)$$

X^* = optimal best value of single response optimization (Refer Table 8.23), for X_i' (Refer Table 8.22)

The weightage should be assigned such that the following condition is satisfied:

$$\sum_{i=1}^{n} W = 1 \quad (8.21)$$

Therefore overall utility was defined as (Walia et al. 2006):

$$U = \sum_{i=1}^{n} U_i \; P_i \quad (8.22)$$

The utility was considered higher the better and hence it was maximized, therefore quality characteristics will be optimized automatically (minimized or maximized)

For MRR; $A = \frac{9}{\log\frac{0.346}{0.01}}$ *:* $A_{mrr} = 5.847$

For Ra; $A = \frac{9}{\log\frac{0.325}{1.77}}$ *;* $A_{Ra} = -12.228$

For RS ; $A = \frac{9}{\log\frac{106.40}{678}}$ *;* $A_{RS} = 11.19$

For MH; $A = \frac{9}{\log\frac{506.21}{55.63}}$*;* $A_{MH} = 9.3833$

For TWR; $A = \frac{9}{log\frac{0.41}{1.81}}$ $A_{TWR} = 13.97$

8.7.2 Algorithm for multi-response optimization for MRR, Ra, RS, MH and TWR in PMND-EDM

1. To find optimum value of response characteristics separately using single response Taguchi optimization technique

2. Construction of preference scales for each response characteristic from the experimental data using Eqs.8.20-8.24.

3. Assignment of weightage to satisfy Eq.8.21.

4. Finding the utility value for each product using Eq.8.22.

5. Application of utilities in the orthogonal array as per Taguchi design of experiments and finding the S/N ratios.

6. Analysis of the results.

7. Determination of optimal setting of process parameters for optimization of the utilities.

8. Prediction of response characteristics by using optimal settings of parameters.

9. Conducting confirmation experiments and their comparison with predicted value for validation of the results.

Taguchi L_9 optimization has been implemented for parameters tool type, flow rate, powder concentration and mist pressure and the results for individual outcomes are shown in Table 8.22 (as per chapter 7) while Table 8.23 shows the values of response at optimal process parameters conditions.

Table 8.22 Individual outcomes for MRR, Ra, RS, MH and TWR in PMND-EDM

Exp.No	MRR (mg s^{-1})			S/N (dB)	Ra (µm^{1})			S/N (dB)	RS (MPa)			S/N (dB)	TWR (mg/min)			S/N (dB)	Micro-hardness (HV)			S/N (dB)
	R1	R2	R3		R1	R2	R3		R1	R2	R3		R1	R2	R3		R1	R2	R3	
1	0.07	0.06	0.09	-24.11	1.61	1.41	1.77	-4.10	565	558	530	-54.82	1.65	1.45	1.81	-4.31	175	100.25	338.93	41.52
2	0.22	0.10	0.21	-18.12	1.66	1.38	1.35	-3.34	621	551	550	-55.19	1.70	1.42	1.39	-3.57	450	350.78	345.08	49.69
3	0.37	0.30	0.36	-11.04	1.46	1.74	1.56	-4.03	510	659	678	-55.85	1.50	1.78	1.60	-4.24	505.63	501.78	540.89	52.47
4	0.01	0.01	0.01	-40.40	1.33	1.19	1.07	-1.59	370	361	340	-51.05	1.37	1.23	1.11	-1.87	59.37	45.96	50.26	32.39
5	0.03	0.02	0.05	-30.29	0.37	0.51	0.74	5.01	145	169	186	-44.48	0.41	0.55	0.78	4.44	112.23	259	189	42.13
6	0.08	0.05	0.01	-32.60	0.87	0.81	0.86	1.44	239	279	280	-48.51	0.91	0.85	0.90	1.04	132.23	55.63	62.38	34.96
7	0.07	0.07	0.19	-23.21	0.73	0.61	0.94	2.24	251	214	311	-48.35	0.77	0.65	0.98	1.81	148.96	192.85	200.56	43.15
8	0.10	0.07	0.10	-22.39	0.51	0.71	0.57	4.40	230	209	191	-46.46	0.55	0.75	0.61	3.84	237	215	350.22	46.23
9	0.08	0.08	0.10	-22.74	1.36	1.51	1.54	-3.35	556	501	587	-54.79	1.4	1.55	1.58	-3.59	201	222.37	245	45.11
	Overall mean MRR ($\overline{MRR}$)= 0.11mg s^{-1}				Overall mean Ra ($\overline{Ra}$) = 1.113 µm				Overall mean RS ($\overline{RS}$)= 394.11 MPa				Overall mean TWR ($\overline{T}$) = 1.15 mg/min				Overall mean micro-hardness ($\overline{MH}$)= 232.86			

Table 8.23 Optimal setting and values of process parameters for different output responses as per single objective optimization

Response	Process parameters at optimum vale	Predicted optimal values
MRR	A1, B3, C3, D3	0.346 mg/s
Ra	A2, B2, C3, D2	0.325 (µm)
RS	A2, B2, C1, D2	106.40 (MPa)
MH	A1, B2, C3, D3	506.21 HV
TWR	A2, B2, C3, D2	0.41 mg/min

Following equation were obtained for preference scale for MRR (P_{MR}), Ra (P_{Ra}), RS (P_{RS}), MH (P_{MH}) and TWR (P_{TWR}), (Walia et al. 2006):

$$P_{mrr} = A_1 * log \frac{X_{mrr}}{0.01} \quad (8.23)$$

$$P_{Ra} = -A_2 * log \frac{X_{Ra}}{1.77} \quad (8.24)$$

$$P_{RS} = -A_3 * log \frac{X_{RS}}{678} \quad (8.25)$$

$$P_{MH} = A_4 * log \frac{X_{MH}}{55.63} \quad (8.26)$$

$$P_{TWR} = -A_5 * log \frac{X_{TWR}}{1.81} \quad (8.27)$$

8.7.3 Calculation of utility value

The selected quality characteristics were assigned with equal weighs (1/5 each), as all the characteristics were important equally while the equation for utility value calculations was given as (Walia et al. 2006):

$$U(n, r) = P_{MRR}(n, r) \times W_{MRR} + P_{Ra}(n, r) \times W_{Ra} + P_{MH}(n, r) \times W_{MH} + P_{RS}(n, r) \times W_{RS} + P_{TWR}(n, r) \times W_{TWR} \quad (8.28)$$

Where n= number of experiments (1, 2, 3…..9); r = number of repetitions. The utilities values were used in L_9 array, for which the experimental results are given in Table 8.24. While, main effects and average values of output responses MRR, Ra, RS, MH and TWR in PMND-EDM are given in Table 8.25. The ANOVA was performed and its pooled data for raw and S/N values is given in Table 8.26. Based upon the results obtained by pooling, the plot between utility and process parameters is shown in Figure 8.1.

Table 8.24 Utilities values of MRR, Ra, RS, MH and TWR

Exp. No.	Utilities values			*S/N* [dB]
	R1	R2	R3	
1	1.11	2.21	2.96	6.41
2	4.22	4.32	4.79	12.95
3	3.66	4.34	4.93	12.68
4	6.01	6.34	6.78	16.09
5	5.1	5.44	5.76	14.70
6	7.2	7.76	7.99	17.67
7	3.32	3.65	3.91	11.19
8	4.21	4.27	4.52	12.73
9	6.11	6.49	6.78	16.20

The average % value was calculated for utility for different parameters. After that main effects % of micro-hardness were calculated by expression (L2-L1) and (L3-L2). Finally the difference between L2, L1 and L3, L2 was calculated. Analysis of variance was done for TWR S/N ratio on the results obtained at 95% confidence level.

Table 8.25 Main effects and average values of output responses MRR, Ra, RS, MH and TWR in PMND-EDM

LEVEL	Tool Diameter (A) S/N	Tool diameter (A) Raw data	Flow rate (B) S/N	Flow rate (B) Raw data	Powder concentration (C) S/N	Powder concentration (C) Raw data	Pressure (D) S/N	Pressure (D) Raw data
L1	8.12	3.61	8.71	4.03	9.77	4.69	9.93	4.66
L2	14.36	6.48	11.67	4.73	13.29	5.76	12.13	5.24
L3	11.58	4.80	13.68	6.14	11.00	4.45	11.99	5
L2-L1	6.24	2.87	2.95	0.70	3.515203	1.06	2.20	0.57
L3-L2	-2.78	-1.68	2.00	1.40	-2.28	-1.30	-0.13	-0.23
DIFFERENCE	-9.02	-4.55	-0.95	0.69	-5.80	-2.37	-2.34	-0.81
*L1, L2, L3 represent levels 1, 2 and 3 respectively of parameters. (L2-L1) is the average main effect when the corresponding parameter changes from Level 1 to Level 2. (L3-L2) is the main effect when the corresponding parameter changes from Level 2 to Level 3.								

Table 8.26 ANOVA pooled S/N and raw data for multi responses MRR, Ra, RS, MH and TWR in PMND-EDM

Parameters	SS (S/N)	SS Raw	Fe Raw	Fe S/N	Ve S/N	Ve Raw	SS' Raw	SS' S/N	P S/N	P Raw	F Ratio Raw	F Ratio S/N
Tool diameter	58.69	37.45	2	2	29.34	18.72	37.0	49.56	39.86	51.1	83.72	6.43
Mist flow rate	37.42	20.72	2	2	18.71	10.36	20.27	28.29	22.75	28.0	46.32	4.10
Metallic powder concentration	19.09	8.68	2	2	9.54	4.34	8.23	9.96	8.01	11.37	19.41	2.09
Mist Pressure	*	1.52	2	*	*	0.76	1.07	*	*	1.48	3.39	*
Error	9.12	4.02	18	2	4.56	0.22	5.81	36.50	29.36	8.03	-	-
Total (T)	124.34	72.40	26	8			72.40	124.34	100	100	-	-

The analysis for utilities value was done for mean responses (mean utility) and S/N ratios by considering the higher the better approach for utility. The data from Table 8.26 was used for plotting of utility in Figure 8.32 with respect to different parameters at different levels. It was observed that process parameters that process parameter A at level 2 (A_2), process parameter B at level 3 (B_3), process parameter C at level 3 (C_3) and process parameter D at level 2 (D_2) were most significant in enhancing the utility of the process within the selected parametric range. It was observed that tool diameter (A), mist flow rate (B), metallic powder concentration (C) and mist pressure (D) were significant in affecting the utility value and the S/N ratios as per ANOVA. The utility increases with increase in dimensions of tool diameter because the flushing takes place more efficiently which provides better cooling condition at the tool tip which brings down the temperature at the sparking ends of the hollow tool electrodes. However with further increase in tool diameters there was no increase in the utility as seen in Figure 8.32 (a).

Secondly flow rate was found to be most influential at 3rd level in increasing the utility value as shown in 8.32 (b). At this level, the flow rate of the dielectric medium at 15 ml/min was most optimum in providing suitable normal discharges at the machining zone along with powder additives which results in improved utility.

The utility value was found to be highest at 3rd level of powder additives (metallic) concentration as shown by the trend of plot in Figure 8.32 (c.) The utility value increased with respect to increase in metallic powder concentration which can be observed in the Figure 8.32 (c). Powder concentration was significant factor affecting the utility. At low concentration the heat dissipation was not proper due to small discharge gap but with increasing of powder concentration, discharge gap was enlarged. This resulted in improvement of cooling and machining process. All these factors resulted in achieving the highest utility value at 3rd level of process parameter. The utility shows the increasing trend when the air pressure changes from 0.4 MPa to 0.5 MPa as shown in Figure 8.32 (d). With increase of air pressure there were more molecules at the inter electrode gap which enhances discharging. Due to this phenomenon, there was improvement in deionization effect. Effects of abnormal short circuit and arc discharge were reduced which eventually led to better heat dissipation and reduced heat transfer. All these factors contributed to increase in utility till 0.5 MPa. But with further increase of pressure the gap voltage increases due to which the plasma generated was not uniformly distributed and improper machining takes place which led to decrease in utility value.

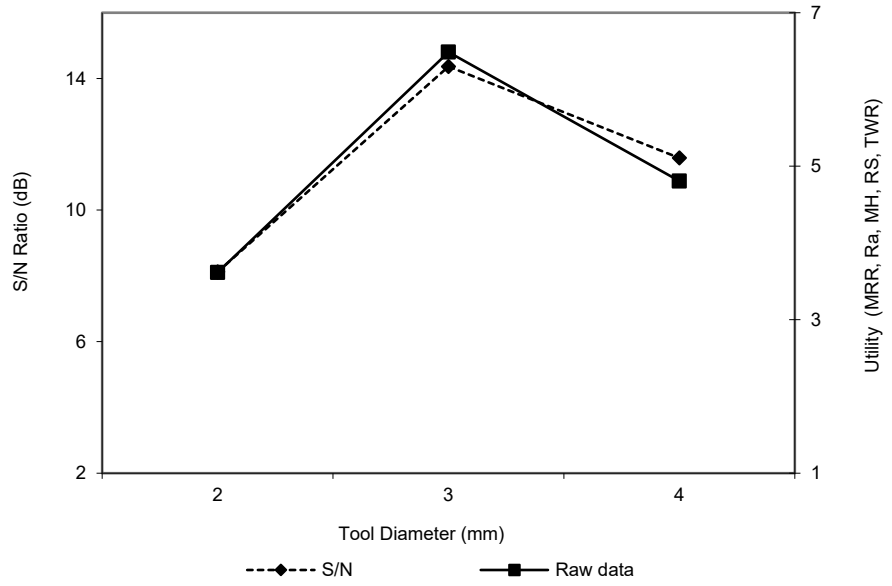

Figure 8.32 (a) Effect of tool type on utility

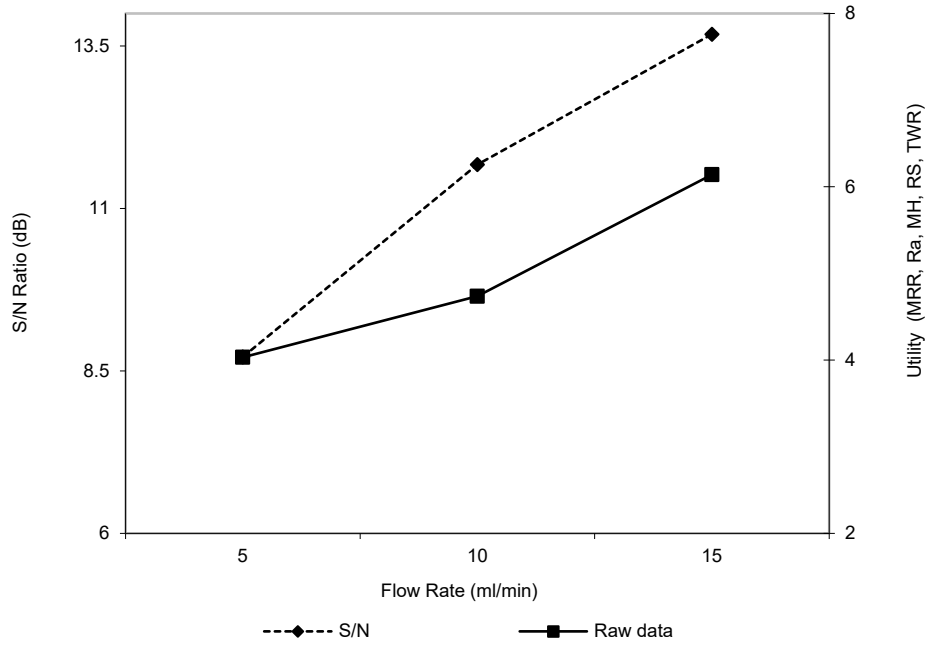

Figure 8.32 (b) Effect of Flow rate on utility

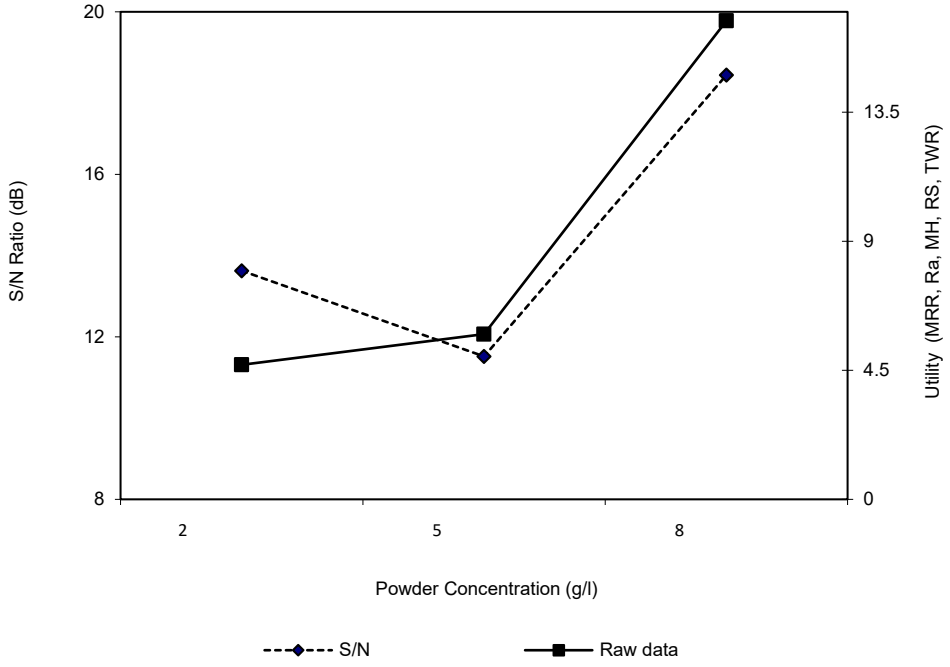

Figure 8.32 (c) Effect of powder concentration on utility

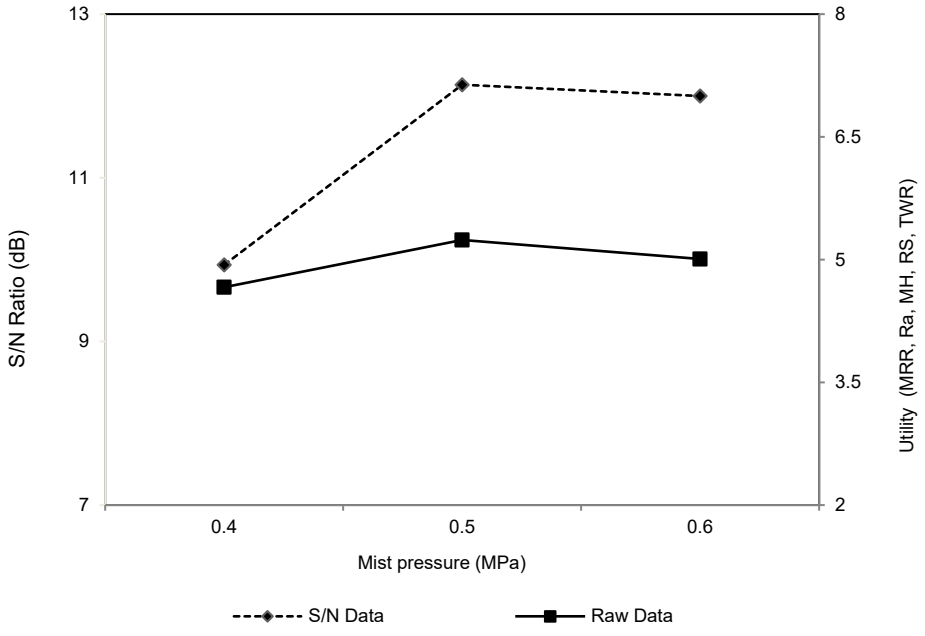

Figure 8.32 (d) Effect of pressure on utility

8.7.4 Estimation of performance characteristics (Utilities of MRR, Ra, MH, RS and TWR)

Estimation of response characteristic can be determined by using Eq. 8.29, (Walia et al. 2006) as:

$$\mu = \overline{A_2} + \overline{B_3} + \overline{C_3} + \overline{D_2} - 3\bar{T} \qquad (8.29)$$

Where μ= Predicted mean; T = Mean MRR, mean RS, mean Ra, mean, MH, mean TWR;

The confidence interval of confirmation experiments at 95 % can be determined by Eq.8.30:

$$CI_{CE} = \sqrt{F_{\alpha}(1, f_e)V_e\left[\frac{1}{n_{eff}} + \frac{1}{R}\right]} \quad (8.30)$$

Where, F_α (1, fe) = the F ratio at the confidence level of (1 –α) against DOF 1, $F_{0.05}$ (1, 18) =3.5546 (Tabulated), $n\_eff = N/(1 + [\text{DOF}])$, N (total number of experiments) = 27, Treatment = 9, repetition = 3. R (sample size for confirmation experiments) = 3, f_e (error DOF) = 26.

(a) Material removal rate

$\mu_{mrr} = \overline{A_2} + \overline{B_3} + \overline{C_3} + \overline{D_2} - 3\overline{MRR} = 0.63$

The predicted optimal range of confidence interval of conformation experiments (CI_{CE}) is:

CI_{CE} = +/- 0.24

$\mu_{mrr} - CI_{CE} < \mu_{mrr} < \mu_{mrr} + CI_{CE}$

0.39 < 0.63 < 0.87

(b) Surface finish

$\mu_{Ra} = \overline{A_2} + \overline{B_3} + \overline{C_3} + \overline{D_2} - \overline{Ra} = 0.79$

The predicted optimal range of confidence interval of conformation experiments (CI_{CE}) is:

CI_{CE} = +/- 0.06

$\mu_{Ra} - CI_{CE} < \mu_{Ra} < \mu_{Ra} + CI_{CE}$

0.73< 0.79 < 0.85

(c) Residual stress

$\mu_{RS} = \overline{A_2} + \overline{B_3} + \overline{C_3} + \overline{D_2} - 3\overline{RS} == 286$

The predicted optimal range of confidence interval of conformation experiments (CI_{CE}) is:

CI_{CE} = +/- 0.67

$\mu_{RS} - CI_{CE} < \mu_{RS} < \mu_{RS} + CI_{CE}$

285.33< 286< 286.67

(d) Micro-hardness

$\mu_{MH} = \overline{A_2} + \overline{B_3} + \overline{C_3} + \overline{D_2} - 3\,\overline{MH} = 249$

The predicted optimal range of confidence interval of conformation experiments (CI_{CE}) is:

CI_{CE} = +/- 0.42

$\mu_{MH} - CI_{CE} < \mu_{MH} < \mu_{MH} + CI_{CE}$

248.58< 248< 249.42

(e) Tool wear rate

$\mu_{TWR} = \overline{A_2} + \overline{B_3} + \overline{C_3} + \overline{D_2} - 3\bar{T} = 1.07$

The predicted optimal range of confidence interval of conformation experiments (CI_{CE}) is:

CI_{CE} = +/- 0.12

$\mu_{TWR} - CI_{CE} < \mu_{TWR} < \mu_{TWR} + CI_{CE}$

0.95 < 1.07 < 1.19

8.7.5 Confirmation of experiments for utilities (MRR, Ra, RS, MH and TWR)

At optimum settings, the experiments were performed as suggested by utility concept and Taguchi analysis. The values obtained are given in Table 8.27. It was noticed that the values lies between the prescribed limit or range with 95 % confidence interval.

Table 8.27 Confirmation experiments for quality characteristics

Exp. No	MRR	Ra	RS	MH	TWR
1	0.16	1.21	271.83	255.01	0.91
2	0.43	0.78	290.12	271.43	1.21
3	0.25	0.98	278.91	266.71	1.01
Overall Average	0.28	0.99	280.28	264.38	1.04

8.8 Gaseous Assisted Powder Mixed Near-Dry Electric Discharge Machining

This section includes further study on another form of hybrid EDM method of machining known as Gaseous Assisted Powder Mixed Near-Dry Electric Discharge Machining. The experiments were

conducted with different combination of dielectric gases in place of compressed air. The effect of different dielectric gases was studied under different experimental scenarios on responses such as material removal, surface finish, micro-hardness and residual stress.

Experimental study was performed for powder mixed near-dry EDM in gaseous medium. Different combination of gases was used in order to study their influences on machining characteristics such as MRR, Ra, RS and micro-hardness. The experiments were performed as per experimental condition (Refer Table 4.3, Chapter 4). Average value of material removal rate by GAPMND-EDM using different experimental scenarios is shown in Table 8.28.

Table 8.28 Average value of Material Removal Rate by GAPMND-EDM using different experimental scenarios

Operating pressure (MPa)	R1	R2	R3	Scenario 1 Average MRR (mg/min)
0.1	0.0886	0.0821	0.0953	0.266
0.2	0.1553	0.1451	0.1656	0.466
0.3	0.1776	0.1841	0.1712	0.533
0.4	0.2333	0.3811	0.0855	0.700
Operating pressure (MPa)	R1	R2	R3	Scenario 2 Average MRR (mg/min)
0.1	0.3803	0.2326	0.0847	0.687
0.2	0.3863	0.3712	0.4014	1.159
0.3	0.531	0.510	0.552	1.593
0.4	0.602	0.576	0.629	1.808
Operating pressure (MPa)	R1	R2	R3	Scenario 3 Average MRR (mg/min)
0.1	0.266	0.391	0.142	0.80
0.2	0.288	0.301	0.276	0.866
0.3	0.377	0.311	0.444	1.133
0.4	0.553	0.421	0.685	1.66
Operating pressure (MPa)	R1	R2	R3	Scenario 4 Average MRR (mg/min)
0.1	0.503	0.612	0.394	1.51
0.2	0.544	0.698	0.390	1.633
0.3	0.587	0.551	0.624	1.763
0.4	0.731	0.881	0.581	2.1938
Operating pressure (MPa)	R1	R2	R3	Scenario 5 Average MRR (mg/min)
0.1	0.343	0.441	0.245	1.03
0.2	0.353	0.310	0.220	1.06
0.3	0.401	0.479	0.320	1.20
0.4	0.600	0.587	0.613	1.80
Operating pressure (MPa)	R1	R2	R3	Scenario 6 Average MRR (mg/min)
0.1	0.747	0.621	0.873	2.241
0.2	0.805	0.987	0.624	2.417
0.3	0.926	0.871	0.982	2.780
0.4	1.126	1.171	1.082	3.379

8.8.1 Effect of Gases with powder additives On MRR in GAPMND-EDM

GAPMND-EDM experiments were performed with metallic powders (copper, zinc, graphite) along with gases (argon and oxygen) at different operating pressure. Among the different metallic powders used, the graphite powder along with dielectric gas proved to be better in terms of higher erosion rate. The probable reason was that graphite powder has higher thermal conductivity as compared to zinc or copper additives along with dielectric gas. Secondly graphite additives have lower density as compared to zinc or copper additives which enables the grain particles of graphite to disperse more uniformly in the dielectric medium thus providing favourable machining conditions for erosion. It was also observe that the MRR increased with increase in dielectric mist pressure. Molten eroded material from the machined surface of the workpiece had a close relationship with the ejection force of the dielectric mist pressure and the dissipation of heat (Bai et al. 2013, c). Some machined samples by GAPMND-EDM is shown in Figure 8.33.

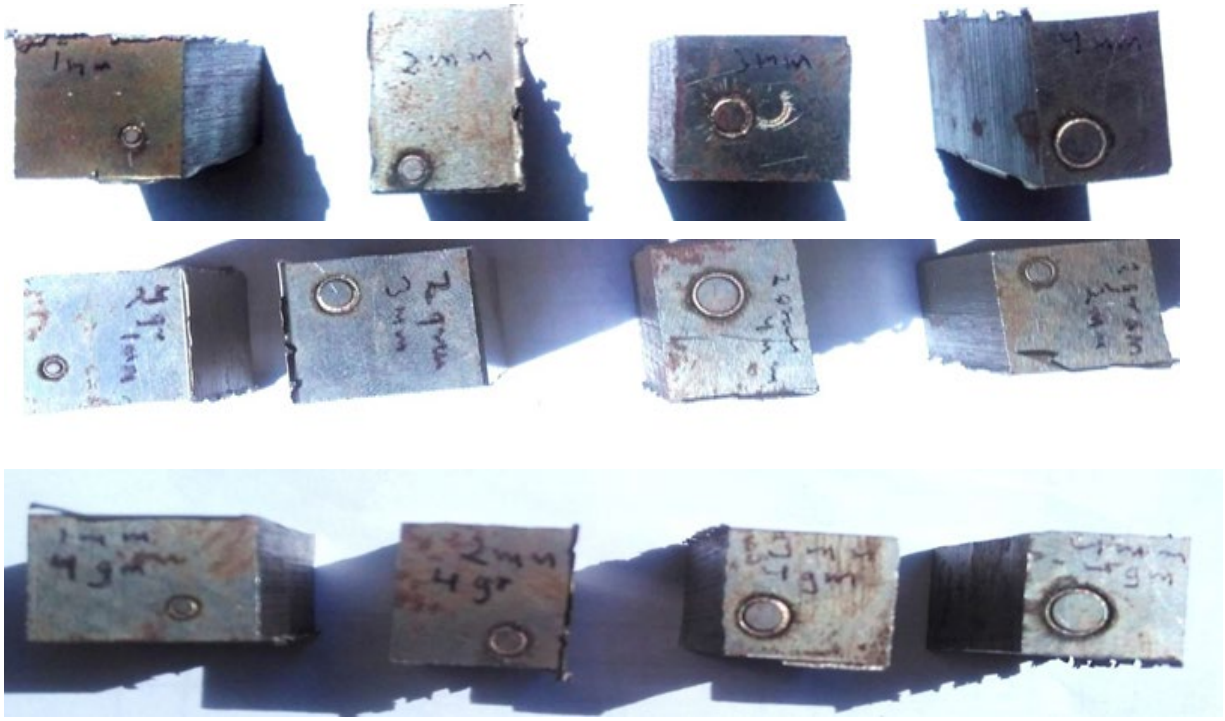

Figure 8.33 Machined samples by GAPMND-EDM

It was also visualized experimentally that among the different combination of metallic powders and gases, the dielectric mixture of graphite powder along with oxygen gas resulted in achievement of highest MRR. The reason attributed to this fact was that oxygen assisted EDM leads to chemical exothermic reaction. These exothermic reactions were responsible for oxidation process, which contributes to higher MRR as compared to argon gas as dielectric medium (Kunieda and Yoshida,

1997, Kunieda et al. 2003). Another fact can also be attributed to this phenomenon was that oxygen has relatively lower ionization energy (12.5 eV) as compared to argon gas (15.69eV). The gas with lower ionization energy has a tendency to ionize more quickly, which results in higher MRR (Li et al. 2006). However lower ionization energy of oxygen solely cannot be held entirely responsible for higher MRR because if ionization energy ratio was taken into consideration between oxygen and argon (12.5/15.69 = 0.796) i.e 0.796. The ratio was not that large as compared to higher differences in MRR ratios (3.379/0.7= 4.82) according to experimental scenario 1 and scenario 6 at 0.4 MPa (Refer Table 4.3, Chapter 4). Phenomenon of higher MRR with oxygen assisted in GAPMND-EDM was due to electronegativity of oxygen gas. The probability of an atom to attract electrons was known as electronegativity phenomenon. The electron affinity energy EAE for oxygen gas is 2.73eV as compared to that of argon gas which is -1.0 eV. The negative energy of argon atom means that first it has to absorb some energy in order to attract electron. Therefore, in comparison to oxygen, the argon gas was not properly ionized and makes it difficult for its deionization which conversely affects the sparks discharges at the machining gap. While due to easy ionization of oxygen gas, the oxygen atom captures the electrons easily and combines with positive ions. This easy phenomenon of deionisation creates a stable discharge in case of oxygen assisted EDM and consequently leads to higher MRR (Liqing and Yingjie, 2013).

Formation of large craters, cracks and pores were formed over the machined sample with oxygen assisted EDM as shown in Figures 8.34 (a, c). While with that of argon assisted dielectric medium only micro pores and pits can be seen on the machined surfaces in Figures 8.34 (b, d, e) due to which the MRR was lower. Large craters can be observed in Figure 8.34 (a) due to enhanced conductivity, which cause generation of spark from a long distance. Among the different metallic powder used, the largest cavities were formed by use of graphite powder because of its lower density and higher thermal/electrical conductivity as compared to other powders.

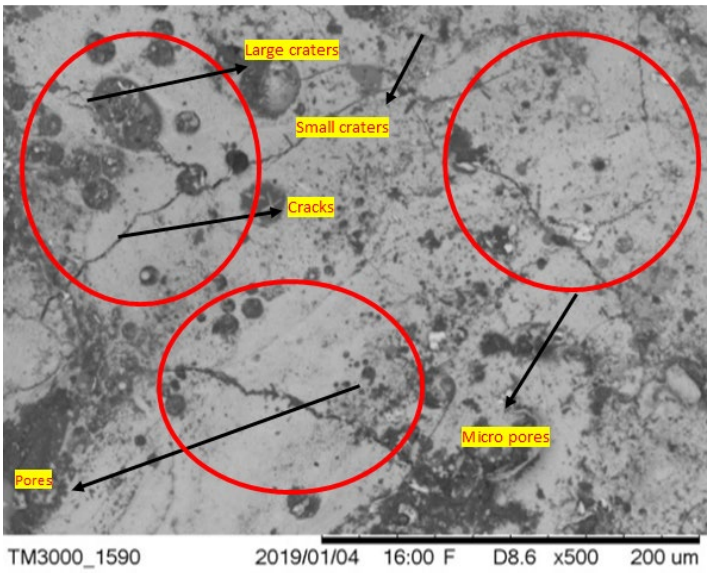

Figure 8.34 (a) SEM image of machined EN-31 sample by oxygen assisted with graphite powder

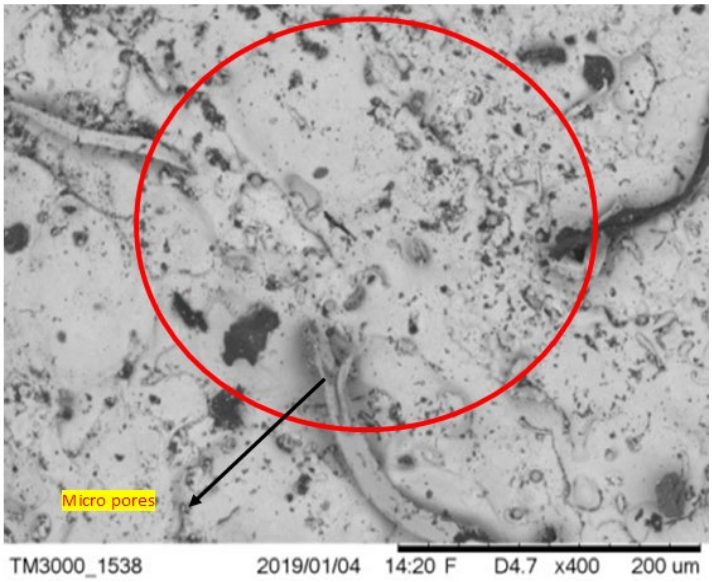

Figure 8.34 (b) SEM image of machined EN-31 sample by argon assisted with copper powder

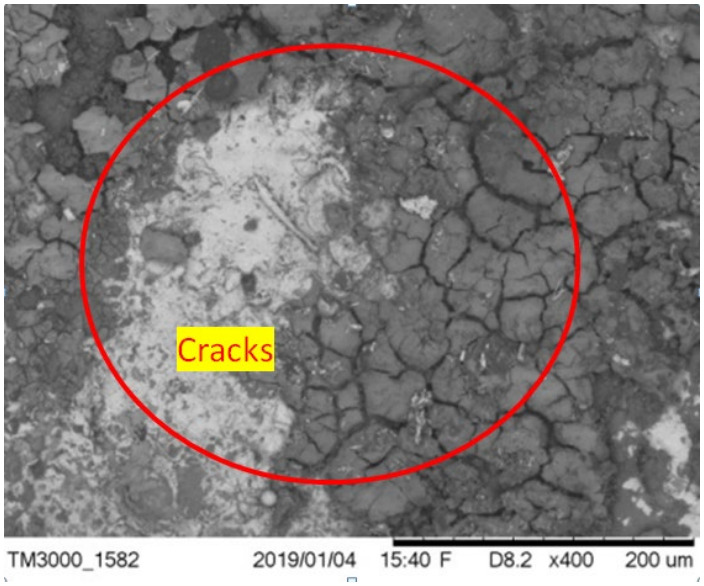

Figure 8.34 (c) SEM image of machined EN-31 sample by oxygen assisted with zinc powder

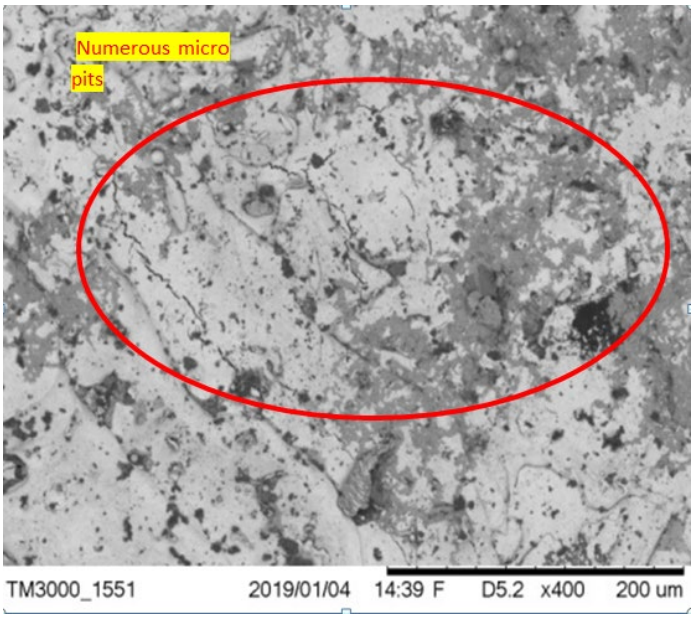

Figure 8.34 (d) SEM image of machined EN-31 sample by argon assisted with copper powder

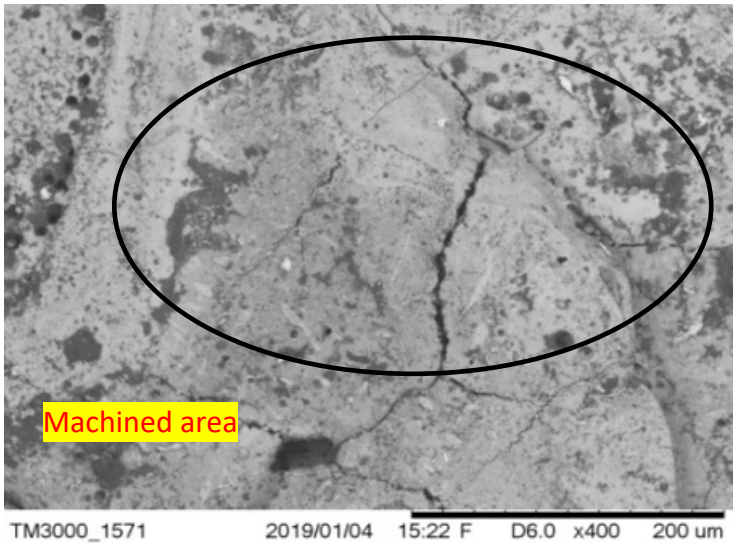

Figure 8.34 (e) SEM image of machined EN-31 sample by argon assisted with zinc powder additives

8.8.2 Effect of Gases with powder additives on Surface finish in GAPMND-EDM

Further analysis was carried out for surface finish by GAPMND-EM under different experimental conditions scenarios (Refer Table 4.3, Chapter 4). The surface finish (Ra) analysis for the machined EN-31 samples by GAPMND-EDM was performed with the help of tomography machine. As compared to conventional EDM, the surface finish obtained by GAPMND-EDM was quite high. The Ra value was found to be finest (1.11 µm) for machined sample with dielectric medium of graphite powder additive with argon gas. Few properties of graphite powder are advantageous in terms of surface, electrical and thermal abilities which were responsible for generation of fine surfaces. Secondly its low electrical resistivity as compared to other powder such as copper or zinc was also advantageous in obtaining a fine surface finish. Graphite has excellent lubricity property which has a very good effect on wetting of the powder particles by the molten machined surface and the well-developed ordered microstructure of graphite material was also an added advantage (Wong et al. 1998). All these conditions lead to formation of smooth machined surfaces as shown in Figure 8.35 (a).

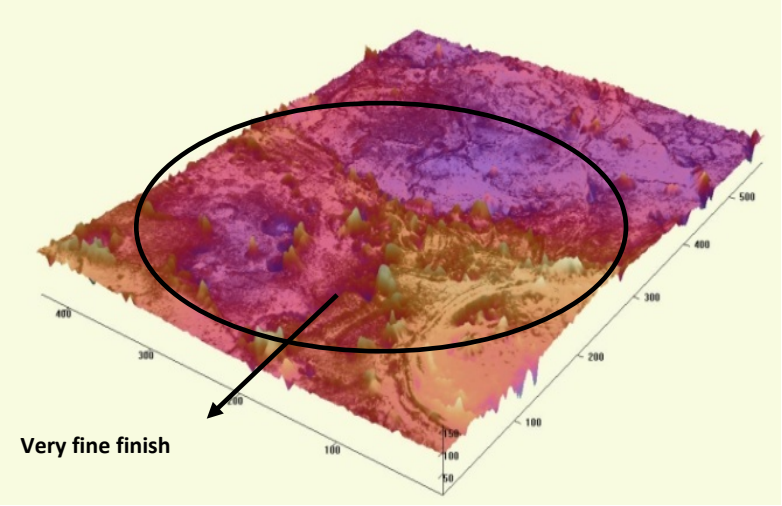

Figure 8.35 (a) Surface profile with graphite additive (powder) in presence of argon gas

Although copper and zinc additives gave fine surface finish results, but not with the same efficiency as graphite powder. Figures 8.35 (b, c) shows the machined surface by different metallic powder additives in presence of argon gas. It can be clearly seen from these images that the surface roughness was quite smoother due to inert gas atmosphere provided for machining purpose. Less oxidation results in stable sparking conditions due to which the arc produced was more uniformly distributed and provides shallow craters over the machined surface which makes it possible to achieve much finer surface.

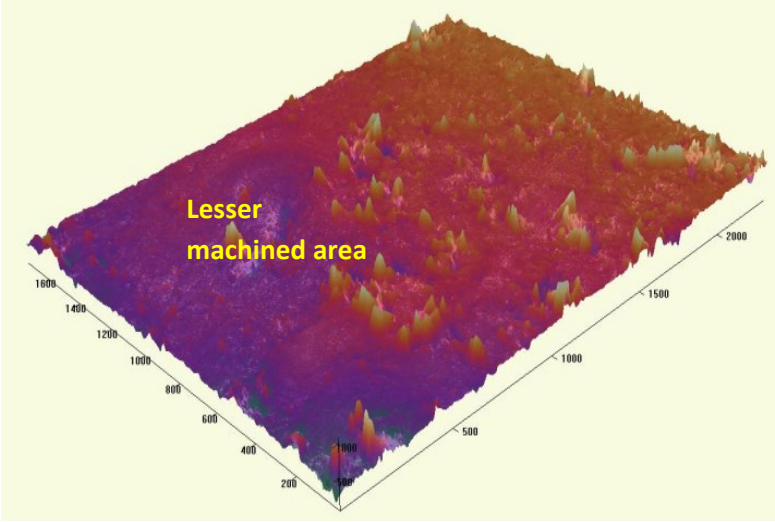

Figure 8.35 (b) Surface profile with copper additive (powder) in presence of argon gas

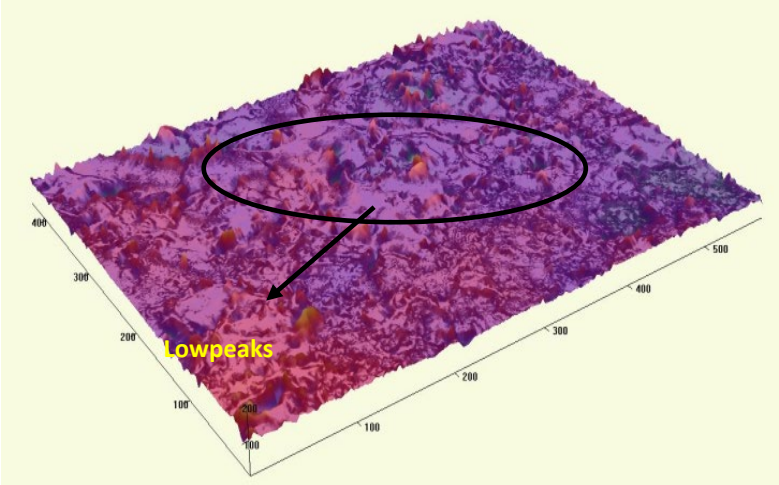

Figure 8.35 (c) Surface profile with zinc additive (powder) in presence of argon gas

The tomography images of machined surface by different metallic powder additives in presence of oxygen gas are shown in Figure 8.35 (d, e, f). It can be seen from the images that the machined surface has higher peaks and irregularities as compared to that of inert gas (Ar) assisted EDM machining. The matter of fact was that higher oxidation rate and exothermic reaction leads to higher erosion rate and comparatively less stable arc at the inter electrode gap, due to which the craters produced were non uniform and hence more surface irregularities leads to lower surface finish.

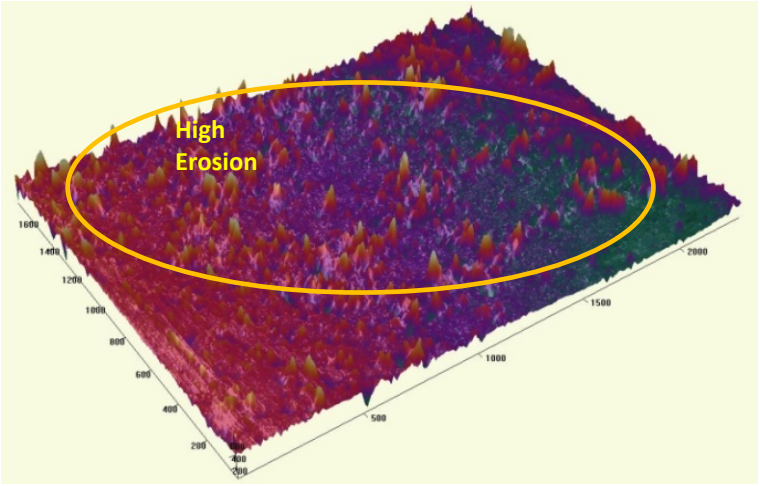

Figure 8.35 (d) Surface profile with copper additive (powder) in presence of oxygen gas

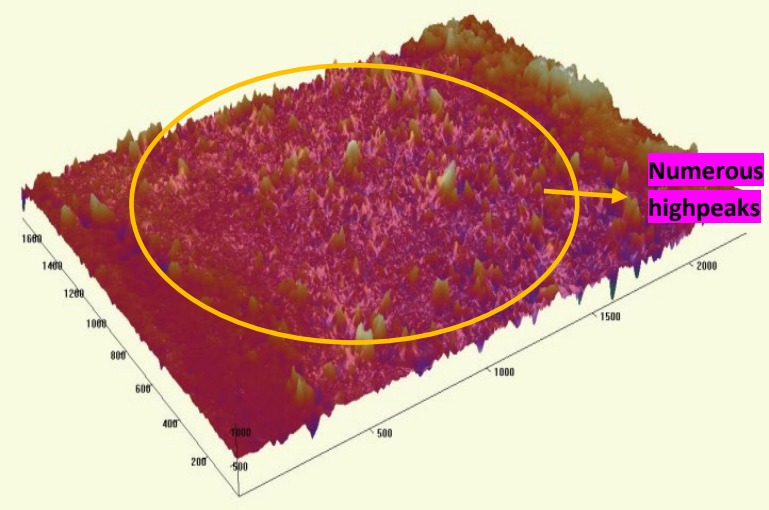

Figure 8.35 (e) Surface profile with graphite additive (powder) in presence of oxygen

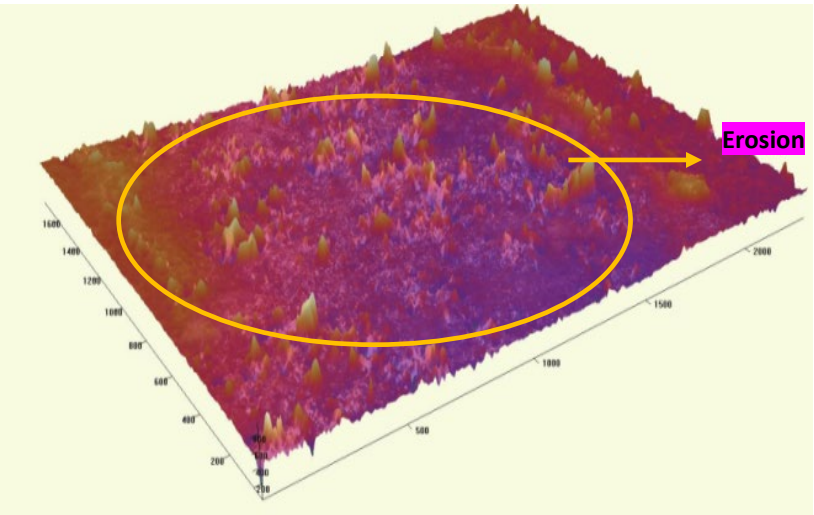

Figure 8.35 (f) Surface profile with zinc additive (powder) in presence of oxygen gas

Overall the surface finish achieved was better than conventional EDM methods and the fact attributed was that the plasma channel at the machining gap gets modified and distributes the plasma energy more uniformly which results in formation of shallow craters over the machined surface (Fong and Chen, 2005).

8.8.3 Effect of Gases with Powder Additives on Micro-Hardness in GAPMND-EDM

It was observed that the micro-hardness at the machined area increased due to surface modification by using powder additives. The metallic powder additives in the dielectric medium (kerosene based dielectric oil and gas) increased the ionization effect at the inter electrode gap (IEG). Pyrolysis effect was observed in the enlarged plasma due to breakage of carbon hydrogen (C-H) bonds which makes it a possible to avail more number of carbon ions which leads to formation of carbides over the

machined surface and eventually leads to formation of hardened surfaces (Ndaliman et al. 2013 b). Larger and distinct plates of γ' phase contributes more effectively in obtaining high micro-hardness (Talla et al. 2016, b).

The micro hardness was found to be maximum of 820.30 Vickers hardness number (HV) in case of zinc additive dielectric medium due to its high hardness and low electrical conductivity value followed by copper powder (671.1 HV) and graphite powder (194.13 HV) as shown in Figure 8.36 (a-c). Among all the three metallic powders, zinc additive laden dielectric medium obtained highest micro-hardness because the smallest spark gap at the machining area due to its low electrical conductivity. This small gap makes favourable conditions for piling of debris and in addition the amount of heat was removed from the machining area owing to low thermal conductivity of zinc powder. Therefore more amount of heat and quenching leads to harder surface (Talla et al. 2016, b)

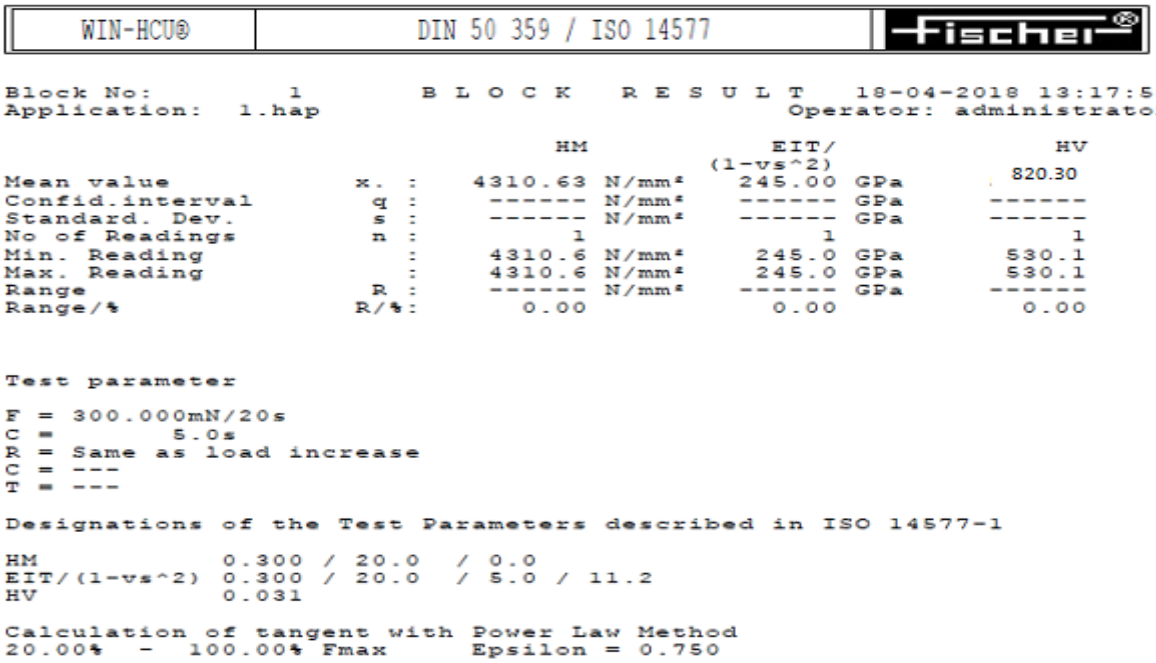

WIN-HCU® | DIN 50 359 / ISO 14577 | Fischer

Block No: 1 B L O C K R E S U L T 18-04-2018 13:17:53
Application: 1.hap Operator: administrator

		HM	EIT/(1-vs^2)	HV
Mean value	x. :	4310.63 N/mm²	245.00 GPa	820.30
Confid.interval	q :	------ N/mm²	------ GPa	------
Standard. Dev.	s :	------ N/mm²	------ GPa	------
No of Readings	n :	1	1	1
Min. Reading	:	4310.6 N/mm²	245.0 GPa	530.1
Max. Reading	:	4310.6 N/mm²	245.0 GPa	530.1
Range	R :	------ N/mm²	------ GPa	------
Range/%	R/%:	0.00	0.00	0.00

Test parameter

F = 300.000mN/20s
C = 5.0s
R = Same as load increase
C = ---
T = ---

Designations of the Test Parameters described in ISO 14577-1

HM 0.300 / 20.0 / 0.0
EIT/(1-vs^2) 0.300 / 20.0 / 5.0 / 11.2
HV 0.031

Calculation of tangent with Power Law Method
20.00% - 100.00% Fmax Epsilon = 0.750

Figure 8.36 (a) The reading of micro-hardness of the machined sample by GAPMND-EDM using zinc additive.

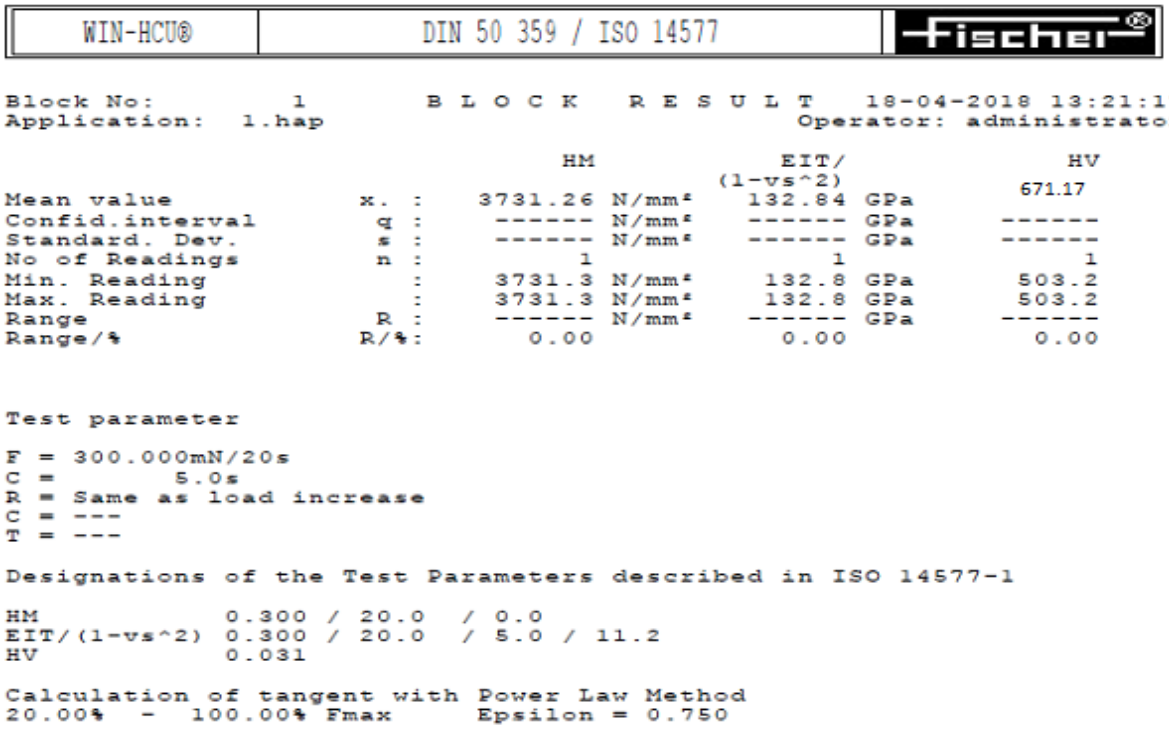

WIN-HCU® | DIN 50 359 / ISO 14577 | Fischer®

Block No: 1 B L O C K R E S U L T 18-04-2018 13:21:17
Application: 1.hap Operator: administrator

			HM		EIT/(1-vs^2)		HV
Mean value	x. :	3731.26	N/mm²	132.84	GPa	671.17	
Confid.interval	q :	------	N/mm²	------	GPa	------	
Standard. Dev.	s :	------	N/mm²	------	GPa	------	
No of Readings	n :	1		1		1	
Min. Reading	:	3731.3	N/mm²	132.8	GPa	503.2	
Max. Reading	:	3731.3	N/mm²	132.8	GPa	503.2	
Range	R :	------	N/mm²	------	GPa	------	
Range/%	R/%:	0.00		0.00		0.00	

Test parameter

F = 300.000mN/20s
C = 5.0s
R = Same as load increase
C = ---
T = ---

Designations of the Test Parameters described in ISO 14577-1

HM	0.300 / 20.0 / 0.0
EIT/(1-vs^2)	0.300 / 20.0 / 5.0 / 11.2
HV	0.031

Calculation of tangent with Power Law Method
20.00% - 100.00% Fmax Epsilon = 0.750

Figure 8.36 (b) The reading of micro-hardness of the machined sample by GAPMND-EDM using copper additive

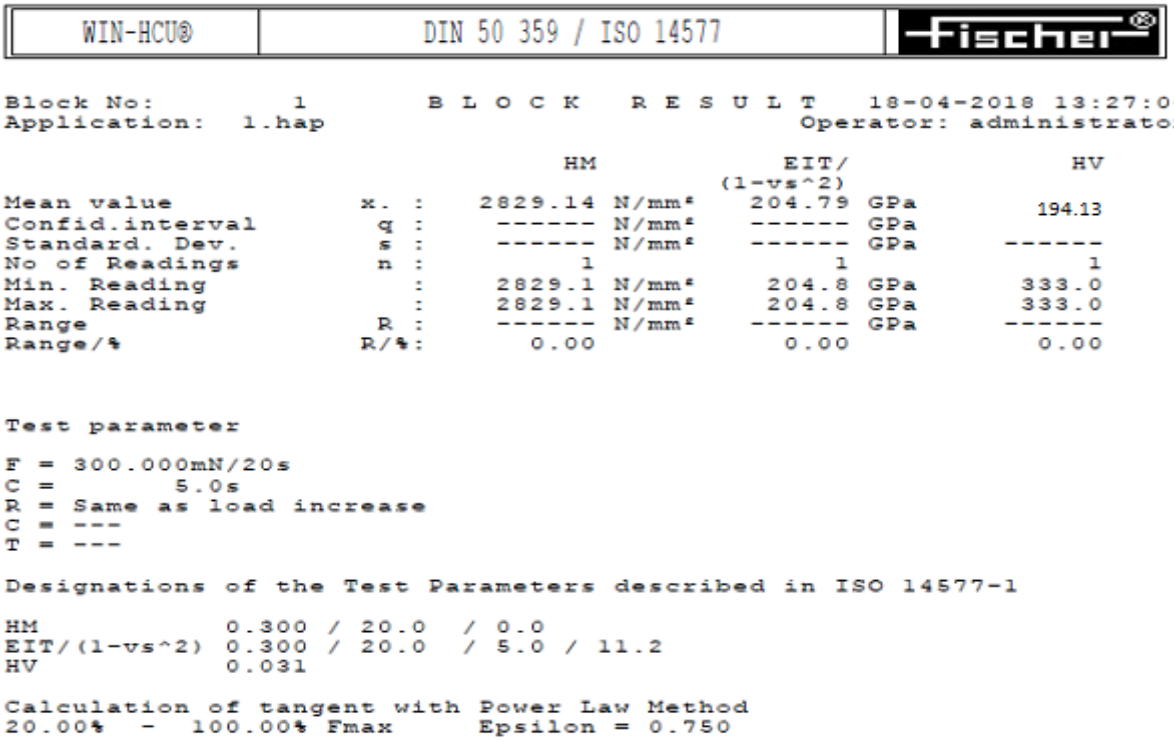

WIN-HCU® | DIN 50 359 / ISO 14577 | Fischer®

Block No: 1 B L O C K R E S U L T 18-04-2018 13:27:00
Application: 1.hap Operator: administrator

			HM		EIT/(1-vs^2)		HV
Mean value	x. :	2829.14	N/mm²	204.79	GPa	194.13	
Confid.interval	q :	------	N/mm²	------	GPa		
Standard. Dev.	s :	------	N/mm²	------	GPa	------	
No of Readings	n :	1		1		1	
Min. Reading	:	2829.1	N/mm²	204.8	GPa	333.0	
Max. Reading	:	2829.1	N/mm²	204.8	GPa	333.0	
Range	R :	------	N/mm²	------	GPa	------	
Range/%	R/%:	0.00		0.00		0.00	

Test parameter

F = 300.000mN/20s
C = 5.0s
R = Same as load increase
C = ---
T = ---

Designations of the Test Parameters described in ISO 14577-1

HM	0.300 / 20.0 / 0.0
EIT/(1-vs^2)	0.300 / 20.0 / 5.0 / 11.2
HV	0.031

Calculation of tangent with Power Law Method
20.00% - 100.00% Fmax Epsilon = 0.750

Figure 8.36 (c) The reading of micro-hardness of the machined sample by GAPMND-EDM using graphite additive

8.8.4 Effect of Gases with powder additives on Residual stress in GAPMND-EDM

Residual stress analysis of the machined samples by GAPMND-EDM was performed at different dielectric medium combination as shown in Figure 8.37. Localised heating and rapid cooling phenomenon results in formation of tensile residual stress in the machined components (Kruth and Bleys, 2000). These residual stress need to be minimized in order to increase the product life. As compared to conventional EDM method, the residual stresses generated in the machined products were lower in metallic powder assisted EDM.

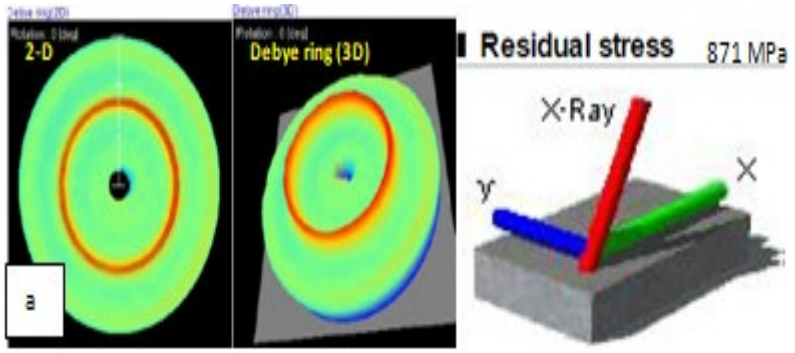

Figure 8.37 (a) Debye Scherer rings with residual stress values of machined EN-31 samples by GAPMND-EDM with graphite and oxygen medium

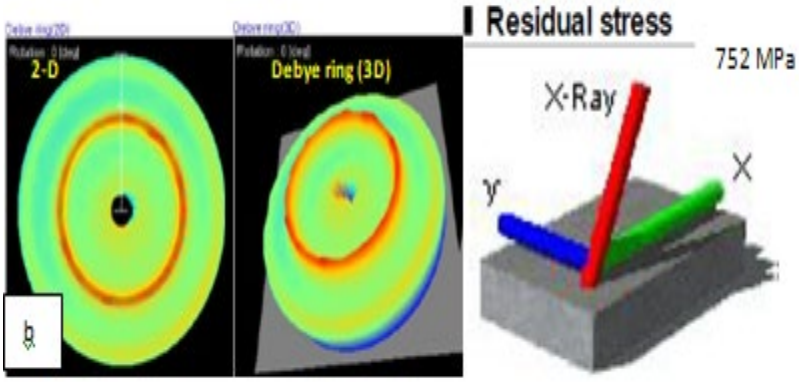

Figure 8.37 (b) Debye Scherer rings with residual stress values of machined EN-31 samples by GAPMND-EDM with copper and oxygen

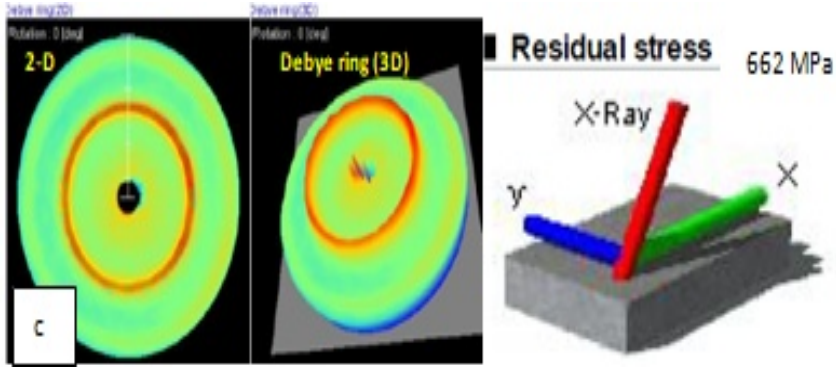

Figure 8.37 (c) Debye Scherer rings with residual stress values of machined EN-31 samples by GAPMND-EDM with zinc and oxygen

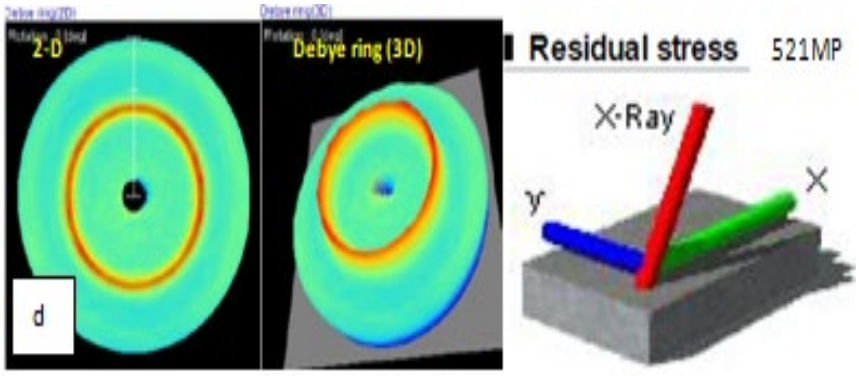

Figure 8.37 (d) Debye Scherer rings with residual stress values of machined EN-31 samples by GAPMND-EDM with argon and graphite

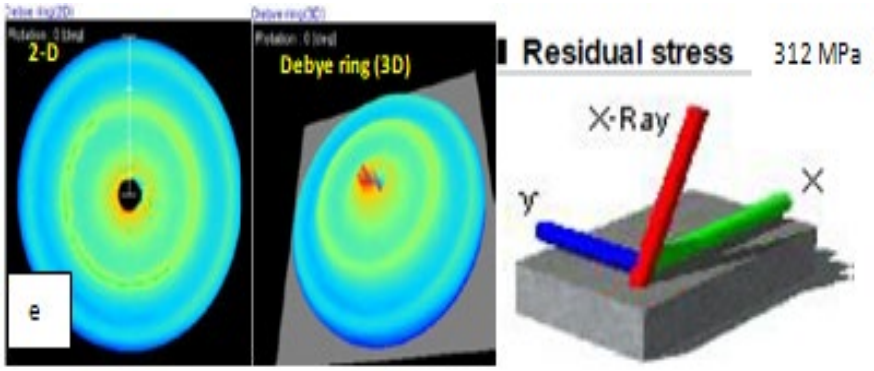

Figure 8.37 (e) Debye Scherer rings with residual stress values of machined EN-31 samples by GAPMND-EDM with argon and zinc

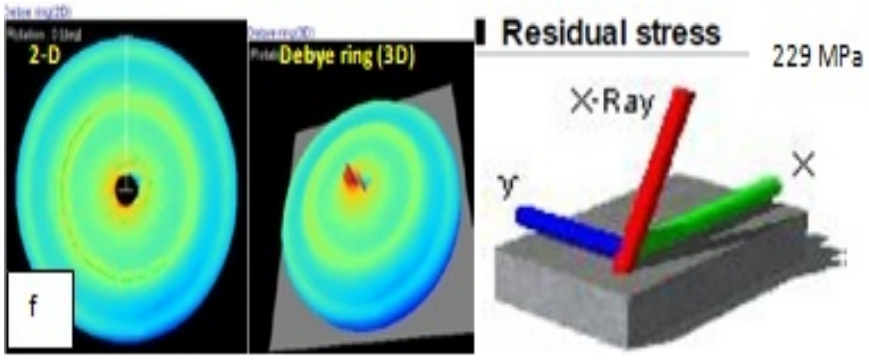

Figure 8.37 (f) Debye Scherer rings with residual stress values of machined EN-31 samples by GAPMND-EDM with argon and copper

The energy density was very high in conventional EDM but with powder suspended dielectric medium, the spark gap gets enlarged due to which the discharge energy density decreases and results in lower value of thermal residual stresses (Talla et al. 2017). The lowest value for residual stress (229 MPa) in machined EN-31 sample was with that dielectric medium of copper additives with argon gas. Heat of fusion was considerably lower which resulted in lower value of thermal stresses

and secondly lesser surface resolidification phenomenon also contributed in reducing thermal residual stresses.

Presence of some micro cracks developed over the machined surface as shown in Figure 8.38, were also responsible for relieving some part of the tensile residual stresses (Rao et al. 2016). At the same time better flushing and cooling conditions were significantly an important factor in diminishing theses induced thermal stresses. Figure 8.39 shows the variation of residual stress induced across the sample depth. High tensile residual stresses increased from the surfaces and reached the maximum value just below the heat effected zone (HAZ) and again falls to low value of compressive residual stress. The compressive stresses found in the affected layer were evident since residual stresses within plastically deformed layers were equilibrated with elastic stresses in the core of the material (Ekmekci et al. 2007). Table 8.29 shows the overall experimental results for the experiments conducted by GAPMND-EDM.

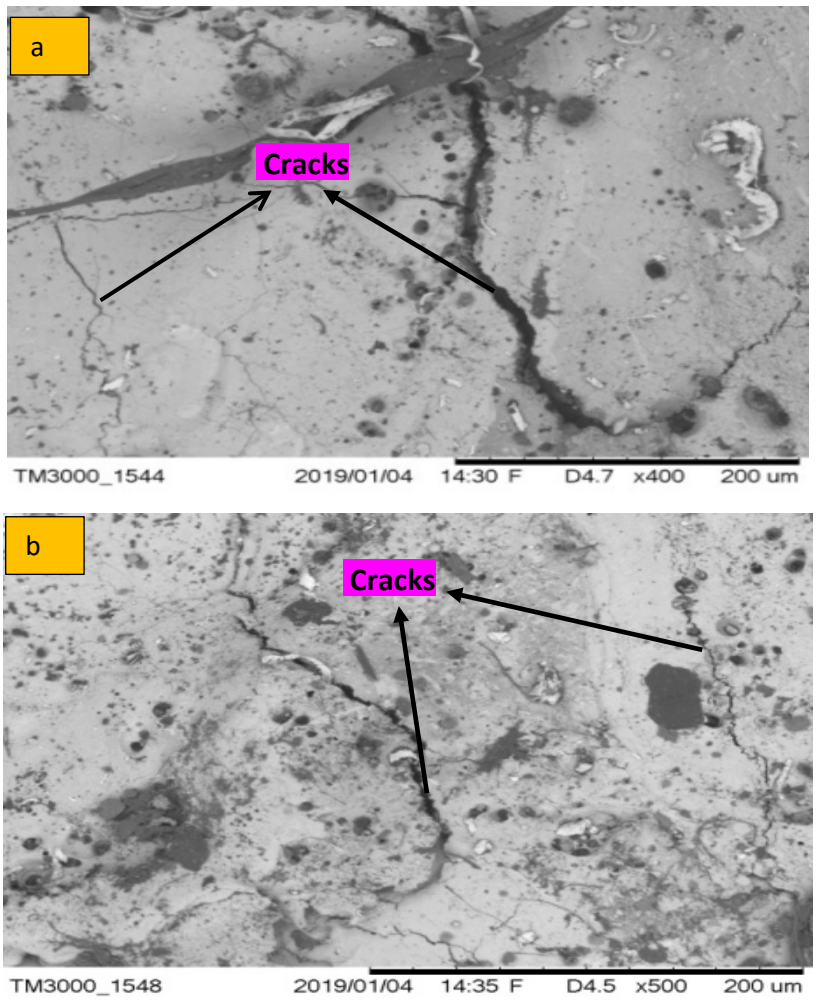

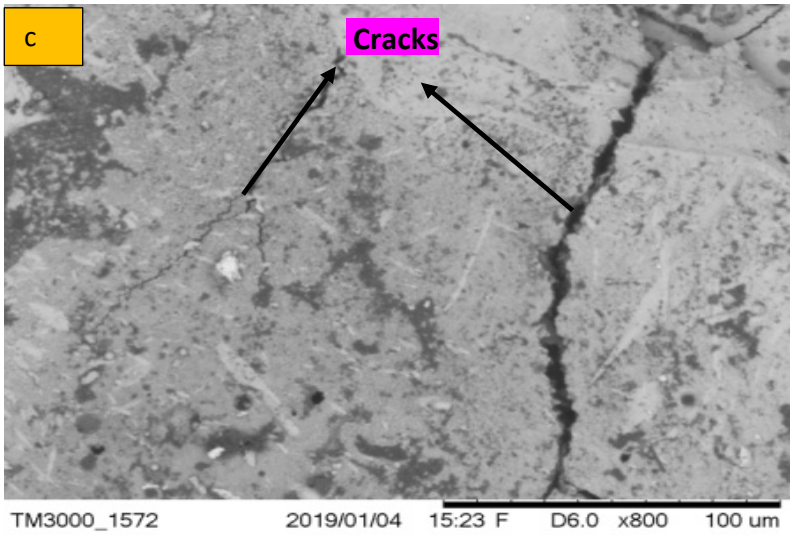

Figure 8.38 [a-c] Images of some machined EN-31 samples with micro cracks

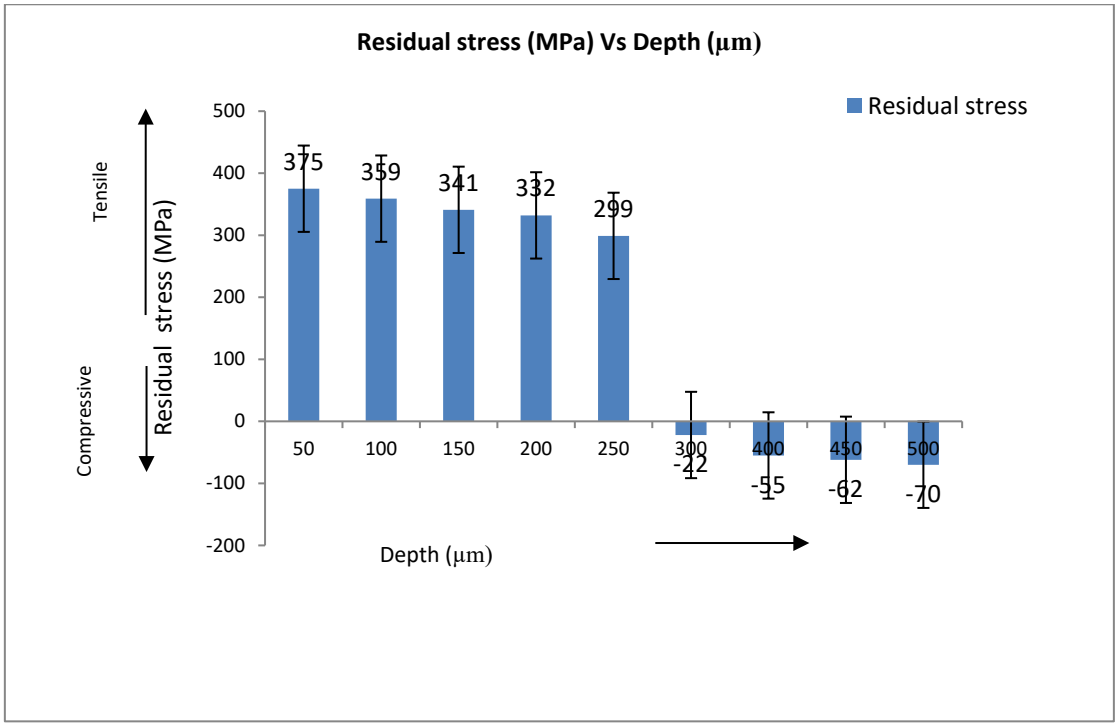

Figure 8.39 Residual stress variations across the depth of the machined sample

Table 8.29 Summary of experimentations conducted by GAPMND-EDM under different experimental conditions

Maximum material removal rate	(Dielectric medium) Graphite additives + O_2 gas at 0.4 MPa	3.379 (mg/min)
Highest Surface finish	Graphite powder +Argon gas at high pressure (Recommended 0.4 MPa)	1.11 (μm)
Highest micro-hardness	Zinc powder + Argon gas	820.30 (HV)
Lowest residual stress with respect to dielectric medium	Copper powder +Argon gas	229 (MPa)
Nature of residual stress with respect to depth of machined sample	Nature of stress Tensile and compressive. Higher tensile stresses just below HAZ	Maximum tensile stress 375 (MPa) Minimum compressive stress-70 (MPa)

8.9 Effect of Different Powder Additives on Machining Performance in PMND-EDM

This section includes comparative study for output performance such as material removal rate, surface finish and tool wear rate by using different metallic powder additives such as aluminium, graphite and silicon powder.

8.9.1 Effect of Different Powder Additives on MRR

As compared to ND-EDM, MRR with metallic powder additives in ND-EDM was found to be more due to reduction of breakdown dielectric strength as shown in Figure 8.40. This uniform dispersion of conductive powders causes increase in inter electrode gap which leads to large discharges (Talla 2016, a). Another contribution is that these metallic additives also help in creating a bridge phenomenon between the electrodes which results in increased thermal conductivity. All these factors are responsible for increasing the frequency of discharges due to which more erosion from the workpiece takes place as compared to conventional EDM (Kansal et al. 2007).

The highest MRR in PMND-EDM was found by using aluminium powder followed by graphite and silicon. The reason attributed was that the Al powder has lowest resistivity (5 μΩ-cm) amongst other metallic powders Gr (30 μΩ-cm) and Si (10000 μΩ-cm). This lowest electrical resisitivity of Al causes sparking to take place from a larger distance at the inter electrode gap (IEG) unlike Gr and Si which has comparatively smaller discharges. This results in increase in sparking frequency and at the same time this increased working gap facilitates easy removal of debris and also improves the flushing conditions.

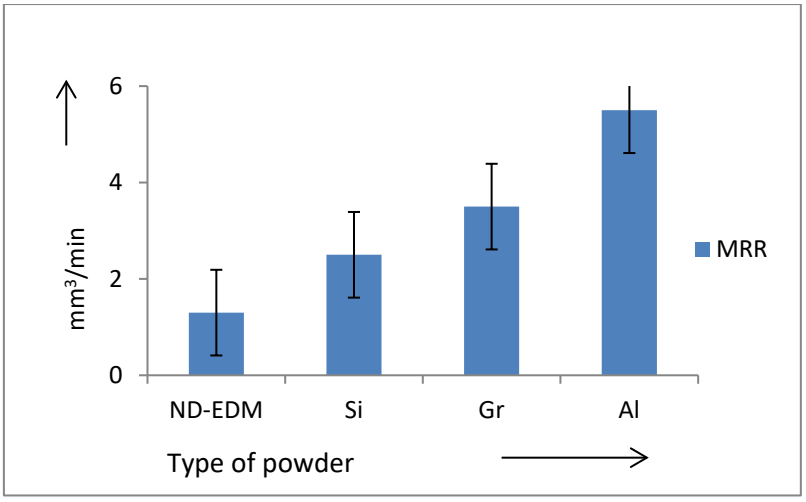

Figure 8.40 MRR Vs different types of machining method

8.9.2 Effect of Different Powder Additives on Surface Finish (Ra)

The addition of metallic powders in the dielectric has reduced the sourface roughness considerably over the machined surface of the workpiece as shown in Figure 8.41. Powder particles enlarge the plasma generated between the electrodes. The discharge energy of the multiple sparks is distributed evenly over a larger area (Fong and Chen 2005). Additionaly the molten metal at the machining gap is not compressed heavily by the gas bubbles and plasma channel which makes the surface less concave and uniformly smooth (Tzeng and Lee 2001). The surface roughness was maximum for ND-EDM due to improper discharges. The surface obtained by ND-EDM has large cracks (Figure 8.42) and these cracks are responsible for corrosion and fatigue failure under tensile loading while the surface defects such as cracks were minimized by powder additives in PMND-EDM. The metallic powders high thermal conductivity was responsible for taking up some part of the residual heat at the sparking zone. Another reason attributed was that the pressure of the plasma channel was considerably lower due to slow cooling rate of the molten material at IEG which leads to formation of micro cracks unlike large defective cracks (Prihandana et al. 2011).

The maximum surface finish was observed with Silicon followed by graphite and aluminium due to its low thermal and electrical conductivity as shown in Figure 8.43 (a-d). Silicon powder particles being smaller in size enter the machining gap in more quantity which results in even distribution of discharges over a large area. Therefore the surface finish achieved was higher in quality as compared to surface machined by other powder additives due to their large particle size (Kung et al. 2009). Even though the electrical conductivity of aluminium is higher than graphite powder but still the surface roughness produced by Aluminium powder was higher. The reason behind this phenomenon is that the density of aluminium is higher than graphite powder, which doesn't allow particles to mix

thoroughly with the dielectric in a uniform manner. Secondly, powder particles of Aluminium powder agglomerates due to Van der Walls forces or electrostatic force when added to the dielectric. Therefore excessive powder particles concentration causes short circuiting and improper discharges which eventually deteriorates the surface finish of the machined samples.

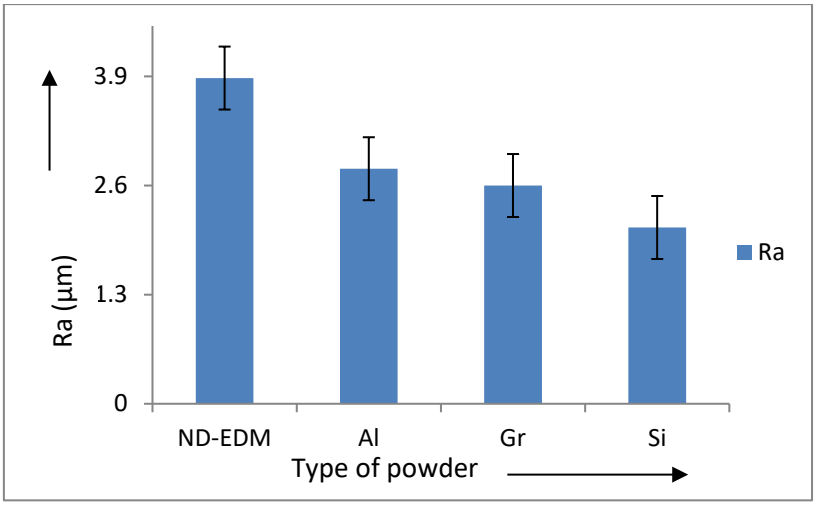

Figure 8.41 Ra Vs different types of metallic powder

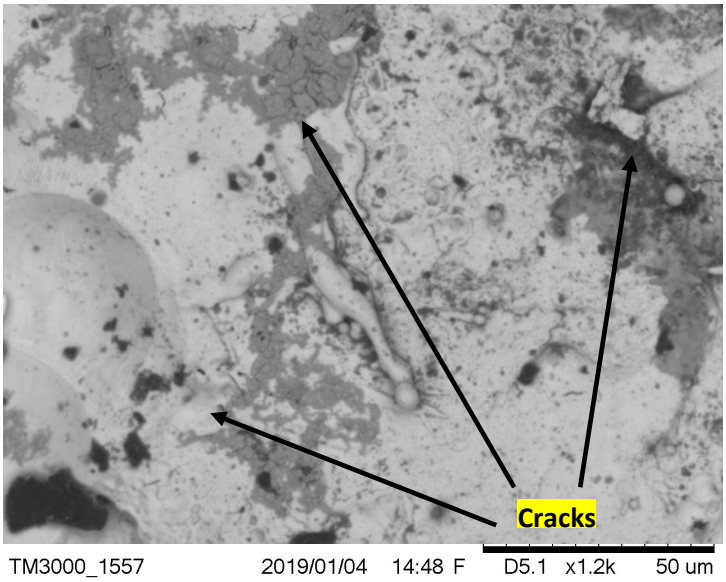

Figure 8.42 Surface cracks over the machined surface by ND-EDM

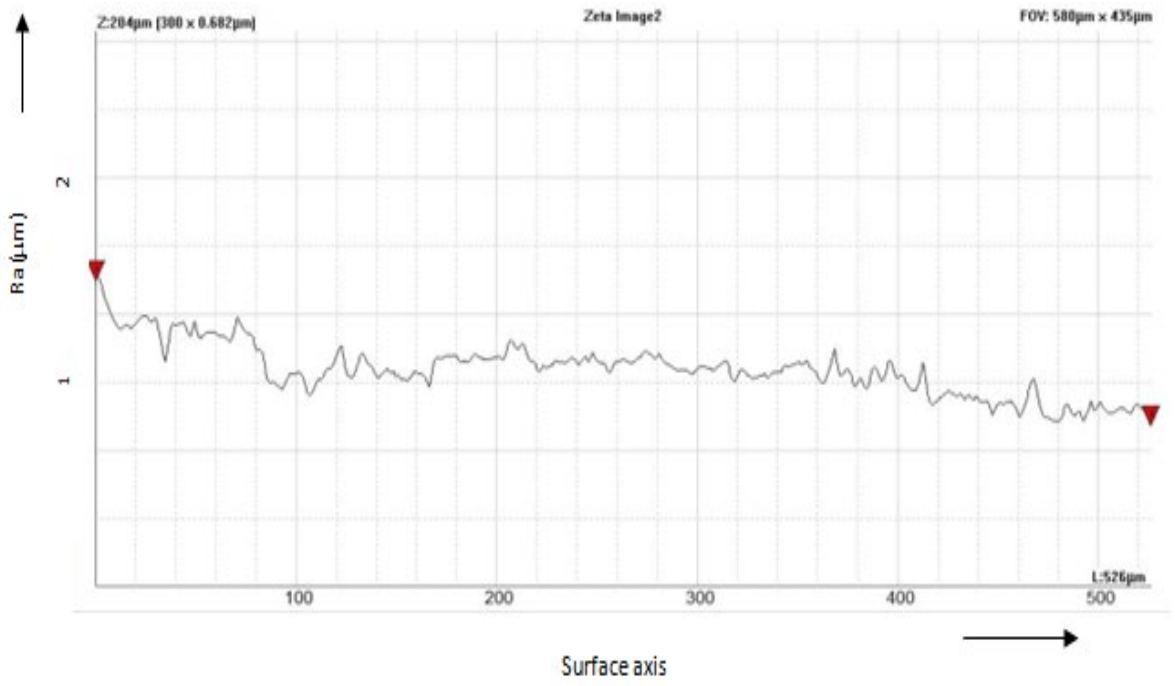

Figure 8.43 (a) Surface profile of machined workpiece sample by Silicon powder

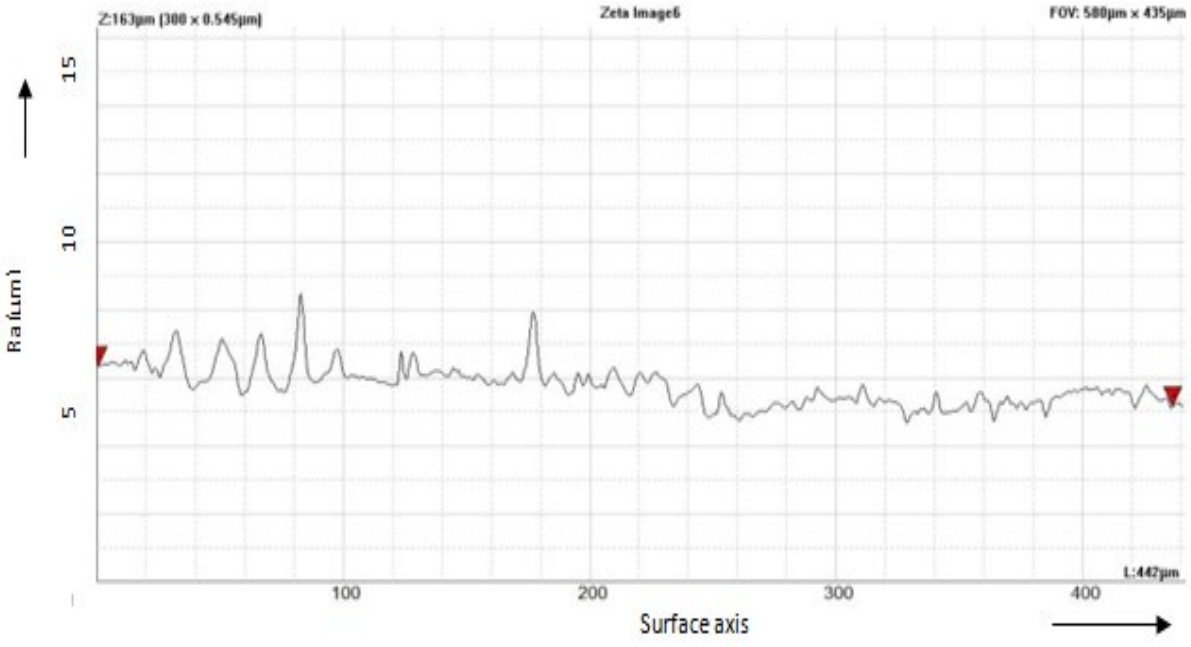

Figure 8.43 (b) Surface profile of machined workpiece by graphite powder

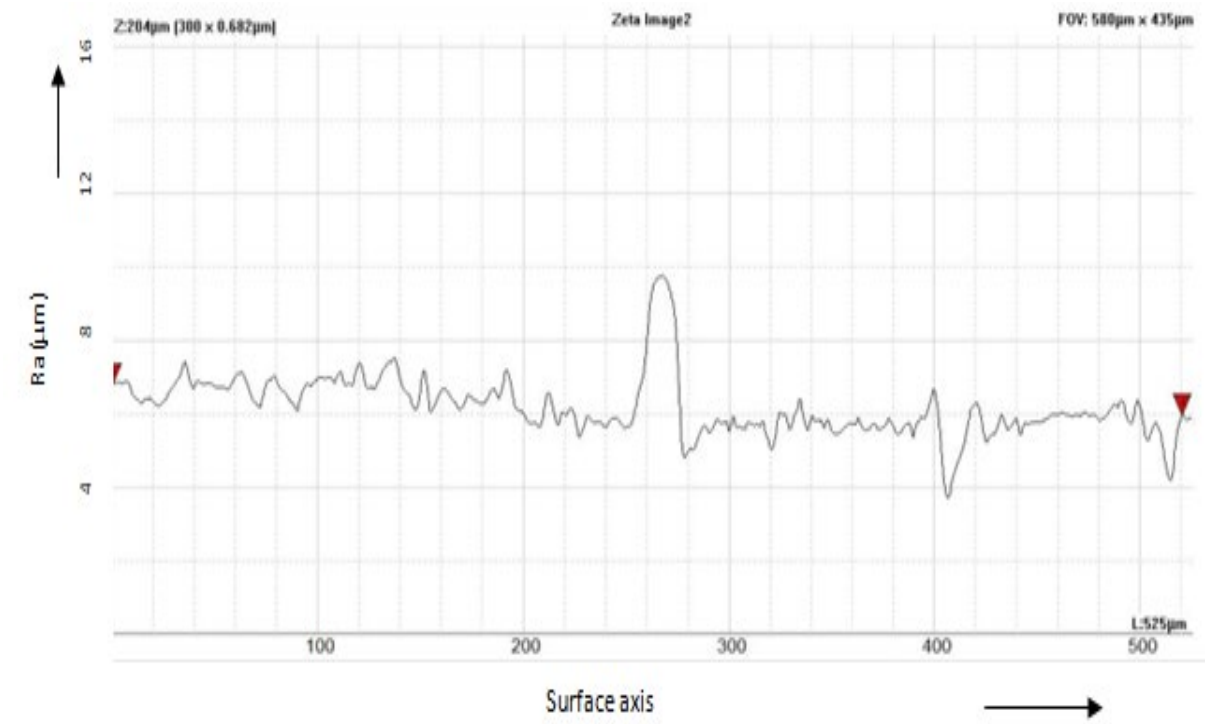

Figure 8.43 (c) Surface profile of machined workpiece by aluminium powder

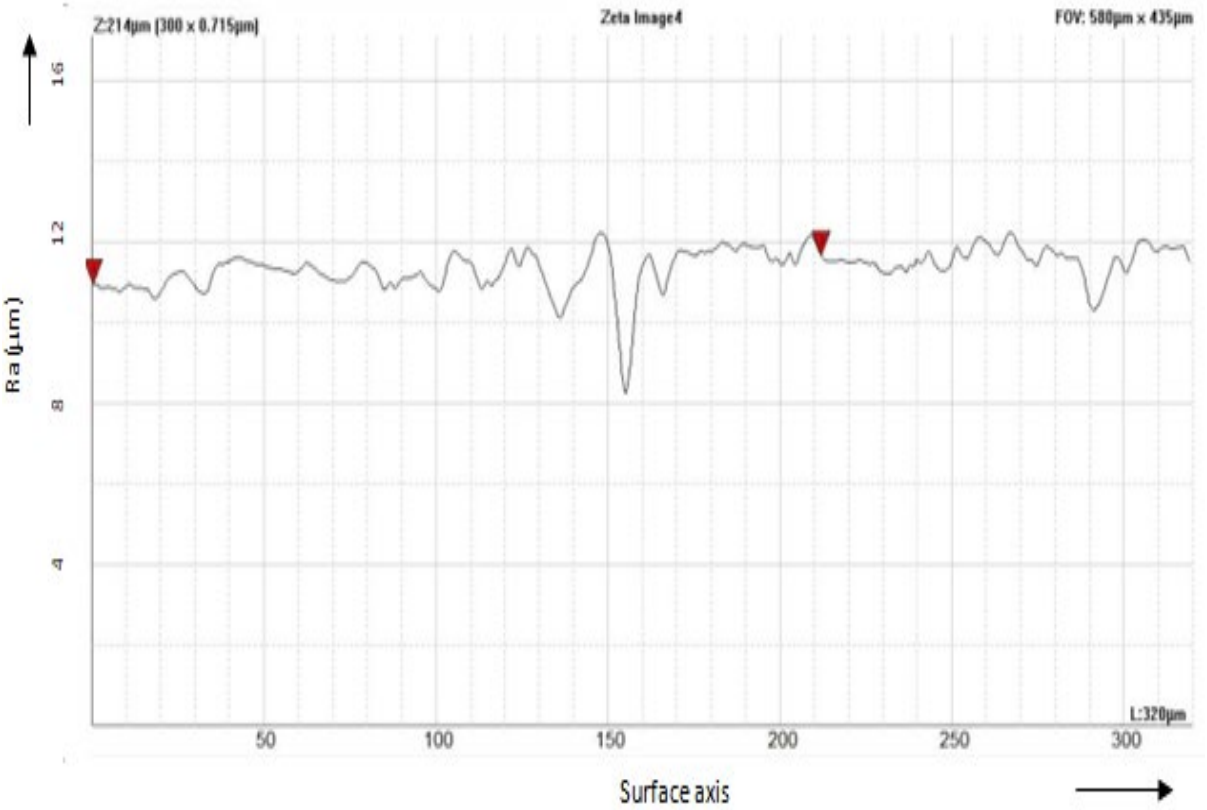

Figure 8.43 (d) Surface profile of machined workpiece by Near Dry machining

Summary

a) The FEM model was validated through experimental and analytical means.
b) This chapter includes result and discussion related to optimization of process parameters and their effect on output performances.
c) The best combination of the parameters was found for improving the machining efficiency.
d) Later confirmation experiments were conducted to verify the results, whether the output results were within the acceptable range or not.
e) Various properties of machined surface were analyzed by Scanning Electron Microscope, profilometer and other instruments.
f) Multi response characteristic optimization was performed using utility function.
g) Study was performed on another form of hybrid EDM method of machining known as Gaseous Assisted Powder Mixed Near-Dry Electric Discharge Machining.
h) The experiments were conducted with different combination of dielectric gases in place of compressed air.
i) The effect of different dielectric gases was studied under different experimental scenarios on responses such as material removal, surface finish, micro-hardness and residual stress.
j) Use of dielectric in form of other gases can significantly improve the machining tendency of the developed setup.

This chapter contains salient conclusions. Important conclusions of the investigation regarding MRR, Ra, TWR, MH and RS are stated in this end part of the thesis. This chapter also introduces scope for further research in this field. Significant findings have been drawn from performed experimentation.

9.1 Conclusion

- Powder mixed near-dry electric discharge machining (PMND-EDM) is an advanced method of machining very hard conductive materials with complex geometries which are difficult to be machined by other conventional method.
- PMND-EDM is an eco-friendly process which uses minute amount of metal working fluids (MWF) along with conductive metallic powders for machining purposes. Improvement in heat distribution by the bridging effect at the machining gap due to presence of metallic powder particles resulted in obtaining better quality surfaces.
- Several experiments were performed as per different experimental conditions with different powder additives and dielectric mediums and it was observed that the dielectric medium composition can be tailored as per the requirement of machining in EDM.
- The analysis for X-ray diffraction of the finished workpiece was performed with X'Pert High Score tool. The oxide layers and molten material on workpiece surface was also observed from SEM images which were responsible for changing the surface properties of the machined samples.
- The MRR increases with an increase in metallic powder concentration of zinc and maximum increase in MRR was 17.85% as compared to ND-EDM.
- Surface finish was improved by 16.36% in PMND-EDM as the sparking was uniformly distributed among the powder particles, which gives even and uniform machined surfaces.
- There was a decrease in residual stress by 56.09% over the machined surfaces in PMND-EDM due to relieving of induced stresses by powder additives.

- The maximum increase in MH was 62.69% over the machined surface in PMND-EDM as compared to ND-EDM due to the formation of hard carbides and oxides over the top layer of the machined workpiece.

- In single response optimization, Tool diameter (2mm), flow rate of mist (15 ml/min), concentration of metallic powder (8 gm/l) and mist pressure (0.6 MPa) of dielectric medium were the most influential values which resulted in obtaining maximum MRR of 0.11 mg s^{-1}.

- Tool diameter (3mm), flow rate of mist (10 ml/min), concentration of metallic powder (8 gm/l) and mist pressure (0.5 MPa) of dielectric medium were the most influential values which resulted in obtaining maximum surface finish (Ra~1.113 μm).

- The optimum tool wear rate was obtained as 1.15 mg/min for Tool diameter (3mm), flow rate of mist (10 ml/min), concentration of metallic powder (8 gm/l) and mist pressure (0.5 MPa) of dielectric medium.

- The optimum residual stress was obtained as 106.32 MPa for Tool diameter (3mm), flow rate of mist (10 ml/min), concentration of metallic powder (2 gm/l) and mist pressure (0.5 MPa) of dielectric medium.

- Tool diameter (2 mm), flow rate of mist (10 ml/min), concentration of metallic powder (8 gm/l) and mist pressure (0.6 MPa) of dielectric medium were the most influential values which resulted in obtaining highest value of micro-hardness was found to be 506.63 HV of the machined sample.

- For the multi response optimization, the optimized results for improved material removal rate, improvement of surface finish, enhanced micro-hardness, reduced residual stress and tool wear rate were 0.63 (mg/s), 0.79 (μm), 249 (HV), 286 (MPa) and 1.07 (mg/min) respectively. The optimized values were obtained at Tool diameter (3mm), flow rate of mist (15 ml/min), concentration of metallic powder (8 gm/l) and mist pressure (0.5 MPa) of dielectric medium.

- The 95% confidence interval of the predicted mean for the material removal rate was $0.39 < MRR < 0.87$; for Surface finish was $0.73 < Ra < 0.85$; for Residual

stress was 285.33< RS< 286.67; for Micro-hardness was 248.58< MH< 249.42; for Tool wear rate was 0.95 < TWR < 1.19.

- Thermo-Electrical modeling was performed for MRR in PMND-EDM. A striking similarity between the values of experimental work, numerical model and FEM model has been observed. The maximum experimental MRR was 7.68 mm^3/min and the error percentage between experimental, mathematical and FEM was under 15%.

- The heat flux transferred to the workpiece from the tool was a function of breakdown time, pulse-on time (35, 65, 200 and 500 μs), current (12 A), voltage (25 V) and flushing efficiency (100%).

- The small variations in time-lag value brought increase in net amount of heat delivered to the workpiece which resulted in increment of MRR in thermo-electric modeling. This increasing and decreasing nature of MRR at various powder concentration values corresponds to various pulse duration values in machining.

- Gaseous assisted powder mixed EDM experimentation was performed for analysis for MRR, Ra, MH and RS. Graphite metallic powder along with oxygen gas was proven to be most superior dielectric combination in terms of obtaining highest MRR (3.379 mg/min) as compared to other dielectric combinations.
- Graphite powder along with argon gas was found to be most suitable dielectric medium as compared to other dielectric mediums in terms of achieving finest surface finish (Ra) of 1.11μm.
- Powder additives in GAPMND-EDM were effective in surface modification and improving micro-hardness of machined parts. The highest MH obtained was 820.30 HV by using dielectric combination of zinc additives with argon gas.
- The residual stress tends to decrease with metallic powder additives and lowest induced tensile residual stress was 229 MPa in case of dielectric combination of zinc along with argon gas.

- A comparative experimental study for machining performance characteristics was performed for PMND-EDM with metallic powders Silicon, Graphite and Aluminium. The highest MRR (4.5 mm^3/min) in PMND-EDM was found by using aluminium powder followed by graphite and silicon. The maximum surface finish

(1.6 μm) was observed with Silicon powder followed by graphite and aluminium powder due to its low thermal and electrical conductivity

9.2 Future Scope

- The modeling can be performed for determining residual stress, surface finish, micro-hardness and tool wear rate in near-dry EDM.
- The modeling can be performed for determining machining characteristics in powder mixed near-dry EDM.
- The modeling can be performed for determining residual stress, surface finish, micro-hardness in gaseous assisted powder mixed near dry EDM.
- This model could be utilized further for determination of development of surface cracks and variation in the properties of dielectric medium while machining.

REFRENCES

[1]. Amorim F.L, Dalcin V.A, Soares P, Mendes L.A, Surface modification of tool steel by electrical discharge machining with molybdenum powder mixed in dielectric fluid, International Journal of Advanced Manufacturing Technology, (2017), 91 (1-4), p.341-350.

[2]. Astakhov V. P, Tribology of Metal Cutting, Elsevier, 2006.

[3]. Bai X, Zhang Q.H, Li T.T, Zhang J.H, Powder Mixed near Dry Electrical Discharge Machining, Advanced Materials Research, (2012, a), 500, p. 253-258.

[4]. Bai X, Zhang Q.H, Li T.T, Zhang Y.H, Research on the medium breakdown mechanism of powder mixed near-dry electrical discharge machining, Chinese Journal of Mechanical Engineering, (2012, b), 48, p. 186-192.

[5]. Bai X, Zhang Q.H, Yang T, Zhang J.H, Tan J, Research on tool wear rate of powder mixed near dry electrical discharge machining, Advanced Materials Research, (2013,a), 652-654, p. 2222-2227.

[6]. Bai X, Zhang Q.H, Yang T.Y, Zhang J.H, Research on material removal rate of powder mixed near-dry electrical discharge machining, International Journal of Advanced Manufacturing Technology, (2013, b), 68, p. 1757-1766.

[7]. Bai X, Zhang Q.H, Zhang J.H, Kong D, Yang T, Machining efficiency of powder mixed near-dry electrical discharge machining based on different material combinations of tool electrode and workpiece electrode, Journal of Manufacturing Processes, (2013, c), 15 (4), p.474-482.

[8]. Bhattacharya A, Batish A, Kumar N, Surface characterization and material migration during surface modification of die steels with silicon, graphite and tungsten powder in EDM process, Journal of Mechanical Science and Technology, (2013), 27, p. 133–140.

[9]. Bhattacharya R, Jain V. K, Ghoshdastidar P. S, Numerical simulation of thermal erosion in EDM process, Institution of Engineers India Part E: production engineering division, (1996), 77, p.13-19.

[10]. Boopathi S, Sivakumar K, Experimental investigation and parameter optimization of near-dry wire-cut electrical discharge machining using multi-objective evolutionary algorithm, International Journal of Advanced Manufacturing Technology, (2013), 67, p.2639–2655.

[11]. Brar B.S, Walia R.S, Singh V.P, Electrochemical-aided abrasive flow machining (ECA2 FM) process: a hybrid machining process, International Journal of Advanced Manufacturing Technology, (2015), 79 (1-4), p.329-342.

[12]. Byrne D.M, Taguchi S, The Taguchi approach to parameter design, Quality Progress, (1987), p.19-26.

[13]. Choudhary S.K, Jadoun R.S, Current Advanced Research Development of Electric Discharge Machining (EDM): A Review, International Journal of Research in Advent Technology, (2014), 2, p.2321-9637

[14]. Chow H.M, Yan B.H, Huang F.Y, Hung J.C, Study of added powder in kerosene for the micro-slit machining of titanium alloy using electro-discharge machining, Journal of Materials Processing Technology, (2000), 101, p.95-103.

[15]. Chundru V.R, Koona R, Pujari S.R, Surface modification of Ti6Al4V alloy using EDMed electrode made with nano- and micron-sized TiC/Cu powder particles, Arabian Journal for Science and Engineering, (2019), 44, p. 1425-1436.

[16]. Derek W.B, Analysis of Optimal Decisions, John Wiley and Sons: New York, (1982), p.257.

[17]. Dhakar K, Dvivedi A, Dhiman A, Experimental investigation on effects of dielectric mediums in near-dry electric discharge machining, Journal of Mechanical Science and Technology, (2016), 30, p.2179-2185.

[18]. Dhakar K, Dvivedi A, Parametric Evaluation on Near-dry Electric Discharge Machining, Materials and Manufacturing Processes, (2015), 31, p. 413-421.

[19]. Dhakar K, Pundir H, Dvivedi A, Optimization and Comparison of Near-Dry Edm and Dry Edm of Inconel 71, Journal of Production Engineering, (2014), 17, p. 25-29.

[20]. Dibitonto D. D, Eubank P. T, Patel M. R, Barrufet M. A, Theoretical models of the electrical discharge machining process, A simple cathode erosion model. Journal of applied physics, (1989), 66(9), p.4095-4103.

[21]. Ekmekci B, Elkoca O, Tekkaya A.E, Residual Stress State and Hardness Depth in Electric Discharge Machining: De-Ionized Water as Dielectric Liquid, Machining Science and Technology, (2007), 9, p.39-61.

[22]. Ekmekci B, Tekkaya A.E, Erden A.D, A semi-empirical approach for residual stresses in electric discharge machining (EDM), International Journal of Machine Tools and Manufacture, (2016), 46, p. 858–868.

[23]. El-Hofy H, Youssef H, Environmental hazards of non-traditional machining, Proceedings of the 4th IASME / WSEAS International Conference on Energy & Environment (EE'09), (2009), p. 140-146.

[24]. Erden A, Bilgin, S, Role of impurities in electric discharge machining, In Proceedings of the Twenty-First International Machine Tool Design and Research Conference, Palgrave, London, (1981), p. 345-350.

[25]. Erden A, Kaftanoglu B, Heat transfer modeling of electric discharge machining, In Proceedings of the Twenty-First International Machine Tool Design and Research Conference Palgrave, London, (1981), p. 351-358.

[26]. Fong T.Y, Chen C.F, Investigation into some surface characteristics of electrical discharge machined SKD-11 using powder-suspension dielectric oil, Journal of Materials Processing Technology, (2005), 170, p.385–391.

[27]. Furutani K, Saneto A, Takezawa H, Mohri N, Miyake H, Accertation of titanium carbide by electrical discharge machining with powder suspended in working fluid, Precision Engineering, (2001), 25 (2), p. 138-144.

[28]. Gao Q, Zhang Q.H, Zhang J.H, Experimental study of powder-mixed near dry electrical discharge machining, Chinese Journal of Mechanical Engineering, (2009), 45, p.169–175.

[29]. Germer L.H, Haworth F E, Erosion of Electrical Contacts on Make, Journal of Applied Physics, (1949), 20, 1085.

[30]. Gill A.S, Kumar S, Investigation of micro-hardness in electrical discharge alloying of En31 tool steel with Cu–W powder metallurgy electrode, Arabian Journal for Science and Engineering, (2018), (43), p. 1499-1510.

[31]. Gill A.S, Kumar S, Surface Roughness and Micro hardness Evaluation for EDM with Cu-Mn Powder Metallurgy Tool, Materials and Manufacturing Processes, (2016), 31, p.514-521.

[32]. Goyal S, Singh R. K, Parametric Study of Powder Mixed EDM and Optimization of MRR and Surface Roughness, International Journal of Scientific Engineering and Technology, (2014), 3, p. 56-62.

[33]. Goyal T, Walia R.S, Sidhu T.S, Multi-response optimization of low-pressure cold-sprayed coatings through Taguchi method and utility concept, The International Journal of Advanced Manufacturing Technology, (2013), 64, p. 903-914.

[34]. http://www.mercatech.com

[35]. https://www.avonbroach.com/

[36]. https://www.basilius.com

[37]. https://www.weibull.com

[38]. Jabbaripour B, Sadeghi M.H, Shabgard M.R, Faraji H, Investigating surface roughness, material removal rate and corrosion resistance in PMEDM of r-TiAl intermetallic, Journal of Manufacturing Processes, (2013), 15, p.158–166.

[39]. Jahan M.P, Rahman M, Wong Y.S, Modelling and experimental investigation on the effect of nano powder-mixed dielectric in micro-electro discharge machining of tungsten carbide. Proceedings of the Institution of Mechanical Engineers, Part B, (2010), 224, p. 1725–1739.

[40]. Jain V. K, Advanced Machining Processes, Allied Publishers, (2009).

[41]. Jameson E.C, Electrical Discharge Machining, Society of Manufacturing Engineers, Technology and Engineering (2001).

[42]. Jeswani M. L, Effects of the addition of graphite powder to kerosene used as the dielectric fluid in electrical discharge machining, Wear, (1981), 70 (2), p. 133-139.

[43]. Ji R, Liu Y, Zhang Y, Wang F, Machining performance of silicon carbide ceramic in end electric discharge milling. International Journal of Refractory Metals and hard Metals, (2011), 29, p.117-122.

[44]. Jilani S. T, Pandey P. C, Analysis and modelling of EDM parameters. Precision Engineering, (1982), 4(4), p.215-221.

[45]. Joshi S. N, Pande S. S, Thermo-physical modeling of die-sinking EDM process, Journal of manufacturing processes, (2010), 12(1), p.45-56.

[46]. Kalajahi M. H, Ahmadi S. R, Oliae S. N. B, Experimental and finite element analysis of EDM process and investigation of material removal rate by response surface methodology, International Journal of Advanced Manufacturing Technology, (2013), 69(1-4), p.687-704.

[47]. Kalpakjian S, Schmid S, Manufacturing Engineering and Technology, 7th Edition, Pearson, (2014).

[48]. Kansal H. K, Singh S, Kumar P, Numerical simulation of powder mixed electric discharge machining (PMEDM) using finite element method, Mathematical and Computer Modelling, (2008), 47(11-12), p.1217-1237.

[49]. Kansal H.K, Singh S, Kumar P, Effect of silicon powder mixed EDM on machining rate of AISI D2 die steel, Journal of Manufacturing Processes, (2007), 9, p. 13–22.

[50]. Kansal H.K, Singh S, Kumar P, Parametric optimization of powder mixed electric discharge machining by response surface methodology, Journal of Materials Processing Technology, (2005), 169 (3), p. 427-436.

[51]. Kao C.C, Tao J, Shih A.J, Near dry electrical discharge machining, International Journal of Machine Tools and Manufacture, (2007), 47, p. 2273–2281.

[52]. Khullar V.R, Sharma N, Kishore S, Sharma R, RSM- and NSGA-II-based multiple performance characteristics optimization of EDM Parameters for AISI 5160, Arabian Journal for Science and Engineering, (2017), 42, p. 1917-1928.

[53]. Khundrakpam N.S, Brar G.S, Deepak D, A Comparative Study on Machining Performance of wet EDM, Near Dry EDM and Powder Mixed Near Dry EDM, International Journal of Applied Engineering Research, (2018), 13, p. 9378-9381.

[54]. Konig W, Klocke F, Manufacturing process 3, Ablation, generation and laser material processing, Springer, Berlin (1997).

[55]. Kozak J, Rajurkar K.P, Hybrid machining processes, Evaluation and development, Proceedings of 2nd International Conference on Machining and measurement of sculptured surfaces, Krakow, (2001), p.501-536.

[56]. Kremer D, Lhiaubet C, Moisan A. A, Study of the effect of synchronizing ultrasonic vibrations with pulse in EDM, Annal CIRP, (1991), 40, p.211-214.

[57]. Kumar A, Kumar S, Mandal A, Dixit A.R, Investigation of powder mixed EDM process parameters for machining Inconel alloy using response surface methodology, Materials Today: Proceedings, (2018,a), 5, p. 6183–6188.

[58]. Kumar M, Datta S, Kumar R, Electro-discharge machining performance of Ti–6Al–4V Alloy: Studies on parametric effect and phenomenon of electrode wear, Arabian Journal for Science and Engineering, (2019), 10, p. 1553-1568.

[59]. Kumar P, Barua P.B, Gaindher J.L, Quality of V-process method through the Taguchi technique, Quality and Reliability Engineering International, (1996), 12, p. 421–427.

[60]. Kumar P, Barua P.B, Gaindher J.L, Quality optimization (multi-characteristics) through Taguchi technique and utility concept, Quality and Reliability Engineering International (2000), 16 p. 475–485.

[61]. Kumar S, Batra U, Surface modification of die steel materials by EDM method using tungsten powder-mixed dielectric, Journal of Manufacturing Procesess, (2012), 14 (1), p. 35-40.

[62]. Kumar S, Grover S, Walia R.S, Analyzing and modeling the performance index of ultrasonic vibration assisted EDM using graph theory and matrix approach, International Journal on Interactive Design and Manufacturing, (2016), 12, p.225-242.

[63]. Kumar S, Grover S, Walia R.S, Effect of hybrid wire EDM conditions on generation of residual stresses in machining of HCHCr D2 tool steel under ultrasonic vibration, International Journal on Interactive Design and Manufacturing, (2018, b), 12, p. 1119-1137.

[64]. Kumar S, Singh R, Batish A, Singh T.P, Singh R, Investigating surface properties of cryogenically treated titanium alloys in powder mixed electric discharge machining. Journal of the Brazilian Society of Mechanical Sciences and Engineering, (2017), 39, p. 2635-2648.

[65]. Kung K.Y, Horng J.T, Chiang K.T, Material removal rate and electrode wear ratio study on the powder mixed electrical discharge machining of cobalt-bonded tungsten carbide, International Journal of Advanced Manufacturing Technology, (2009), 40, p. 95–104.

[66]. Kunieda M, Miyosh Y, Takaya T, Nakjima N, Yu Z. B, Yoshida M, High Speed 3D Milling by Dry EDM, CIRP Annal, (2003), 52, p. 147-150.

[67]. Kunieda M, Yoshida M, Electrical Discharge Machining in Gas, CIRP Annal, (1997), 46, p. 143–146.

[68]. Kuriakose S, Mohan K, Shunmugam M.S, Data mining applied to wire-EDM process, Journal of Materials Processing Technology, (2003), 142, p. 182–189

[69]. Li L, Zhao L, Li Z.Y, Feng L, Bai X, Surface characteristics of Ti-6Al-4V by SiC abrasive-mixed EDM with magnetic stirring, Materials and Manufacturing Processes, (2016), 32 (1), p. 83-86.

[70]. Li L.Q, Zhao W.S, DI S.C, WANG Z.L, Experimental Study on Electrical Discharge Machining in Gas, Chinese Journal of Mechanical Engineering, (2006), 42, p.203-216.

[71]. Lin Y.C, Hung J.C, Chow H.M, Wang A.C, Chen J.T, Machining Characteristics of a Hybrid Process of EDM in Gas Combined with Ultrasonic Vibration and AJM, Procedia CIRP , (2016) 42, p.167-172

[72]. Liqing L, Yingjie S, Study of dry EDM with oxygen-mixed and cryogenic cooling approaches, The Seventeenth CIRP Conference on Electro Physical and Chemical Machining (ISEM) Procedia CIRP, (2013), 6, p. 344 – 350.

[73]. Liu J. F, Guo Y. B, Thermal Modeling of EDM with Progression of Massive Random Electrical Discharges, Procedia Manufacturing, (2016, a), 5, p.495-507.

[74]. Liu J.F, Guo Y.B, Residual stress modeling in electric discharge machining (EDM) by incorporating massive random discharges, Procedia CIRP, (2016, b), 45, p. 299-302.

[75]. Madhu P, Jain V. K, Sundararajan T, Rajurkar K. P, Finite element analysis of EDM process, Processing of Advanced Materials (UK), (1991), 1(3), p.161-173.

[76]. Mai C, Hocheng H, Huang S, Advantages of carbon nanotubes in electrical discharge machining, International Journal of Advanced Manufacturing Technology, (2012), 59, p.111–117.

[77]. Mane S.G, Hargude N.V, Parametric Optimization Of Near Dry Electrical Discharge Machining Process For Aisi Sae D-2 Tool Steel, International Journal of Advanced Research in Engineering and Technology, (2015), 6 (1), p. 99-114.

[78]. Marafona J, Chousal J. A. G, A finite element model of EDM based on the Joule effect. International Journal of Machine Tools and Manufacture, (2006), 46(6), p.595-602.

[79]. Marashi H, Jafarlou D. M, Sarhan A. A, Hamdi M, State of the art in powder mixed dielectric for EDM applications, Precision Engineering, (2016), 46, p.11-33.

[80]. Marty C.C, Investigation of surface temperature in electro-discharge machining. Journal of Engineering for Industry, (1977), 99(3), p.682-684.

[81]. Masuzawa T, Tsukamoto J, Fujino M, Drilling of Deep Microholes by EDM, CIRP Annals, (1989), 38, p. 195-198

[82]. McGeough, J.A, Electro discharge machining in Advanced Methods of Machining, Advanced Methods of Machining, 1st edition. Chapman and Hall, USA, ISBN 0-412-31970-5, (1988), 130.

[83]. Menzies I, Koshy P, Assessment of abrasion assisted material removal in wire EDM, CIRP Annals - Manufacturing Technology, (2008), 57 (1) p. 195–198.

[84]. Merdan M.A.E.R, Arnell R.D, The surface integrity of adie steel after electrodischarge machining: 2 residual stress distribution, Surface Engineering, (1991), 7, p.154–158.

[85]. Mishra, P.K, Non-Conventional machining, The institution of Engineers-India, (1997), p.106-107.

[86]. Murali M.S, Yeo S.H, Process Simulation and Residual Stress Estimation of Micro-Electro discharge Machining Using Finite Element Method**,** Japanese Journal of Applied Physics, (2005), 44, p. 5254-5263.

[87]. National Institute of Occupational, Safety and Health, centre for disease control and prevention, (1983) https://www.cdc.gov/noes/default.html

[88]. Ndaliman M.B, Khan A.A, Ali M.Y, Influence of dielectric fluids on surface properties of electrical discharge machined titanium alloy, Proc IMechE, Proceedings of the Institution of Mechanical Engineers, Part B, (2013, b), 227, p.1310–1316.

[89]. Ogata Y.M, Residual stress on surface machined by wire electric discharge, International Journal of the Japan Society for Precision Engineering, 1991, 25, p. 273–278.

[90]. Ojha K. Garg R.K, Singh K.K, Experimental Investigation and Modeling of PMEDM Process with Chromium Powder Suspended Dielectric, International Journal of Applied Science and Engineering, (2011), 9 (2), p.65-81.

[91]. Opoz T.T, Yasar H, Ekmekci N, Ekmekci B, Particle migration and surface modification on Ti6Al4V in SiC powder mixed electrical discharge machining, Journal of Manufacturing Processes, (2018), 31, p. 744-758.

[92]. Pandey A and Singh S, Current research trends in variants of Electrical Discharge Machining: A review, International Journal of Engineering Science and Technology, (2010), 2, p. 2172-2191.

[93]. Pandey P.C, Shan H.S. Modern Machining processes, Tata McGraw Hill, (2003), p.92-93.

[94]. Patel J. B, Darji R. S, Dalai M, Powder mixed edm for improvement of mrr and surface finish: a review, International Journal of Recent Scientific Research, (2018), 9(3), p. 25218-25226.

[95]. Patel M. R, Barrufet M. A, Eubank P. T, Dibitonto D. D, Theoretical models of the electrical discharge machining process II. The anode erosion model, Journal of applied physics, (1989), 66(9), p. 4104-4111.

[96]. Pattabhiraman A, Marla D, Kapoor S.G, Atomized Dielectric Spray-Based Electric Discharge Machining for Sustainable Manufacturing, Journal of Micro and Nano-Manufacturing, (2015), 3, p. 1- 8.

[97]. Prabhu S, Uma M, Vinayagam B.K, Adaptive neuro-fuzzy interference system modelling of carbon nanotube-based electrical discharge machining process, Journal of the Brazilian Society of Mechanical Sciences and Engineering, (2013), 35, p.505–516.

[98]. Prabhu S, Vinayagam B.K, AFM Nano Analysis of Inconel 825 with Single Wall Carbon Nano Tube in Die Sinking EDM Process Using Taguchi Analysis, Arabian Journal for Science and Engineering, (2013), 38, p. 1599–1613.

[99]. Prihandana G.S, Mahardika M, Hamdi M, Wong Y.S, Miki K, Mitsui K, Study of Workpiece Vibration in Powder-Suspended Dielectric Fluid in Micro-EDM Processes, International Journal of Precision Engineering and Manufacturing, (2013), 14, p. 1817-1822.

[100]. Prihandana G.S, Mahardika M, Hamdi M, Wong Y.S, Mitsui K, Accuracy improvement in nanographite powder-suspended dielectric fluid for micro-electrical discharge machining processes, International Journal of Advanced Manufacturing Technology, (2011), 56, p.143–149.

[101]. Prihandana G.S, Sriani T, Mahardika M, Hamdi M, Miki N, Wong Y.S, Application of powder suspended in dielectric fluid for fine finish micro-EDM of Inconel 718, International Journal of Advanced Manufacturing Technology, (2014), 75, p. 599–613.

[102]. Rahul, Datta S, Biswal B.B, Mahapatra S.S, A Novel Satisfaction Function and Distance-Based Approach for Machining Performance Optimization During Electro-Discharge Machining on Super Alloy Inconel 718, Arabian Journal for Science and Engineering, (2017), 42, p. 1999-2020.

[103]. Rana R, Walia R.S, Murtaza Q, Tyagi M, Parametric Optimization of Hybrid Electrode EDM Process, AES-ATEMA, International Conference 29 international conference TORONTO, Canada (2016).

[104]. Rao P.S, Ramji K, Satyanarayana B, Effect of wire EDM conditions on generation of residual stresses in machining of aluminum 2014 T6 alloy, Alexandria Engineering Journal, (2016), 55 (2), p. 1077-1084.

[105]. Razak M. A, Abdul A.M, Nanimina A.M, Improving EDM Efficiency with Silicon Carbide Powder-Mixed Dielectric Fluid, International Journal of Materials, Mechanics and Manufacturing, (2015), 3, p.40-43.

[106]. Ross P.J, Taguchi techniques for quality engineering, (1988), McGraw-Hill Book Company, New York.

[107]. Ross P.J, Taguchi techniques for Quality Engineering, (1996), McGraw-Hill Book Company, New York.

[108]. Sahu S.K, Jadam T, Datta S, Dhupal D, Nandi G, Application of SiC Power Added in Kerosene Dielectric Media for Electro-Discharge Machining of Inconel 718 Super Alloys: Effect of Powder Concentration, Materials Today: Proceedings, (2018), 5, p. 20297–20305.

[109]. Schulze H. P, Herms R, Juhr H, Schaetzing W, Wollenberg G, Comparison of measured and simulated crater morphology for EDM. Journal of Materials Processing Technology, (2004), 149(1-3), p.316-322.

[110]. Shabgard M, Seydi S, Seyedzavvar M, Novel approach towards finite element analysis of residual stresses in electrical discharge machining process, International Journal of Advanced Manufacturing Technology, (2016), 82, p. 1805-1814.

[111]. Shah A, Prajapati V, Patel P, Pandey A, Development of Pulsed Power DC Supply for Micro-EDM (2007).

[112]. Shen Y, Liu Y, Zhang Y. Y, Dong H, Sun W, Wang X, Zheng C, Ji R, High-speed dry electrical discharge machining, International Journal of Machine Tools and Manufacture, (2015), 93, p. 19-25.

[113]. Shen Y, Liu Y, Sun W, Zhang Y, Dong H, Zheng C, Ji R, High-speed near dry electrical discharge machining, Journal of Materials Processing Technology, (2016), 233, p.9-18.

[114]. Shobert E.I, What happens in EDM Electrical Discharge Machining: Tooling, Methods and Applications, Society of Manufacturing Engineers, Dearborn, Michigan, (1983), p.3–4.

[115]. Singh B, Kumar J, Kumar S, Experimental Investigation on Surface Characteristics in Powder-Mixed Electro discharge Machining of AA6061/10%SiC Composite, Materials and Manufacturing Processes, (2014), 29, p.287–297.

[116]. Singh B, Kumar J, Kumar S, Investigation of the Tool Wear Rate in Tungsten Powder-Mixed Electric Discharge Machining of AA6061/10%SiC Composite, Materials and Manufacturing Processes, (2016), 31, p.456–466.

[117]. Singh B, Kumar J, Kumar S, Influences of Process Parameters on MRR Improvement in Simple and Powder-Mixed EDM of AA6061/10%SiC Composite, Materials and Manufacturing Processes, (2015), 30, p.303–312.

[118]. Singh G, Singh G, Singh K, Singla A, Experimental studies on material removal rate, tool wear rate and surface properties of machined surface by powder mixed electric discharge machining, Materials Today: Proceedings, (2017), 4 (2), p.1065-1073.

[119]. Singh H, Experimental study of distribution of energy during EDM process for utilization in thermal models, International Journal of Heat and Mass Transfer, (2012), 55 (19-20), p.5053-5064.

[120]. Singh J, Satsangi P. S, Walia R. S, Singh V.P, Micro-hardness and machined surface damage study for continuous and discontinuous ultrasonic vibration assisted electrical discharge machining, Materials and Manufacturing Processes, (2011,a).

[121]. Singh J, Sharma R.K, Assessing the effects of different dielectrics on environmentally conscious powder-mixed EDM of difficult to machine material (WC-Co), Frontiers of Mechanical Engineering, (2016), 11, p. 374-387.

[122]. Singh J, Walia R.S, Satsangi P, Singh V, FEM modeling of ultrasonic vibration assisted work-piece in EDM process, International Journal of Mechanical Systems Engineering, (2011,b), 1, p. 8-16.

[123]. Singh S, Singh J, Optimization Of Powder Mixed Electric Discharge Machining Using ASTM A-105 Steel By Response Surface Methodology, International Journal of Enhanced Research In Science Technology & Engineering, (2014), 3, p. 291-303.

[124]. Singh S, Yeh M.F, Optimization of Abrasive Powder Mixed EDM of Aluminum Matrix Composites with Multiple Responses Using Gray Relational Analysis, Journal of Materials Engineering and Performance, (2012), 21, p. 481–491.

[125]. Singh T, Dvivedi A, Developments in electrochemical discharge machining: A review on electrochemical discharge machining, process variants and their hybrid methods, International Journal of Machine Tools and Manufacture, (2016), 105, p. 1-13

[126]. Skrabalak G, Kozak J, Study on Dry Electrical Discharge Machining, Proceedings of the World Congress on Engineering 2010, 3.

[127]. Skrabalak G, Kozaka J, Zyburaa M, Optimization of dry EDM milling process, Procedia CIRP 6, (2013) p. 332 – 337

[128]. Snoyes R, VanDijck F.S, Investigations of EDM operations by means of thermo mathematical models, (1971), Annals of CIRP, 20(1), p. 35-36.

[129]. Sundriyal S, Walia R.S, Vipin, Tyagi M, Investigation on surface finish in powder mixed near dry electric discharge machining method, Materials Today: Proceedings DOI: 10.1016/j.matpr.2019.09.031.

[130]. Sundriyal S, Vipin, Walia R.S, Experimental investigation on micro-hardness of EN-31 die steel in powder mixed near dry electric discharge machining method, Strojniski vestnik- Journal of Mechanical Engineering, (2020,a), 66, (3), p. 184-192.

[131]. Sundriyal S, Vipin, Walia R.S, Powder Mixed Near Dry Electric Discharge Machining Parameter Optimization for Tool Wear Rate, Advances in Unconventional Machining and Composites, Springer Nature Singapore Pte Ltd (2020,c).

[132]. Sundriyal S, Vipin, Walia R.S, Study on influence of metallic powder in near dry electric discharge machining, Strojniski vestnik – Journal of Mechanical Engineering, (2020,b), 66(4), p. 243-253.

[133]. Talla G, Gangopadhyay S, Biswas C.K, Effect of powder- suspended dielectric on the EDM characteristics of Inconel 625, Journal of Material Engineering and Performances, (2016,b), 25 (2), p. 704-717.

[134]. Talla G, Gangopadhyay S, Biswas C.K, Influence of graphite powder mixed EDM on the surface integrity characteristics of Inconel 625, Particulate Science and Technology, (2017), 35 (2), p. 219-226.

[135]. Talla G, Powder-mixed Electric Discharge Machining (PMEDM) of Inconel 625, Ph.D Thesis, National Institute of Technology Rourkela, (2016, a).

[136]. Tan P. C, Yeo S.H, Tan Y.V, Effects of nanopowder additives in micro-electrical discharge machining, International Journal of Precision Engineering and Manufacturing, (2008), 9, p. 22-26.

[137]. Tanimura T, Isuzugawa K, Fujita I, Iwamoto A, Kamitani T, Development of EDM in the Mist, Proceedings of Ninth International Symposium of Electro Machining, (1989), 9, p. 313-316.

[138]. Tao J, Shih A. J, Ni J, Experimental study of the dry and near-dry electrical discharge milling processes, Journal of Manufacturing Science and Engineering, (2008), 130 (1).

[139]. Tao J, Shih A. J, Ni J, Near-Dry EDM Milling of Mirror-Like Surface Finish, International Journal of Electrical Machining, (2008), p. 29-33.

[140]. Tlili A, Ghanem F, Salah N. B, A contribution in EDM simulation field, The International Journal of Advanced Manufacturing Technology, (2015), 79(5-8), p.921-935.

[141]. Tripathy S, Tripathy D. K, An approach for increasing the micro-hardness in electrical discharge machining by adding conductive powder to the dielectric, Materials Today: Proceedings, (2017, b), 4 (2), p. 1215-1224.

[142]. Tripathy S, Tripathy D.K, Optimization of process parameters and investigation on surface characteristics during EDM and powder mixed EDM, Innovative Design and Development Practices in Aerospace and Automotive Engineering. Lecture Notes in Mechanical Engineering, (2017, a) Springer, p. 385-391.

[143]. Tsai H.C, Yan, B.H, Huang, F.H, EDM performance of Cr/Cu based composite electrodes, International Journal of Machine Tools and Manufacturing, (2003), 43 (3), p.245–252.

[144]. Tzeng Y.F, Lee C.Y, Effects of Powder Characteristics on Electro-discharge Machining Efficiency, International Journal of Advanced Manufacturing Technology, (2001), 17, p. 586–592.

[145]. Upadhyay L, Aggarwal M, Pandey P, Performance analysis of magneto rheological fluid assisted electrical discharge machining, Materials and Manufacturing Processes, (2017), 33(11).

[146]. Van Dijck, F. S, Dutre W. L, Heat conduction model for the calculation of the volume of molten metal in electric discharges, Journal of Physics D: Applied Physics, (1974), 7(6), p.899.

[147]. Vignesh M, Ramanujam R, Laser Laser-assisted high speed machining of Inconel 718 alloy, High Speed Machining, (2020), p. 243-262

[148]. Walia R.S, Shan H. S, Kumar P, Effect of providing a rotating rod inside the hollow cylindrical workpiece on the material removal in AFM, Proceedings of 21st AIMTDR Conference, (2004), p. 143-148.

[149]. Walia R.S, Shan H.S, Kumar P, Multi-response optimization of CFAAFM process through Taguchi method and utility concept, Materials and Manufacturing Processes, (2006), 21 (8), p**.** 907-914.

[150]. Wang T, Wu C, Liu H, Chen M, Cheng J, Su D, On-machine electric discharge truing of small ball-end fine diamond grinding wheels, Journal of Materials Processing Technology (2020).

[151]. Wang T, Chen Y, Kunieda M, Study on wire electric discharge machining in gas, Chinese journal of mechanical engineering, (2003).

[152]. Wang X, Liu Y, Zhang Y, Sun Q, Li Z, Shen Y, Characteristics of plasma channel in powder-mixed EDM based on mono pulse discharge, International Journal of Advanced Manufacturing Technology, (2016), 82, p. 1063-1069.

[153]. Wong Y.S, Lim L.C, Rahuman I, Tee W.M, Near-mirror-finish phenomenon in EDM using powder-mixed dielectric, Journal of Materials Processing Technology, (1998), 79, p.30-40.

[154]. Wu K.L, Yan B.H, Huang F.Y, Chen S.C, Improvement of surface finish on SKD steel using electro- discharge machining with aluminum and surfactant added dielectric*,* International Journal of Machine Tools and Manufacture, (2005), 45, p. 1195–1201.

[155]. Yadav V, Jain V.K, Dixit P.M, Thermal stresses due to electrical discharge machining. International Journal of Machine Tools and Manufacture, (2002), 42, p.877–888.

[156]. Yang X, Han X, Zhou F, Molecular dynamics simulation of residual stress generated in EDM. Procedia CIRP, (2013), 6, p.433 – 438.

[157]. Yeo S. H, Kurnia W, Tan P. C, Critical assessment and numerical comparison of electro-thermal models in EDM. Journal of materials processing technology, (2008), 203(1-3), p.241-251.

[158]. Zain Z. M, Ndaliman M.B, Khan A.A, Ali M.Y, Improving micro-hardness of stainless steel through powder-mixed electrical discharge machining, Journal of Mechanical Engineering Science, (2014), 228, p. 3374–3380.

[159]. Zhang Q.H, Zhang J.H, Deng J.X, Qin Y, Niu Z.W, Ultrasonic vibration electrical discharge machining in gas, Journal of Material processing Technology, (2002), 129, p. 135-138.

[160]. Zhao W.S, Meng Q.G, Wang Z.L, The application of research on powder mixed EDM in rough machining, Journal of Materials Processing Technology, (2002), 129 (1-3), p. 30-33.

[161]. Zhao Y, Kunieda M, Abe K, EDM mechanism of single crystal SiC with respect to thermal, mechanical and chemical aspects, Journal of Materials Processing Technology, (2016), 236, p.138-147.

[162]. Zingerman A.S, Propagation of a discharge column, Soviet Physics-Technical Physics, (1956), 5, p. 992-996.

[163]. Zou R, Yu Z, Yan C, Li J, Liu X, Xu W, Micro electrical discharge machining in nitrogen plasma jet, Precision Engineering, (2018), 51, p.198–207.

Research Publications

International Journal

[1]. S. Sundriyal, Vipin, R.S. Walia, Experimental Investigation on Micro-hardness of EN-31 Die Steel in Powder Mixed near Dry Electric Discharge Machining Method, **Strojniski vestnik** – J. Mech. Engg. **66**, 184-192, (2020). **(SCI, Impact factor: 1.139)**

[2]. S. Sundriyal, Vipin, R.S. Walia, Study on Influence of Metallic Powder in Near- Dry Electric Discharge Machining, **Strojniski vestnik** – J. Mech. Engg. **66,** 243-253, (2020). **(SCI, Impact factor: 1.139)**

[3]. S. Sundriyal, J. Yadav, Vipin, R.S. Walia, R. Kumar, Thermal-physical based modeling of material removal in Powder Mixed Near Dry Electric Discharge Machining, Journal of Materials Engineering and Performnace (2020). **(SCI, Impact factor: 1.652)**

[4]. S. Sundriyal, Vipin, R.S. Walia, Experimental studies on parametric effect and phenomenon of metallic powder additives in Near Dry Electric Discharge Machining, Scientia iranica **(accepted, SCI Impact factor: 1.025)**

[5]. S. Sundriyal, Vipin, R.S. Walia, Experimental Study On Gaseous Assisted Powder Mixed Near Dry Electric Discharge Machining, Part E: Journal of Process Mechanical Engineering **(Revision 1, SCI Impact factor: 1.60)**

[6]. S. Sundriyal, Vipin, R.S. Walia, Study On Performance Enhancements In Powder Mixed Near Dry Electric Discharge Machining, **IJEMS (SCI – Under review, Impact factor: 0.54)**

[7]. S. Sundriyal, R.S. Walia, Vipin, M. Tyagi, Investigation on surface finish in powder mixed near dry electric discharge machining method, **Materials Today**: Proceedings DOI: 10.1016/j.matpr.2019.09.031. **(Scopus Indexed)**

[8]. S. Sundriyal, Vipin, R.S. Walia, Near Dry and Powder Mixed Near Dry Electric Discharge Machining, International Journal of Engineering and Advanced Technology (IJEAT) ISSN: 2249 – 8958, Volume-9 Issue-1, October 2019. **(Scopus)**

[9]. S. Sundriyal, Vipin, R.S. Walia, Powder Mixed Near Dry Electric Discharge Machining Parameter Optimization for Tool Wear Rate, Advances in Unconventional Machining and Composites, Springer Nature Singapore Pte Ltd (2020). (**Book chapter**)

International conference

- S. Sundriyal, Vipin, R.S. Walia, Effect Of Process Parameters On Kerf In Wire Electric Discharge Machining, Dr B R Ambedkar National Institute Of Technology Jalandhar-144011, India Department Of Industrial And Production Engineering IVth International Conference On Production And Industrial Engineering, CPIE-2016

- S. Sundriyal, R.S. Walia, Vipin, M. Tyagi, Investigation on surface finish in powder mixed near dry electric discharge machining method, 2 nd International Conference on Computational& Experimental Methods in Mechanical Engineering (ICCEMME-2019)

- Sanjay Sundriyal, R.S Walia, Vipin, Himmat Singh and Parvesh Ali Optimization Of Process Parameters In Wire Electrical Discharge Machining, ICAPIE 2016.

- S. Sundriyal, Vipin, R.S. Walia, Powder Mixed Near Dry Electric Discharge Machining Parameter Optimization for Tool Wear Rate, Advances in Unconventional Machining and Composites, Springer Nature Singapore Pte Ltd (2020). AIMTDR 2018

- S. Sundriyal, Vipin, R.S. Walia, Experimentation for Micro-hardness and Residual Stress in Gaseous Assisted Powder Mixed Near Dry Electric Discharge Machining, ICAPIE 2019.